UNIVERSITÉ DU QUÉBEC À CHICOUTIMI

THESIS PRESENTED TO THE

UNIVERSITY OF QUEBEC AT CHICOUTIMI

IN PARTIAL FULFILLMENT OF

THE REQUIREMENTS FOR THE DEGREE OF

DOCTOR OF PHILOSOPHY IN ENGINEERING

BY

OSSAMA ELSEBAIE

EFFECTS OF STRONTIUM-MODIFICATION, IRON-BASED INTERMETALLICS AND AGING CONDITIONS ON THE IMPACT TOUGHNESS OF Al-(6-11)%Si ALLOYS

APRIL 2010

UNIVERSITÉ DU QUÉBEC À CHICOUTIMI

THÈSE PRÉSENTÉE À

L'UNIVERSITÉ DU QUÉBEC À CHICOUTIMI

COMME EXIGENCE PARTIELLE

DU DOCTORAT EN INGÉNIERIE

PAR

OSSAMA ELSEBAIE

EFFETS DE LA MODIFICATION PAR LE STRONTIUM, LES INTERMÉTALLIQUES À BASSE DE FER ET LE VIEILLISSEMENT SUR LA RÉSILIENCE DES ALLIAGES Al-(6-11)%Si

AVRIL 2010

RÉSUMÉ

La résilience est une propriété mécanique qui a pris de l'importance au cours des dernières années. Les données de la résilience sont utilisées pour optimiser les paramètres de conception puisqu'elles fournissent un moyen de comparaison et d'évaluation de la ductilité des alliages dans des conditions de haut taux de déformation. L'un des tests les plus répandus pour mesurer l'énergie de résilience d'un matériau donné est l'essai de résilience Charpy, qui a évolué pour devenir aujourd'hui un outil qualitatif pour la sélection des matériaux et pour étudier les effets des changements de microstructure sur la ténacité des matériaux. Le but principal de ce travail est d'étudier les effets de la modification au Sr, des phases intermétalliques à base de fer et des conditions de vieillissement sur la résilience des alliages commerciaux 356 et 319. La parfaite compréhension de tels paramètres quant à ces alliages serviront également de base de référence pour la caractérisation des propriétés de résilience du nouvel alliage Al-Si 396, lequel étant présentement étudié dans le cadre du programme de recherche de développement d'alliage. Les résultats obtenus de cette étude ont été analysés par rapport aux effets de ces paramètres sur l'énergie totale absorbée (E_T), de l'énergie initiation de fissure (Ei) et de l'énergie de propagation de la fissure (Ep). La rupture se produisant dans les alliages 356, 319, et 396 non-modifiés et modifiés au Sr contenant différents niveaux d'additions a également été étudiée. L'énergie totale absorbée a été mesurée en utilisant une machine d'essai de résilience Charpy, de modèle SI-1D3 de SATEC Systems Inc. couplée à un système d'acquisition de données. Ces tests ont été effectués sur des échantillons sans entaille afin de mettre en évidence le rôle des paramètres métallurgiques sur l'initiation et la propagation de la fissure. Les dimensions de l'échantillon selon la norme ASTM-E23 sont de 10 x 10 x 55 mm. Les résultats de l'examen microstructural révèlent que l'alliage 356 non modifié tel que coulé affiche de grosses particules aciculaires de silicium eutectique. Dans l'alliage 356 tel que coulé, la phase π-fer précipite soit en liaison étroite avec les plaquettes de la phase β-fer ou encore en particules indépendantes en forme de script. D'autre part, les aiguilles β-fer et les particules π-fer semblent être se former loin des colonies de silicium eutectique modifié pour l'alliage 356 modifié. La mise en solution dissout complètement les particules de petite taille de la phase π dans la matrice, en particulier pour l'alliage 356 contenant de faibles niveaux de fer. Les particules de grande taille de la phase π semblent se dissoudre partiellement dans la matrice puisque le temps de mise en solution est insuffisant pour produire une dissolution complète. Il sera également observé que certaines aiguilles β subissent une striction et mènent ultimement à une fragmentation en plus petites aiguilles. Les résultats obtenus ont révélé que l'augmentation du niveau de fer diminue significativement les valeurs de l'énergie de résilience des alliages 356 et 319. L'ajout de 0,1% en poids de Mn aux alliages 319 et 356 non-modifiés semble avoir aucun effet observable sur les valeurs de l'énergie de résilience, en particulier par rapport aux valeurs obtenues pour les mêmes alliages ne contenant que du Fe. L'augmentation du niveau de Mn à 0,38% en poids produit une légère amélioration dans les valeurs de l'énergie de résilience pour les alliages 356 et 319 non-modifiés et modifiés par rapport aux alliages contenant uniquement du fer pour les conditions tel que coulé et après mise en solution. L'alliage 319 contenant différents niveaux de Fe-Mg combinée affiche des valeurs de l'énergie de résilience plus faible

que celui ne contenant que du fer, quel que soit le niveau de fer. Une telle baisse de la valeur de l'énergie de résilience est plus prononcée après l'ajout de 0,28% en poids de Mg. La même observation a été faite dans le cas des additions combinées de Fe, Mn et Mg, à l'exception des conditions modifiées et après la mise en solution, où leurs valeurs de l'énergie de résilience demeurent presque inchangées. L'ajout de 200 PPM Sr dans les alliages 356 et 319 tel que coulés améliore légèrement les valeurs de l'énergie de résilience. Le traitement thermique couplé à la modification au Sr améliore l'énergie globale de résilience pour les alliages 356 et 319, en particulier pour les faibles niveaux d'additions. Les alliages modifiés montrent des valeurs plus élevées d'énergie de résilience par rapport aux alliages non modifiés dans les mêmes conditions, quel que soit le niveau des ajouts. L'augmentation du temps de vieillissement artificiel de l'alliage 356 non-modifié et modifié à 180°C jusqu'à 8 h diminue la valeur d'énergie de résilience comparée à celle obtenue après la mise en solution. D'autre part, le sur revenu à 220°C augmente progressivement les valeurs d'énergie de résilience en augmentant le temps de vieillissement jusqu'à 12 h. Une amélioration considérable de la valeur de l'énergie de résilience d'environ 20 J et 18 J a été observée pour les alliages 356 modifiés contenant 0,15% de Fe et l'addition combinée de 0,22% et 0,14% Mn, respectivement. L'alliage 319 contenant du fer présente le même comportement après un vieillissement à 180°C et à 220°C, toutefois, les valeurs de l'énergie de résilience après le vieillissement à 220°C pour différents temps sont légèrement inférieures à celles obtenues à 180°C. Les alliages 319 modifiés et non-modifiés contenant 0,18% Fe vieillis à 180°C pendant 12 h donnent la valeur d'énergie de résilience d'environ 12 J, la plus élevée parmi tous les alliages impliqués. Une variation similaire dans les valeurs de l'énergie de résilience des alliages 319 contenant des additions combinées de Fe-Mn et Fe-Mg est observée après un vieillissement à 180 ° C et 220 ° C à différents temps de vieillissement. Une légère augmentation de la valeur de l'énergie de résilience est observée pour les alliages 319 non-modifiés et modifiés après un vieillissement à 180°C soit pour 2 ou 12 h à comparer aux valeurs obtenues pour les alliages tel que coulés. Les alliages 319 modifiés contenant 0,3% en poids de Fe-Mn ont démontré des valeurs d'énergie de résilience plus élevées pour tous les temps de vieillissement à 220°C que celles obtenues pour les mêmes alliages mais après la mise en solution. Les valeurs de l'énergie de résilience pour l'alliage 396 présentent une amélioration similaire à celle observée pour les alliages hypoeutectiques 356 et 319 modifiés et traités thermiquement. Toutefois, l'alliage 396 donne des valeurs de résilience inférieures à celles obtenues pour les alliages 356 et 319. Le contenu quasi eutectique de silicium ~ 11% en poids avec la fraction volumique élevée de composés intermétalliques y compris les phases contenant du Cu et du Fe fourni un grand nombre de sites d'initiation de fissures et réduit ainsi les valeurs de l'énergie de résilience de l'alliage 396. L'effet des constituants de la microstructure est plus prononcé à une faible vitesse refroidissement (SDAS ~120μm). Le comportement des alliages 396 est similaire pour les deux conditions de refroidissement, cependant les alliages refroidis à l'air, afficher les valeurs de l'énergie de résilience plus élevées que pour les alliages refroidis dans le four. L'augmentation du temps de vieillissement à 44 h à la température maximale du vieillissement de 180° C ne produit pratiquement pas de changement perceptible dans les valeurs de l'énergie résilience pour tous les alliages 396 étudiés. Le vieillissement artificiel à 240°C pendant 44 h produit une augmentation importante des valeurs de l'énergie de résilience à la suite de l'adoucissement, indépendamment de la composition

des alliages. Le comportement à la rupture des alliages 356 non-modification contenant 0,15% de Fe est principalement contrôlée par les particules aciculaires de la phase Si eutectique tandis que les plaquettes β-fer agissent en tant que sites d'initiation de fissures et facilitent la propagation des fissures pour les alliages non modifiés contenant 0,8 % de Fe. Les plaquettes β-fer et les particules de la phase π-fer contribuent largement à l'initiation et à la propagation de la fissure pour les alliages 356 modifiés contenant 0,9% de Fe. La fracture des alliages 319 est régie principalement par la phase intermétallique Al_2Cu ainsi que les deux phases de fer : α-fer et β-fer. La propagation de la fissure des alliages 396 se produit principalement à travers les phases intermétalliques Al_2Cu ou α-fer.

ABSTRACT

Impact toughness is a property which has been acquiring increased importance in recent years. Impact toughness data is being used for optimizing design parameters since it can provide a means for comparing and assessing alloy ductility under conditions of a high rate of deformation. One of the most prevalent tests for measuring the impact energy of any particular material is the Charpy impact test which has currently evolved into a qualitative tool for the selection of materials and for studying the effects of microstructural changes on material toughness. The main intention of the current study is to investigate the effects of Sr-modification, Fe-based intermetallic phases and aging conditions on the impact toughness of commercially used 356 and 319 alloys. A Full understanding of such parameters with respect to these alloys would also serve as a reference base for characterizing the impact properties of the newly developed 396 Al-Si alloy, currently being studied as a part of an ongoing research program on alloy development. The results obtained from the current study were analyzed in term of the effects of this range of parameters on the total absorbed energy (E_T), crack initiation energy (E_i) and crack propagation energy (E_p). The fracture occurring in non-modified and Sr-modified 356, 319, and 396 alloys containing different levels of additions was also investigated. The total absorbed energy was measured using a computer-aided instrumented Instron Charpy impact testing machine, model SI-1D3 from SATEC Systems Inc. This testing was conducted on unnotched samples in order to emphasize the role of metallurgical parameters on both crack initiation and crack propagation processes. The dimensions of the sample according to ASTM-E23 standard are 10 x 10 x 55 mm. The results of microstructure examination reveal that the as-cast non-modified 356 alloys display large acicular eutectic Si particles. The π-iron phase was found to precipitate either in close association with the β-iron phase platelets or else in the form of independent script-like particles in the as-cast 356 alloys. Both β-iron needles and π-iron script-like particles seem to be segregated away from the modified eutectic Si colonies in the Sr-modified 356 alloys. Solution heat treatment results in dissolving the small-sized particles of the π-phase completely in the matrix, particularly in the 356 alloys containing low levels of iron. The large-size particles of π-phase appear to partially dissolve into the matrix after solution treatment due to insufficient solution time to produce complete dissolution. It will also be observed that there are a number of thin β-needles undergo necking and ultimately leads to fragmentation into small needles. The results obtained from the Charpy impact test revealed that increasing the level of iron additions diminishes the impact energy values of both 356 and 319 alloys to a noticeable degree. The addition of 0.1 wt% Mn to both non-modified 356 and 319 alloys seems to have no observable effect on the impact values, particularly when compared to the values obtained for the same alloys containing only Fe. While increasing the level of Mn addition up to 0.38 wt% produces a slight improvement in the impact energy values for both non-modified and Sr-modified 356 and 319 alloys compared to that of those containing only iron under the same as-cast and solution-treated conditions. The 319 alloys containing various levels of combined additions of Fe-Mg display lower impact values than those containing only iron, irrespective of the level of iron content. Such a drop in the impact values is more pronounced at an addition of 0.28 wt% Mg. The same observation was

obtained in the case of combined additions of Fe, Mn and Mg with the exception of the modified solution heat-treated conditions, where their impact values remain almost unchanged.

Introducing 200 ppm Sr to both as-cast 356 and 319 alloys was found to slightly improve the impact energy values. The application of solution heat treatment in conjunction with Sr-modification significantly was found to improve the overall impact energy of both as-cast 356 and 319 alloys, particularly at low levels of additions. The Sr-modified alloys show higher impact energy values compared to non-modified alloys in the same conditions, regardless of the level of additions. Artificial aging of non-modified and Sr-modified 356 alloys at a peak-aging temperature of 180°C diminishes the impact energy values with an increase in the aging times up to 8 hrs compared to those obtained under the solution heat-treated alloys. On the other hand, aging at an over-aging temperature of 220°C gradually increases the impact energy values with further aging time up to 12 hrs. A significant improvement in impact values of about 20 J and 18 J was observed for both Sr-modified 356 alloy containing 0.15 wt% Fe and combined addition of 0.22 wt% Fe and 0.14 wt% Mn, respectively. The impact behavior of iron-containing 319 alloys exhibit the similar behavior at both 180°C and 220°C aging temperatures, however, the impact values obtained after aging cycle of 220°C for various aging times show slightly lower impact values than those obtained after 180°C aging cycle. The Sr-modified and non-modified 319 alloys containing 0.18 wt% Fe aged at 180°C for 12 hrs display the highest impact energy values of ~ 12 J among all the 319 alloys involved. A similar variation in the impact energy values of 319 alloys containing combined additions of Fe-Mn and Fe- Mg is observed after aging at both 180°C and 220°C temperatures for different aging time. A slight increase in the impact values of both non-modified and Sr-modified 319 alloys may be observed after aging at 180°C either for 2 hrs or 12 hrs compared to the impact values obtained for as-cast alloys. The Sr-modified 319 alloys containing 0.3 wt% Fe-0.09 wt% Mn-0.09 wt% Mg was observed to exhibit higher levels of impact values for all the aging time at 220°C than those obtained for the same alloys under solution heat-treated conditions. The impact energy values of newly-developed 396 alloys exhibit a similar improvement to that observed in hypoeutectic 356 and 319 alloys with the application of Sr-modification and solution heat treatment. The 396 alloys, however, display lower impact values than those obtained for 356and 319 alloys. The near-eutectic Si content of ~ 11 wt% together with the high volume fraction of intermetallics including Cu- and Fe-containing phases provide a wide number of crack initiation sites and thus reduces the impact energy values of these 396 alloys. The effect of microstructural constituents is more pronounced at low cooling rate conditions with an SDAS of ~ 120 μm. The impact behavior of aged 396 alloys is similar under both cooling rate conditions; the air-cooled alloys (SDAS ~ 45 μm), however, display higher impact values than do furnace-cooled alloys (SDAS ~ 120 μm). Increasing the aging time up to 44 hrs at the peak-aging temperature of 180°C produces virtually no discernible change in the impact values of all the 396 alloys investigated. Artificial aging at 240°C for 44 hrs produces a significant increase in the impact values as a result of the softening, regardless of alloy composition.

The fracture behavior of non-modified 356 alloys containing 0.15 wt% Fe is mainly controlled by the acicular eutectic Si particles whereas β-iron platelets act as crack initiation sites and provide further path for final crack propagation in non-

modified alloys containing 0.8 wt% Fe. The β-iron platelets and π-iron phase particles contribute largely to crack initiation and propagation in the Sr-modified 356 alloys containing 0.9 wt% Fe. The fracture of 319 alloys is governed mainly by the Al_2Cu intermetallic phase as well as both α-iron and β-iron phases. Crack propagation occurs mainly in the 396 alloys via the Al_2Cu and/or α-iron intermetallic phases.

ACKNOWLEDGMENTS

I would like to convey my gratefulness to my supervisor, Prof. Fawzy H. Samuel for encouraging me to complete my doctoral degree; without his incessant supervision and support it would have been impossible to do so. I am very grateful to him for helping me so generously over the last four years. I feel honored to have been able to work with someone whose dedication and contribution to the field of science will be a constant inspiration to me throughout my life.

I would also like to thank my co-supervisor, Prof. Agnes Marie Samuel, who provided me with helpful suggestions on improving the quality of my research, and for her invaluable insights and comments during the final stages of writing my thesis.

Financial support in the form of scholarships received from the Natural Sciences and Engineering Research Council of Canada (NSERC), the Fondation de l'Université du Québec à Chicoutimi (FUQAC), General Motors Powertrain Group (U.S.A), and Corporativo Nemak (Mexico) is gratefully acknowledged.

I would like to extend my appreciation to Mr. Alain Bérubé of the TAMLA group, at UQAC, for his assistance with the castings and sample preparation, as well as to Mr. Lang Shi of the Microanalysis Laboratory, Earth and Planetary Sciences, McGill University for carrying out EPMA analyses. Appreciation is also due to Madame Marion Sinclair for her great help in editing my thesis.

Acknowledgment goes to my wife Hayam and my kids for their unfailing support and encouragement during the time it took to write my thesis.

TABLE OF CONTENTS

LIST OF TABLES

LIST OF FIGURES

CHAPTER 2

CHAPTER 1

INTRODUCTION

CHAPTER 1

INTRODUCTION

1.1 INTRODUCTION

Al-Si cast alloys are being used increasingly for various applications because of their high strength-to-weight ratio, superior casting characteristics, high wear resistance and high corrosion resistance. The foregoing features make it possible to produce different lightweight high-strength components from Al-Si alloys. Using such components in the automobile industry will reduce fuel consumption, save energy, and cut down on environmental pollution. Furthermore, Al-Si alloys may also be used for aerospace and defense applications.[1]

The impact toughness of Al-Si alloys is regulated to a high degree by their microstructure which depends significantly on alloy chemistry, melt treatment processes, heat treatment, and solidification conditions. The microstructure of Al-Si alloys usually consists of α-Al dendrites, eutectic Si particles, and intermetallic phases.[2]

Numerous intermetallic phases may be formed in the Al-Si alloy system as a result of the reaction of Al with the elements present in the alloy. Some of these intermetallic phases, such as Mg_2Si and Al_2Cu, improve the strength values of such alloys through the precipitation-hardening which occurs during the application of a T6 temper, whereas others, like the Fe-bearing intermetallic phases, can have a seriously deleterious effect on mechanical properties. The β-Al_5FeSi iron intermetallic phase is considered to be one of the most detrimental iron intermetallic phases, in which the

plate-like morphology of the phase creates potential crack initiation sites and ultimately leads to the impairment of the ductility and fracture toughness of these Al-Si alloys.[3]

Modification is one of the most frequently applied melt treatment processes for Al-Si alloys. In this process, the addition of controlled amounts of such modifying elements as Sr and Na may advantageously transform the morphology of the eutectic Si particles from a coarse, acicular form into a fine fibrous one. This alteration in the morphology and size of eutectic Si particles will tend to lessen the number of crack initiation sites and greatly improve the impact toughness of these alloys.

A heat treatment process is applied to Al-Si cast alloys with the aim of improving the as-cast structure in view of the fact that the mechanical response of this structure is undesirable from the design point of view. It is recommended also that the solution heat treatment temperature should be carefully controlled to avoid the incipient melting of the last solidified phases in the Al-Si alloy system, for example, the Al_2Cu phase in the case of Al-Si-Cu alloys. There is a possibility of avoiding such localized melting by the expediency of applying multi-stage solution heat treatments thus leading to a decrease in cavity formation associated with the former. This type of treatment would consequently increase alloy soundness which would in turn improve the mechanical properties of the castings.[4] The coarsening of the Si particles during solution heat treatment increases the proportion of the soft ductile α-aluminum dendrites in the matrix, causing an increase in the crack propagation resistance of the matrix and, as a result, an improvement in the impact toughness.[5]

In recent years, studies involving parameters such as intermetallic phases, Sr-modification and heat treatment conditions which affect the impact and fracture properties of Al-Si alloys have become increasingly important in describing the fracture

resistance of these alloys; they are also crucial to establishing safe design components and to predicting the critical size of cracks or discontinuities.[6] The effects of this particular range of parameters on the impact toughness of Al-Si alloys will therefore be investigated and discussed in the current study, as will be their concomitant fracture mechanisms.

1.2 OBJECTIVES

The intention of this study is to investigate the effects of Sr additions, intermetallic phases, cooling rate, and heat treatment on the impact properties of a series of Al-Si casting alloys. The study will be carried out through an examination of the following:

- the effects of various intermetallic phases present in the microstructure on the Charpy impact properties of a variety of popular 319 and 356 alloys; such phases will include the Al_2Cu, Mg_2Si, and Fe-containing intermetallics;
- the influence of the heat treatment process in terms of different aging temperatures and times on the Charpy impact properties of 319 and 356 alloys containing different addition levels of Fe, Mn, and Mg;
- the effects of Sr addition, cooling rate, and different aging conditions on the Charpy impact properties of newly developed 396 Al-Si alloys containing two addition levels of Mn;
- the fracture mechanism in terms of the crack initiation and crack propagation processes occurring in non-modified and Sr-modified 319, 356 and 396 alloys containing different levels of additions, observed in the as-cast and heat-treated conditions.

CHAPTER 2

REVIEW OF THE LITERATURE

CHAPTER 2

REVIEW OF THE LITERATURE

2.1 INTRODUCTION

At present, aluminum-silicon (Al-Si) alloys are the most commonly used aluminum casting alloys mainly because of their high strength-to-weight ratio, superior castability and low thermal expansion coefficient, as well as high wear and corrosion resistance. These alloys have found widespread use in the production of numerous components in a number of sectors including the automotive, aerospace and defence industries.

Aluminum-silicon cast alloys are widely applied in the automotive industry where high strength and light weight products are required. The resulting low mass components used in vehicle construction have been observed to lead to greater load capacity and reduced fuel consumption.[7]

The performance of Al-Si alloys depends mainly on their microstructure which includes α-Al dendrites, eutectic Si particles, and a variety of intermetallic phases which are determined by the type and the amount of alloying additives used. The combination of controlled additions of alloying elements, together with the application of suitable melt treatment processes and the appropriate heat treatment, are the most frequently used means of regulating the microstructure of Al-Si alloys during their solidification.[8]

The eutectic Si phase is usually observed in the form of coarse acicular particles in the as-cast microstructure of Al-Si alloys. The sharp corners at the tips of these Si

particles may act as stress concentration sites in the matrix. Consequently, the presence of such particles tends to accelerate the formation of microvoids and to decrease the resistance of the matrix to crack initiation, possibly leading to rapid failure. The morphology of the eutectic Si phase may be modified from its original acicular form to a fine fibrous one through the addition of such elements as Sr and Na to the alloy. This type of modification process, as applied to the eutectic Si phase morphology, results in a reduction of the number of crack initiation sites in the matrix, improving, at the same time, the overall impact toughness of these alloys.[9]

Copper is considered to be one of the major alloying elements in the 319-type alloys. The presence of Cu in these alloys makes them heat-treatable, and can consequently improve their strength by means of a precipitation-hardening mechanism. Copper reacts with aluminum to form the Al_2Cu intermetallic phase; it may then subsequently precipitate during solidification either in the form of fine eutectic Al-Al_2Cu colonies, or block-like particles, and/or a mixture of both types, depending on the cooling rate and the amount of modifier introduced. [10]

Of all the intermetallic phases formed in Al-Si alloys, the iron-containing intermetallic phases, particularly the plate-like β-Al_5FeSi particles, are considered to be the most detrimental to the mechanical properties of such alloys. This plate-like phase possesses sharp corners at its ends and may act as a stress raiser, eventually promoting the initiation of microcracks in the matrix. Furthermore, the plate-like shape of these particles presents a high aspect ratio resulting in maximum obstruction to the movement of dislocations. The addition of controlled amounts of certain neutralizing elements such as Mn, Cr, and Ca may decrease the detrimental effects of β-iron platelets by transforming them into the more compact α-iron Chinese script phase. [11, 12, 13, 14]

In the presence of high levels of iron in Al-Si-Mg alloys, an alternative iron-containing intermetallic phase, labeled π-$Al_8FeMg_3Si_5$, was reported to precipitate in the form of Chinese-script particles; this phase has also been found to grow from the surfaces of the β-iron platelets. [15, 16] The size and morphology of this π-iron phase strongly affects the strength and ductility of Al-Si-Mg alloys. This phase has been observed to diminish the strength values of the alloys since its formation reduces the amount of Mg available for dissolution in the matrix. The proportion of solid solution of Mg with aluminum is thus decreased which also reduces the precipitation of the Mg_2Si hardening phase to a high degree during subsequent heat treatment stages. It was also found that the π-iron phase has the potential for decreasing elongation values to a significant degree, particularly in the case of alloys containing high levels of Mg; also, it tends to promote the formation of an excessive proportion of shrinkage porosity defects in the castings. [17, 18]

By applying a suitable heat treatment process such as a T6 temper to Al-Si alloys, it becomes possible to produce a combination of optimum strength through precipitation-hardening and improved alloy ductility. The main requirement in the selection of the solution heat treatment temperature is to avoid the localized melting phenomenon known as 'incipient melting' which results in the formation of cavities and lowers the alloy soundness. For example, the solution heat treatment temperature for A319 alloys is restricted to 495°C so as to avoid the possibility of any localized melting of the Al_2Cu phase in the grain boundary regions. [9] A decrease in the harmful effects caused by β-iron platelets through their fragmentation and/or dissolution in the matrix is one of the main benefits of applying a solution heat treatment to Al-Si-Cu alloys. [19]

Impact toughness is a property which has been acquiring increased importance in recent years. Impact toughness data is being used for optimizing design parameters since it can provide a means for assessing alloy ductility under conditions of rapid loading or of a high rate of deformation.[2] One of the most prevalent tests for measuring the impact energy of any particular material is the Charpy impact test which has currently evolved into a tool for the selection of materials and toughness evaluation.

The impact toughness of Al-Si alloys is controlled to a significant extent by the morphology and size of the eutectic Si particles, as well as by the size of the α-Al dendrites. The size and morphology of the intermetallic phases which form in the interdendritic regions between aluminum and the alloying additives also have a strong influence on the impact toughness of these alloys.[19, 20, 21, 22]

2.2 ALUMINUM-SILICON ALLOY SYSTEM

Aluminum alloys containing Si as a major element are known as Al-Si alloys and belongs to the 3xx.x series of cast alloys. These alloys may be divided into these main categories: hypoeutectic, eutectic or hypereutectic depending on the Si-content which may vary from 6 to 11 wt% in the hypoeutectic alloys, and from 12 to 20 wt% in the hypereutectic alloys, the eutectic composition being ~ 12 wt% Si. The 3xx.x series are outstanding in that they are relatively high in silicon thus providing superior casting characteristics such as high melt fluidity and high mold filling capability. The intensified response of this type of alloy to heat treatment improves the strength properties involved. As a result, the 3xx.x series are the most widely used to date and are also the best choice for producing extremely complex and large-size castings.[23]

The 319-group of aluminum alloys is considered to be the most popular type from among the Al-Si-Cu alloy systems; the group is thus used in numerous industries for automobile, aerospace, and defense applications. The A319-type alloys are characterized by high castability, high strength-to-weight ratio, high corrosion resistance, and high thermal conductivity. Such characteristics make these alloys a particularly popular choice for producing a number of critical automotive components including pistons, engine blocks, and water-cooled cylinder heads requiring the application of the permanent mold casting process. [24, 25, 26]

Alloy A319 is also a general all-purpose alloy used preferentially in the automotive industry for sand castings to manufacture crankcases for both internal combustion and diesel engines, and either gasoline or oil tanks, as well as oil pans.[7, 26] The strength of this type of alloy may be further improved through the application of the full T6 heat treatment process.

Alloy A356 is the alloy with the highest level of purity of all Al-Si-Mg alloys and which usually becomes hardened by the precipitation of the Mg_2Si phase. This alloy is generally characterized by excellent castability, high weldability, and high corrosion resistance. Apart from its high purity, A356 alloy combines optimum tensile and physical properties to be observed after the application of the requisite heat treatment. The foregoing makes this alloy an appropriate choice for a wide variety of military and industrial applications such as airframe castings, aircraft and missile components, and automotive parts.[7, 26]

Alloy A413 is considered to be a binary Al-Si alloy suitable for the production of die castings because of its high Si-content of about 11 wt % which gives the alloy its high castability status.[7] This alloy is characterized by moderate strength and ductility

values in conjunction with good wear and corrosion resistance. Alloy A413 is also a general-purpose alloy which may be used for producing numerous large castings, including complicated parts with thin sections, and fatigue-resistant castings. This alloy is a recommended choice for food and dental equipment, and also for critical components in marine, ornamental and architectural applications. [26]

2.3 MODIFICATION

Modification is a melt treatment process frequently applied in the foundry industry and refers to the changes created in the morphology of the eutectic Si phase. It is a process which is usually applied to both hypo- and hyper-eutectic Al-Si alloys, and it is effectuated by means of the addition of various elements such as Na and Sr. The modification process involves converting the morphology of the eutectic Si phase from its initial coarse acicular structure to a fine fibrous one. The eutectic Si phase appears in the form of small individual particles on a conventionally polished surface, although in actual fact, it forms a coral- or seaweed-like structure beneath a deeply etched surface, as shown in Figure 2.1. Sodium and strontium are among the modifying elements which are preferred for the purpose because of the substantial effect they produce at low addition levels. The degree of modification depends on the amount of Sr added and the time evolved between the addition and casting process. [5, 26]

Crossley and Mondolfo [27] proposed a physical model to explain the modifying action of Sr addition. These researchers assumed that the eutectic Si grows at a faster rate than aluminum, thus resulting in sharp acicular particles in the unmodified structure. The addition of Sr reduces the surface tension of aluminum and hence, it increases the contact angle between aluminum and silicon, thereby allowing the

aluminum to envelop and to obstruct the growth of the Si phase as well as to promote that of the aluminum dendrites. The eutectic Si then begins to acquire a coral-like morphology which is characteristic of a chemically modified structure. [26]

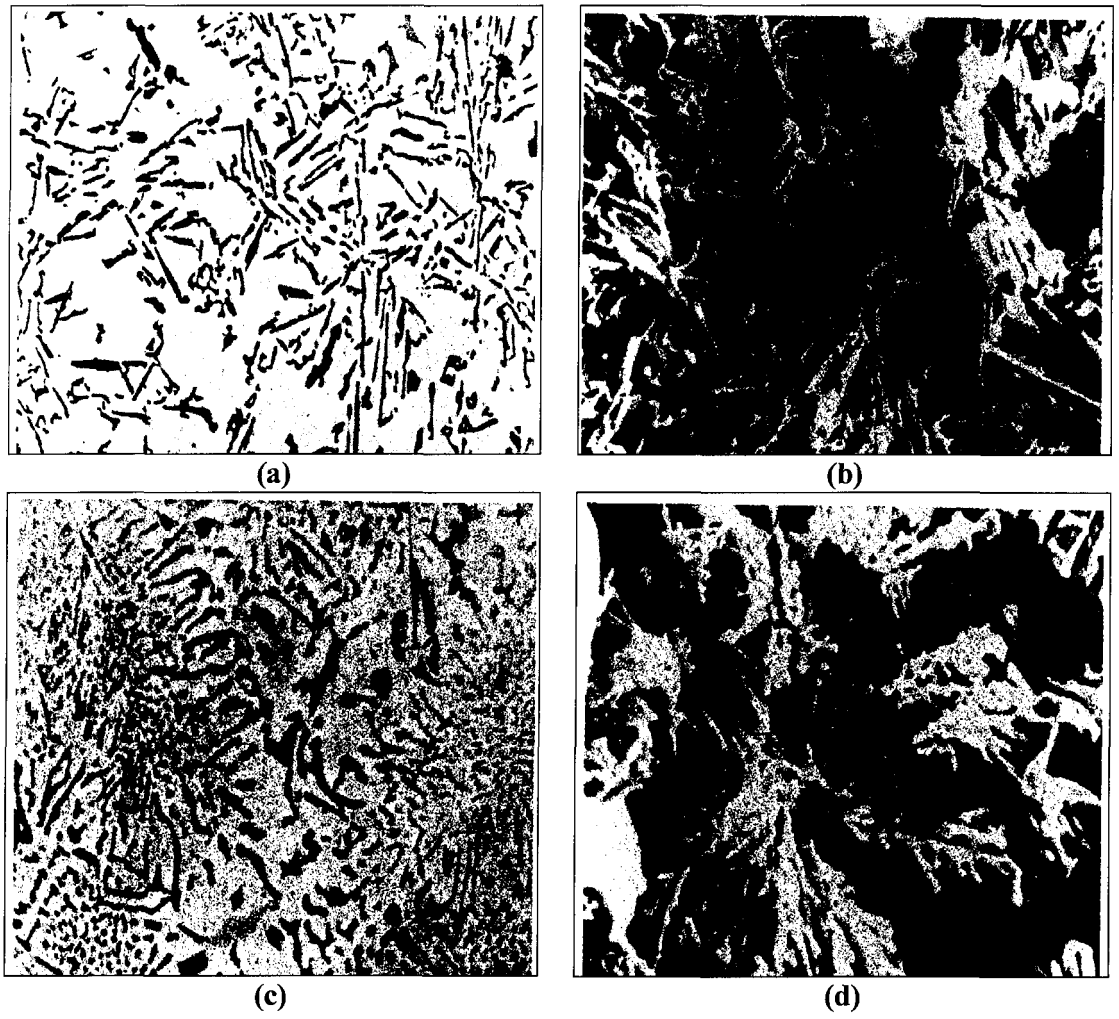

Figure 2.1 Effects of modification on the morphology of the eutectic Si phase in 356 alloys, (a) and (c) optical micrographs of non-modified and modified samples, normal-etched, at 300X; (b) and (d) SEM micrographs of non-modified and modified samples, deep-etched, at 2000X. [26]

2.4 HEAT TREATMENT

Heat treatment is a thermal process which aims at modifying the metallurgical microstructure of an alloy, thereby obtaining the desired physical and mechanical properties for meeting the requirements of specific applications. The versatility of aluminum alloys offers a range of possible heat treatment processes for obtaining a suitable combination of physical and mechanical properties in the casting. Apart from the phase and morphological changes accompanying high temperature treatment, internal residual stresses, caused either by solidification or by quenching, and microsegregation tend to become minimized. [24] The age-hardening treatment process, as applied to Al-Si alloys, comprises a sequence of three basic processing steps, namely, solution heat treatment, quenching, and aging.[24, 26]

Solution heat treatment is undertaken to dissolve maximum amounts of the soluble phases which had formed earlier during and after solidification of the alloy. Other effects such as the spheroidization of undissolved constituents and homogenization may also occur. [26] This particular step in the heat treatment process is carried out for an estimated sufficient period of time at the safest maximum temperature relative to the melting temperature of the last solidified phase. This solution temperature should be lower than the solidus temperature; otherwise it is liable to cause localized melting at the grain boundary and, hence, to affect both alloy soundness and mechanical properties adversely. It should be noted here that the solution temperature and time parameters are both significant aspects of the solution heat treatment process. [24, 28]

Eutectic Si particles undergo shape changes during the solution heat treatment of Al-Si alloys such as the A319 and A356 cast alloys; thus the fibrous eutectic Si particles in the modified alloys will be seen to undergo necking and gradual separation into small

segments, as shown in Figure 2.2. The fragmented particles begin to spheroidize and coarsen in response to the Ostwald ripening phenomenon. These fibrous Si particles in the modified alloys spheroidize more rapidly than the plate-like Si particles in the non-modified alloys.[29, 30, 31, 32] The Ostwald ripening mechanism [33] involves the separation of smaller particles, followed by the diffusion of these particles throughout the matrix to attach themselves to the surface of larger particles in a process of mass transfer, as it were. The eutectic Si particles coarsen as the solution heat treatment proceeds, regardless of the prior morphology of the Si particles. [26, 34]

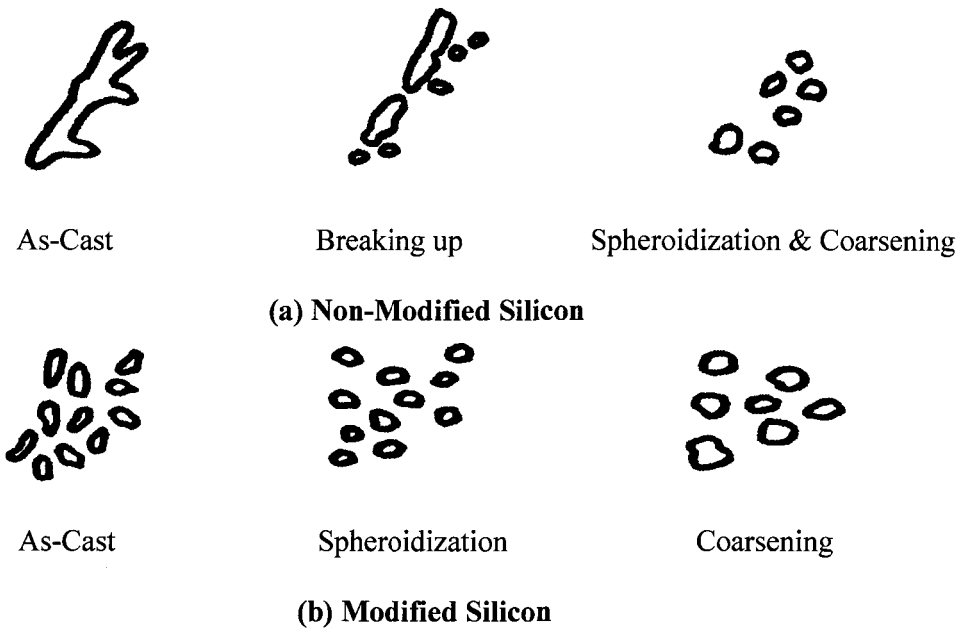

Figure 2.2 Schematic diagram showing modification of Si particles during solution heat treatment of Al-Si alloys which are: (a) non-modified and, (b) modified. [32]

The effects of solution heat treatment on the size and morphology of β-Al_5FeSi platelets has attracted a great deal of attention because of the deleterious effects that these platelets have on the strength and ductility of aluminum-silicon alloys. Narayanan

et al., [35] in their study of the dissolution of the β-Al_5FeSi phase in a 319 alloy containing 1.0% Fe, observed necking and fragmentation of this phase along its plate widths and a concomitant dissolution of the phase at the platelet tips with increasing solution temperatures. Villeneuve and Samuel[36] further studied the fragmentation and dissolution of the β-Al_5FeSi phase during the solution heat treatment of Al-13%Si-Fe alloys. They proposed that dissolution occurred in the presence of high Sr-content according to the following reaction:

$$Al + \beta\text{-}Al_5FeSi \Rightarrow Al_6Fe + Si$$

This dissolution of β-phase particles was reported to begin through (i) necking at the thin parts of the platelets- or needles as they appear in an optical micrograph, (ii) fragmentation into small segments, and (iii) dissolution by the rejection of both iron and Si into the matrix at the needle tips. Narayanan *et al.* [35] reported that the size and volume fraction of the β-Al_5FeSi phase, however, did not decrease monotonically with increasing solution temperatures, but instead increased in alloys which had been solution-treated at around 520°C or higher. These researchers proposed that such an effect may be ascribed to the formation of the liquid phase as a result of localized melting occurring in interdendritic and grain boundary regions. They concluded also that solution temperature has a greater impact on the dissolution of iron-based intermetallics than does solution heat treatment time.

Since this phenomenon of the fragmentation and dissolution of the β-Al_5FeSi phase is considered to be a diffusion-controlled process, it is controlled by both solution temperature and time parameters to a high degree. Increasing these parameters makes it possible to overcome the diffusivity problem of iron in solid aluminum to some degree. A complete dissolution of iron-based intermetallic phases, however, is less likely to

occur because of the negligible solubility of iron in solid aluminum. The π-iron intermetallic phase thus only transforms to another small-sized β-iron platelets having a less detrimental morphology with regard to the mechanical properties. The increased possibility of the incipient melting phenomenon occurring with such elevated solution temperatures would result in limiting the use of this approach.[37]

Zheng [38] investigated the effects of solution time on the transformation of the π-phase to β-platelets in an Al-7%Si-0.45%Mg-0.15%Fe alloy. The volume fraction measurements revealed that the transformation of the π-phase to β appears to be slow at the beginning. Increasing the solution time by about 10 to 20 min leads to accelerate the rate of this transformation. After 360 min, the rate becomes slower and also it may not be complete, as shown in Figure 2.3.

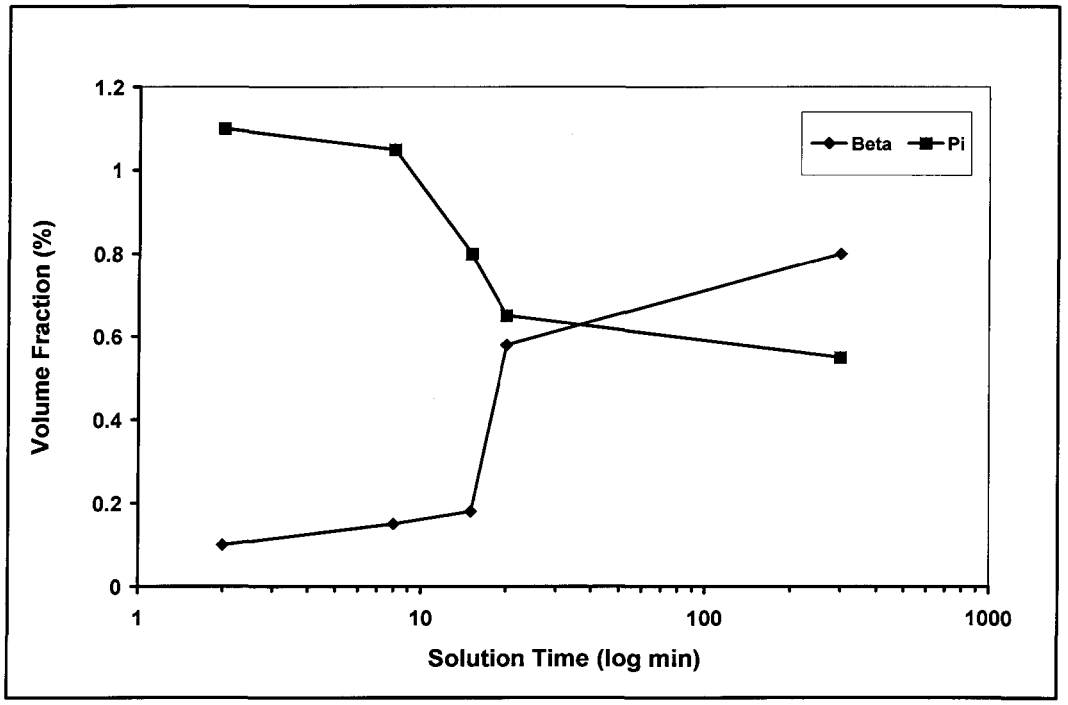

Figure 2.3 Effect of solution heat treatment time at 540°C on the amount of the volume fraction of both π- and β-iron phases present in an Al-7%Si-0.4%Mg-0.15%Fe alloy.[38]

Similarly, Taylor *et al.*[39, 40] investigated the effects of solution heat treatment on the amounts of intermetallic phases formed in Al-7Si-Mg cast alloys. The results reveal that solution heat treatment diminishes the volume fraction of Mg_2Si for all the alloy compositions involved, although it substantially reduces the volume fraction of the π-phase, particularly in the alloys containing Mg additions ranging from 0.3% to 0.4%, as shown in Figure 2.4. The reduction in the volume fraction of the π-phase after solutionizing treatment may be a result of the decomposition of this phase, liberating Mg which subsequently dissolves into the aluminum in solid solution, and resulting in the formation of fine precipitates of an iron-based intermetallic free of Mg. The transformation process of π-phase to β seems to be a time- and composition-dependent reaction. The energy dispersive X-ray (EDX) spectrum obtained for this new phase is observed to be similar to that of the β-phase; it may thus probably be assumed that it has a composition similar to that of the β-Al_5FeSi phase.

Quenching is the second, as well as the most critical, step in the heat treatment process. It is usually set in motion following the solutionizing step so as to sustain the supersaturated solid solution and a considerable concentration of vacancies. Also, the induced residual stresses and the warpage or distortion of the castings involved may be reduced after quenching. The effectiveness of the quenching stage depends to a large extent on the quench medium used and the quench interval applied. The quench medium should have sufficient volumetric heat-extraction capacity and uniformity to produce a high cooling rate. A rapid quench-rate ensures that all precipitates are retained in solid solution. Higher potential strength and improved corrosion and stress-corrosion performance can be achieved by using a quench medium such as water which produces fast quench rates.[26, 29, 41]

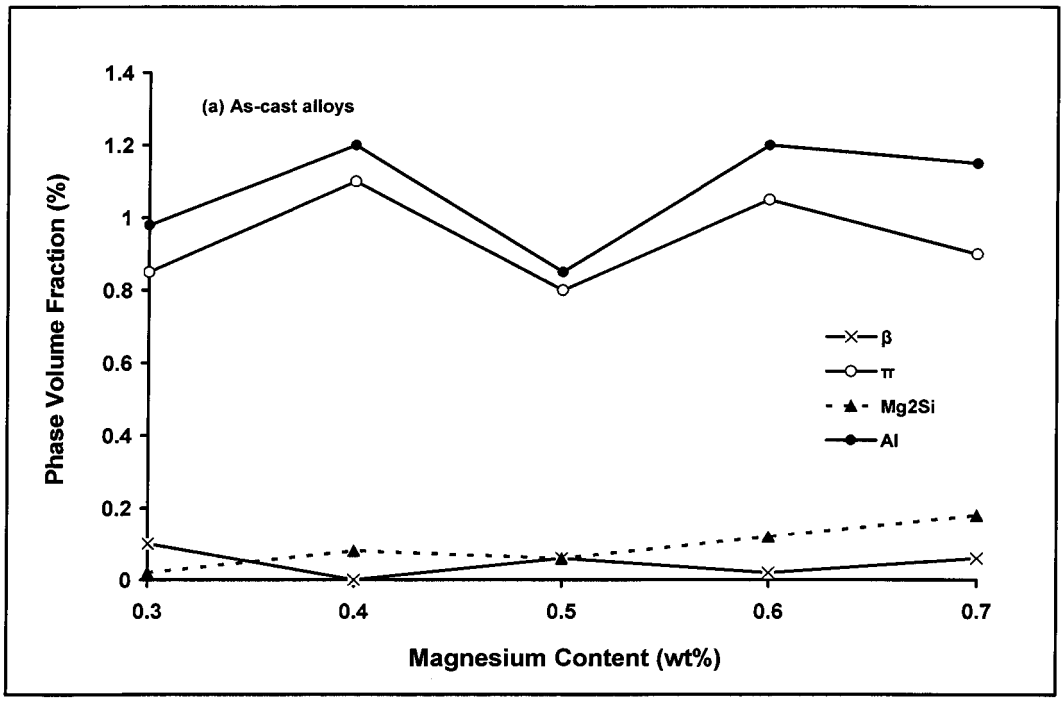

(a)

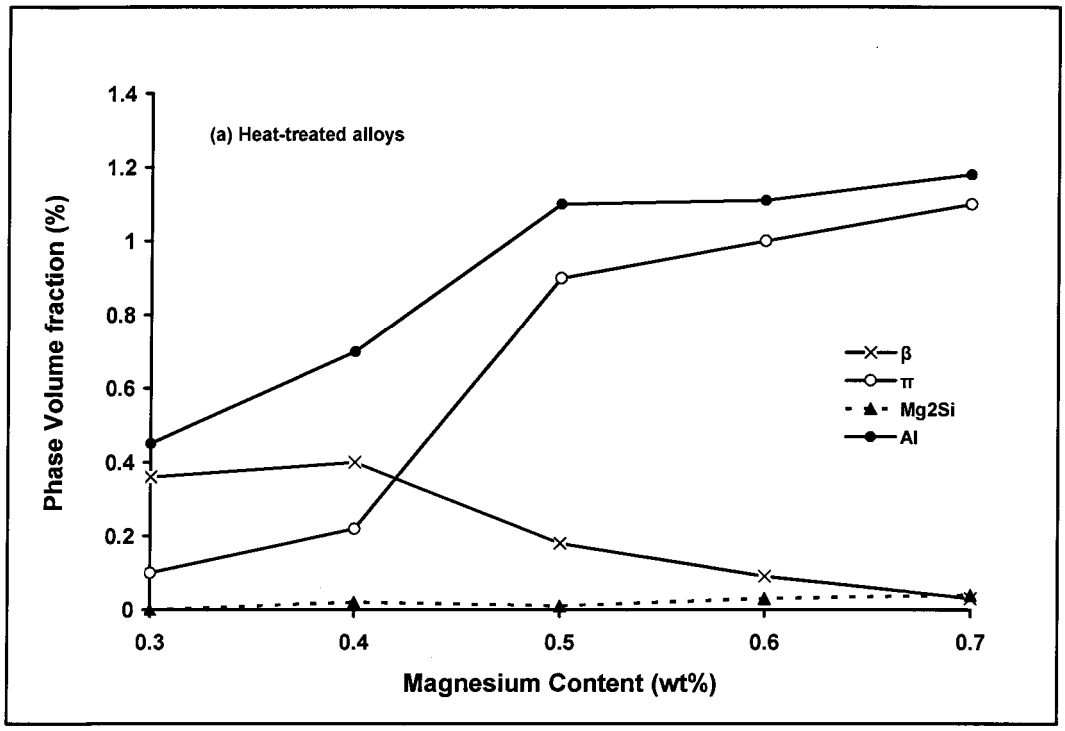

(b)

Figure 2.4 Variation of the volume fraction of all intermetallic phases with Mg content in the Al-7Si-0.12Fe-xMg alloy under the: (a) as-cast and (b) solution heat-treated conditions.[39]

Aging is the last step of the full heat treatment process. This step is undertaken to allow the hardening phases to precipitate out of the solid solution and to strengthen the alloy matrix. Hardening is generally defined as a sequence of metallurgical changes in the microstructure which leads to an intensification in its resistance to deformation.[26] Most aluminum alloys become age-hardened naturally to some degree after quenching. The extent of these metallurgical changes depends on the alloy composition and a combination of time-temperature conditions.[24] Some types of aluminum alloys, such as A356 alloys, are naturally aged at room temperature to improve the uniformity of vacancy distribution and hence, to diminish the precipitate-free zones (PFZ).[42] The hardening process of other aluminum alloys may be accelerated by heating the as-quenched alloy to intermediate temperatures in a process known as artificial aging. The presence of an excess concentration of vacancies promotes diffusion and the formation of GP zones. [24]

2.4.1 Precipitation-Hardening of the Al-Si-Cu and Al-Si-Cu-Mg Alloy Systems

The strength of as-cast Al-Si-Cu alloys is lower than the required values in the standard specifications for particular applications. Consequently, these alloys are usually subjected to a specific heat treatment process with a view to achieving an optimum combination of strength and ductility. Copper, as one of the main alloying elements in such alloys together with magnesium, produces a significant improvement in alloy strength through the precipitation-hardening process. During the solution heat treatment of these alloys, Cu or Mg dissolves in the matrix to form a supersaturated solid solution with aluminum. As mentioned earlier, the alloys are then rapidly quenched in warm water to preserve the supersaturated solid solution obtained as well

as to provide a substantial concentration of vacancies in the matrix to advance the precipitation process. Also, a noticeable improvement in the tensile strength is to be observed after solution treatment. Such A319 alloy, however, is not thermodynamically stable and thus a precipitation sequence may occur over time, leading to dimensional changes. Consequently, artificial aging following the quenching stage is usually undertaken to provide both sufficient time and the temperature required for the precipitation of the Al_2Cu hardening phase.

The precipitation-hardening process for the 319 alloy begins upon heating the quenched alloy to the appropriate temperatures. The precipitation sequence in these alloys may be summarized as follows: [7, 41, 43]

$$\alpha_{ssss} \longrightarrow \underset{}{\text{GP (I) Zones}} \longrightarrow \underset{\text{(Coherent)}}{\text{GP (II) Zones } (\theta'')} \rightarrow \underset{\text{(Semi-Coherent)}}{(\theta')} \rightarrow \underset{\text{(Non-Coherent)}}{\theta \text{ (equilibrium } Al_2Cu \text{ phase)}}$$

In the early stages of the aging process, the supersaturated solid solution is transformed into thin plates of Cu-rich regions called Guinier-Preston zones or GP (I) zones. A slight strengthening of the matrix will be observed at this underaged stage. Further aging time results in the transformation of GP (I) zones into ordered coherent precipitates which are referred to as GP (II) zones or the θ'' phase. The precipitated particles retard the motion of dislocations in two distinct ways: These coherent precipitates create coherent strain fields around them which interact strongly with the stress fields of the dislocations (*i.e.* coherency strengthening). The particles may be sheared by the dislocations, as shown in Figure 2.5. This type of strengthening is known as chemical hardening, where the strength increases as a result of increasing the stress required to force a dislocation through a coherent precipitate. This stress is required to form a new interfacial area between the matrix and precipitate. Consequently, these

interactions between dislocation and precipitated particles provide the matrix with maximum strength which is usually reached at the peak-aging condition. [44, 45]

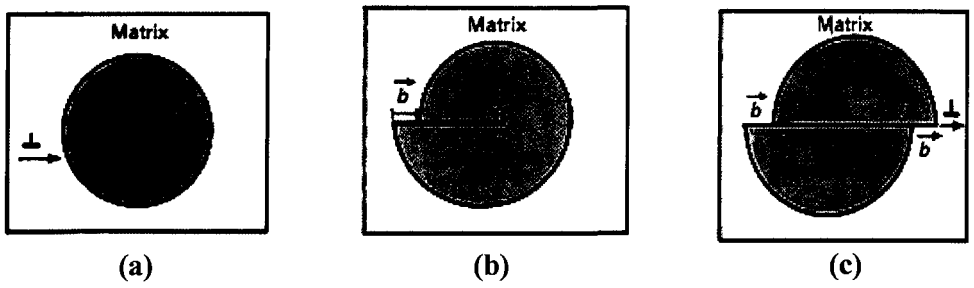

Figure 2.5 Schematic diagram representing the interaction of the dislocation/precipitated particles: (a) dislocation moves on the slip plane, (b) dislocation starts shearing the precipitated particles, and (c) dislocation cuts the particle and new surface is formed. [45]

Increasing the aging time leads to the formation of the semi-coherent precipitates θ' which are then transformed into the non-coherent equilibrium θ phase during the final stage of aging (*i.e.* in the over-aging stage). [41] The dislocations are able to move easily either by means of the phenomenon of obstacle by-passing (cross-slip) or bending (looping) around the coarsened θ (Al_2Cu) precipitates present at this stage in response to the Orowan mechanism,[44, 45, 46] as may be seen in Figure 2.6 .As a result, the strength of the matrix decreases and the alloy softens in these over-aging conditions.[44] The various strengthening mechanisms occurring during solution and aging treatments may be illustrated and summarized in the schematically plotted graph shown in Figure 2.7. [47]

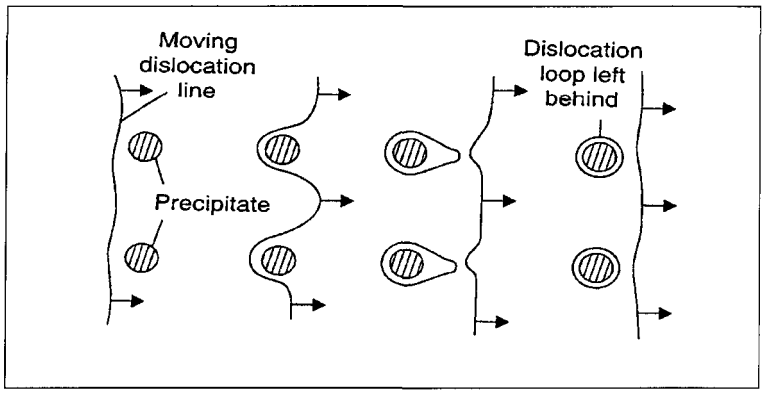

Figure 2.6 Schematic diagram showing the motion of a dislocation known as "bending around precipitated particles", triggered by the Orowan mechanism.[46]

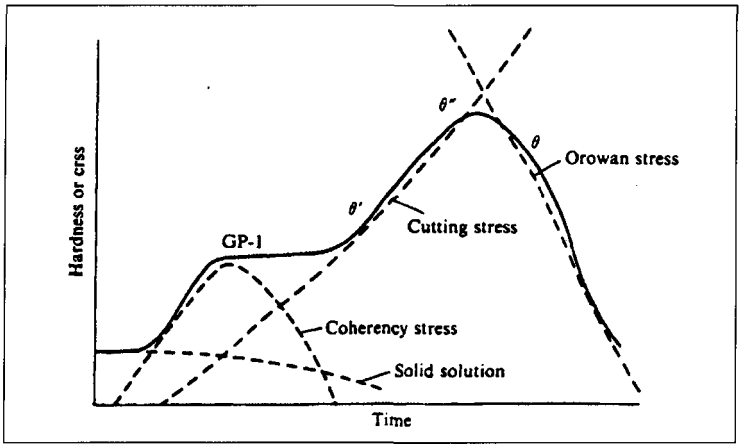

Figure 2.7 Interplay of various precipitation-hardening mechanisms at successive stages in the hardness-time curve.[47]

In the early aging stages of Al-Si-Cu-Mg alloys, fine and profuse GP zones of Al_2Cu and Mg_2Si become distributed homogenously throughout the matrix. Two aging peaks may be observed with further aging. The first peak is higher than the second one, particularly at higher aging temperatures, as may be seen clearly in Figure 2.8. After 6 hrs of aging, it is possible to observe the first peak resulting from the precipitation of high-density GP II zones. Further aging makes it possible for the GP II zones to

dissolve and for plate-like metastable phases to form; these phases had been observed earlier to nucleate on dislocations and to remain semi-coherent with the matrix. These semi-coherent precipitates can effectively hinder and retard the motion of dislocations, providing a certain strengthening effect to the matrix, and leading to the formation of the second peak at 12 hrs of aging. The hardness values of the Al-Si-Cu-Mg alloys, thereafter, display a noticeable reduction with extended aging time, regardless of the aging temperature, as a result of alloy-softening in the overaging stage. The precipitation process of such Al-Si-Cu-Mg alloys is expected to be as follows:[48, 49]

α_{ssss} → formation of GP zone → dissolution of GP zone → formation of metastable phase→ formation of equilibrium phase.

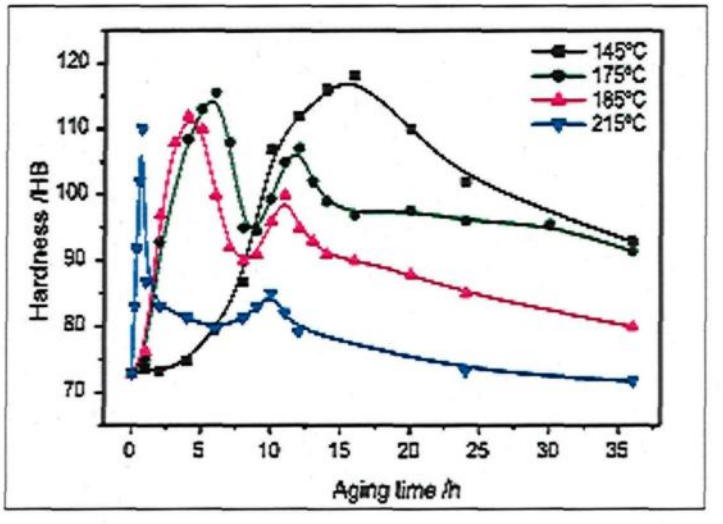

Figure 2.8 Age-hardening curves of Al-Si-Cu-Mg alloy aged at different temperatures.[48]

2.4.2 Precipitation-Hardening of the Al-Si-Mg Alloy System

Magnesium silicide is the soluble hardening phase in this particular type of alloy system. The precipitation of the metastable phase tends to increase the energy required

for the deformation of the crystal lattice.[24] This precipitation can occur very rapidly even at room temperatures within a short period of time. The presence of excess silicon in solid solution after the formation of Mg_2Si precipitates tends to accelerate the precipitation process. The presence of excess silicon reduces the solid solubility of Mg_2Si in the α-aluminum matrix and increases the solvus temperature at a given level of Mg_2Si. Thus, a finer dispersion of precipitates may be formed in the alloys containing excess silicon. The precipitation sequence in these alloys may be summarized as follows:[50]

$$\alpha_{ssss} \longrightarrow \underset{\text{(Coherent)}}{\text{GP Zones}} \rightarrow \underset{\text{(Coherent)}}{\text{GP Zones } (\beta'')\text{ needles}} \rightarrow \underset{\text{(Semi-Coherent)}}{\beta'\text{rod-like}} \longrightarrow \underset{\text{(Non-Coherent)}}{\beta\text{ (equilibrium platelets)}}$$

The precipitation process begins with the decomposition of the supersaturated solution through the clustering of silicon atoms. This clustering results in the formation of spherical Guinier-Preston (GP) zones which are coherent with the matrix. The zones are needle-shaped and extend in the [100] direction of the cubic aluminum matrix. These GP zones are disordered, and they display a high vacancy content, although as aging increases they acquire an ordered structure. Guinier-Preston zones are relatively stable and may exist up to temperatures of about 260°C. With increasing aging treatment, the needle-like GP zones (β'') begin to grow forming rods typical of an intermediate phase (β') and then, eventually, platelets (β) begin to appear. The β' rod-like particles are semi-coherent with the matrix phase, and the rod axes are parallel to the cube matrix directions to form cubic or hexagonal structures. The final equilibrium Mg_2Si (β) forms non-coherent platelets with the aluminum matrix, and has an ordered face-centered cubic structure, with the Mg atoms located at tetrahedral positions. The maximum hardness is obtained even before the platelets begin to form. The maximum

size of the Mg_2Si particles is found to be of the order of 0.03 μm, before the hardness begins to decrease in the over-aging condition. [29, 51, 52]

2.5 BACKGROUND DATA ON IMPACT TOUGHNESS

Impact strength may be viewed as having pivotal importance when considering the properties of alloys for various industrial applications; testing for this parameter has the potential for providing a useful method for evaluating the ductility of an alloy under high loading conditions.[2] The factors affecting the toughness of a structure include low test temperatures, extra loading, and the high strain rates which result from various types of impact; these may be accompanied by a phenomenon known as the stress concentration effect occurring in the presence of notches and cracks. All these parameters tend to accelerate the time-to-fracture of a material, giving rise to the need for investigating impact toughness in order to determine the possibility of producing a material which would tolerate the service conditions imposed upon it. [6]

As a tool for materials selection in design, the Charpy impact test may be used to evaluate the impact toughness of a variety of materials such as steel and aluminum; it may also be used for quality control to ensure that the material being produced reaches a minimum specified toughness level. The importance either of describing the behavior of the alloys, or of predicting their fracture toughness, may be summarized in the following checklist:

(a) to discover the appropriate alloy and its heat treatment process type in order to obtain the highest toughness values;

(b) to choose a suitable alloy for a particular application;

(c) to establish safe levels of design stresses;

(d) to predict the critical size of cracks or discontinuities under specific service conditions in alloy design.[6]

The toughness values of aluminum alloys are relatively low, although the presence of large shear lips on the fracture surface is indicative of ductile failure. In spite of the fact that toughness has a tendency to increase with increasing temperatures as the ductility of aluminum increases, this parameter is not particularly sensitive to temperature as a general rule, or in any other respect. Most commercial aluminum alloys are brittle, displaying low ductility upon fracture because of their instability and the existence of self-propagating crack growth in the elastic region. Nonetheless, various types of high strength aluminum alloys may be useful and highly practical in aerospace applications where maximum strength and low-ductility failure is a distinct consideration. Accordingly, further quantitative evaluation of fracture behavior through measuring fracture toughness under certain conditions is strongly recommended for these specific alloys.[6]

2.5.1 Definition of Impact Toughness

Impact toughness or impact energy is usually defined as the total absorbed energy required to fracture a material under high strain or rapid loading. Since impact toughness is a critical mechanical property for certain applications, the method for testing it will affect the impact values obtained to a significant degree. The most common tests for measuring the impact energy of aluminum alloys are: (a) the Charpy Impact Test, and (b) the Izod Test.

The Charpy Impact Test is a popular test for measuring the toughness of the materials; it should be remembered, however, that it was developed before the theory of

fracture mechanics was formulated. The total absorbed energy required for breaking the material is measured by the high strain rate fracture of a standard notched or unnotched specimen. In this test, a heavy pendulum hammer falling from a fixed height strikes against a test specimen which is supported at both ends like a simple beam, as shown in Figure 2.9. The striker hits the test specimen at a constant velocity between 3 and 6 m/s determined on the basis of the specifications listed in the instruction book for the ASTM E 23 standard test method. The total absorbed energy dissipated in breaking the test specimen is then measured based on the difference in the potential energy of the striking pendulum. [45, 53] The impact energy obtained from the Charpy Impact Test also correlates with the area located under the stress-strain curve obtained from the normal tensile test, namely toughness.

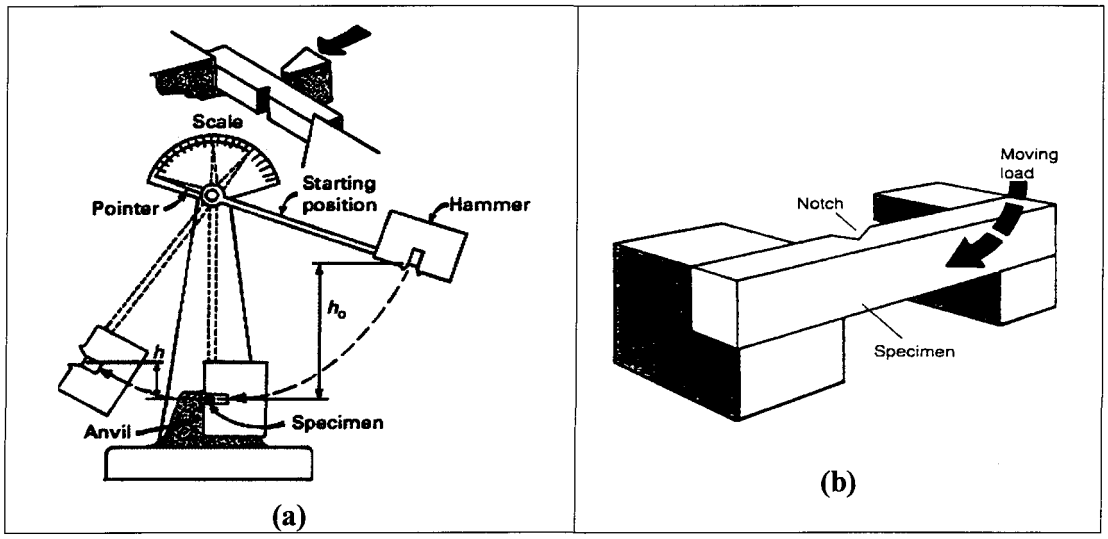

Figure 2.9 Schematic diagram of the Charpy Impact Testers showing: (a) analog basic pendulum type machine; and (b) simple beam test specimen.[45]

The Charpy impact energy is measured by evaluating the whole energy required to break the specimen. Thus, this parameter includes the elastic strain energy, the plastic

work done during yielding, and the energy involved in creating the fracture surface. The elastic energy is usually not a significant fraction of the total energy which is dominated by the plastic work. The total impact energy (E_T) is the sum of the energy required to initiate the crack (Ei) and the energy for causing the crack to propagate (E_p).[2] Also, the total absorbed impact energy may be represented by the area located under the load-time curve which is obtained from an instrumented Charpy impact machine, as shown in Figure 2.10.[54]

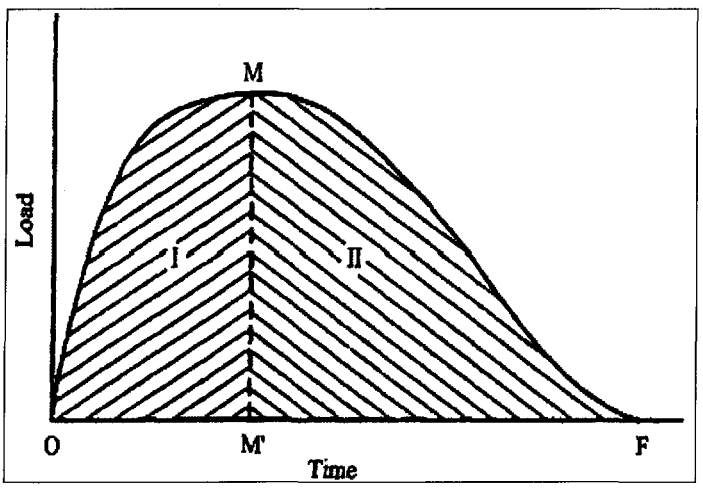

Figure 2.10 Schematic diagram representing the relation between load and time in the Charpy Impact Test where M = Maximum load; I = Crack initiation impulse; II = Crack propagation impulse; OM' = Crack initiation time; M'F = Crack propagation time.[54]

Figure 2.11 represents the shape of the load-time curves obtained from the Charpy Impact Test, where it indicates the deformation, and fracture history of the test pieces. The load-time curve may be interpreted using concepts similar to those employed for a conventional tensile test. The curves may be subdivided into two zones: either elastic or plastic zones, as defined by the dashed lines in each case. The initial load fluctuation on these curves is not a real effect of the material properties since it is

caused by the inertial loading of the hammerhead as a result of the acceleration of the specimen from rest. The initial rise in the load corresponds to the elastic zone, in other words up to the yield load L_y. At higher loads, prior to the maximum load L_{max}, the specimen deforms plastically, while beyond L_{max} the load decay is indicative of controlled crack propagation.[2]

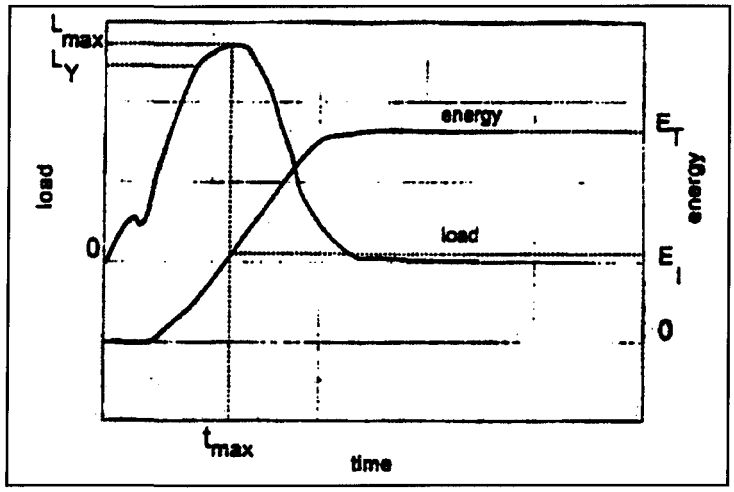

Figure 2.11 Schematic representation of the results obtained from the instrumented Charpy Impact Test. [2]

The Charpy Impact Test is used as an economical quality control method for evaluating notch sensitivity, impact toughness, and the embrittlement of engineering metals and materials. In addition, Charpy impact testing may be used to measure the impact toughness of a wide range of mass-produced materials such as plate-shaped metals, forged parts, bar products, welded structures for construction purposes, and so forth. The ASTM standards (ASTM 1990) E23, other international standards, and the Indian standards (BIS 1988) IS1757 all stipulate the requirements for test specimens, anvil supports, striker dimensions and tolerance, as well as for the machine verification and the determination of fracture appearance. The main differences between ASTM E

23 and other standards are the criteria for machining tolerance, dimensions, and the tip geometry of the striker. Also, the ASTM E 23 standard test method is usually used for all notched bar impact testing of metallic materials, while the Indian IS1757 standard test is used only for measuring the Charpy V-notch impact energy values of metallic materials. [53]

The Izod Impact Test is used most frequently to evaluate the relative toughness or impact toughness of materials in quality control applications, in this regard it is judged to be a rapid and economical test, applied more for the sake of comparison than to formulate a definitive evaluation. The Izod test is similar to the Charpy V-notch test, for which the same testing machine may be used. The difference between both these tests is to be found in the specimen geometry and calculation of the impact toughness. The Izod test involves a cantilever-beam with a falling pendulum striking the specimen above the notch, as shown in Figure 2.12. The specimen has a V-notch which is located toward one end of the specimen instead of in the middle, as it is in the Charpy V-notch specimen. The advantage of the Izod test is that several notches may be made in a single specimen. [53]

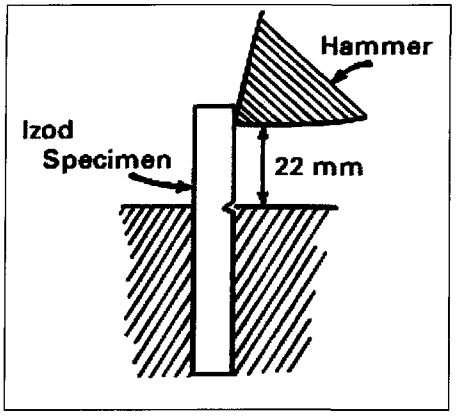

Figure 2.12 Schematic diagram of the Izod Impact Test showing the test configuration and the cantilever beam test specimen.[45]

2.6 PARAMETERS CONTROLLING IMPACT TOUGHNESS OF ALUMINUM-SILICON ALLOYS

2.6.1 Effects of Impact Specimen Geometry (Notch Type)

The Charpy impact energy (CIE) depends on the size and the geometry of the test specimen to a large degree. Thus, a standard specimen size is used to make it possible to compare between different materials. In the presence of a notch, the impact energy will be much lower than that for an unnotched specimen. This type of unnotched impact specimen provides highly accurate results, drawing attention to the fact that the impact values depend on the microstructure rather than on the specimen configuration. [2]

The presence of a notch in the impact test specimen will tend to have a negative effect on the impact energy values obtained. The stress concentration at the notch may then result in the following occurrences in the plastic area of that notch: (i) severe plastic deformation; (ii) an increase in work-hardening; and (iii) an intensification of the tensile stresses. All of the foregoing lead to a significant drop in the work done by plastic deformation; consequently, the fracture of the specimen occurs rapidly at lower impact energy values. Owing to the fact that the impact toughness of some materials is more highly sensitive to notches than others, the standard notch tip radius and notch depth are used for comparing between different materials. In this respect, the Charpy Impact Test may be used as an indicator for the notch sensitivity of a given material.

Tsukuda *et al.* [55] measured the impact energies of unnotched, U-notched and V-notched samples of 356 alloys under the same test conditions. They reported that, from among the three sample types, the V-notched samples displayed the lowest impact values while the U-notched samples exhibited 65% higher impact energy than did the

V-notched ones. On the other hand, the greatest improvement in impact energy was to be observed in the unnotched specimens, representing an increase of about 240%.

In their study carried out on the impact properties of Al-Si-Mg alloys, Shivkumar *et al.* [56] reported that low Charpy impact energy values were obtained for both non-modified and Sr-modified notched samples in the as-cast condition, *i.e.* 2 J and 10.8 J, respectively. The unnotched specimens of Al-Si alloys were reported to display higher impact values as confirmed by Paray *et al.* [2] who investigated the impact properties of a series of Al-Si foundry alloys; they found that the unnotched samples displayed higher Charpy impact values for both non-modified and Sr-modified 356 alloys in the as-cast conditions, specifically, 15.1 J and 22.8 J, respectively.

Srivasta *et al.* [57] demonstrated that when measuring the impact energy values using unnotched specimens there is a reduction of about 80% in the values obtained as opposed to results from unnotched samples. It should be noted, furthermore, that a small shallow scratch measuring 0.1 mm on the surface of the specimen reduces the absorbed impact energy by about 30%.

2.6.2 Effects of Microstructure

The microstructure of Al-Si alloys plays an important role in determining the desired mechanical properties. This microstructure generally consists of the soft α-Al dendrites, hard and brittle eutectic Si particles, and a variety of interdendritic intermetallic phases as well. The size and morphology of the eutectic Si particles may be modified through the addition of controlled amounts of certain elements such as Sr, and Na. The size of the Si particles then decreases and they become converted from the original coarse acicular form into finely-distributed fibrous particles. This

transformation in the morphology of the eutectic Si phase results in considerable improvement in the strength properties and ductility of these alloys. Consequently, there is a closely-knit relationship between microstructure and ductility which governs the impact toughness of an alloy to a great extent. In general, the microstructure of Al-Si alloys is regulated to a considerable degree by alloy composition, solidification conditions, melt treatment and heat treatment; as a result, all these parameters will tend to have a noticeable effect on the impact properties of these Al-Si alloys.

2.6.2.1 Alloy Composition

Alloying elements such as Cu, Mg, Ni, Mn, and Fe, are added to the binary Al-Si alloys to improve their mechanical properties. Such elements may react with Al to form numerous intermetallic phases which usually precipitate in the interdendritic regions. Intermetallic phases such as Mg_2Si and Al_2Cu strengthen the Al-Si alloys by means of a precipitation mechanism during the application of artificial aging, mainly T6 temper, although Fe-containing intermetallic phases result in a deterioration of the mechanical properties.

Iron is considered to be a major impurity commonly found in Al-Si alloys; this element is capable of forming many types of intermetallic phases which are seriously detrimental to the mechanical properties of Al-Si alloys. The β-Al_5FeSi iron platelet-like phase is also considered to be one of the most harmful of the iron-bearing phases. Appearing in the form of needles in a two-dimensional micrograph, this phase is often also termed as 'needle-like'. The platelet morphology of the β-Fe phase provides further stress raiser sites at the sharp edges of their tips ultimately leading to an impairment of the ductility and impact toughness of these alloys. This type of disadvantageous effect

which the β-needlelike iron phase is known to have on the mechanical properties of Al-Si alloys may be eliminated by adding a certain amount of neutralizing elements such as Mn, Cr and Ca. [58, 59]

Since the chemical composition of Al-Si alloys influences their impact toughness to a significant degree, the effects of the major elements present in Al-Si alloys on this parameter will be the subject of the following subsections.

2.6.2.1.1 Si-Content

Extensive studies were carried out by Tsukuda *et al.* [60] on the effects of different addition levels of Si, from 1-13%, on the impact strength of Al-Si-0.15%Sb alloy; they observed that Charpy impact energy values decreased rapidly at a Si-content of 6-8% or more for both as-cast and solution heat-treated alloys, as shown in Figure 2.13. The increased probability of crack initiation with increasing Si-content may explain the sharp deterioration in impact strength, particularly in the case of the as-cast alloy.

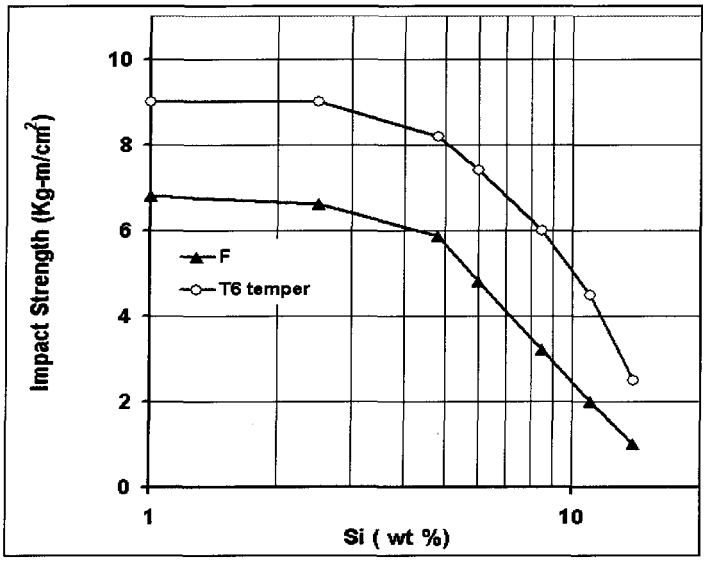

Figure 2.13 Effects of silicon on impact strength of Al-Si-0.03%Mg-0.02%Fe 0.15%Sb alloy. Permanent mold casting, F and T6 temper. [60]

Kawamoto *et al.* [61] investigated the relationship between fracture properties and the microstructure of hypereutectic Al-Si alloy castings. The results they obtained indicate that increasing the Si-content of the alloy from 10 to 20% causes a noticeable decrease in the U-notch Charpy impact values, as may be seen in Figure 2.14. This decrease in impact values may be explained by the fact that the presence of coarse primary Si particles in the hypereutectic alloy increases the number of crack initiation sites in the matrix, thereby leading to a reduction in crack initiation resistance.

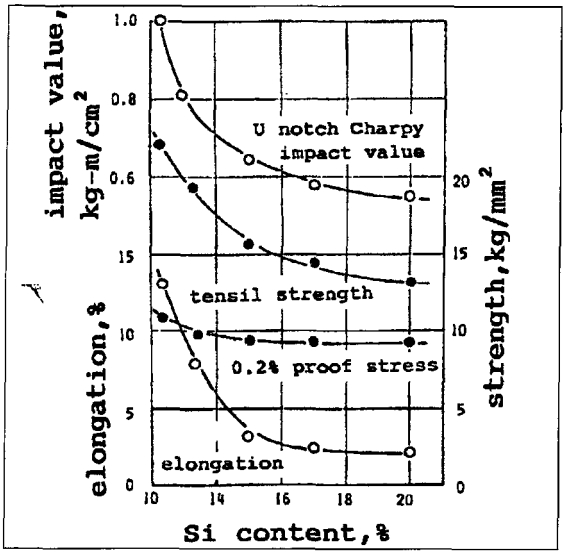

Figure 2.14 Relationship between Si-content and the mechanical properties of Al-Si alloy castings. [61]

Also, the influence of Si-content on the toughness of various Al-Si cast alloys was studied by Thakur *et al.* [62] The results they obtained reveal that the toughness decreases significantly with increasing Si-content upon the transition from hypoeutectic (4% Si) to hypereutectic alloys (17%Si), as is clearly shown in Figure 2.15. An increase in the Si-content implies that there is an increase in the number of crack

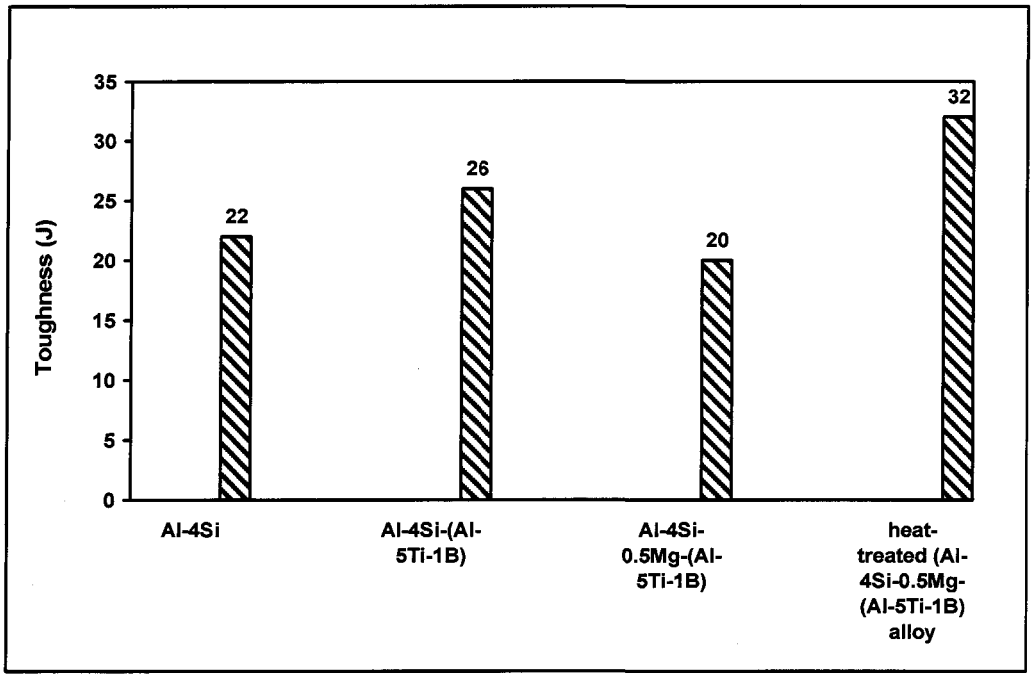

(a)

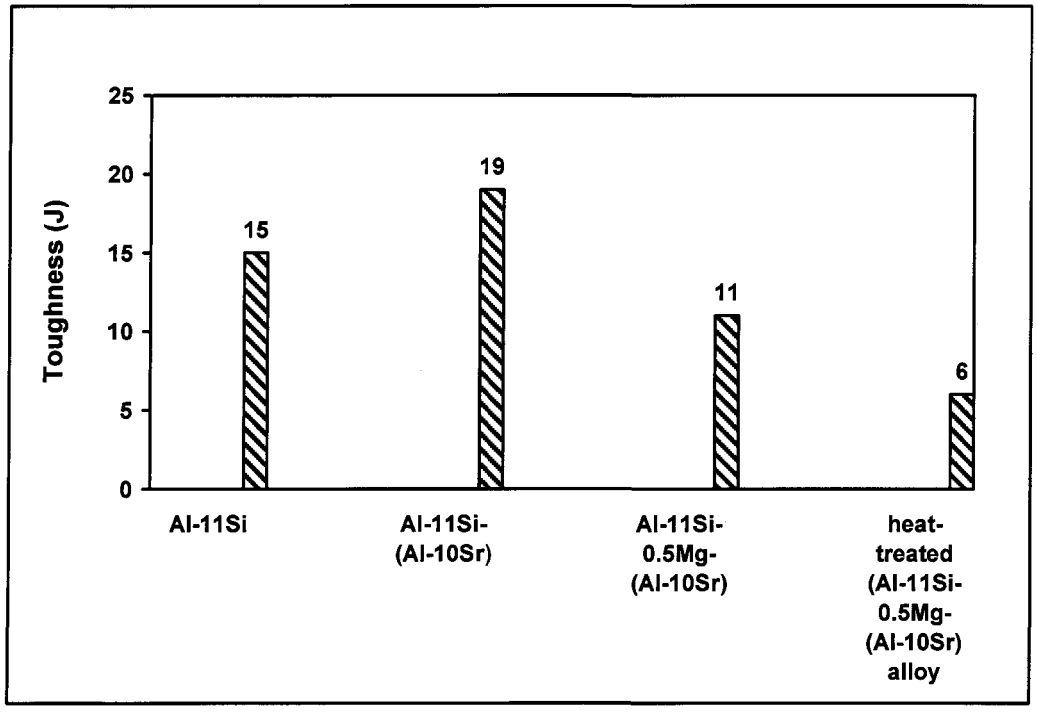

(b)

Figure 2.15

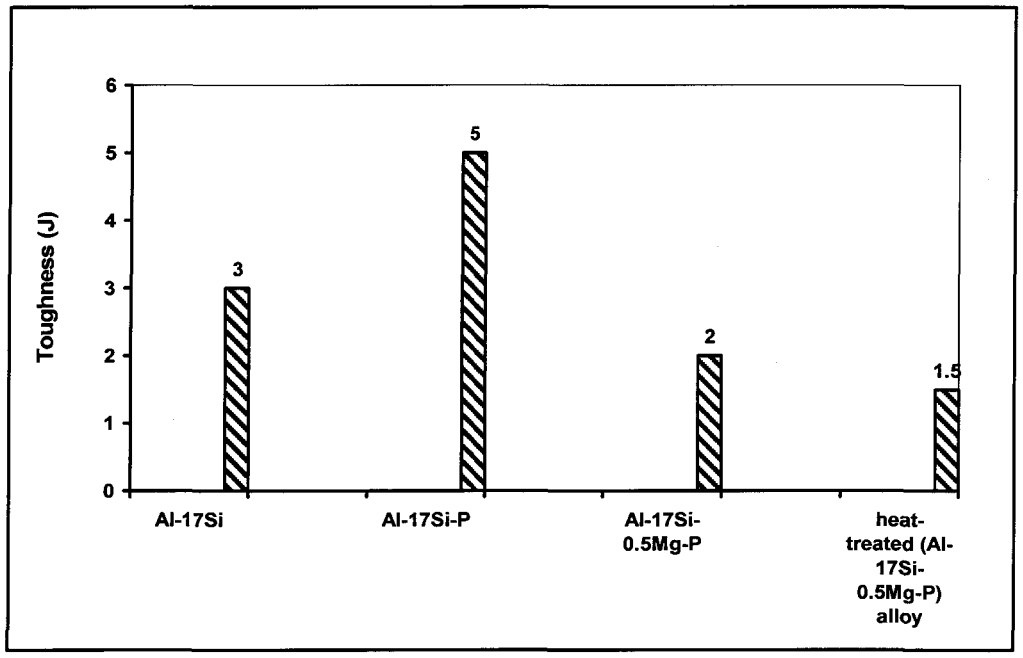

(c)

Figure 2.15 Relationship between Si-content and the toughness of various Al-Si cast alloys: (a) hypoeutectic alloy, (b) eutectic alloy, and (c) hypereutectic alloy. [62]

initiation sites and, as a result, the possibility of crack formation intensifies. This increase in Si-content also indicates that there will be a decrease in the proportion of the soft ductile α-aluminum dendrites in the matrix and separates the eutectic Si phase. The significant decrease which was observed in the overall impact toughness of the alloys may thus be ascribed to all of the above reasons.

2.6.2.1.2 Mg-Content

Magnesium is usually added to Al-Si alloys to increase strength values through precipitation of the hardening Mg_2Si phase during the aging process. The effects of Mg addition on eutectic Si particles was extensively studied by Moustafa *et al.*;[63, 64, 65] their results reveal that an addition of 0.4% Mg increases not only the Si-particle size in the

non-modified alloys, but it also negates the modifying action of Sr, where it changes the well-modified Si particles into partially-modified ones. Thus, increasing the Mg content by 0.4% or more would result in a decrease in the impact energy of Al-Si alloys.

Tsukuda *et al.* [60] studied the variation of the impact strength of Al-Si alloys at various levels of Mg addition. They found that increasing the amount of Mg added from 0.15 to 0.6% resulted in an acute drop in the impact strength values of Al-7%Si alloys in both the as-cast and heat-treated T6 conditions for all levels of iron-content, as shown in Figure 2.16 (a), and (b).

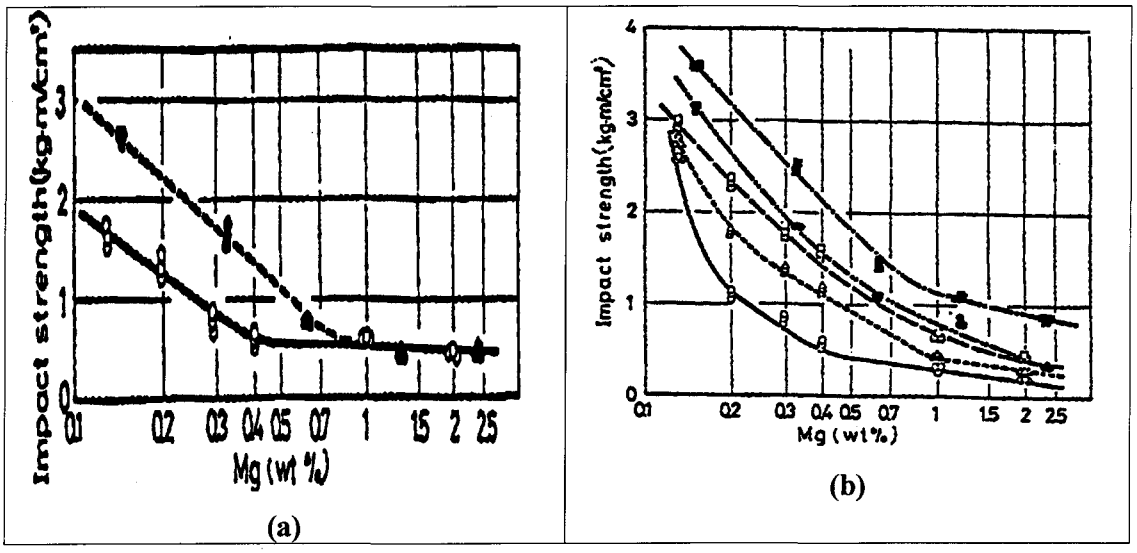

Figure 2.16 Effects of magnesium on impact strength of Al-7%Si-0.006%Fe-0.07%Ti-0.005%Na and Al-7%Si-0.2%Fe-0.13%Ti-0.005%Na alloys. Permanent mold castings: (a) as-cast; and (b) T6 tempered. [60]

Murali *et al.* [66] made an extensive examination of the influence of different levels of Mg addition on the fracture toughness of an Al-7Si-0.3Mg casting alloy displaying low iron-content, in this case 0.2%. The researchers found that a reduction of

about 50 % in the absorbed impact energy was observed upon increasing the level of Mg addition from 0.32% to 0.65%, *i.e.* from 9.7 J to 5 J, as shown in Figure 2.17.

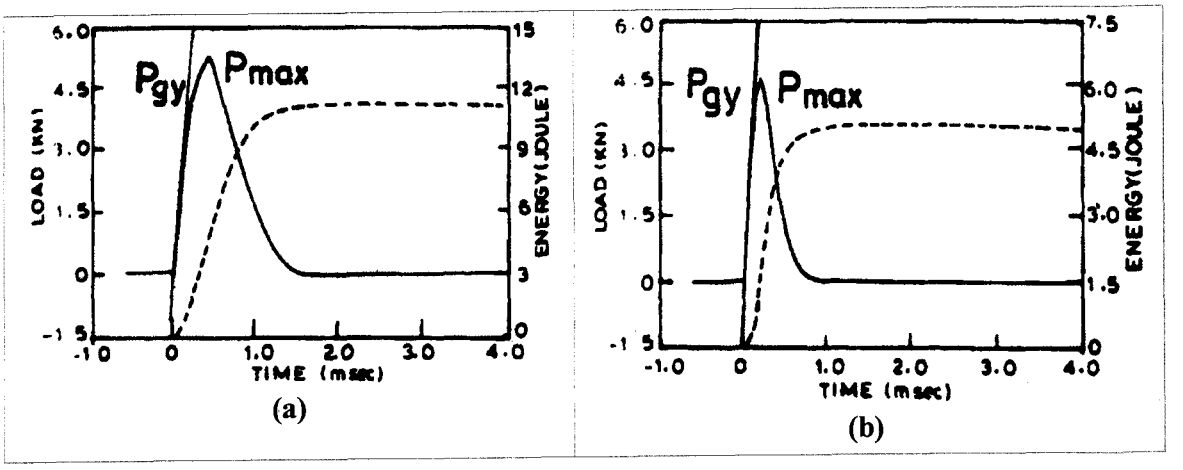

Figure 2.17 Load-time and Charpy impact energy-time curves of an Al-7Si-Mg alloy at addition levels of (a) 0.32% Mg and (b) 0.65% Mg. [66]

Nakayama *et al.* [67] investigated the effects of different levels of Mg-content, from 0.3 to 1%, on the mechanical properties of an Al-2%Si casting alloy which was subjected to solution heat treatment at high temperatures and aged between 145°C and 200°C for long times. The researchers observed that both the absorbed impact energy and the elongation-to-fracture values of the alloys containing 0.6% Mg diminished noticeably as a result of the precipitation of the Mg_2Si strengthening phase in the eutectic regions. In view of the fact that the precipitated amount of the hard, brittle Mg_2Si phase increases with an increase in the Si-content of the alloy, the Al-7%Si-0.3%Mg alloy acquires lower absorbed impact energy and elongation-to-fracture values than the lower Si-content Al-2%Si-0.3%Mg alloy.

An investigation carried out by Thakur *et al.* [62] concerning the influence of Mg additions on the toughness of eutectic Al-11Si alloys revealed that the value of this

parameter is reduced by ~ 42% after the addition of 0.5% Mg, as shown in Figure 2.18. Such a decrease in toughness may be attributed to the formation of the hard and brittle Mg_2Si intermetallic phase as well as to an increase in the number of crack initiation sites accompanied by high levels of Si in the alloy.

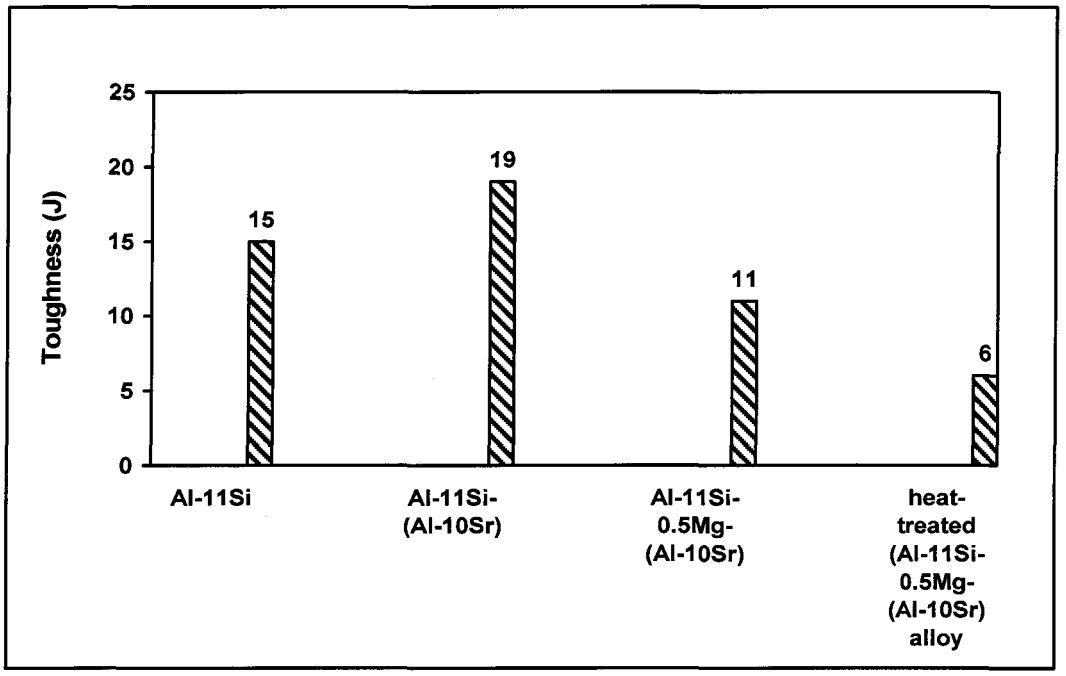

Figure 2.18 Influence of Mg addition on the toughness of a refined hypoeutectic Al-11%Si cast alloy. [62]

Data reported in a study carried out by Tavitas-Medrano *et al.* [68] regarding the influence of Mg addition on the impact energy of 319-type alloys revealed that the addition of 0.4 wt% Mg reduces the impact energy values of both non-modified and modified A319 alloys. This reduction in impact values may be ascribed to the fact that the addition of Mg increases the strength values by a means of precipitation-hardening at the expense of ductility. The precipitation of both Al_2Cu and Mg_2Si particles during artificial aging at 150°C for 4 hrs, *i.e.* during the underaging stage, increases strength

values to an acceptable level and concurrently improves the impact values of Sr-modified A319 alloys (~ 24 J).

2.6.2.1.3 Iron-Content

Natural impurities exist normally in aluminum-silicon casting alloys; significant expenditures are incurred for their removal or elimination. Iron is the most obvious undesirable element to be found in aluminum-silicon alloys.[37, 69] Although the presence of iron diminishes tool wear and prevents soldering with a die in the production of die casting parts, it has a deleterious effect, particularly on the ductility and fracture toughness properties of aluminum alloys. This detrimental effect of iron may be a result of its low solid solubility in the α-aluminum matrix (< 0.04 wt%) and also of its associated greater ability to form a variety of insoluble, brittle needlelike Fe-base intermetallic phases for particular levels of constituent elements including Al_3Fe, Al_6Fe and Fe-Al-Si phases. The chemical composition and morphology of such phases also depends on the solidification conditions. Fe-bearing intermetallic phases may precipitate in other morphological forms besides needles, like Chinese script and star-like particles. [15, 69, 70] Stress concentration may occur at the sharp edges of the needle-like intermetallic phases, causing a decrease in crack initiation resistance and, consequently, bringing about a noticeable drop in the impact toughness of the Al-Si alloys.

Reducing, or completely avoiding, the formation of the β-Al_5FeSi iron platelike phase would result in neutralizing its adverse influence on the mechanical properties, thereby improving the ductility and toughness of the alloys. Numerous investigators[71, 72, 73, 74] have proposed that avoiding the formation of such a phase entirely or otherwise

decreasing its amount in Al-Si alloys may be accomplished by: (a) adding a certain quantity of specified elements such as Mn and Cr, known as correctors; (b) increasing the cooling rate; (c) superheating the melt; and (d) applying suitable chemical and thermal modification processes.

Vorren *et al.* [12] investigated the effects that different iron contents (0.15, 0.2, 0.3, 0.4, 0.6, and 0.8%) would have on the Charpy impact energy of Al-7Si-0.3Mg alloys. They found that as the iron-content decreased from 0.3% to 0.15%, a slight increase in the fracture toughness could be obtained, representing an increase of about 20%-25%. Similarly, Tsukuda *et al.* [60] found that an increase in the iron-content gradually decreases the impact strength of the Na-modified as-cast Al-7Si-0.3Mg alloy. A sharp decrease in the impact strength was also observed in T6 heat-treated alloys with increasing Fe-content from 0.2 to 0.75% Fe, as shown in Figure 2.19.

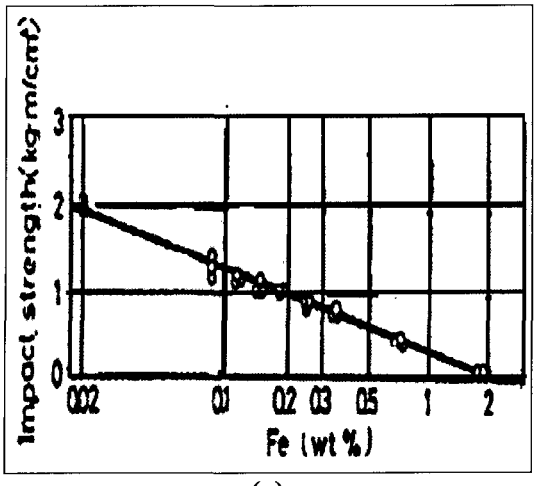

(a)

Figure 2.19

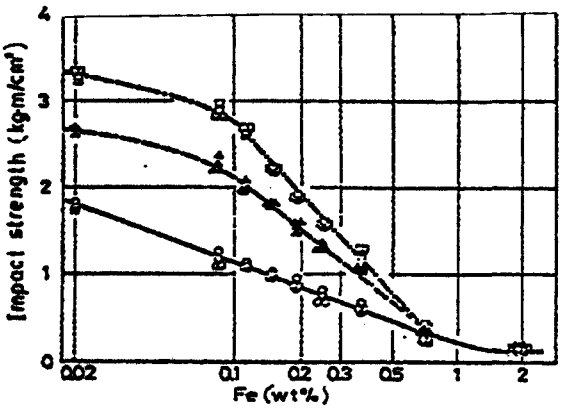

(b)

Figure 2.19 Effects of iron on the impact strength of an Al-7%Si-0.23%Mg-0.13%Ti-0.005%Na alloy. Permanent mold casting: (a) as-cast; and (b) T6 temper.[60]

Data reported in a study carried out by Kaneko *et al.* [75] regarding the influence of iron on the Charpy impact behavior of squeeze-cast Al-7Si-0.3Mg alloys, reveal that an increase in the iron-content from 0.15 to 0.3% results in a decrease in Charpy impact energy from 1.5 to 1.2 J/mm^2. A further increase in the iron-content causes a sharp reduction in the Charpy impact energy values. Based on the reduction in these values, the researchers proposed that the maximum iron-content for obtaining optimum mechanical properties should be 0.3%.

Similar results were reported in the investigation carried out by Murali *et al.* [66] concerning the effects of different levels of iron addition on the impact properties of the Al-7Si-0.3Mg alloy. The researchers found that increasing the iron content from 0.2% to 0.8% decreases the absorbed impact energy to a significant degree, representing a reduction of about 87%, as shown Figure 2.20.

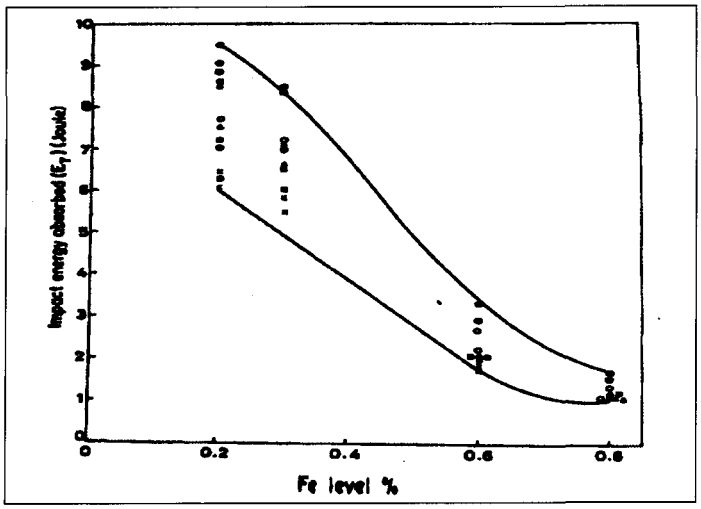

Figure 2.20 Effects of iron-content on the total energy absorbed E_T of an Al-7Si-0.38Mg casting alloy.[66]

Similarly, Kobayashi [76] reported in his review on the fracture characteristics of Al casting alloys, that the dynamic fracture toughness (*i.e.* impact toughness) and dynamic crack propagation resistance of Al-6Si-3Cu-0.3Mg-0.2Fe alloy tend to decrease with increasing Fe-content, as shown in Figure 2.21. The Ca-modified alloy exhibits higher levels of toughness than the non-modified alloys. From these observations, Kobayashi concluded that a significant improvement in the toughness of Al-Si alloys may be obtained by Ca-modification of the harmful β-Al_5FeSi needlelike intermetallic phase.

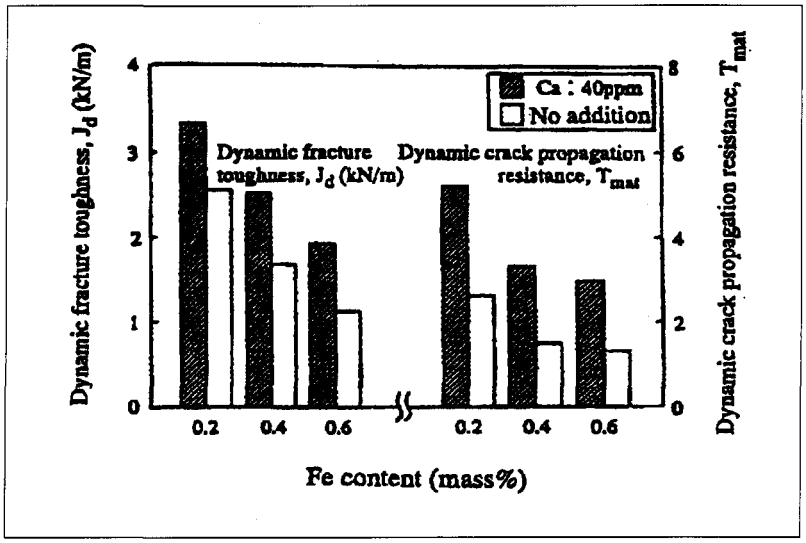

Figure 2.21 Effects of the Fe-content on the dynamic fracture toughness and dynamic crack propagation resistance of Ca-modified and non-modified heat-treated Al-Si-Cu-Mg-Fe alloys.[76]

Kumari *et al.*[77] investigated the effect of individual or combined additions of Mn and Ca on the mechanical characteristics of Al-7Si-0.3Mg-0.6Fe alloys. The researchers pointed out that an improvement of about 27% in the impact strength may be obtained by the addition of 0.3% Mn as a result of the transformation of the platelet-like β-Fe intermetallic into the α-Fe intermetallic with its more compact Chinese script form. The impact strength, however, becomes reduced in the presence of high levels of Mn addition of ~0.5% because of the formation of star-like sludge particles. The addition of 0.05% Ca refines the long β-iron platelets through their fragmentation; the impact strength is then subsequently improved by about 80%. The combined addition of Ca and Mn improves the impact strength to a high degree, *i.e.* an 85% improvement may be observed, as shown in Figure 2.22.

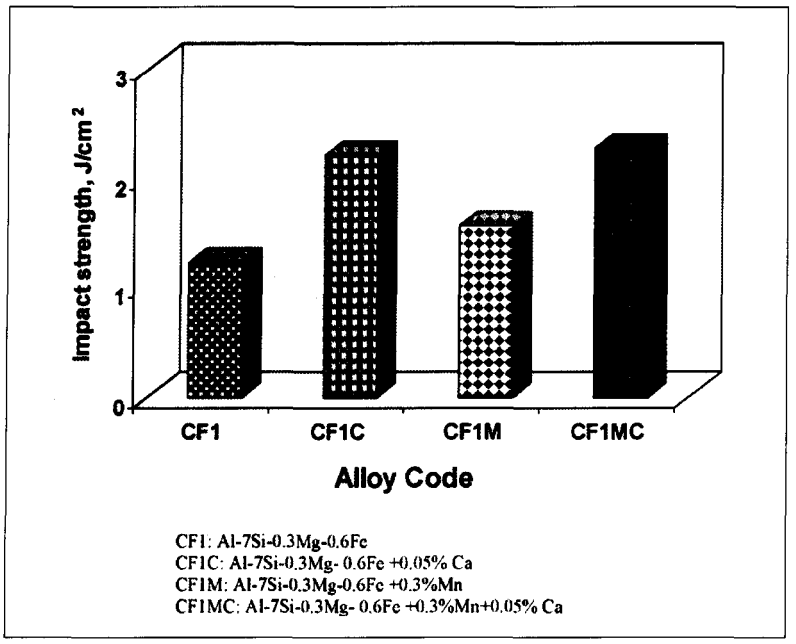

Figure 2.22 Effects of individual and combined additions of Ca and Mn on the impact strength of Al-7Si-0.3Mg-0.6Fe alloy.[77]

Li *et al.* [8] also studied the effects of various levels of iron addition on the impact properties of AA319-type alloys. They concluded that the addition of iron results in an acute reduction in the impact energy of these alloys, regardless of the cooling rates. They attributed this unfavorable effect of iron to the presence of sharp corners at the edges of the β-iron platelets and to the fact that these corners act as crack initiation sites in the matrix.

2.6.3 Effects of Cooling Rate

It has frequently been reported that increasing the cooling rate results in an intensified fineness of dendrite arm spacing (DAS), finer eutectic structure, and a decrease in the size of the intermetallic phases; it will also lead to the occurrence of lower amounts of porosity as well as to its improved distribution. An appreciable and

beneficial effect may thus be obtained with regard to the strength properties and fracture toughness of Al-Si alloys.[1]

The investigation carried out by Vorren *et al.* [12] on the effects of iron on the Charpy impact energy values of Al-7Si-0.3Mg alloys reveals that a high cooling rate can reduce the amount of β-Al_5FeSi platelets to a noticeable degree. Thus, the detrimental effect of this particular phase on the impact values will also be reduced. From Figure 2.23, it will be observed that the fracture toughness of Al-7Si-0.3Mg alloys increases with an increase in the cooling rate for all the alloys, regardless of the iron-content, as confirmed by the small DAS values. It is worth noting that higher fracture toughness values may be obtained in the case of alloys displaying lesser levels of iron, namely 0.15%Fe.

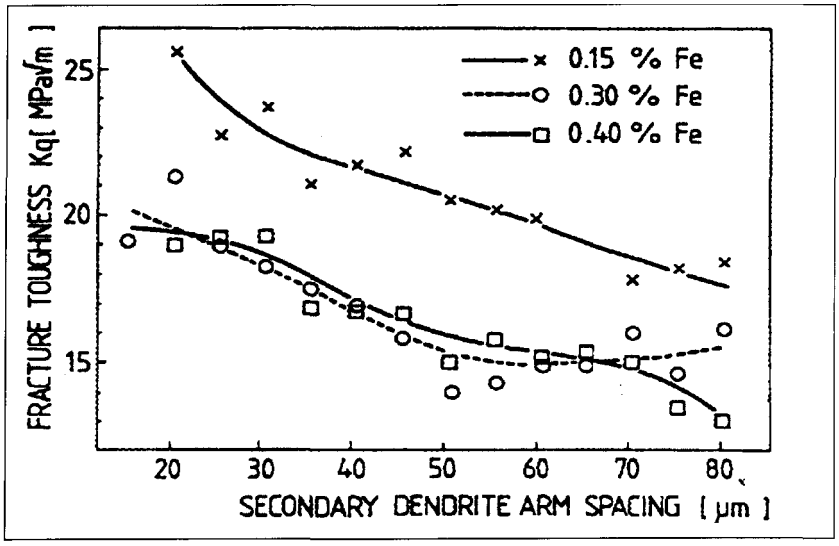

Figure 2.23 Fracture toughness versus secondary dendrite arm spacing at different levels of iron-content (0.15, 0.3 and 0.3%) in AlSi7Mg0.3 alloys. [12]

Kato and Kobayashi [78] studied the effects of solidified microstructures on the fracture toughness of unidirectionally solidified Al-Si system alloys. They reported that

the absorbed impact energy of the Al-7%Si alloy is reasonably enhanced with increasing cooling rates, as shown in Figure 2.24. The increase in impact energy may be ascribed to a decrease in primary and secondary dendrite arm spacing and to the refining of Si particles through the application of a rapid cooling rate. On the other hand, the impact energy of Al-7%Si-0.3%Mg is affected only slightly by the cooling rate because of the formation of brittle, hard Mg_2Si particles in the matrix.

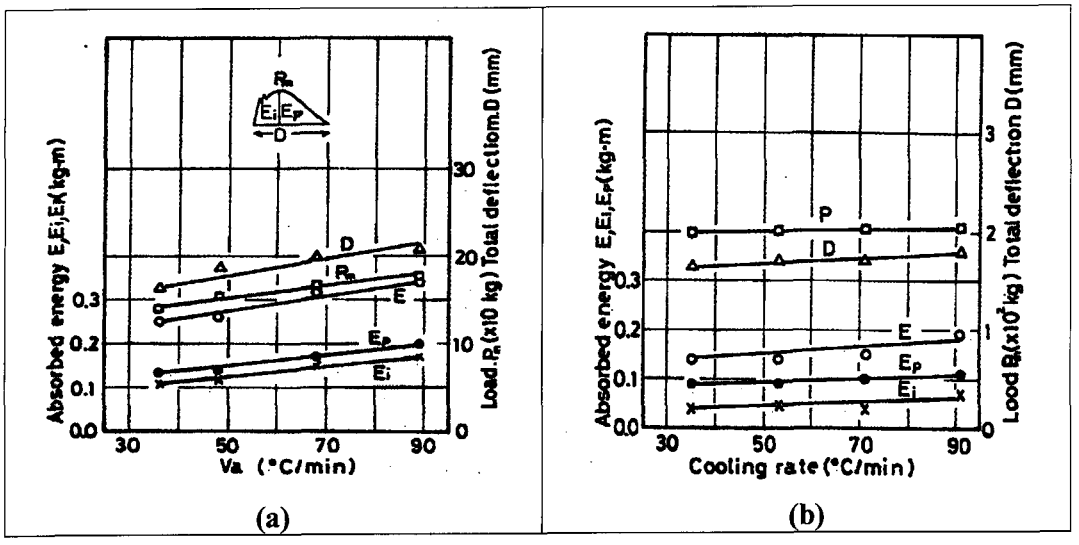

Figure 2.24 Relation between toughness and cooling rate of (a) as-cast Al-7%Si alloy; and (b) as-cast Al-7%Si-0.3%Mg alloy. [78]

In a recent study carried out by Merlin *et al.* [79] on the impact behavior of low-pressure die casting automotive wheels, the results revealed that the impact energy values of A356 alloys display an inverse correlation with the secondary dendrite arm spacing (SDAS). The finer the microstructure (*i.e.* the smaller the SDAS), the greater the impact energy values which may be obtained. These findings are in agreement with the study carried out by Murali *et al.* [66] concerning the effects of solidification rate on the fracture toughness of Al-7Si-0.3Mg casting alloys. Their results indicate that

solidification rate affects the fracture behavior of such alloys to a significant extent, particularly at low Fe and Mg contents. The higher the solidification rate, the higher the ductility which may be obtained, and hence a noticeable improvement in the impact energy will also be observed, as shown in Figure 2.25.

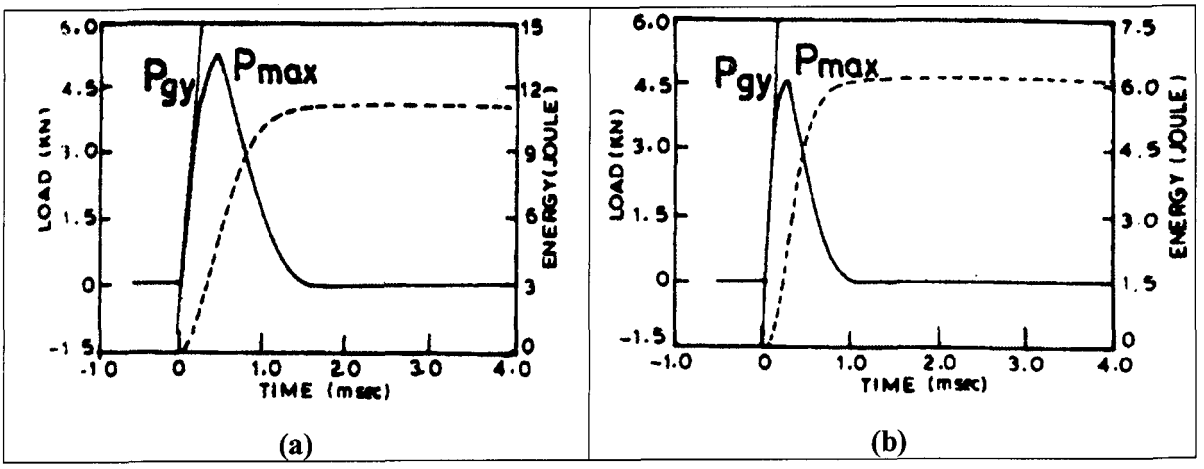

Figure 2.25 Load-time and Charpy impact energy-time curves of Al-7Si-0.3Mg-0.2Fe alloy (a) at high cooling rates, and (b) at low cooling rates.[66]

Li *et al.* [8] investigated the parameters controlling the impact properties of Al-Si-Cu alloys. Their results reveal that the total absorbed impact values show a significant decrease upon increasing the DAS values (*i.e.* causing a decrease in cooling rate) for all the alloys studied under T5 condition, as shown in Figure 2.26. They ascribed this reduction in the impact values to the fact that the size and volume fraction of detrimental β-iron platelets increases upon decreasing the cooling rate and increasing the iron-content of the alloys in question.

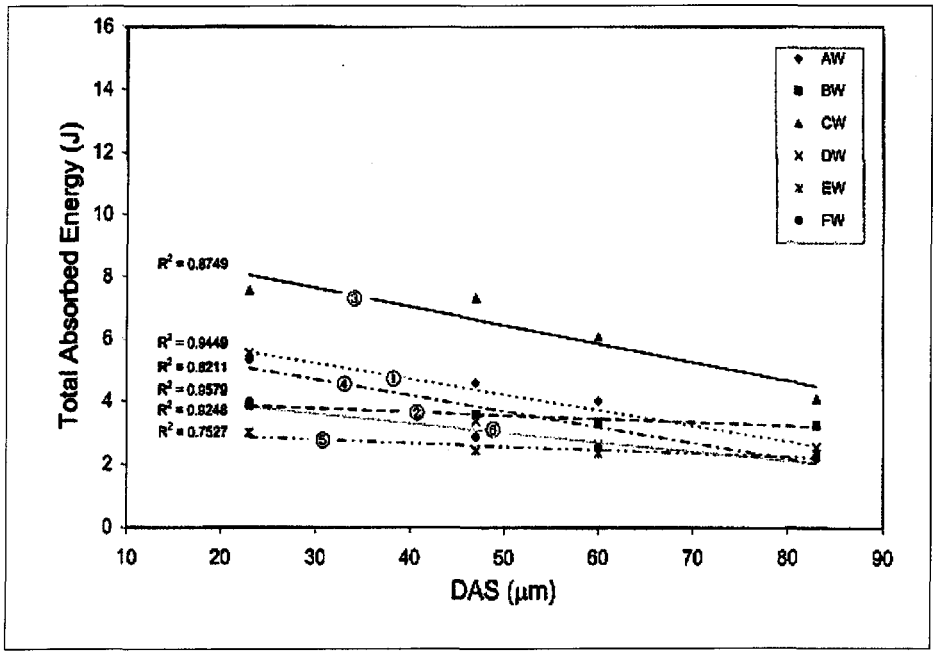

Figure 2.26 Total absorbed energy as a function of DAS for the A319 alloys studied under T5 condition (AW: 319 alloy, BW: 319 + 0.4Fe + Sr, CW: 319 + Sr, DW: 319 +1.2Fe+ Sr, EW: 319 + 1.2Fe, and FW: 319 +1.2Fe + Sr + P).[8]

2.6.4 Effects of Modification

The sharp corners to be found at the edges of acicular eutectic Si particles may act as stress concentration sites, thereby accelerating the initiation and propagation of cracks. This decrease in resistance to both crack initiation and crack propagation results in the rapid failure of the alloy component. Modification is known to be one of the main melt treatment processes and is thus usually applied to Al-Si cast alloys to transform the morphology of undesirable coarse Si into finely distributed fibrous particles. This modification of eutectic Si morphology significantly reduces crack initiation sites and, consequently, leads to a considerable improvement in the elongation which regulates the impact toughness of these alloys to a great extent.[80]

In their work concerning the effects of Sr addition on the fracture characteristics of high purity A356 casting alloys, Kobayashi *et al.* [81] reported that the Charp impact energy (CIE) value was significantly enhanced by the addition of 100 ppm Sr, as shown in Figure 2.27. The increase in the Charpy impact energy may be attributed to the refinement and spheroidization of the acicular Si particles after Sr-addition. On the other hand, increasing the level of Sr-addition by more than 100 ppm increases the cohesion of eutectic Si particles as well as leads to the formation of a higher degree of porosity. [56] The size of Si particles begins to increase with over-modification, resulting in a decrease in the total absorbed impact energy of the A356 alloys under investigation.

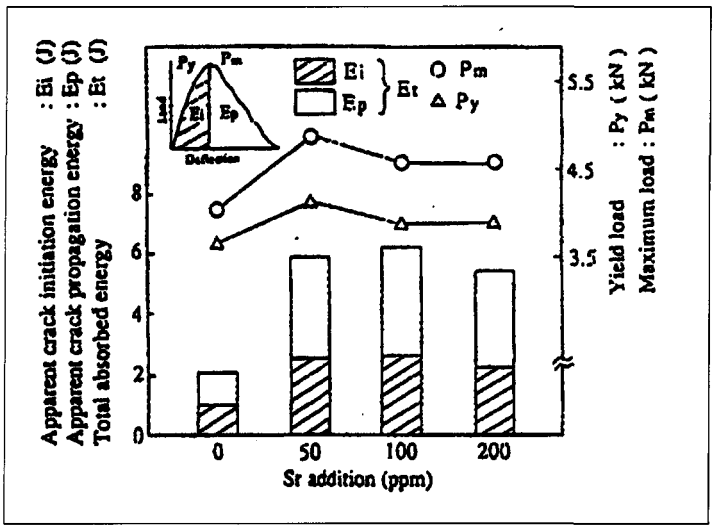

Figure 2.27 Effects of Sr addition on the impact energy of pure Al-Si-Mg alloys. [81]

Closset [82] reported that adding 200 ppm of Sr to both as-cast and heat-treated A413 alloys improves the impact strength by ~ 200%, and ~ 283%, respectively. The application of modification process with an appropriate heat treatment may result in a significant improvement (775%) in the impact strength. The same effects of Sr addition

were also observed for A356 alloys in which the impact values of as-cast non-modified alloys improved by percentage of ~97%. These results were confirmed by a study carried out by Paray *et al.*,[2] who reported an improvement of 65% in the impact strength of the as-cast 356 alloy after Sr-modification.

Hafiz and Kobayashi [83] investigated the influence of Sr level on impact toughness in terms of the crack initiation and crack propagation energies of high purity eutectic Al-Si alloys. The researchers revealed the effective role of Sr-modification in improving the impact values, showing an overall increase of about 438%, for the alloys which had been solidified in a steel mold as shown in Figure 2.28. These results are similar to those reported in other studies carried out by the same researchers.[84,85] The improvement in the total absorbed energy, as confirmed by the increase in both crack initiation and crack propagation energy values, may be attributed to the modification effect of Sr on the eutectic Si particles and the subsequent increase in the proportion of the soft ductile α-aluminum dendrites in the matrix.

The effects of Sr-modification on the Charpy impact energy of Al-Si-Cu alloys solidified in both a sand mold and a water-cooled copper mold were studied by Shivkumar *et al.*[19] They found that the impact energy increased from 0.6 J to 1.4 J after Sr-modification of the as-cast sand castings, representing an increase of approximately 133%. Also, Sr-modification brought about a significant increase in the impact energy of the Cu metallic mold castings from 0.7 J to 2 J, representing an improvement of about 185%.

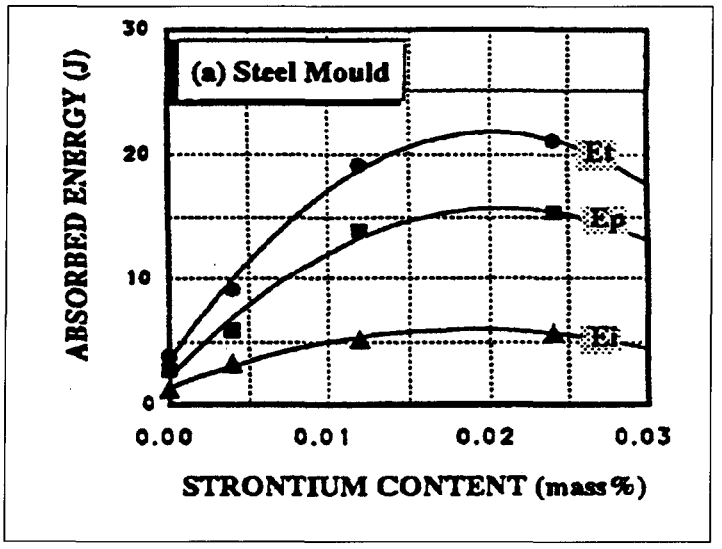

Figure 2.28 Impact strength of eutectic Al-Si alloy as a function of Sr-content. [83]

2.6.5 Effects of Heat Treatment

It was also frequently reported that by applying solution heat treatment to Al-Si alloys it was possible to cause changes in their microstructure, particularly in the morphology of the eutectic Si particles. In the early stages of heat treatment, the platelike Si particles begin to break up into smaller particles through a process known as necking and fragmentation. They then start to spheroidize to attain a rounded form.[32, 34] As the solution time and/or temperature increases, the spheroidized particles start to coarsen during a stage in which they attain a critical volume in accordance with the Ostwald ripening phenomenon.[86] In this manner, the eutectic Si particles thus undergo a sequence of necking, fragmentation, spheroidization, and ultimate coarsening.

The impact properties of Al-Si alloys depend strongly on the morphology of the eutectic Si phase and the proportion of ductile α-Al dendrites in the matrix which separates the brittle Si particles. The spheroidization of eutectic Si particles decreases

the crack initiation sites and increases the bonding of Si with the soft α-aluminum matrix, resulting in an improvement in the resistance to crack initiation (RCI). The coarsening of the eutectic Si particles during solution treatment increases the inter-particle spacing and hence, increases the proportion of ductile α-aluminum dendrites in the matrix, thereby leading to an improvement in the resistance of these alloys to crack propagation (RCP).[5, 87]

It should also be observed that solution heat treatment can minimize the detrimental effects of β-Al_5FeSi on the impact toughness of Al-Si alloys as confirmed by Shivkumar *et al.*[19] in their study on the impact properties of Al-Si-Cu alloys. Their results reveal, among other things, that the β-Al_5FeSi needles undergo necking and then fragmentation into smaller pieces, the thickness of which was also observed to decrease with an increase in solution treatment time.

Paray *et al.* [32] studied the influence of heat treatment, in terms of solution treatment time and artificial aging time, on the impact properties of non-modified and Sr-modified 356 alloys. They found that the unmodified samples which had been solution heat-treated for even 1 hour and aged for 4 hours, exhibited greater impact energy values than did those in the as-cast non-modified and Sr-modified conditions. The appreciable improvement in both crack initiation and propagation energies emphasizes the positive influence of heat treatment on the impact strength. The changes in the microstructure resulting from prolonged solution treatment time (*e.g.* 2 and 4 hours) would, as a matter of course, tend to improve the impact values significantly. The impact values of the Sr-modified A356 alloy increased by a percentage of about 150% compared to the non-modified alloy after solution treatment at 538°C for 13 h followed by aging at 154°C for 8 h. Thus, Sr modification in combination with adequate

solution heat treatment will clearly be observed to improve the impact toughness of Al-Si alloys to a considerable extent.

The effects of heat treatment on the impact strength of Al-7%Si-0.3%Mg alloys were investigated by Tsukuda *et al.*,[55] who found that by increasing both solution heat treatment temperature and time, the impact strength would also increase, as shown in Figure 2.29. They observed that the impact strength decreased as well upon increasing both aging temperature and time, as may be seen in Figure 2.30. The higher impact strength values were obtained after aging for 2 h at 120°C aging temperature.

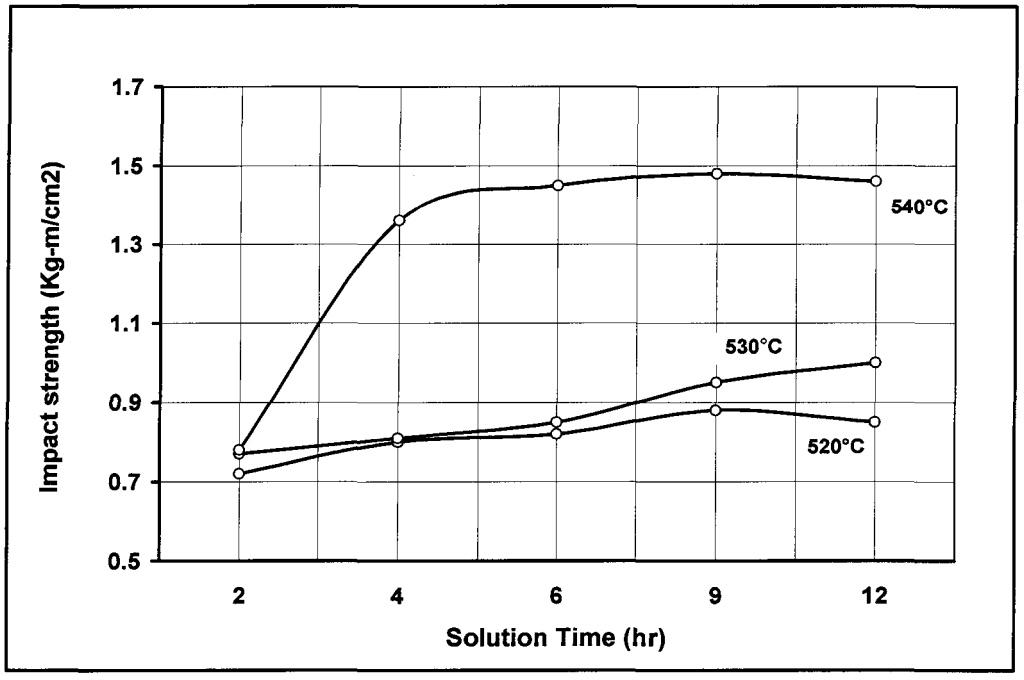

Figure 2.29 Effects of solution temperature and time on the impact strength of Al-6.8Si-0.3Mg-0.2Fe-0.12Ti alloys.[55]

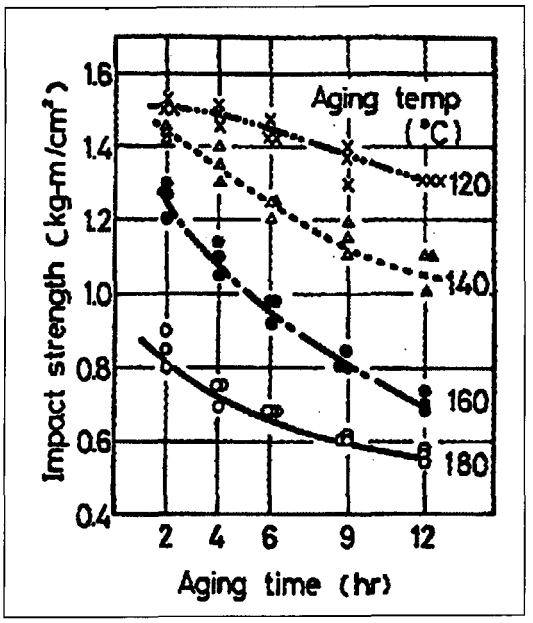

Figure 2.30 Effects of aging temperature and time on the impact strength of heat-treated Al-6.8Si-0.3Mg-0.2Fe-0.12Ti alloys. [55]

Nakayama *et al.* [67] studied the influence of aging time on the absorbed impact energy of an Al-2%Si casting alloy containing various levels of Mg (0.3 to 1%). They found that the impact energy values decreased sharply with an increase in the aging time, regardless of the aging temperature, as shown in Figure 2.31. The impact values, however, show a noticeable restoration after ~ 11 hr of aging at 200°C for Al-2%Si-0.3%Mg and also a slight recovery for Al-7%S-0.3%Mg at 145°C.

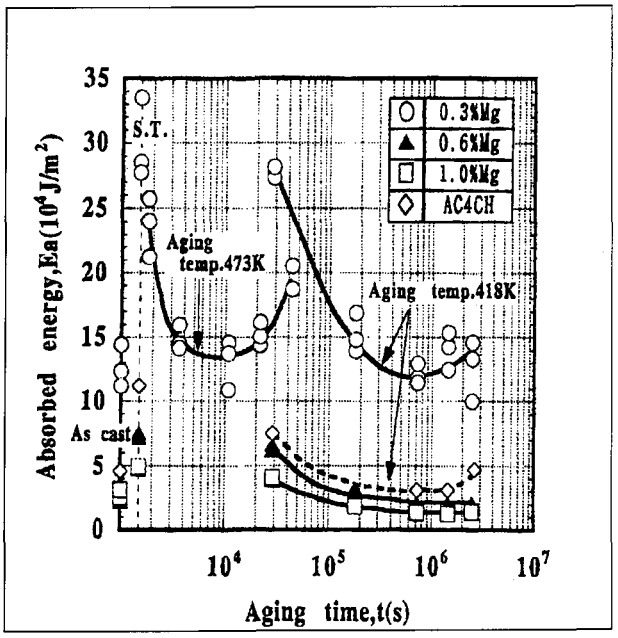

Figure 2.31 Effects of aging time on the absorbed impact energy of Al-2%Si-(0.3 to 1%) Mg and Al-7%Si-Mg alloys. [67]

2.7 FRACTURE OF ALUMINUM-SILICON ALLOYS

Extensive studies have been carried out since the 1960s on the fracture mechanisms of Al-Si cast alloys.[88, 89, 90] Hafiz and Kobayashi [84] investigated the relationship between microstructure and fracture behavior in Al-Si casting alloys. According to their results, the voids are initiated at the sharp edges of silicon particles at the outset of the process; the individual voids then grow and coalesce creating microcracks in the eutectic region. These, in turn, link up to form one major crack which ultimately propagates and leads to the final fracture.

Similar results were observed in a study which was undertaken, also by Hafiz and Kobayashi, [83, 85] to understand the mechanism involved in the fracture of modified and non-modified eutectic Al-Si alloys. These researchers were able to point out that it

is the fracture of Si particles which initiates the first microcrack rather than the decohesion of the Si particles at the silicon matrix interface. Thereafter, these microcracks grow and coalesce, then propagate through the eutectic phase, resulting in final fracture which is of a brittle type in the non-modified alloy, but displays a ductile mode in the case of the Sr-modified alloy. Based on these findings, the researchers proposed that the morphology and distribution of the Si particles governs the fracture profile to a large extent.

In their work on the effects of microstructure on the fracture mechanism of A356 alloys, Voigt and Bye [91] reported that both the crack initiation and its subsequent propagation are triggered by the fracture of the silicon particles at relatively low strain values. Further deformation, through a process of coalescence, leads to a joining up of microcracks with other neighboring microcracks in the same eutectic region to initiate the primary crack, or otherwise to the link-up with the propagating crack front. The fracture process tends to follow the path taken by eutectic regions, ultimately resulting in a transgranular mode of fracture in the sample.

Wang and Cáceres [92] also investigated the fracture mode of A356 and A357 alloys. They postulated that the fracture mechanism may take place in three main stages, as follows: (i) the crack forms as a result of the fracture of silicon particles or their decohesion from the aluminum matrix interface at low plastic strains; (ii) the cracked particles generate localized shear bands with further deformation, and thereafter adjacent cracked particles connect together to form microcracks in the eutectic regions; and (iii) the microcracks join together, propagate, and result in the final fracture. The fracture mechanism in terms of void nucleation and coalescence steps may be observed illustrated schematically in Figure 2.32. [93]

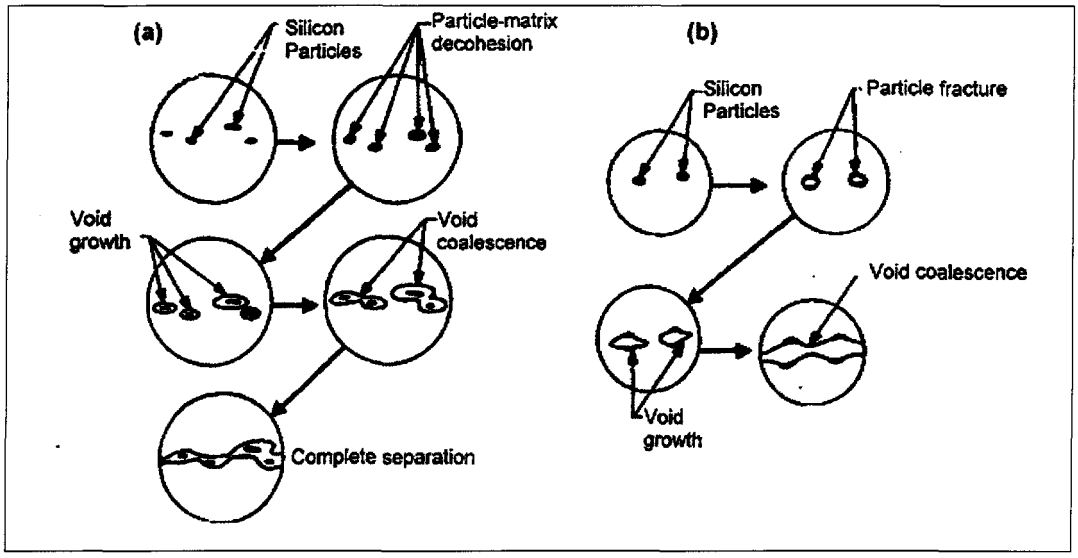

Figure 2.32 Schematic illustration of fracture mechanism (*i.e.* void coalescence) based on Si particles: (a) initiation by Si particle/Al matrix interface decohesion, and (b) initiation by Si particle fracture.[93]

2.7.1 Effects of Microstructure

The microstructure of Al-Si cast alloys consists mainly of a soft ductile α-aluminum matrix and of hard brittle eutectic Si particles as well as the interdendritic phases which form between Al and other elements. The morphology of eutectic silicon particles was reported to affect the fracture behavior of these alloys to a significant degree. Other microstructural constituents such as dendrite arm spacing and iron-containing intermetallic phases also have an influence on fracture characteristics.

The modification of eutectic Si particles by adding Na, Sb, and Sr was, therefore, expected to affect the fracture behavior of commercial hypoeutectic Al-Si alloys substantially, as shown when investigated by Fatahalla *et al.* [94] Their results reveal that the Na- and Sr-modified alloys tend to fracture in a ductile transgranular manner with dimpled and rippled surfaces, whereas a brittle intergranular mode was observed in the non-modified alloys.

Saigal and Berry [95] showed that increasing either the size or the aspect ratio of the Si-particle produces an undesirable effect on the crack initiation resistance of the matrix by decreasing the stress required for initiating the crack in the matrix. Hafiz and Kobayashi [84] also pointed out that a low aspect ratio and improved sphericity of silicon particles increases the resistance of Al-Si alloys to fracture. They ascribed this improvement in fracture resistance to the influence which modified silicon particles tend to have on void nucleation and which is also considered to be the first stage in crack formation.

The study carried out by Dighe and Gokhale [96] on the relationship between microstructure and the fracture path in A356 alloys reported that such a path was found to be instigated primarily by the debonding and breaking up of the largest silicon particles which comprise less than 1% of the overall proportion of whole Si particles in the microstructure of the alloy. Cáceres and Griffiths [97, 98] observed that large and long silicon particles in non-modified Al-7Si-0.4Mg casting alloys are more sensitive to cracking than they are in the modified alloys. The cracking of coarse silicon particles occurs in non-modified structures at low strains and the broken particles may be observed at both cell and grain boundaries. On the other hand, the breaking up of the Si particles is more gradual in finer modified structures and the cracks are then initiated only at the grain boundaries.

The effects of primary Si on the fracture behavior of hypereutectic Al-Si alloys were investigated in a study carried out by Okabayashi *et al.*[99] They pointed out that crack propagation is controlled to a great extent by the primary Si particles, where the cracks propagate as a result of the consecutive cleavage of these particles.

Samuel and Samuel [100] investigated the fracture behavior of 319.2 end chill castings. They found that the fracture mode is mainly transgranular in the alloys where dendrite arm spacing is small in the vicinity of the chill end with a SDAS of ~15 μm, whereas the mode subsequently becomes intergranular in the alloys with large dendrite arm spacings of ~93 μm. This intergranular fracture surface emphasizes the brittleness, or low ductility, of alloys having large dendrite arm spacings.

The results obtained by Surappa *et al.* [101] on the deformation and fracture of cast A356 alloys indicate that the fracture starts with the formation of microcracks at the brittle grain boundaries as well as with the cleavage of the platelike iron intermetallic phase in sand-cast alloys, namely those displaying a low cooling rate and large SDAS. Thus, the fracture path follows an intergranular mode, as may be seen clearly in Figures 2.33(a) and (b). However, small β-iron platelets may be fractured by cleavage in the interdendritic boundary regions in die-cast alloys, namely those with high cooling rates and low SDAS values; as a result, microcracks are formed, then propagate, and thus the fracture process seems to display a transgranular mode in these alloys.

Wang and Cáceres [92] found that the cracking of Si particles tends to occur at the grain boundaries of those Al-Si-Mg alloys which display small dendrite arm spacing values of ~17 μm and thus, the fracture path takes a predominantly intergranualr mode. On the other hand, the fracture tends to occur along the cell boundaries for samples with large dendrite arm spacing values of ~ 65 μm and thus the fracture mode is considered to display a transgranular mode. In a similar study, Cáceres *et al.* [102] observed that Al-Si-Mg alloys having large cell size, *i.e.* high DAS values, tend to display a transgranular fracture path, whereas for fine cell size alloys having low DAS values, the fracture path

proceeds along the grain boundaries following an intergranular mode, regardless of the magnesium content of the alloy.

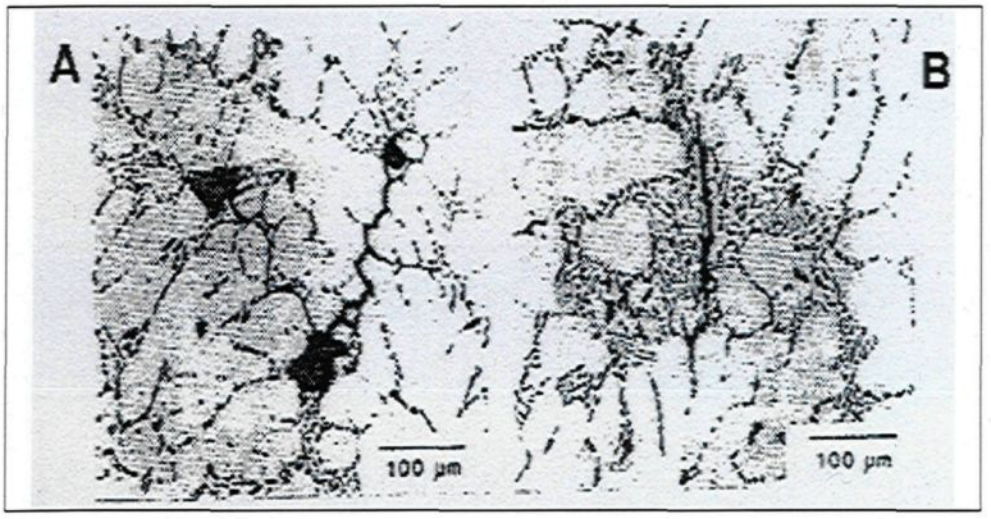

Figure 2.33 Fracture in sand-cast 356 alloys showing (a) grain boundary cracks; (b) fractured β-iron intermetallic particles. [101]

Villeneuve and Samuel [36] observed that cracks formed within the β-Al_5FeSi platelets rather than at the β/aluminum interface in tensile-fractured samples of as-cast Al-13%Si-1.5%Fe alloy, as shown in Figure 2.34. This datum may be attributed to the brittle nature of the β-iron phase, where the platelets split into two halves. These researchers also found that the addition of either Sr, or Sr + Be, to Al-Si-Cu (319) cast alloys will cause the β-Al_5FeSi needles to break up into small fragments. Also, their findings included the fact that these β-Al_5FeSi needles can be transformed into the α-$Al_{15}(FeMn)_3Si_2$ phase which then occurs in the form of Chinese script particles after the addition of Mn in a Mn-to-Fe ratio of ~0.7; otherwise, these needles are transformed into sludge upon the addition of 0.1% Cr. All of the foregoing conditions, resulting from the addition of neutralizers, tend to diminish the amount of brittle β-Al_5FeSi needles

present in the matrix and thus, these alloys will be observed to display a dimpled rupture fracture surface.[103]

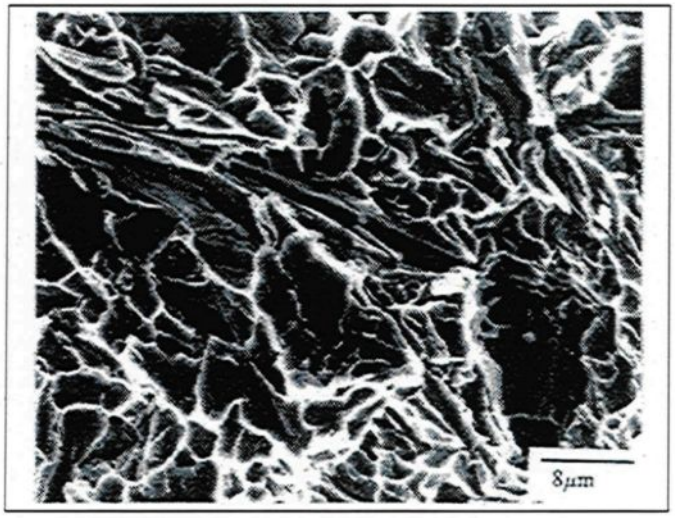

Figure 2.34 Fracture surface of a tensile-fractured as-cast Al-13%Si-1.5%Fe alloy sample.[36]

Murali *et al.*[104] investigated the effects of iron-content on the fracture toughness of squeeze-cast Al-7Si-0.3Mg alloys using standard Charpy V-notch impact test specimens. According to their results, it was possible to observe the occurrence of brittle intergranular fracture resulting from the cleavage of brittle β-Al_5FeSi needles in the alloy containing 0.7% iron.

An in-situ study of the microstructure as it occurs during the tensile deformation of Al-Si alloy castings was carried out by Kato [105] using scanning electron microscopy. The results show that the β-iron needlelike phase cracks easily in the earlier stages of deformation, whereas the α-iron Chinese-script phase is capable of withstanding higher stresses. The crack tends to be activated predominantly at the sharp corners of the

silicon particles when the β-iron needlelike phase is transformed into the α-iron Chinese script phase.

According to recent studies carried out by Li *et al.* [8] on the factors controlling the performance of AA319-type alloys, crack initiation occurs through the fragmentation of the brittle β-iron platelets, Si particles, and Al_2Cu particles in the Sr-modified alloys in both T5 and T6 conditions, as shown in Figure 2.35(a). Subsequently, the crack propagates according to several modes: *i.e.* through the cleavage of the brittle β-Al_5FeSi platelets; through the fracture of undissolved Al_2Cu particles or the insoluble Al_7FeCu_2 intermetallic phase; and through the break-up of the Si particles, all of which as may be observed in Figure 2.35(b). Alternatively, the crack is triggered mainly through the fracture of acicular Si particles and propagates through the void coalescence mechanism in the samples obtained from the T5-non-modified AA319 alloy.

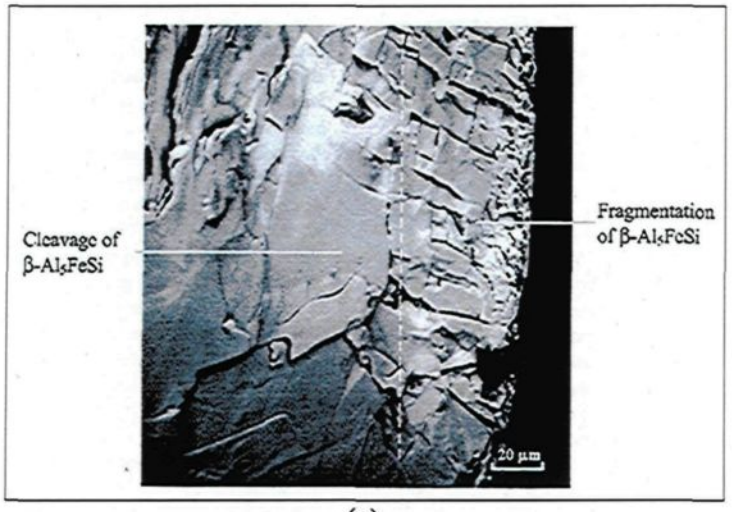

(a)

Figure 2.35

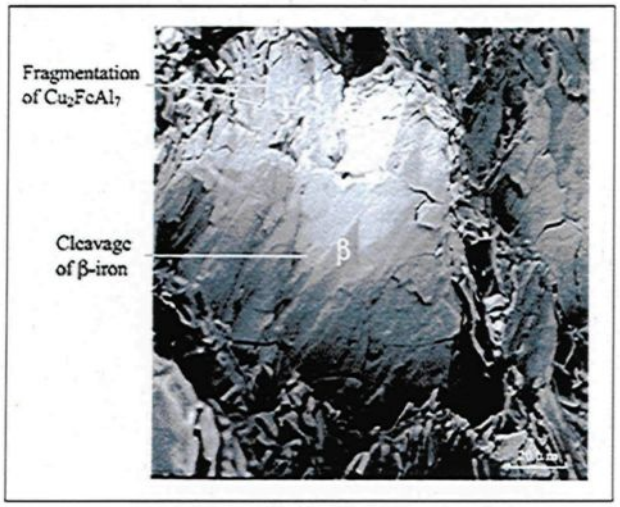

(b)

Figure 2.35 Backscattered SEM micrographs showing the fracture surface of a Sr-modified T6-AA319 alloy with ~1.2%Fe: (a) fragmentation of β-Al_5FeSi during crack initiation followed by cleavage (at the edge), and (b) fragmentation of Al_7FeCu_2 and cleavage of β-iron (at the center).[8]

CHAPTER 3

EXPERIMENTAL PROCEDURES

CHAPTER 3

EXPERIMENTAL PROCEDURES

3.1 INTRODUCTION

The impact behavior of the hypoeutectic 356, 319, and near-eutectic 396 alloys was investigated for the purposes of the present study because of the essential qualities displayed by them with regard to automotive applications. Different levels of Fe, Mg, and Mn were added, either individually or in combination, to both 319 and 356 alloys, thereby covering a wide range of possible industrial compositions for these alloys. Strontium as a modifying agent was implemented with a view to studying the effects of modification on the impact energy values of 319 and 356 alloys. Two different addition levels of Mn together with two different levels of Sr-modification were applied to 396 alloys at two distinct cooling rates, always ensuring that the same aging conditions were applied to all three alloys.

A microstructural examination in terms of eutectic Si particle characterization as well as identification of intermetallic phases was carried out based on the fact that such microstructural constituents regulate the impact energy of the Al-Si alloys to a great extent. The experimental work pertaining to this study was carried out in accordance with the following procedural steps:

3.2 CLASSIFICATION AND PREPARATION OF IMPACT TEST SAMPLES

This part of the experimental work was undertaken in order to prepare the specimens for Charpy impact testing; the samples required were sectioned from the hardness blocks obtained from hypoeutectic 356 and 319 alloys, as well as from the near-eutectic new-developed 396 alloys. This step was undertaken so as to obtain the identical casting and heat treatment conditions and hence the same microstructure. Also, such a step would ensure obtaining relatively reliable results for the comparison purposes between the hardness behavior and impact properties of the three alloys. The task was organized in the following sequence:

1. Classifying the hardness block samples which were obtained by the research group based on the type of alloy involved, the alloying element added, cooling rate, and the relevant heat treatment applied in terms of aging temperature and time, as presented in Table 1.
2. Cutting the hardness block sample into four bars for each alloy/heat treatment condition (see Figure 3.1).
3. Milling the bars to get the exact dimensions for the Charpy impact specimens according to the ASTM E23 standard (10×10×55mm), as shown in Figure 3.1(c). This particular ASTM standard is used to describe the requirements of V-notch impact tests. In the present study, however, unnotched specimens were used because of the fact that aluminum alloys are fragile, and consequently, the presence of notches will contribute to decreasing the absorbed impact energy, and therefore not provide estimates of the actual impact toughness of the alloys in question.

Table 1 Chemical composition, additives and heat treatment conditions used in preparing the alloys investigated for the present study

Alloy	Alloy Code	Chemical Composition & Additives	Heat Treatment Procedures
319	22	(Al-6.5% Si-3.5% Cu) + 0 Fe	SHT* 8h @ 495°C Quenching in warm water (65°C) Aging @ 180°C, 220°C for 2, 4, 6, 8,12 h
	8	(Al-6.5% Si-3.5% Cu) + 0.2Fe	
	9	(Al-6.5% Si-3.5% Cu) + 0.4Fe	
	10	(Al-6.5% Si-3.5% Cu) + 0.8Fe	
	11	(Al-6.5% Si-3.5% Cu) + 0.2Fe + 0.1 Mn	
	12	(Al-6.5% Si-3.5% Cu) + 0.4Fe+ 0.2 Mn	
	13	(Al-6.5% Si-3.5% Cu) + 0.8Fe+ 0.4 Mn	
	14	(Al-6.5% Si-3.5% Cu) + 0.2Fe + 0.1 Mn	
	15	(Al-6.5% Si-3.5% Cu) + 0.8Fe+ 0.1 Mn	
	16	(Al-6.5% Si-3.5% Cu) + 0.2Fe+ 0.3 Mn	
	17	(Al-6.5% Si-3.5% Cu) + 0.8Fe + 0.3 Mn	
	18	(Al-6.5% Si-3.5% Cu) + 0.2Fe + 0.1 Mn + 0.1 Mg	
	19	(Al-6.5% Si-3.5% Cu) 0.8Fe+ 0.4 Mn + 0.1 Mg	
	20	(Al-6.5% Si-3.5% Cu) + 0.2Fe+ 0.1 Mn + 0.3 Mg	
	21	(Al-6.5% Si-3.5% Cu) + 0.8Fe + 0.4 Mn + 0.3 Mg	
356	1	(Al-7%Si-0.35%Mg)+ 0 Fe	SHT 8h @ 540°C Quenching in warm water (65°C) Aging 24 h @ 25°C Aging @ 180°C, 220°C for 2, 4, 6, 8,12 h
	2	(Al-7%Si-0.35%Mg)+ 0.2Fe	
	3	(Al-7%Si-0.35%Mg)+ 0.4Fe	
	4	(Al-7%Si-0.35%Mg)+ 0.8Fe	
	5	(Al-7%Si-0.35%Mg) + 0.2Fe + 0.1 Mn	
	6	(Al-7%Si-0.35%Mg) + 0.4Fe+ 0.2 Mn	
	7	(Al-7%Si-0.35%Mg) + 0.8Fe+ 0.4 Mn	
396	E1	(Al-11Si-2.5Cu-0.45Fe-0.3Mg) + 0.46 Mn + 0 Sr	SHT 8h @ 490°C Quenching in warm water (65°C) Aging @ 150°C, 180°C, 200°C, 220°C and 240°C for 2, 4, 6, 8,12, 16, 20, 24, 30, 36, 44 h
	E2	(Al-11Si-2.5Cu-0.45Fe-0.3Mg) + 0.46 Mn + 0.016 Sr	
	E3	(Al-11Si-2.5Cu-0.45Fe-0.3Mg) + 0.46 Mn + 0.03 Sr	
	E4	(Al-11Si-2.5Cu-0.45Fe-0.3Mg) + 0. 65 Mn + 0 Sr	
	E5	(Al-11Si-2.5Cu-0.45Fe-0.3Mg) + 0.46 Mn + 0.016 Sr	
	E6	(Al-11Si-2.5Cu-0.45Fe-0.3Mg) + 0. 65 Mn + 0.03 Sr at two cooling rates	

* SHT: Solution Heat Treatment.

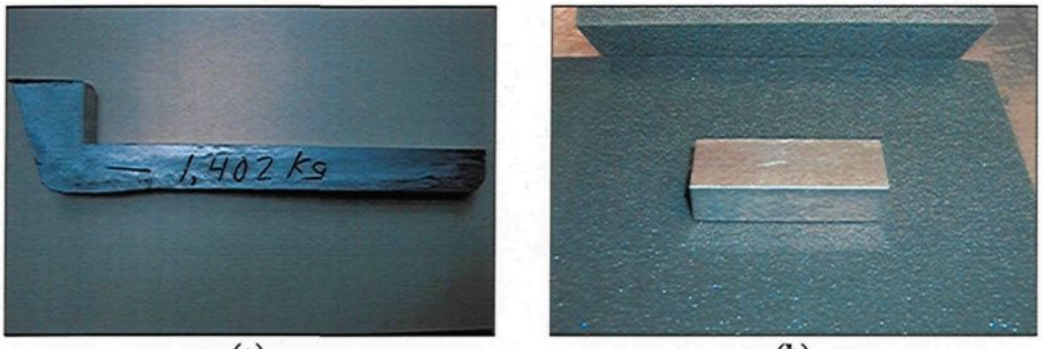

(a) (b)

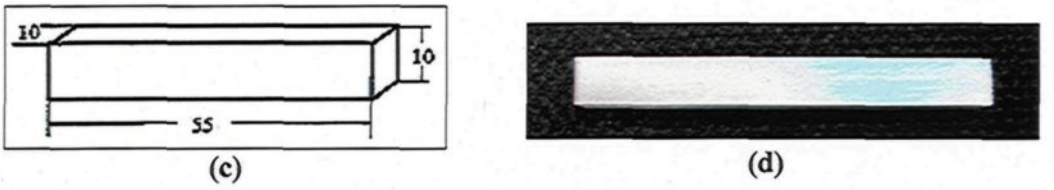

Figure 3.1 Sequence of extracting the Charpy unnotched impact specimens from the hardness block samples: (a) actual casting obtained, (b) hardness block, (c) the dimensions of unnotched impact specimen; and (d) actual unnotched impact specimen.

Casting Procedures

All the alloys to be investigated were melted using an electric induction furnace, as shown in Figure 3.2 (a). The melting temperature was maintained at 730 ± 5°C; the molten metal was degassed using pure dry argon injected into the molten metal (30 ft^3/h) by means of a rotary degassing impeller made of graphite; the degassing time/speed was kept constant at 30 min/150 rpm in order to obtain a lower hydrogen level of ~ 0.1 mL/100g in the melt. All the molten alloys were grain-refined after degassing, using Al-5wt%Ti-1wt%B master alloy.

The first group of non-modified and Sr-modified 319 and 356 alloys containing different levels of additives, namely Fe, Mn, and Mg, were cast in an L-shaped permanent steel mold which had been preheated to 450°C prior to pouring; the alloys were then cooled in atmospheric air after pouring to promote high cooling rates, as represented by small SDAS value.

The second group of near-eutectic 396 alloys, containing different levels of Mn and Sr, were cast as follows: (i) in an L-shaped permanent steel mold preheated to 450°C and then cooled in atmospheric air so as to create a high cooling rate as evidenced by a low SDAS value; and (ii) in an L-shaped permanent steel mold which

had been preheated to 750°C, and then cooled slowly to 450°C after pouring inside the furnace to generate a low cooling rate, as supported by the ensuing high a SDAS value.

All the Sr-modified alloys of the first and second group were obtained by adding about 200-250 ppm of Sr to the degassed non-modified alloy melt. The Sr was added using Al-10%Sr master alloy, in the form of rods. The Sr was usually added to the melt prior to casting using a graphite bell immersed into the melt, following which degassing was carried out for 15 min before pouring. Two levels of Mn (0.45 – 0.65 wt%) and three levels of Sr (0, 200, and 350 ppm) were added to the 396 alloy for castings solidified at both high and low cooling rates.

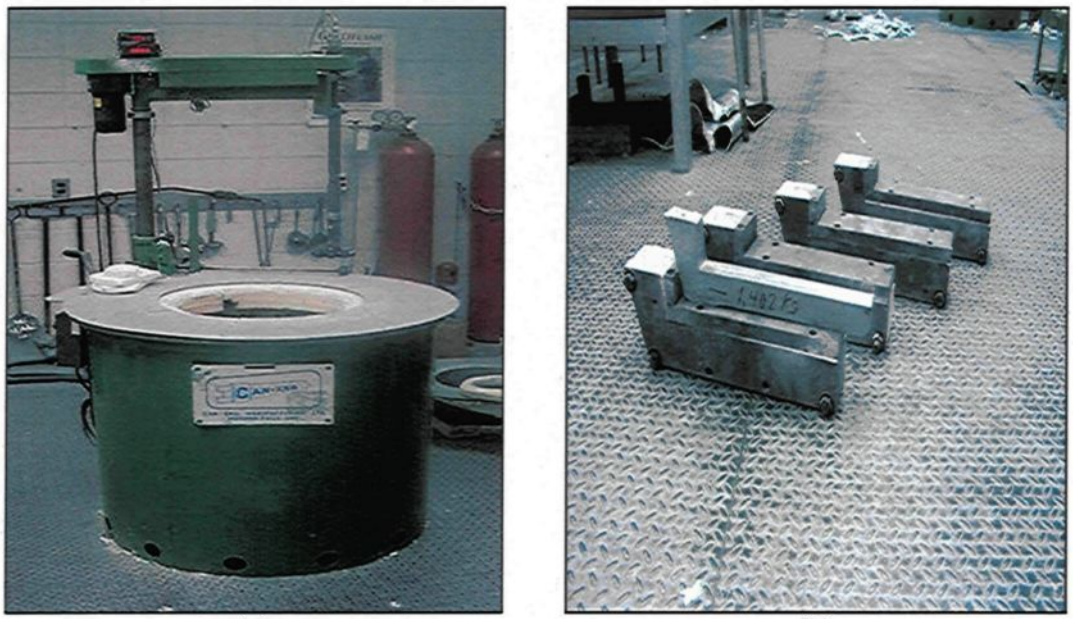

(a) (b)

Figure 3.2 (a) Electric resistance furnace, and (b) L-shaped permanent steel mold and actual casting obtained.

Samples for chemical analysis were also taken simultaneously for each melt composition/casting. The chemical compositions representing the average of three

spectrometric analyses for all the alloys investigated are listed in Appendix 1 under Tables 3, 4, and 5 inclusively.

Heat Treatment Procedures

The castings obtained from the 319, 356, and 396 alloys were machined and milled, then cut into three hardness rectangular blocks for solution heat treatment and aging under a T6 regime, as shown in Figures 3.1(a) and (b). A Blue M forced-air electric furnace, model SPX, equipped with a programble temperature controller (± 1°C), was used for the full heat treatment process, as shown in Figure 3.3. The details of the entire T6 heat treatment regime are summarized in Table 1.

Figure 3.3 Blue - M forced-air electric furnace used for heat treatment.

3.3 CHARPY IMPACT ENERGY MEASUREMENT

Charpy Impact Testing was performed on unnotched samples machined from all the non-modified and Sr-modified alloys in the as-cast and heat-treated conditions. The use of an unnotched test specimen emphasizes on the dependence of the impact energy values on the metallurgical parameters rather than on the specimen configuration. The surfaces of the specimens were polished with sandpaper to remove any irregularities resulting from the machining process. This testing was carried out using a computer-aided instrumented Instron Charpy Impact Testing machine, model SI-1D3 from SATEC Systems Inc., as shown in Figure 3.4. The Charpy impact testing starts when the pendulum swings from a given height to strike the unnotched specimen at a constant velocity of ~ 5.2 m/sec, which falls within the range of the ASTM E 23 standard of 3 to 6 m/s.

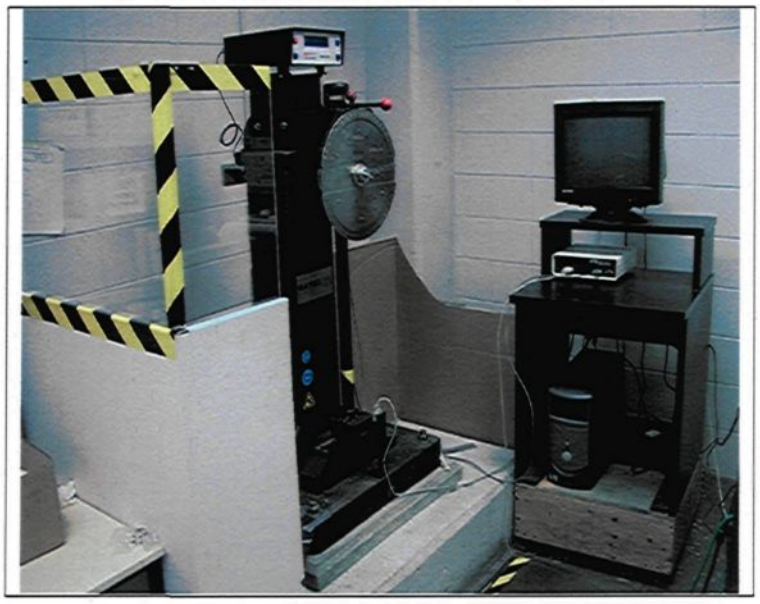

Figure 3.4 A computerized instrumented SATEC Instron Charpy impact machine, model SI-1D3, connected to an Instron Dynatup data acquisition system.

An Instron Dynatup data acquisition system was connected to the pendulum of the impact machine so as to monitor the behavior of the test specimen by measuring the load, total impact energy, crack initiation energy, and crack propagation energy as functions of the total time-to-fracture, as shown in Figure 3.5. The absorbed impact energy measured is calculated on the basis of the difference between the potential energies of the pendulum before and after impact. The average value of the energies obtained from four tested impact specimens for each alloy condition was taken as the representative value for that particular condition.

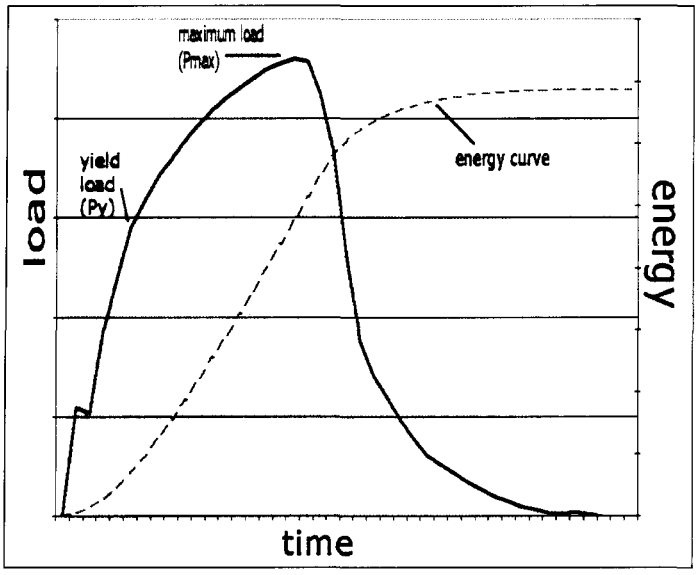

Figure 3.5 Typical load-time curve obtained using the data acquisition system.

3.4 METALLOGRAPHIC EXAMINATION

For the purposes of a microstructural examination, samples were sectioned from the different castings and then prepared for examination using a number of metallographic techniques.

3.4.1 Preparation of Samples

Samples for metallographic examination were sectioned from the castings corresponding to each alloy condition; they were then mounted in bakelite and polished using a BUEHLER variable speed grinder-polisher to obtain the desired fine finish using 1 μm diamond paste. Table 2 shows the details of the grinding and polishing stages which were applied. After every stage of polishing, the samples were washed using a soap-alcohol mixture, and then dried by forced air to avoid the carryover of any contaminate to the next step. The polished samples were then used for the designated microstructural examination.

Table 2 Grinding and polishing procedures used for metallographic samples

Stage	Abrasive	Speed (rpm)	Time (min)	Lubricant	Force (lb)
1	120	120	Until flat	Running water	30
2	240	120	1	Running water	30
3	320	120	1	Running water	30
4	400	120	1	Running water	30
5	600	120	1	Running water	30
6	800	120	1	Running water	30
7	Diamond (6 μm)	120	6	MetaDi fluid	30
8	Diamond (1 μm)	120	6	MetaDi fluid	30
9	Buehler MasterMet	90	4	Water droplets	30

3.4.2 Eutectic Si-Particle Characteristics

Characterization of the eutectic Si particles was carried out for all the alloy conditions involved using a CLEMEX image analyzer in conjunction with an Olympus optical microscope, as shown in Figure 3.6. The Si-particle characteristics were measured for each field by traversing the entire surface of each sample in a regular,

systematic manner. The average values obtained for the eutectic Si particle characteristics are the averages of the readings obtained from the examination of fifty fields per sample. Measurements were carried out at magnifications of 500X and 1000X for the non-modified and Sr-modified alloy samples, respectively. From these measurements, it was possible to determine the following characteristics:

- average Si-particle area (μm^2) and standard deviation;
- average Si-particle length (μm) and standard deviation;
- roundness ratio of Si particles (%);
- aspect ratio, i.e. ratio of maximum to minimum dimensions of the Si particles; and
- density of the Si particles in counts per unit area (number of particles/mm^2).

Figure 3.6 An optical microscope - image analyzer system used for quantitative microstrctural analysis.

3.4.3 Identification of Intermetallic Phases

An electron probe microanalyzer (EPMA) was employed to measure the surface fraction of the intermetallic phases for the as-cast and heat-treated samples obtained

under the variety of conditions involved. Wavelength dispersion spectroscopy (WDS) analyses and energy dispersive X-ray spectrometry (EDX) facilities were used for phase identification purposes. These data provide a useful means for calculating the closest appropriate stoichiometric formula for the various intermetallic phases present in the microstructure of the alloys investigated.

Figure 3.7 shows the WD/ED Combined Microanalyzer located at the McGill Microprobe Laboratory which was used for intermetallic phase identification purposes. This particular version is model JXA-8900R, operating at 20 kV and 30 nA, with an electron beam size of ~ 1μm.

Figure 3.7 Electron probe microanalyzer (EPMA) used for quantification and identification of intermetallic phases.

3.4.4 Fractography

An optical microscope was used to examine both the fracture path and the components of microstructure involved in the crack formation occurring on and below

the surface of metallographic samples which were sectioned off perpendicular to the fracture surface. The longitudinal section indicated by the white line in Figure 3.8(a) shows how the samples were extracted. The fracture surfaces of the Charpy specimens after the test were examined and analysed using scanning electron microscopy (SEM) to monitor the crack propagation path and the fracture mode. Samples were cut approximately a 6mm from the fracture surface, as shown in Figure 3.8(b), the upper part of which was used for fractographic examination. Extra care was taken during the cutting to avoid contamination of the fracture surface.

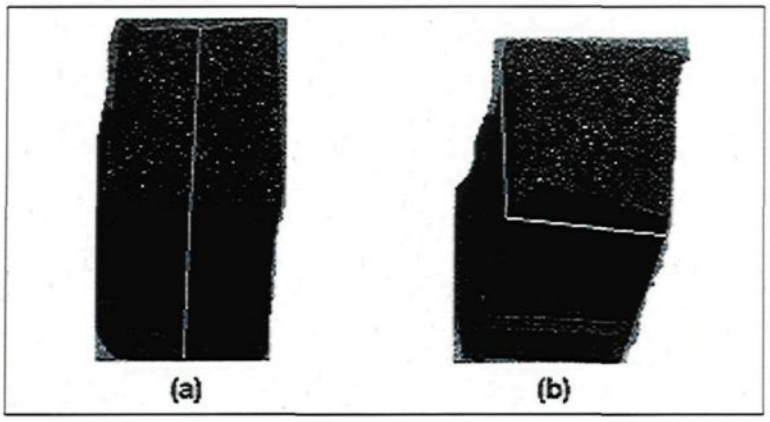

Figure 3.8 An actual unnotched impact-tested specimen showing the location of metallographic samples used for fractographic examination using: (a) optical microscopy, and (b) SEM.

3.5 ANALYSIS OF RESULTS AND DISCUSSION

This part of the study will be completed by carrying out the following activities:

- Analyzing the effects of Fe-based intermetallic phases and heat treatment conditions on the Charpy impact energy of 356 and 319 alloys;

- Studying the effects of Mn and Sr additions as well as the cooling rate on the impact properties of newly developed 396 Al-Si alloys;
- Investigating the fracture mechanisms involved including fracture path and fracture mode using optical microscopy and SEM techniques.

CHAPTER 4

MICROSTRUCTURE AND HARDNESS

CHAPTER 4

MICROSTRUCTURE AND HARDNESS

4.1 INTRODUCTION

The main parameters controlling the microstructure of aluminum-silicon casting alloys include composition, melt treatment, solidification conditions, and the heat treatment process. The microstructure plays a vital role in regulating the mechanical properties of these alloys and, hence, their performance for the desired applications. The principal microstructural constituents of the as-cast aluminum-silicon alloy structure are primary grains of α-Al dendrites, the eutectic Si phase between the dendrites, and secondary eutectic phases such as Mg_2Si or Al_2Cu, as well as ternary phases like iron-bearing intermetallic compounds.

Hardness is a crucial mechanical property which makes it possible to provide a primary assessment of the mechanical properties of an alloy component and hence, to predict its performance under industrial conditions. This property may be defined as the capability of a material to resist permanent indentation or localized plastic deformation when it comes into contact with an indenter under load. [106, 107]

The Brinell hardness testing technique was applied in the present study. In this case, a spherical indenter made of hardened steel or tungsten carbide is forced into the surface of the metal to be tested; the diameter of this indenter is 10.00 mm (0.394 in.). Standard loads ranging between 500 and 3000 kg are applied as compressive loads in 500-kg increments. During the test, the load is applied on the specimen surface and is

maintained constant for a specified time between 10 and 30 sec. The harder the material to be tested, the greater the applied load which will be required. The Brinell hardness number (BHN) is a function of both the magnitude of the load and the diameter of the resulting indentation. This diameter is measured with a special low-power microscope, utilizing a scale which is etched onto the eyepiece. The diameter measured is then converted to the appropriate hardness number using a chart; only one scale is used with this technique.[107]

In this chapter, features of the microstructure including eutectic Si, iron-based intermetallic compounds, and precipitation-hardened phases will be discussed in an attempt to facilitate an understanding of their influence on hardness behavior as presented in the following subsections for the series of Al-Si casting alloys, namely, 356, 319 and 396 alloys investigated in this study. Also, an understanding of this inter-relationship between microstructure and hardness will be useful in the interpretation of the Charpy impact energy results for the same alloys to be discussed in the subsequent chapters of this thesis.

4.2 MICROSTRUCTURE

An examination of the microstructure makes it possible to grasp the complex process-structure-property inter-relationship and would, therefore, also help in the assessment of the performance of aluminum-silicon casting components under a variety of service conditions. The main constituents of the microstructure of the 356 alloys investigated, as an example, will be presented in the following subsections in terms of a qualitative study obtained by means of optical micrographs. In addition, quantitative measurements of the total volume fraction of all intermetallic phases present in the

microstrcture were carried out for non-modified and Sr-modified alloys under as-cast and solution heat-treated conditions.

4.2.1 Iron-Based Intermetallic Phases

It will be noted, from Figure 4.1, that the β-Al_5FeSi phase appears in the form of randomly distributed needles when observed in a two-dimensional optical micrograph, whereas it assumes a plate-like morphology when viewed in three dimension by means of a scanning electron microscope. The π-$Al_9FeMg_3Si_6$ phase is observed to form independent script-like particles, as shown in Figures 4.1(a) and (b). This iron-intermetallic phase is often observed to be closely connected to/nucleated on the β-phase platelets, forming distinctive platelet particles, as shown in Figures 4.1(c) and (d). This observation may suggest that, as a result of the peritectic reaction, the π-iron phase appears to precipitate during solidification at a temperature just after the formation temperature of the β-Al_5FeSi platelets.[16]

These findings are in agreement with those obtained in a study carried out by Taylor [108] on the effects of iron in Al-Si alloys. The results reveal that the π-iron phase may grow in close association with the β-iron phase platelets or else that it may precipitate in the form of independent script-like particles in the case of as-cast alloys; this is shown clearly in Figures 4.2(a) and (b).

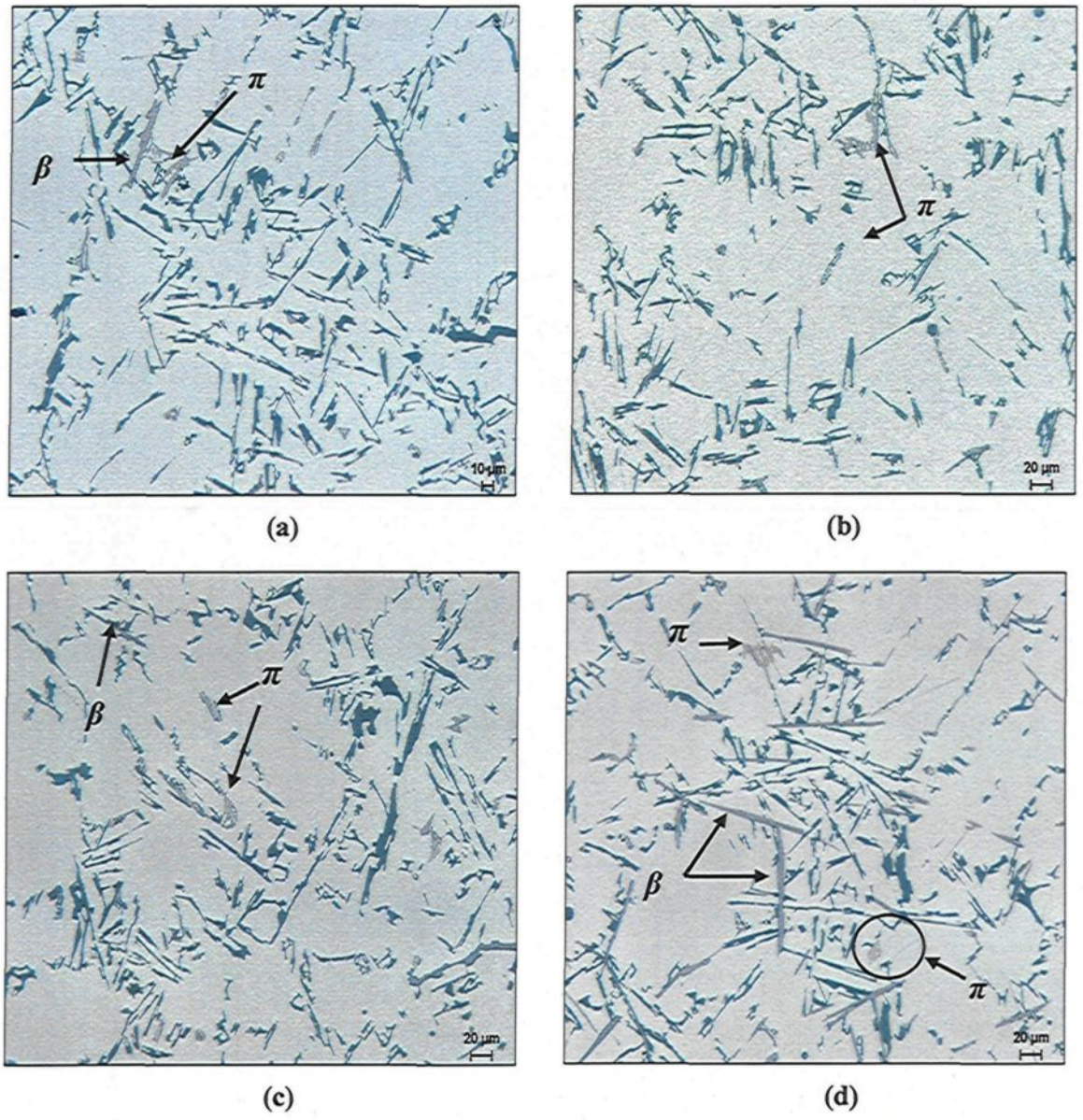

Figure 4.1 Optical micrographs showing the formation of β-Al_5FeSi and π-$Al_8FeMg_3Si_6$ iron intermetallic phases present in the as-cast microstructure of the non-modified 356 alloy containing: (a) 0.1% Fe, (b) 0.25% Fe, (c) 0.4 %Fe, and (d) 0.8% Fe.

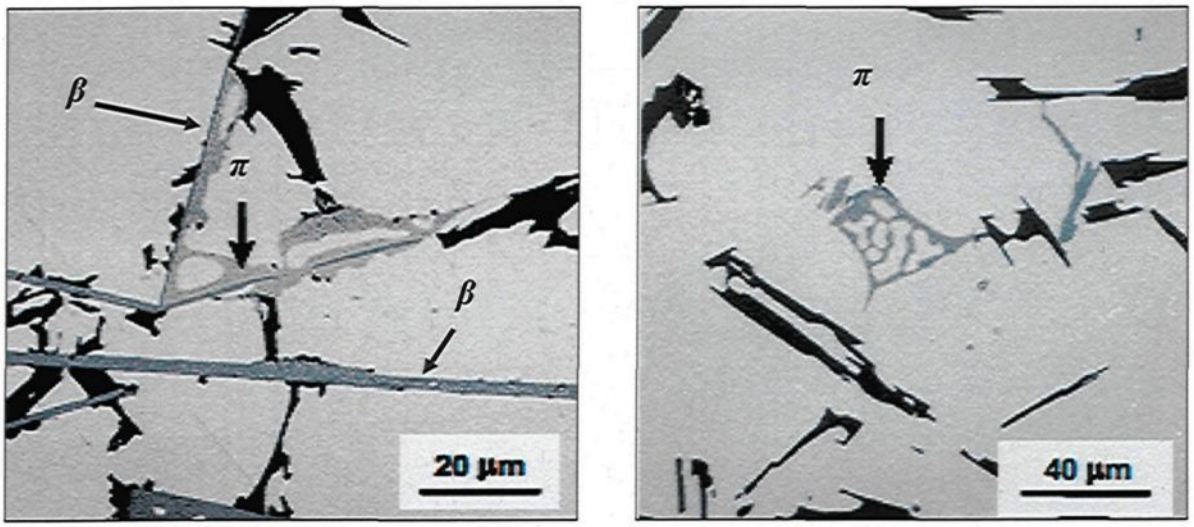

(a) (b)

Figure 4.2 Optical micrographs of Al-5%Si-1%Cu-0.5%Mg-(Fe) alloys showing the formation mechanism of π-$Al_8FeMg_3Si_6$ phase: (a) π-phase growing from the β-platelet phase, and (b) an independent script-like π-phase particle. [108]

Figure 4.3 shows the as-cast microstructures of Sr-modified 356 alloys containing four levels of iron. It will be observed that both β-iron needles and π-iron script-like particles seem to be segregated away from the eutectic Si colonies in the presence of Sr. It is also worth noting, from Figures 4.3(c) and (d), that both of these iron-based phases acquire large-size particles, particularly in the alloys containing high levels of Fe.

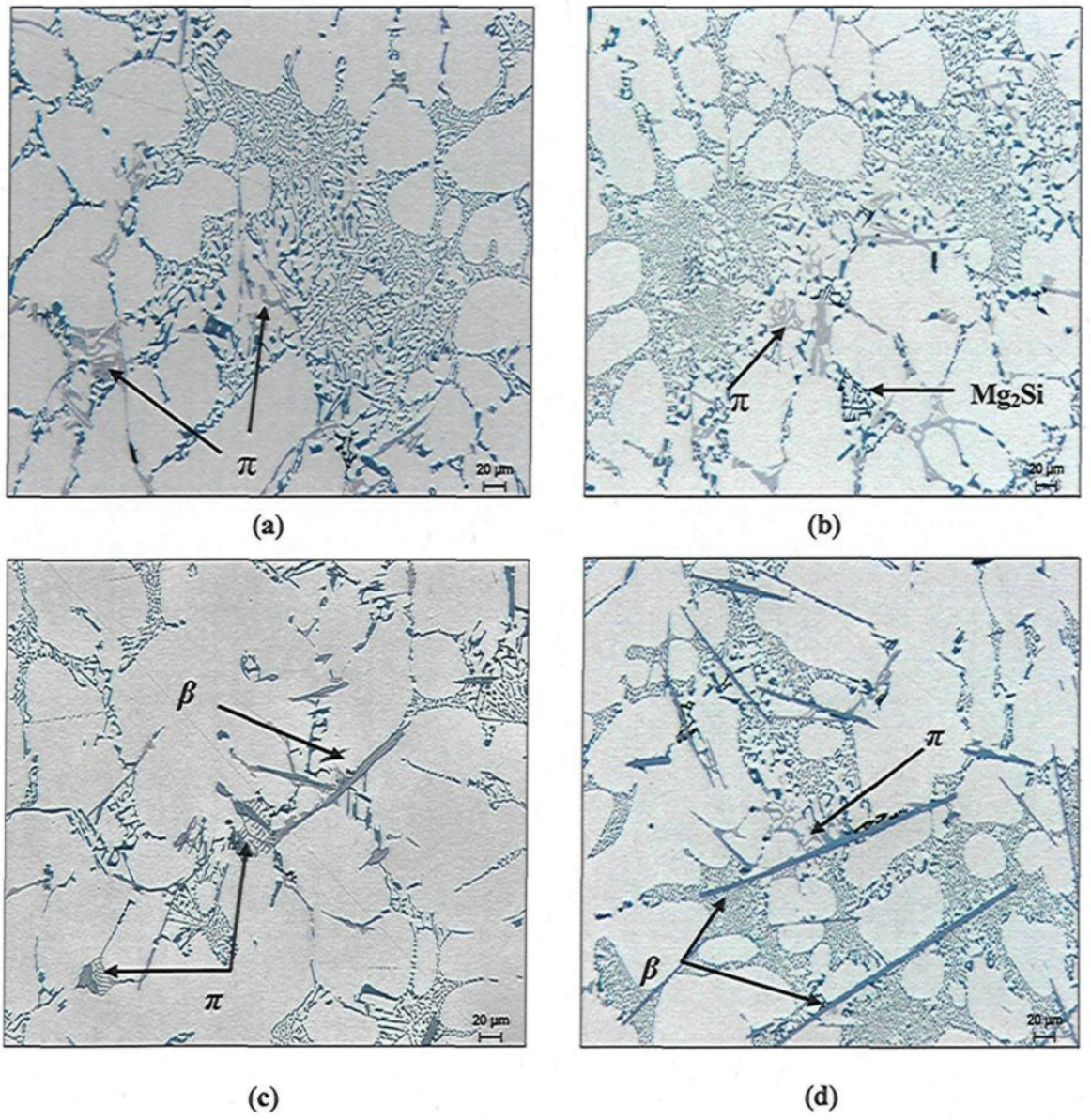

Figure 4.3 Optical micrographs showing the segregation of both β- and π-iron intermetallic phases away from the eutectic Si regions in the as-cast microstructure of Sr-modified 356 alloys containing: (a) 0.1% Fe, (b) 0.25% Fe, (c) 0.43% Fe, and (d) 0.87% Fe.

4.2.2 Effect of Solution Heat Treatment

As frequently reported in a number of earlier studies, [31, 32, 109] the eutectic Si phase is observed to undergo shape changes after the alloys are subjected to solution heat treatment, at 540°C for 8 hrs for the 356 alloys illustrated in Figure 4.4. The fine Chinese-script Mg_2Si phase usually found in the interdendritic regions of the as-cast microstructure is not observed to be present after applying the solution treatment, which supports the assumption of their complete dissolution in the α-aluminum solid solution.

In addition to the previously observed changes in the as-cast structure, the small-sized particles of the π-$Al_8FeMg_3Si_6$ phase tended to disappear during solution treatment, particularly for the alloys containing low levels of iron, most likely as a result of their complete dissolution in the matrix. This π-phase may also decompose by means of discharging its Mg into the aluminum solid solution, leading to its transformation into clusters of fine-scale needles of a Mg-free iron-bearing intermetallic phase, as shown appearing inside the circled areas in Figure 4.4. It may also be observed that this transformation of the π-phase into clusters of a new phase is almost complete in low Fe-containing alloys, and this newly formed phase is thought to possess a composition similar to that of the β-iron phase. [39, 110]

Both the script-like and blocklike π-phase forms, which are present in high Fe-containing alloys, appear to partially dissolve into the matrix after solution treatment because they acquire large-size particles, as shown in the circled area in Figure 4.4 (c) and (d) also showing some minor evidence of fragmentation, rounding, and dissolution. It may thus be concluded that the large particles of π-phase seem to be predominantly resistant to changes during solution treatment. The solutionizing time at such

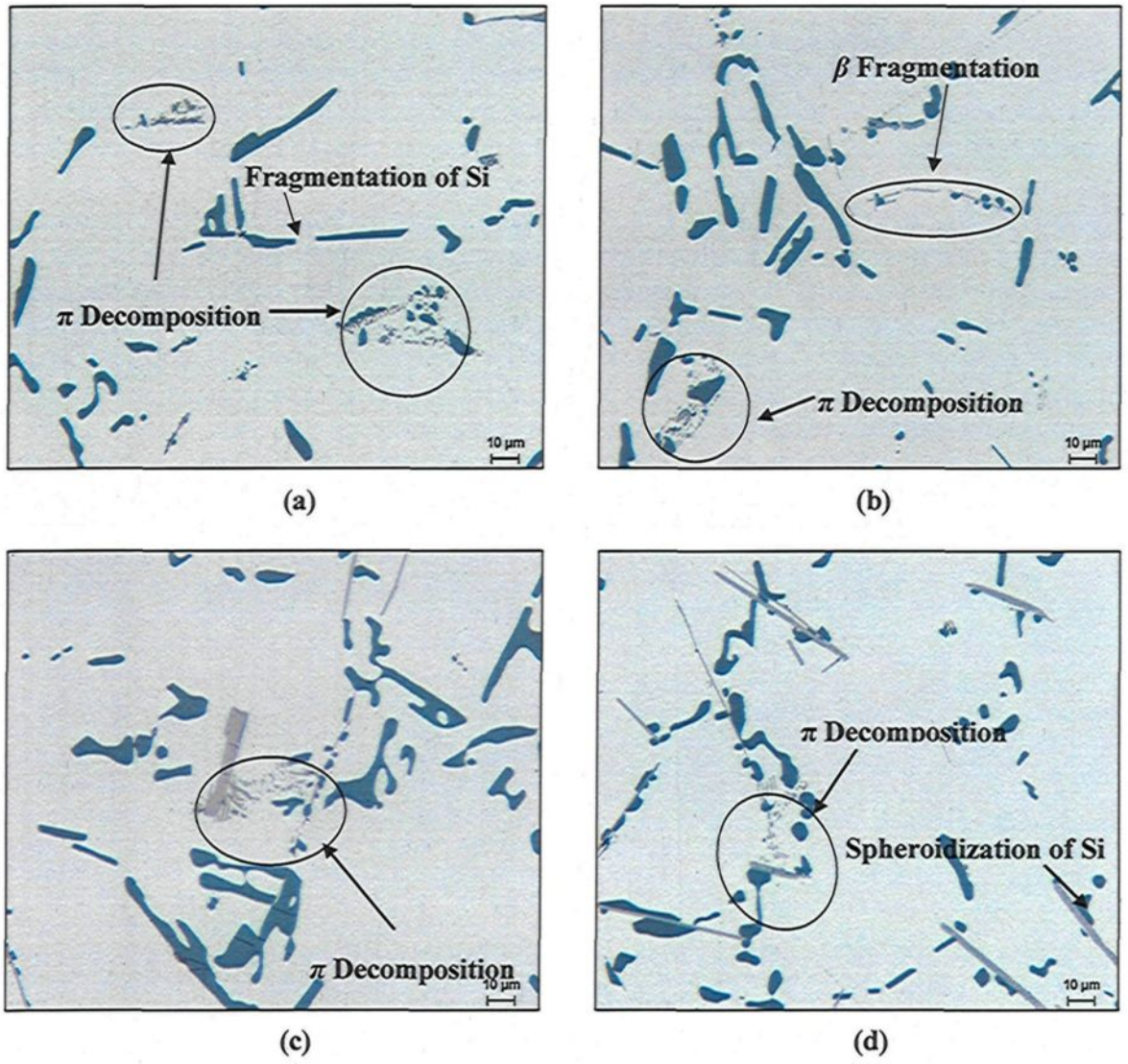

Figure 4.4 Optical micrographs of non-modified solution heat-treated 356 alloys containing: (a) 0.1% Fe, (b) 0.25% Fe, (c) 0.8% Fe, and (d) 1% Fe, showing decomposition of the π-phase and the formation of small new β-needles in the microstructure.

temperatures appears to be insufficient to overcome the low diffusivity of iron in solid aluminum or to complete the decomposition of these coarse π-particles. The above observations emphasize the fact that both solution heat treatment parameters and alloy composition have the effect of controlling the dissolution and/or decomposition of the

π-phase to a large degree; they are also in good agreement with the results obtained in a study carried out by Wang and Davidson [111] on the solidification and precipitation behavior of Al-Si-Mg alloys. It will also be observed that there are a number of thin β-needles which become elongated to the point of necking; they then begin to manifest various states of breakdown, disintegrating into smaller segments, as shown inside the oval area in Figure 4.4(b).

Figure 4.5 shows quantitative measurements for the total surface fraction of the intermetallic phases present in the as-cast and solution-treated microstructures of a 356 alloy containing various levels of iron. It is obvious that solution heat treatment results in reducing the total surface fraction of the intermetallic phases for both non-modified and Sr-modified alloy conditions. The apparent absence of particles of the Mg_2Si phase in Figure 4.4 confirms the complete dissolution of this phase after solution treatment.

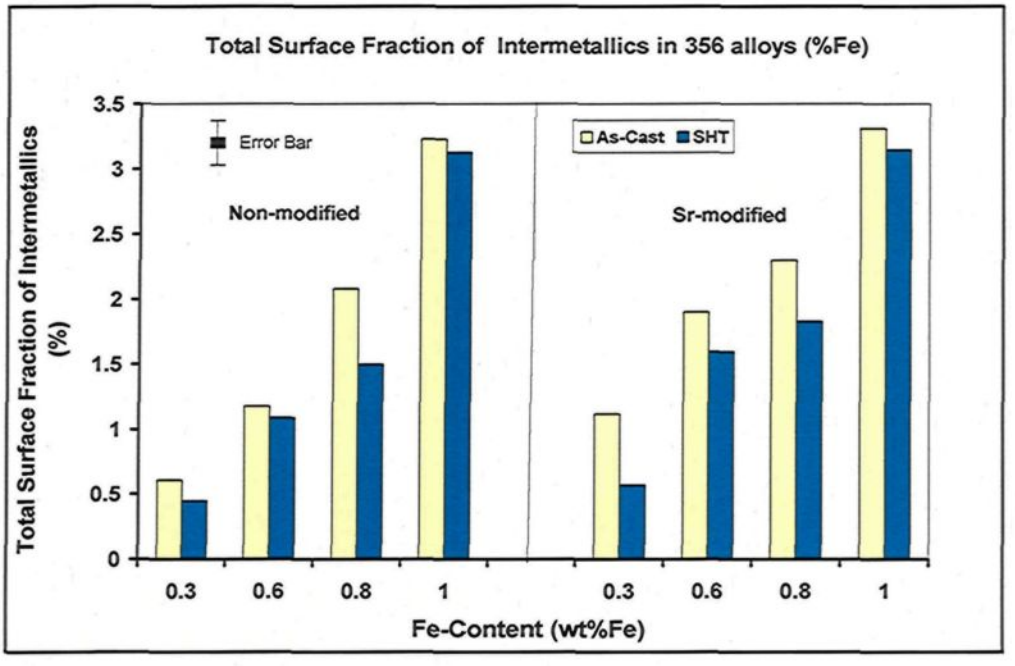

Figure 4.5 Effects of solution heat treatment and Fe-content on the total surface fraction of intermetallic phases observed in an as-cast 356 alloy for the non-modified and Sr-modified cases.

Such a reduction in the total surface fraction of the intermetallics supports the conclusions which were drawn regarding the dissolution and transformation of the π-iron phase, as may be observed from the optical micrographs shown in Figure 4.4. The transformation of the π-phase into fine β-needles also highlights the drop in the total surface fraction of intermetallics considering that the π-phase is less dense and occupies a larger volume fraction than that of the β-phase. It is worth noting that the total surface fraction of intermetallic phases appears to increase with an increase in the level of iron-content, regardless of alloy conditions.

Similar observations were made in the case of Sr-modified solution heat-treated 356 alloys, as shown in Figure 4.6. It should also be noted that the β-iron needles undergo some degree of necking and fragmentation, as represented by the arrows in Figure 4.6(c).

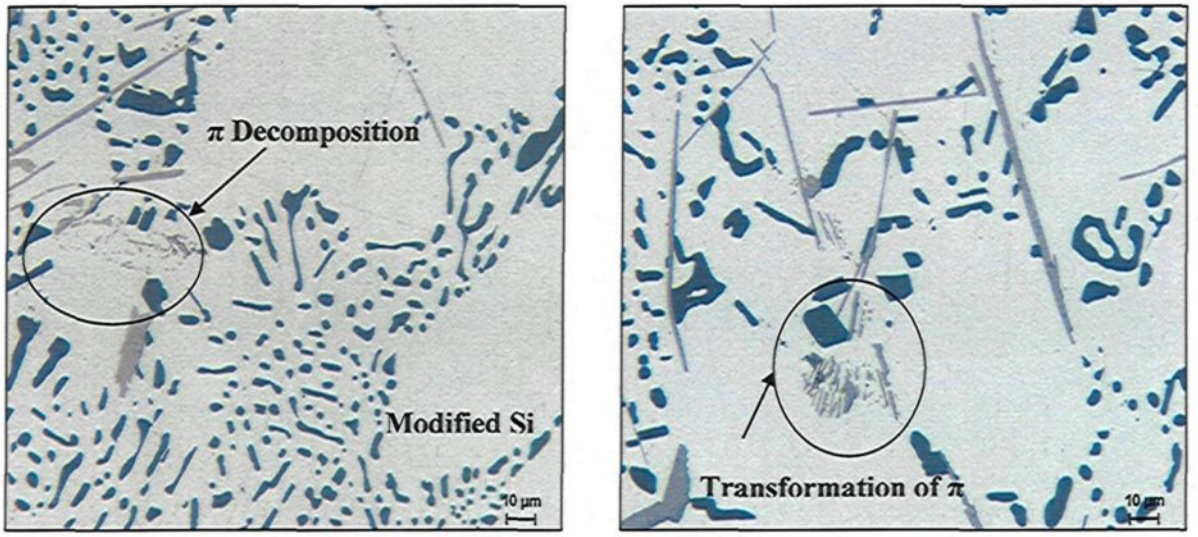

(a) (b)

Figure 4.6

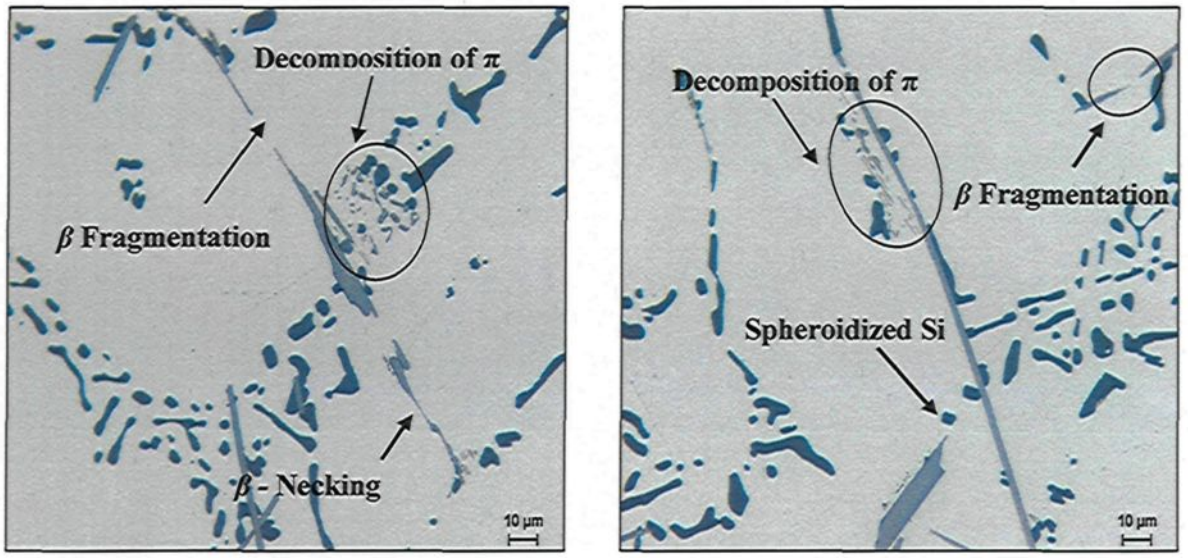

(c) (d)

Figure 4.6 Optical micrographs of Sr-modified solution heat-treated 356 alloys containing: (a) 0.1% Fe, (b) 0.2% Fe, (c) 0.35% Fe, and (d) 0.9% Fe, showing the decomposition of the π-phase and the formation of small new β-needles in the microstructure.

4.3 HARDNESS OF 356 ALLOYS

The type, size, and distribution of the hardening phases which precipitate during the aging process depend to a great extent on the chemical composition of the alloy, on the alloying additives, and on both aging temperature and time. These precipitated phases contribute strongly to the improvement of the hardening of the alloy, particularly at the peak-aged stage. In addition, the distribution of Si particles and the intermetallic phases present in the microstructure play a vital role in determining the hardness and strength values of aluminum-silicon casting alloys. All the foregoing factors emphasize the importance of studying the complex process-structure-property interdependence to be observed in aluminum-silicon alloys.

4.3.1 Effects of Aging Temperature

Figure 4.7 represents the hardness behavior of both non-modified and Sr-modified A356 alloys after aging for 4 hrs at different aging temperatures. [112] It will be observed that changing the aging temperature from 155°C in the case of the under-aged stage to 180°C in the peak-aged stage transforms the GP zones (β'') to semi-coherent β' rod-like particles. This transformation to semi-coherent particles intensifies the internal stresses on the atomic lattice, making the motion of dislocations more difficult. These aspects were observed in the behavior of both non-modified and Sr-modified alloys displaying maximum hardness value after 4 hrs of aging.

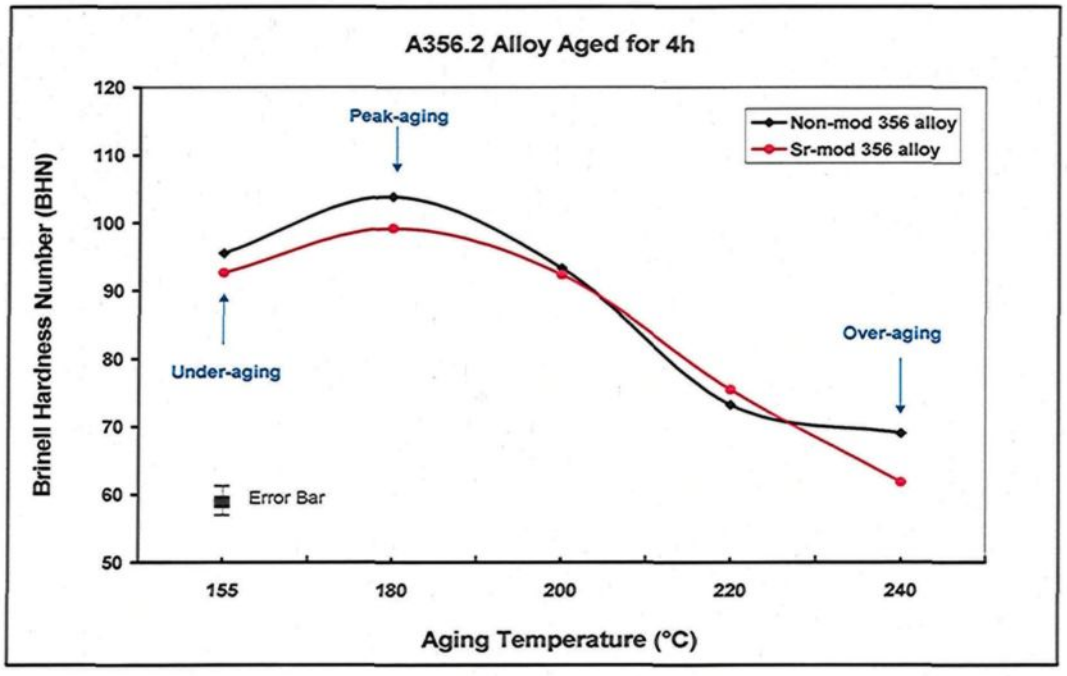

Figure 4.7 Hardness behavior of non-modified and Sr-modified 356 alloys aged for 4 hrs at different temperatures. [112]

Similarly, as reported in previous studies on the aging characteristics of 356 type-alloys, peak hardness was observed after 4 hrs of aging at 180°C, regardless of the alloy composition for both non-modified and Sr-modified alloys, as shown in Figure 4.8. It will also be observed that 356 alloys containing high levels of iron, namely 1 wt%, exhibit the highest hardness values, a fact which may be attributed to the high volume fraction of the intermetallic phases, particularly with regard to iron-based intermetallics, as is evident from Figure 4.5. Further aging at 220°C is observed to soften the alloy and hence a reduction in the hardness values is obtained in this stage (termed over-aging). It is clear that the changes in the morphology of the precipitation-hardened phases during the various stages of aging have a great impact on hardness behavior. Also, the alloys containing high iron levels in both non-modified and Sr-modified cases exhibit higher hardness values.

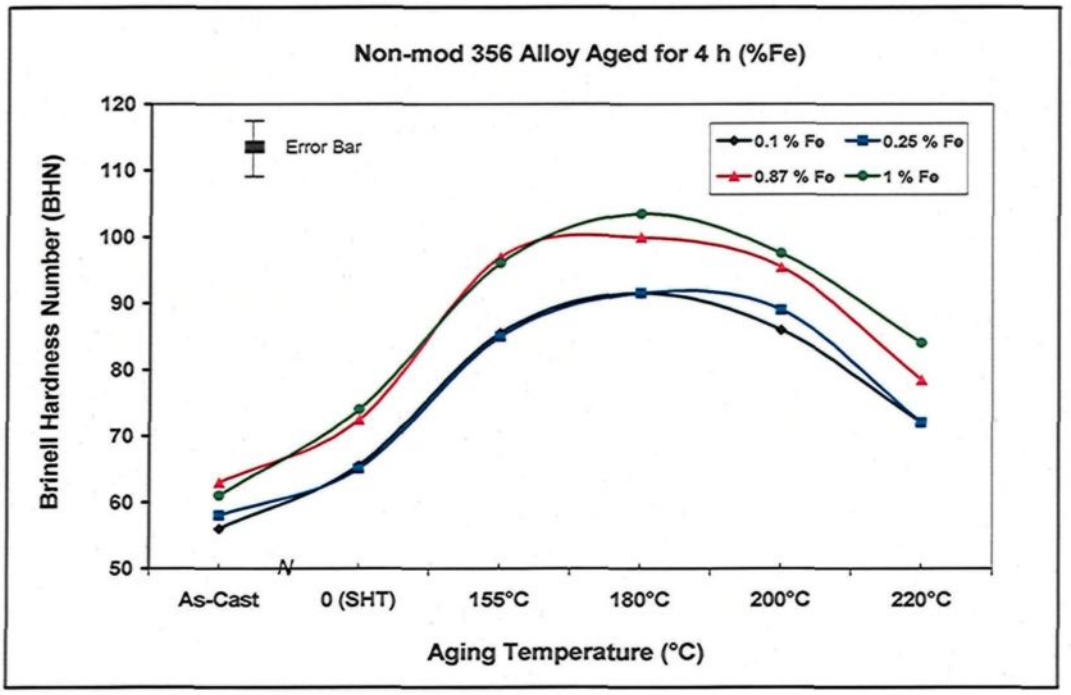

(a)

Figure 4.8

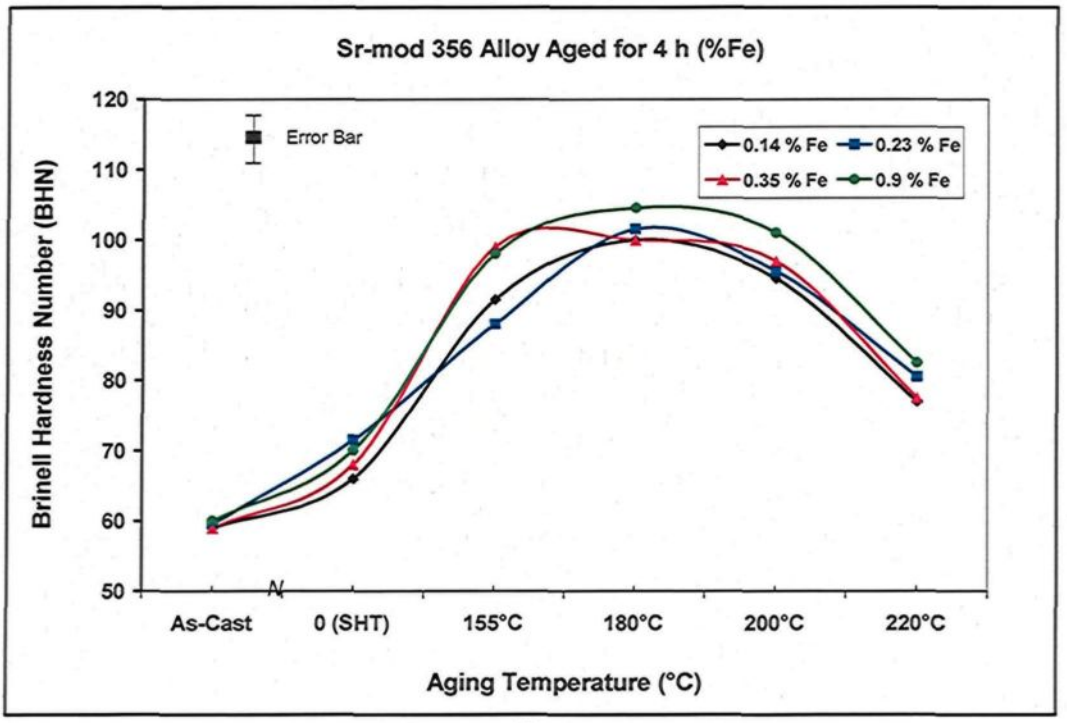

(b)

Figure 4.8 Hardness behavior of 356 alloys containing four levels of iron and aged for 4 hrs at different temperatures: (a) non-modified alloys, and (b) Sr-modified alloys.

4.3.2 Effects of Aging Time at 180°C

The effects of various aging times at 180°C on the hardness values of 356 alloys are shown in Figure 4.9. An aging time of 2 hrs is sufficient to reach the maximum hardness peak at this temperature in the case of both non-modified and Sr-modified alloys. Increasing the aging time further appears either to bring about slight changes in the hardness values or to leave them almost unchanged, thereby showing a plateau spread. The alloys containing high levels of iron acquire a higher volume fraction of iron-intermetallic phases, and they thus show higher hardness values regardless of alloy conditions.

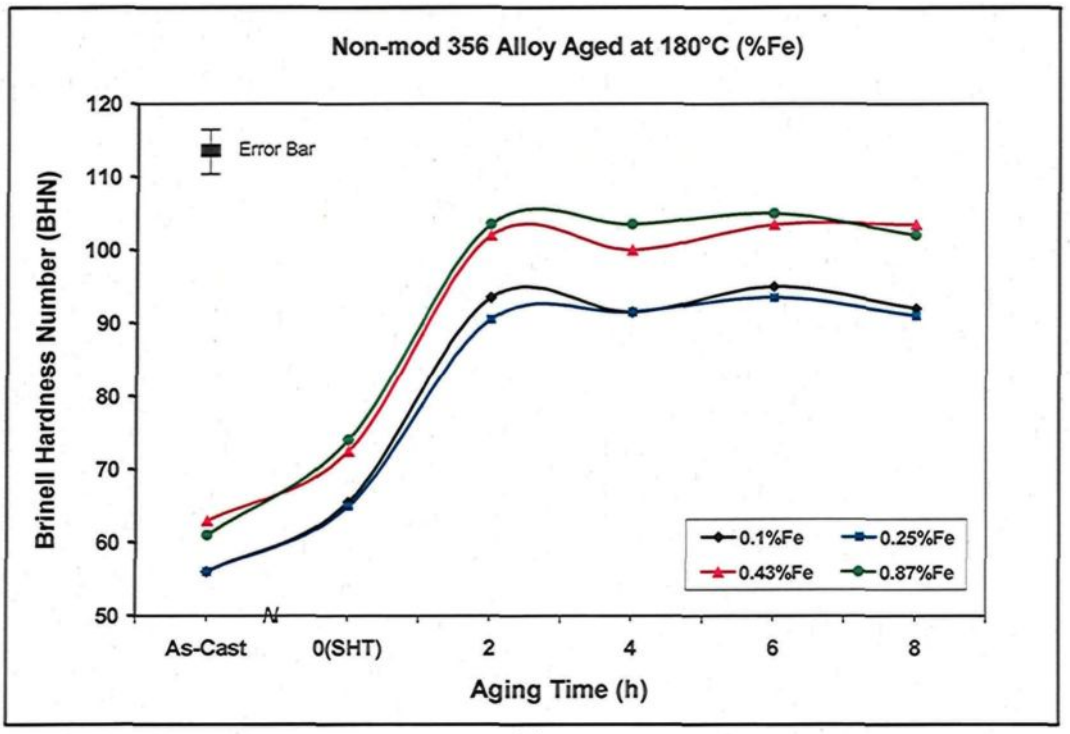

(a)

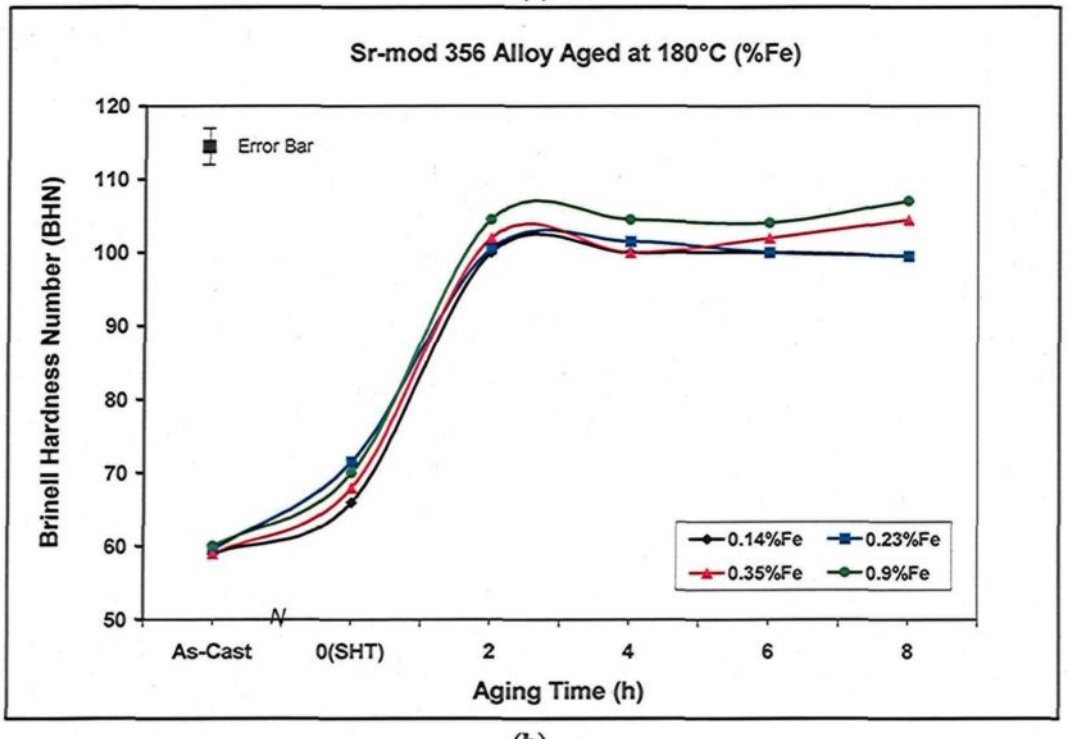

(b)

Figure 4.9 Effects of aging time on the hardness behavior of 356 alloys containing four levels of iron and aged at 180°C: (a) non-modified alloys, and (b) Sr-modified alloys.

4.3.3 Effects of Aging Time at 220°C

It is worth noting, from Figure 4.10, that aging at higher temperatures results in the maximum hardness value in the peak-aging stage after relatively short aging times, 2 hrs in this case. Such an aging temperature of 220°C provides the thermal activation energy required to nucleate and grow the β'(Mg_2Si) intermediate hardening phase. Increasing the aging time further results in a noticeable drop in the hardness values as a result of the coarsening of the hardening phase, in turn leading to softening in both non-modified and Sr-modified alloys. As before, alloys containing high levels of iron, namely 0.8 wt%, exhibit higher hardness values as a result of their high volume fraction of hard iron-bearing intermetallic phases, as may be observed from Figure 4.5.

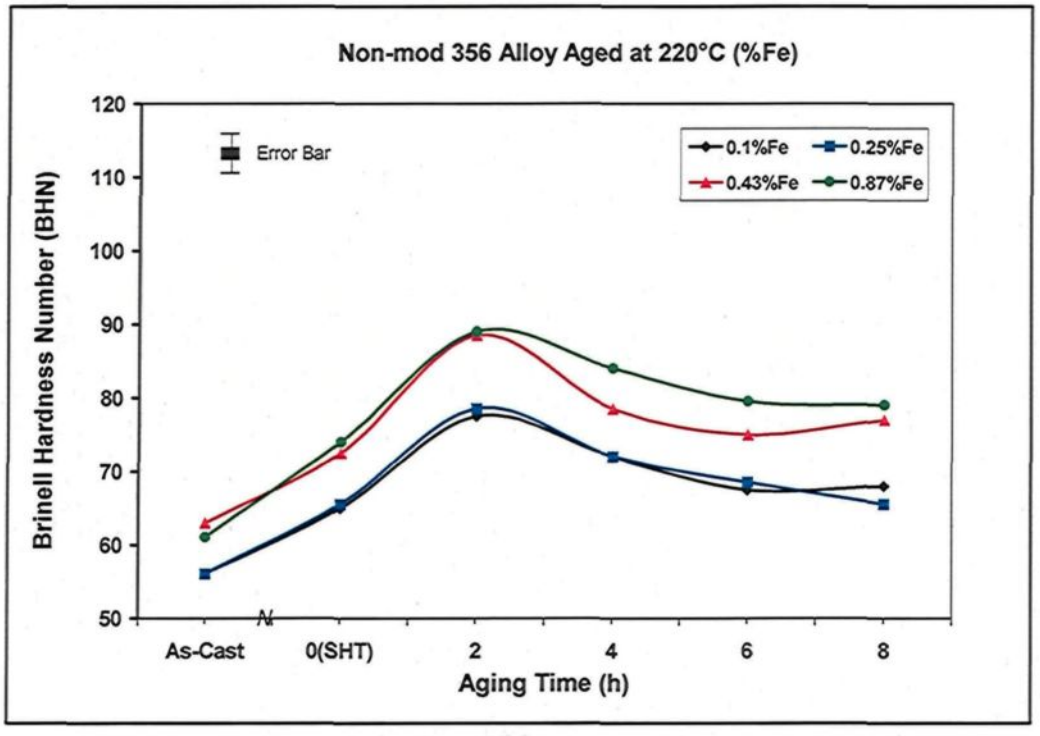

(a)

Figure 4.10

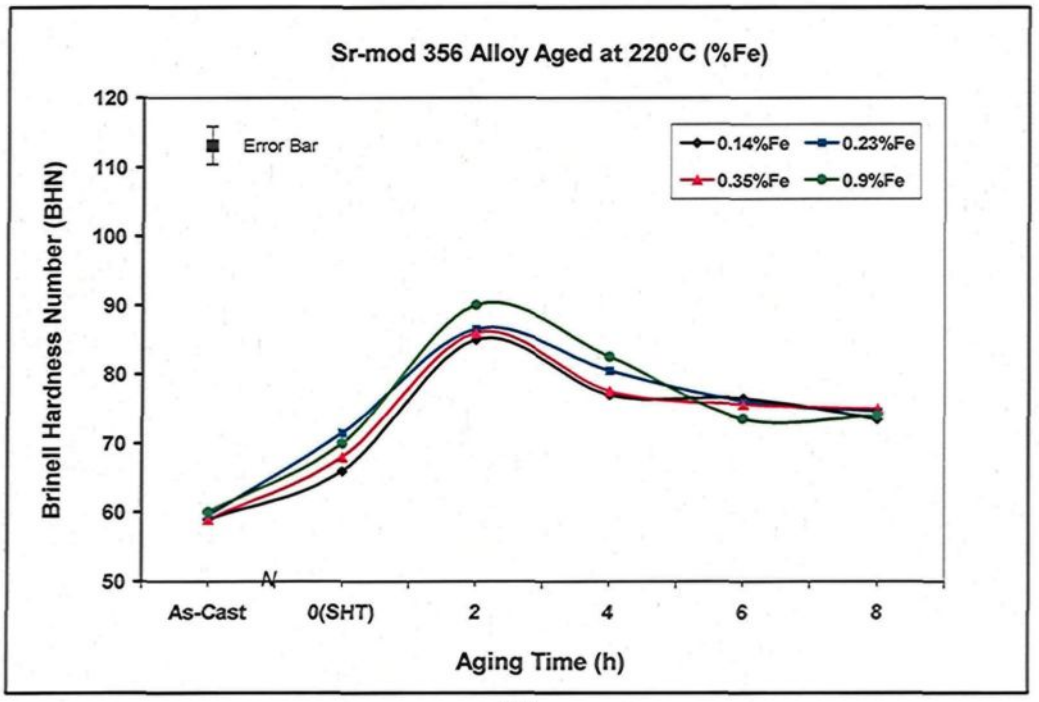

(b)

Figure 4.10 Hardness values as a function of aging times for 319 alloys aged at 220°C: of (a) non-modified alloys, and (b) Sr-modified alloys.

4.4 HARDNESS OF 319 ALLOYS

Figure 4.11 shows the variation of hardness values in A319 alloys in the presence of different aging temperatures during the aging process, as reported in a previous study.[112] This figure provides a clear description of the relationship which exists between the precipitation sequence of the hardening phase and the hardness values themselves, representing an example of a key microstructure-property inter-relationship. Two different peaks of maximum hardness are obtained for non-modified alloys, at 200°C and 240°C aging temperatures.

On the other hand, peak hardness may also be observed after 4 hrs of aging at 200°C in the case of Sr-modified alloys for which the formation of a coherent Al_2Cu phase produces the maximum impedance for dislocation motion at this stage. The

coarsening of the Al_2Cu phase with the application of further aging results in noticeable alloy softening and a drop in hardness values.

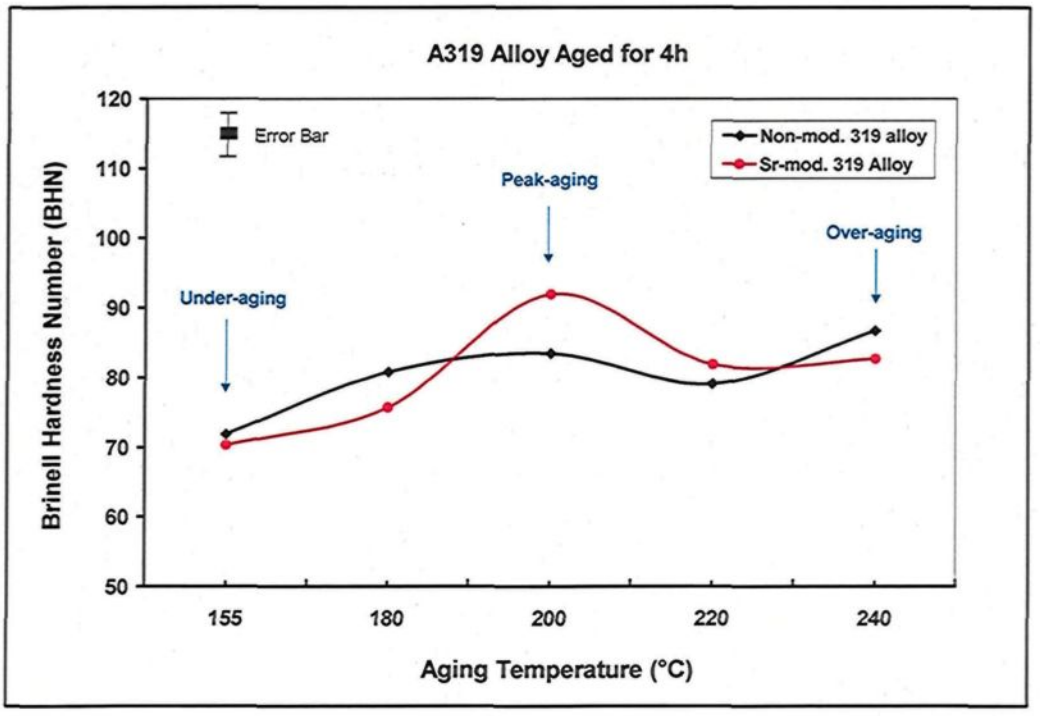

Figure 4.11 Variation of hardness values with aging temperature for non-modified and Sr-modified 319 alloys after 4 hrs aging. [112]

4.4.1 Effects of Aging Temperature

Chemical composition is frequently reported to influence the precipitation behavior of an alloy under aging conditions. The response of 319 alloys seems to be somewhat diverse as opposed to those containing Mg as a major alloying element such as 356 alloy. Figure 4.12 shows the hardness values of 319 alloys which were obtained from the work of Tash *et al.* [113] It will be observed from the fugure that the hardness values increase with increasing aging temperatures, regardless of the alloy composition

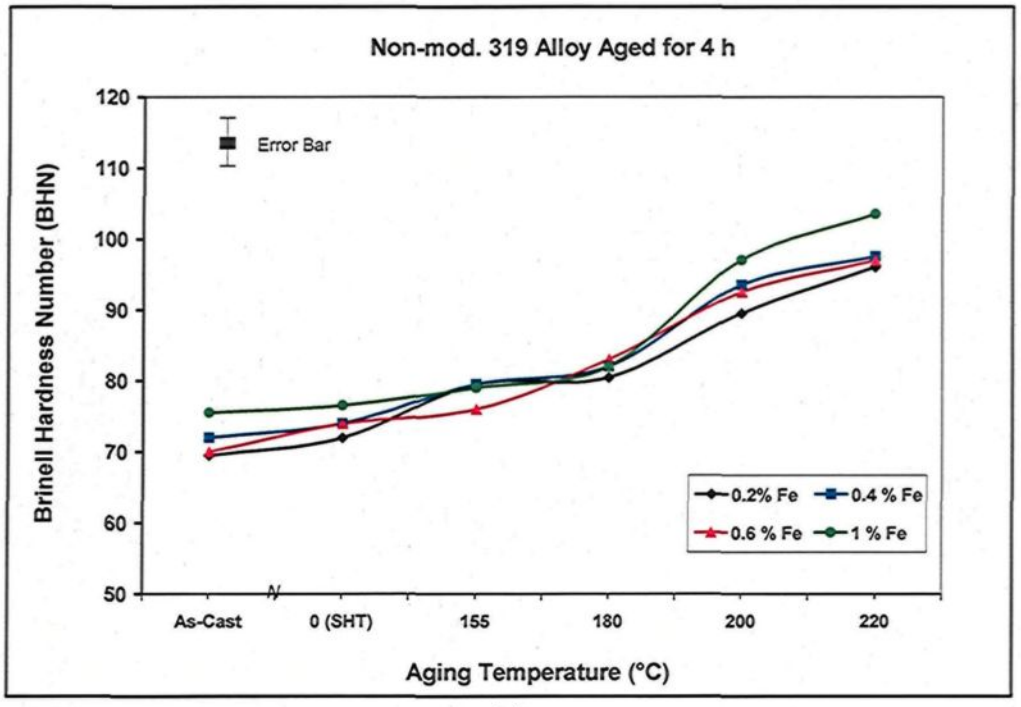

(a)

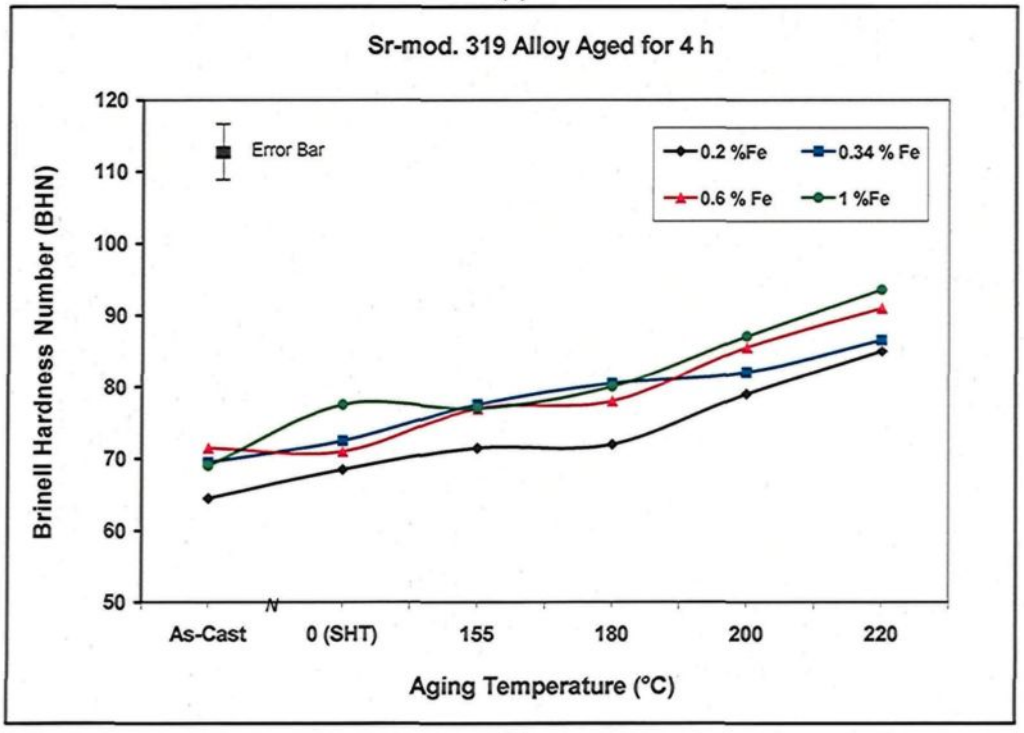

(b)

Figure 4.12 Hardness behavior of 319 alloys containing four levels of iron and aged for 4 hrs at different temperatures: (a) non-modified alloys and (b) Sr-modified alloys.

and the condition prevailing. Aging at high temperatures such as 220°C appears to result in higher hardness values than those obtained at 200°C. Also, as to be expected from the high volume fraction of the intermetallics present, the 319 alloys containing high levels of iron show higher hardness values in the entire range of alloys at almost all aging temperatures.

The non-modified alloys have higher hardness values compared to the Sr-modified alloys, as may be seen clearly in Figure 4.12. The fragmentation and partial dissolution of hard β-iron particles as a result of application of both Sr addition and solution treatment may explain the reason for obtaining lower hardness values in the case of Sr-modified alloys. In addition to the above reasons, the increase in the proportion of the soft ductile α-Al in the matrix resulting from the depression of the eutectic temperature with the addition of Sr would tend to enhance the lower hardness values obtained in this case.

4.4.2 Effects of Aging Time at 180°C

Figure 4.13 shows the effects of various aging times at 180°C on the hardness behavior of 319 alloys. It will be observed that increasing the aging time only causes slight changes in the hardness values, whereas 8 hrs of aging time results in a noticeable increase in the hardness values for all the non-modified alloys, as shown in Figure 4.13 (a). On the other hand, the hardness values for Sr-modified alloys remain virtually unchanged with increase in aging time.

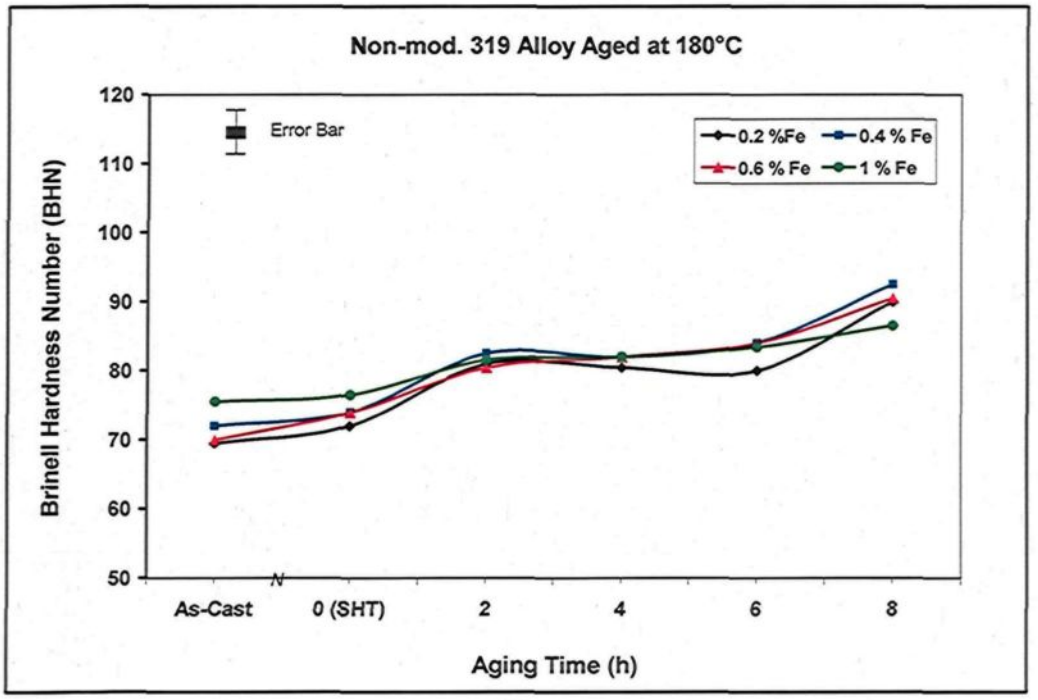

(a)

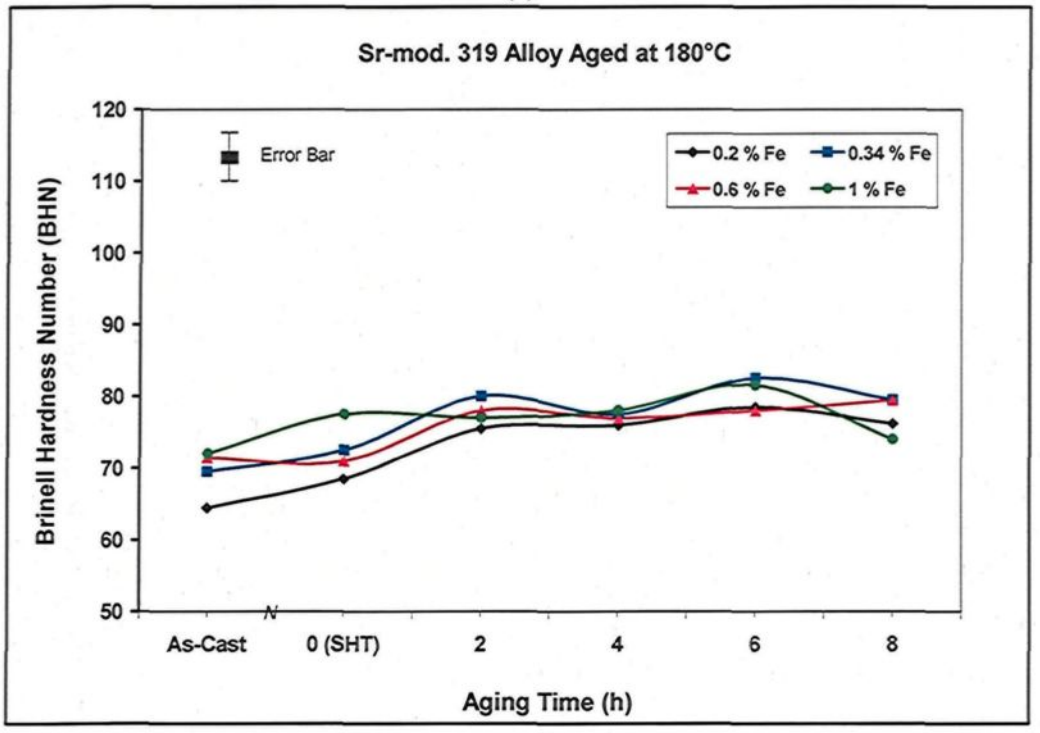

(b)

Figure 4.13 Effects of aging time on the hardness behavior of 319 alloys containing four levels of iron and aged at 180°C for different times: (a) non-modified alloys, and (b) Sr-modified alloys.

4.4.3 Effects of Aging Time at 220°C

The hardness behaviour of 319 alloys at 220°C is somewhat different from that observed at 180°C aging temperature when comparing Figure 4.14 with Figure 4.13. It is clear also from Figure 4.14 that the hardness values are higher at 220°C than at 180°C. The hardness values show a slight decrease or remain almost unchanged with increasing time up to 8 hrs, regardless of alloy composition, as shown in Figure 4.14. The application of relatively high aging temperatures, for long aging times in this case, provides the driving force and the thermal energy for the rapid coarsening of the precipitation-hardened particles, resulting in a softening of the alloys. The aging process is known to have no effect on the morphology of the iron-based intermetallic phases, thus the high Fe-content alloys always display higher hardness values.

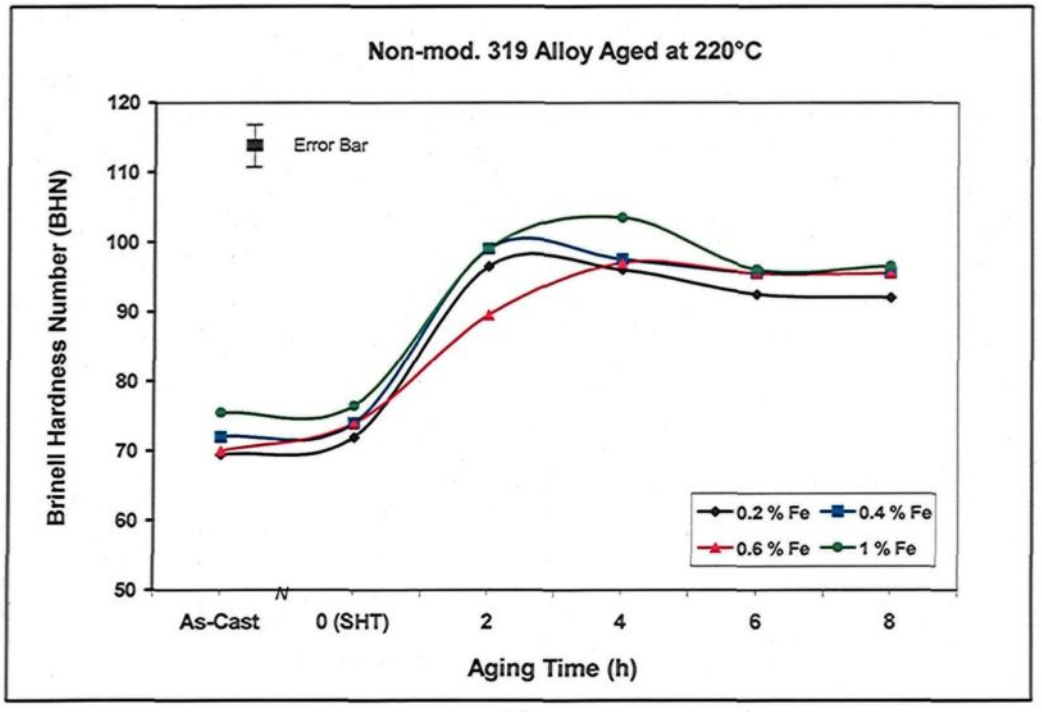

(a)

Figure 4.14

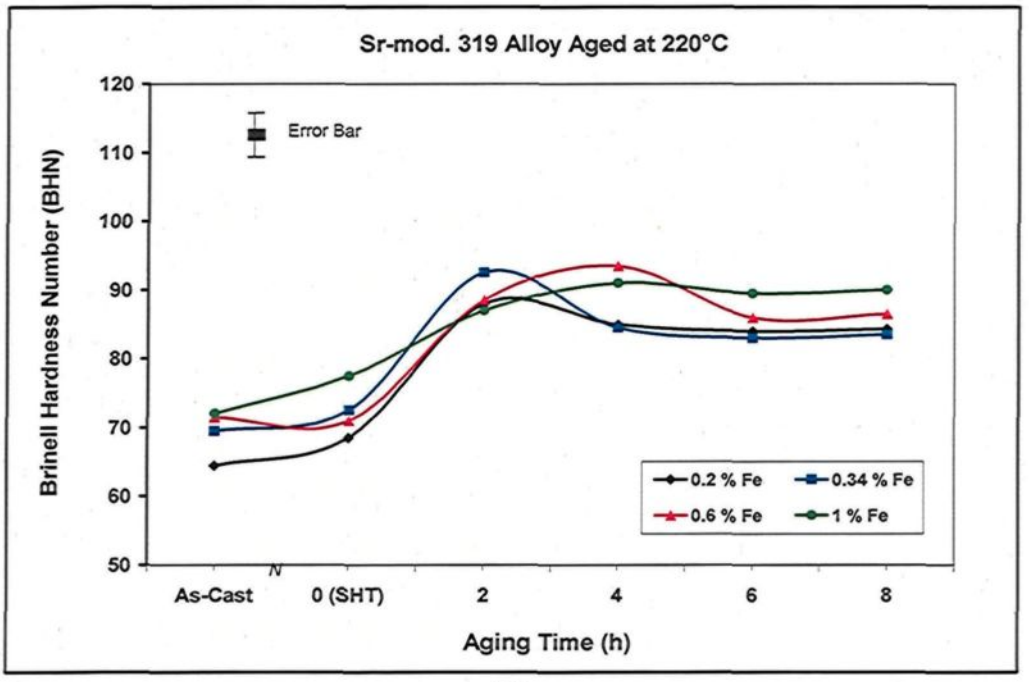

(b)

Figure 4.14 Effects of aging time on the hardness behavior of 319 alloys containing four levels of iron and aged at 220°C for different times: (a) non-modified alloys, and (b) Sr-modified alloys.

4.5 HARDNESS OF NEAR-EUTECTIC 396 ALLOYS

4.5.1 Effects of Aging Temperature

Near-eutectic 413 type alloys containing ~11 wt% Si are known for their weak response to precipitation hardening because of the low Cu content in such alloys. [112] The newly developed 396-type alloys contain 2.7 wt% Cu and 0.4 wt% Mg, where these alloying elements improve the response and precipitation behavior of these alloys during the aging process.

Figure 4.15 reveals the effects of aging temperature on the hardness values of 396 alloys containing 0.46 wt% Mn. It is clear that a period of 4 hrs of aging at 180°C is capable of producing the maximum hardness value during the peak-aging stage. As the

aging temperature increases, the precipitated particles coarsen, leading to a softening of the alloys; consequently, a continuous reduction in the hardness values is observed.

These 396 alloys containing a high Mn-content of 0.46 wt% display higher hardness values compared to both 319 and 356 alloys. The high Mn-to-Fe ratio of ~1.1 in the 396 alloy promotes the precipitation of the iron-bearing intermetallic phase in the form of sludge particles having a sludge factor of ~1.4, which increases the hardness values for such alloys. Again, it is obvious that the features of the microstructure regulate the hardness values of these alloys to a strong degree.

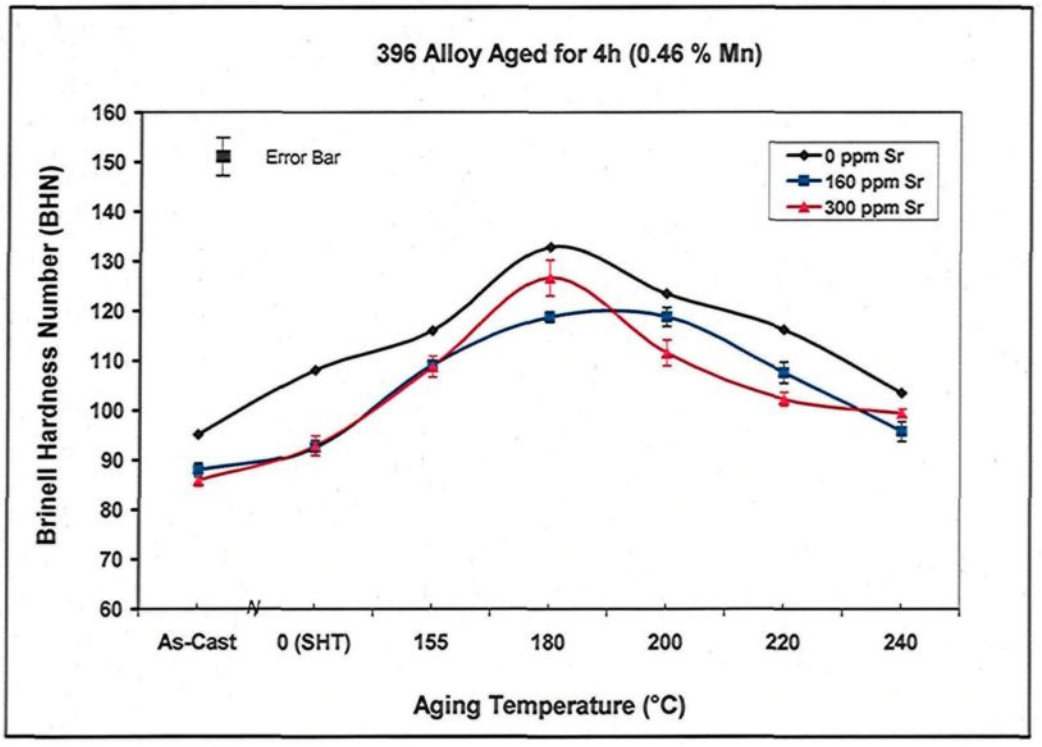

Figure 4.15 Hardness behavior of 396 alloys containing 46 wt% Mn and three levels of Sr addition, and aged for 4 hrs at different temperatures.

4.5.2 Effects of Aging Time

The effects of aging time on the hardness values of 396 alloys at aging temperatures of both 180°C and 220°C is shown clearly in Figure 4.16. It will be observed that the hardness values increase after 2 hrs of aging at 180°C compared to the solution heat-treated condition. The hardness values remain almost unchanged with further aging times, as shown in Figure 4.16 (a). The same effects of aging time may be observed at 220°C aging temperature, although, a gradual and steady reduction in hardness values is observable with further aging times for all the 396 alloys investigated, as is clearly evident from Figure 4.16(b). Also, aging at high temperatures, such as 220°C, results in alloy softening which implies that lower hardness values will be obtained in this case compared to those obtained at 180°C.

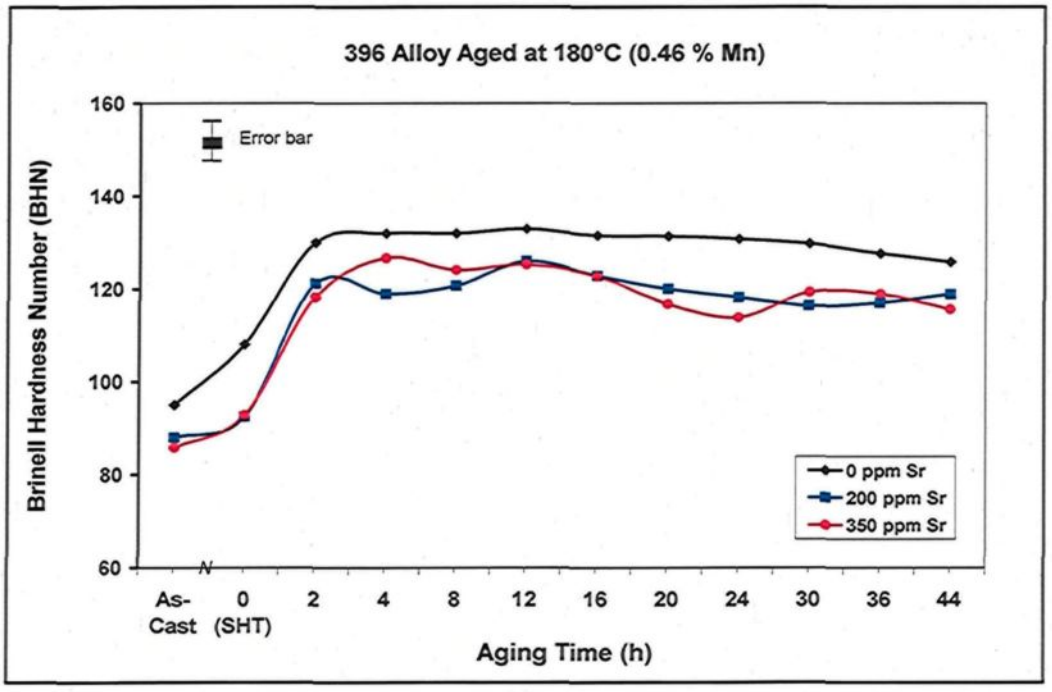

(a)

Figure 4.16

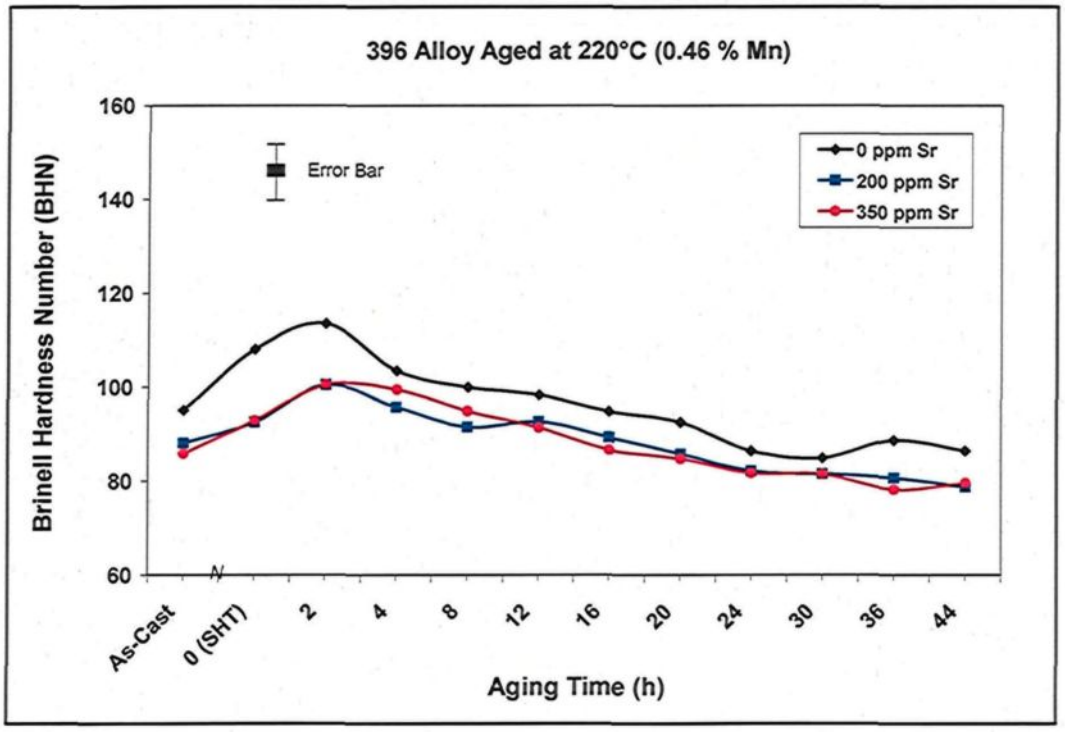

(b)

Figure 4.16 Effects of aging time on the hardness values of 396 alloys containing 0.46 wt% Mn and three levels of Sr addition, aged at (a) 180°C, (b) 220°C.

CHAPTER 5

IMPACT TOUGHNESS OF HYPOEUTECTIC ALLOYS

CHAPTER 5

IMPACT TOUGHNESS OF HYPOEUTECTIC ALLOYS

5.1 INTRODUCTION

Toughness is a mechanical term which is used in several contexts; it may be defined as a measure of the ability of a material to absorb energy up to the point of fracture. The geometry of the test specimen and the manner of load application are among the significant factors involved in determining this property. For high strain-rate loading conditions (dynamic), toughness may be assessed by the application of an impact test in the presence of a notch which acts as a point of stress concentration. Fracture toughness, furthermore, is a property which gives an indication of the resistance of a material to fracture when a crack is present. For a low strain rate situation (static), toughness may be ascertained from the results of a tensile test through an examination of the stress-strain curves. In this case, toughness may be considered as the area under the curve up to the point of fracture. The units for toughness are the same as for resilience, *i.e.* energy per unit volume of material. Tough materials are frequently known to incorporate considerable values of strength and ductility which is a further essential mechanical property to be considered when measuring the toughness of any material; this parameter is a measure of the degree of plastic deformation that the material has sustained at fracture. Impact toughness may, therefore, be used as a significant assessment factor for the ductility of a material under a high rate of

deformation. A material which undergoes little or no plastic deformation upon fracture is termed a brittle material, whereas that which undergoes a large amount of plastic deformation is known as a ductile material. Figure 5.1 illustrates the mechanical behavior of both ductile and brittle materials. Although a brittle material displays higher yield strength values than a ductile one, it appears to have lower toughness values which may be a result of the lack of ductility. Ductile materials are, therefore, considered to be tougher than brittle ones. This fact may be deduced by comparing the area under the stress-strain curves of both material types, as shown in Figure 5.1. It will be observed that the area $AB'C'$ of the ductile material is greater than the ABC area of the brittle material. [107]

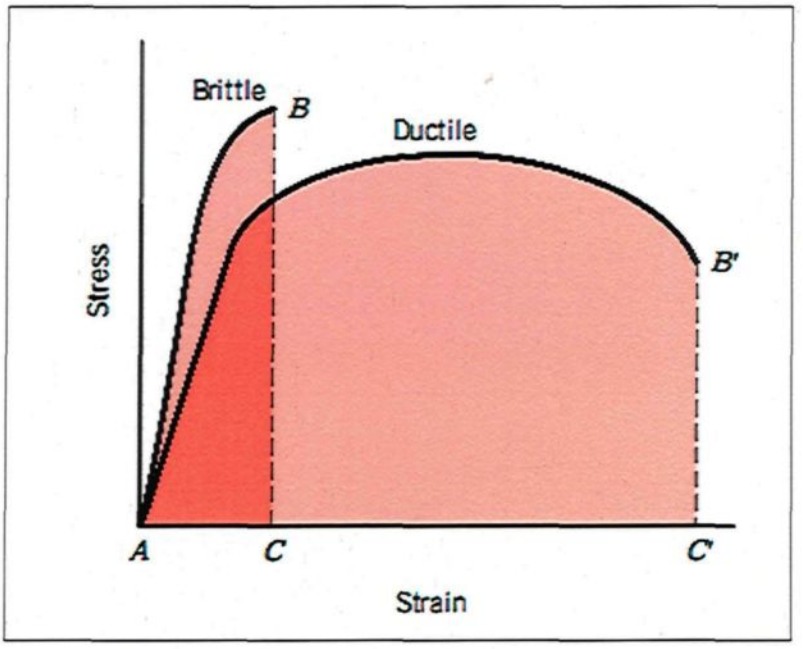

Figure 5.1 Schematic diagram showing the stress-strain curve obtained from a tensile test. [107]

A large number of studies have been undertaken to investigate the effects of alloying elements and heat treatment on the impact toughness of Al-Si alloys. These studies, did not, however, examine or discuss in any detail all of the relevant factors involved in studying this specific property. In the present work, the influence of individual additions of Fe or combined additions of Fe, Mn, and Mg on the impact toughness was investigated concomitantly with the accompanying aging conditions, to acquire a clear understanding of this pivotal property, in order to reach a balanced compromise between the impact toughness and hardness values. This aspect of the study would facilitate in designing and selecting the proper chemical composition and heat treatment suitable for a specific alloy in order to meet the service conditions required of Al-Si castings. The results of the Charpy impact energy properties for both 356 and 319 hypoeutectic alloys will be introduced and discussed in this chapter to evaluate the toughness behavior of such essential Al-Si cast alloys when subjected to high rates of deformation.

5.2 356 ALLOYS

According to the data presented in the chapter reviewing the literature, it is clear that both the structural fineness and the morphology of the microstructural constituents govern the impact toughness to a large degree. These constituents often include α-aluminum dendrites, the eutectic Si phase, and a variety of interdendritic intermetallic phases. The microstructural constituents are also observably affected by the aging treatment conditions applied.

5.2.1 Effects of the Addition of Fe

The effects of the addition of iron, solution heat treatment, and Sr modification on the impact values of the 356 alloy are listed in Table 6 (see Appendix 2). The absorbed impact values appear to decrease considerably with an increase in the iron content from 0.1 wt% to 0.9 wt% Fe for all the 356 alloys conditions, as shown in Figure 5.2. Increasing the volume fraction of the harmful β-iron platelets with increasing iron content provides more sites for crack nucleation and thus facilitates the initiation of cracks which may explain the reduction in the impact energy values.

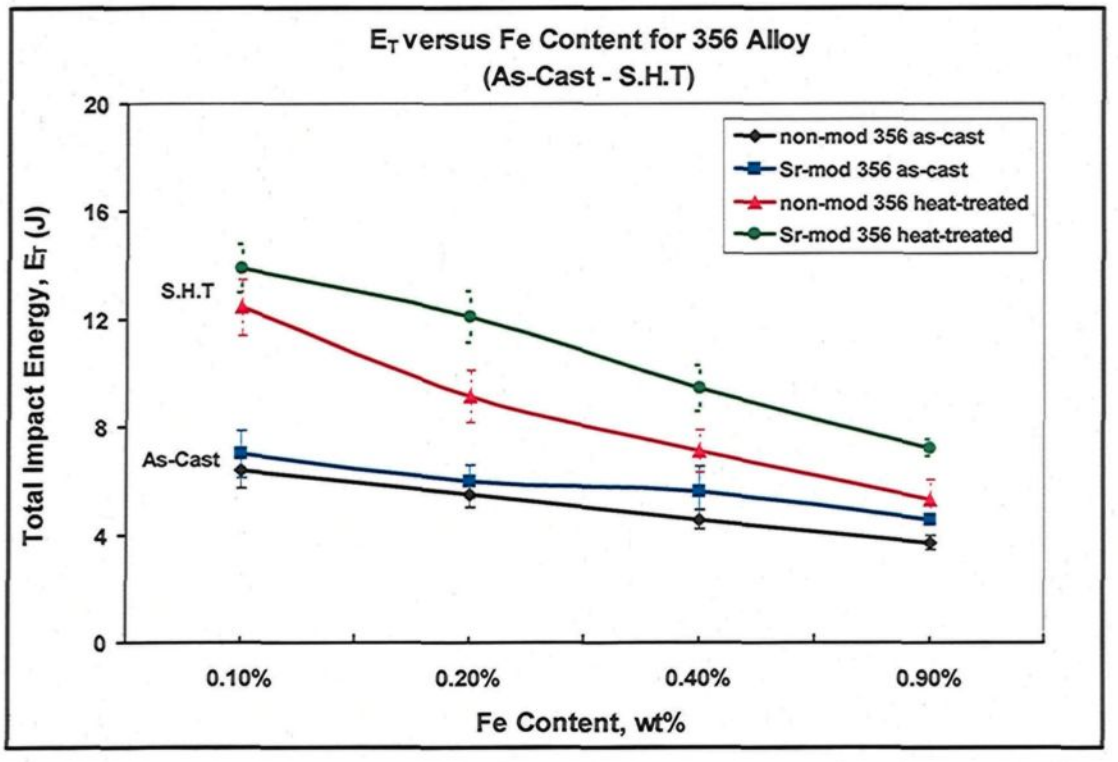

Figure 5.2 Total impact energy as a function of Fe content for non-modified and Sr-modified 356 alloys in the as-cast and solution heat-treated conditions.

These findings are in fairly satisfactory concurrence with a previous study carried out by Ma *et al.* [114] on the effects of Fe content on the impact toughness of 356 alloys. The authors revealed that, regardless of the cooling rate, the lowest iron-containing alloys display the highest impact energy values, particularly in the case of the Sr-modified alloys.

With the addition of Sr to the 356 alloys, the morphology of the eutectic Si phase changes to a fibrous form, leading to a reduction in the number of crack initiation sites in the matrix. As a result, the impact values show an improvement because of the increase in the energy for crack initiation in the matrix, regardless of the level of iron content. This improvement, however, seems to be fairly slight because of the apparent increase in the level of porosity in the microstructure associated with the addition of Sr; this increase in porosity may be considered one of the main disadvantages of using Sr as a modifying agent for Al-Si alloys.[19, 56, 115]

The T4 temper applied at 540°C for 8 hrs followed by natural aging for 24 hrs at room temperature significantly improves the impact energy values of both non-modified and Sr-modified 356 alloys containing 0.1 wt% Fe; this represents an increase of about 95% and 117%, respectively. The improvement observed in the impact values after the application of the T4 temper supports the work of Shivkumar *et al.* [56] on the impact properties of A356 alloys. Their results reveal that the application of solution treatment at 550°C for a relatively short solution time, *e.g.* 2 hrs, is capable of producing a considerable enhancement in the impact energy values of both non-modified and Sr-modified alloys, as is shown clearly in Figure 5.3. The maximum impact energy was 26 J, obtained after a solution time of 168 hrs.

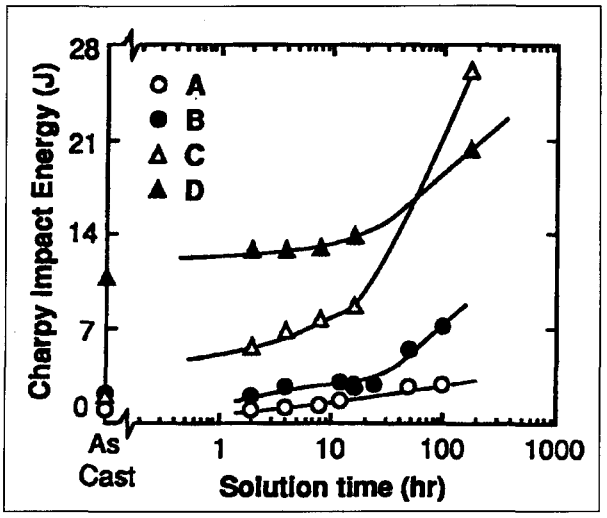

Figure 5.3 Effects of solution time on the Charpy impact energy in A356 castings. Sand castings: A, non-modified; B, Sr-modified; Metallic mold castings: C, non-modified; D, Sr-modified. [56]

With a view to evaluating the impact behavior of 356 alloys, the individual or combined effects of the application of Sr-modification and solution treatment on such behavior may be analyzed based on the fracture mechanism of the alloys under investigation. The fracture process of Al-Si alloys consists mainly of two components, the initiation of microcracks and the propagation of these cracks to form the final fracture. Microcracks are often initiated at the sites or regions of high stress concentrations present in the matrix. [44] For Al-Si alloys, these sites are likely to have originated at the sharp edges found at the extremity of acicular Si particles and β-iron platelets as well as at the interface between the second phase particles and the matrix. According to the chemical composition of the alloys investigated and the conditions involved in the present study, such sources for crack initiation are expected to be present in the matrix in large amounts. The purpose of Sr-modification, in this instance, is mainly to eliminate the area of high stresses located at

the extremities of Si particles and β-iron platelets. The slight increase observed in the impact values of 356 alloys after Sr-modification, however, makes it possible to conclude that the morphology of the eutectic phase, in this case, is not the only parameter controlling impact behavior; it should also be kept in mind that there is still the role of iron-based intermetallic phases which should be taken into consideration.

Solution heat treatment contributes significantly to decreasing the number of crack initiation sites through the spheroidization of eutectic Si particles, the dissolution of the brittle Mg_2Si phase, and the fragmentation of β-iron platelets as well as the transformation of the π-iron phase, as may be seen in Figure 4.6. All of the foregoing microstructural changes appear to improve the crack initiation resistance (CIR) of the matrix.

The propagation of microcracks in the matrix is governed by the ductility of the matrix to a great degree. Increasing the proportion of ductile α-Al dendrites in the matrix would certainly improve its resistance to crack propagation where the presence of large ligaments of this ductile matrix may act as an effective barrier to the advance and continuity of crack growth. Such an improvement in the crack propagation resistance (CPR) of the matrix may be obtained by increasing the proportion of ductile α-Al phase in the matrix through (i) the addition of Sr which depresses the eutectic temperature, [79] and (ii) the application of solution treatment leading to an increase in the inter-particle spacing which associated with the spheroidization and coarsening of the eutectic Si phase. [5, 56, 87]

All of the preceding data provides an indication that applying chemical modification together with solution treatment would result in significant improvements in the overall

impact energy values as a matter of course, together with the improvements occurring in both the crack initiation and crack propagation resistance of the matrix.

5.2.1.1 Effects of Aging Time at 180°C

The impact properties of 356 alloys are strongly regulated by the morphology and size of both eutectic Si and Mg_2Si phases as well as the iron-based intermetallic compounds. It is evident from the values of the impact energies listed in Table 7 (see Appendix 2) that aging at 180°C for different aging times from 2 hrs to 8 hrs reveals a negative effect on the impact behavior, as is also shown in Figure 5.4. This observation is evident from a comparison of Figure 5.4 with Figure 5.3 which show clearly the beneficial effect of solution heat treatment. These results are, in fact, to be expected since the aging process (T6 temper) is often applied to improve the strength of as-cast Al-Si-Mg alloys through precipitation-hardening, at the expense of ductility. These β'-Mg_2Si second phase particles with their needle-like shape impede the motion of dislocations leading to an increased buildup of such dislocations known as pile-ups. The micro-stresses originating at the interface between the second phase particles and the matrix as a result of dislocation pile-ups intensify the possibility of microcrack initiation at these interfaces.[44, 46] The impact properties, thus, continue to decrease with further increases in the aging time up to 8 hrs for both non-modified and Sr-modified 356 alloys, as shown in Figure 5.4. This reduction is thought to be primarily a result of the reduction in the resistance of the matrix to microcrack initiation.

Increasing the aging time to 12 hrs, however, results in a slight recovery in the impact energies of these alloys for both cases. Such minor restoration in impact energies

values may be ascribed to the coarsening of the Mg_2Si particles, leading to easy motion of dislocations and alloy softening which together increase the ductility of the matrix. All of the foregoing contribute to further increasing both the crack initiation and crack propagation resistance which implies that higher energies will be required for initiating and propagating the microcracks.

These results appear to be in good agreement with those obtained from the work of Nakayama *et al.* [67] regarding the effects of Mg additions and aging conditions on the impact energy of Al-Si alloys. The authors reported that the impact behavior displays a similar tendency after aging for greater periods of time at 145°C for both Al-2Si-0.3Mg and Al-7Si-0.3Mg alloys, as shown in Figure 2.31. Tsukuda *et al.*, [55] on the other hand, found that the impact values continue to diminish with further aging times of up to 12 hrs, as shown in Figure 2.30.

It will also be observed from Figure 5.4 that the Sr-modified 356 alloys display higher impact property values than non-modified ones for all aging times, regardless of the iron content. These higher values may be attributed to the microstructural differences between the Sr-modified and non-modified alloys in terms of the morphology and size of both eutectic Si particles and the iron-based intermetallics. From the data reported in the literature concerning the effects of iron in Al-Si alloys, it appears that there are no studies revealing or discussing any changes in the morphology and size of the iron-bearing intermetallic phases during the aging process. The impact energy values of high Fe-containing alloys thus remain virtually the same as those obtained under solution-treated

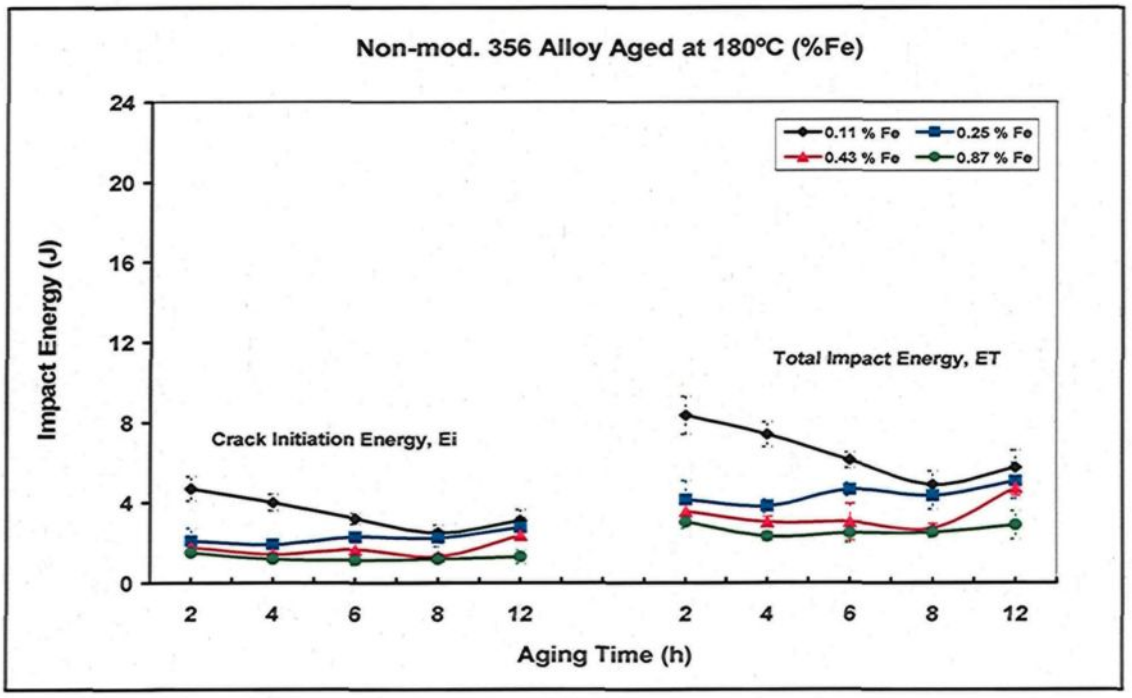

(a)

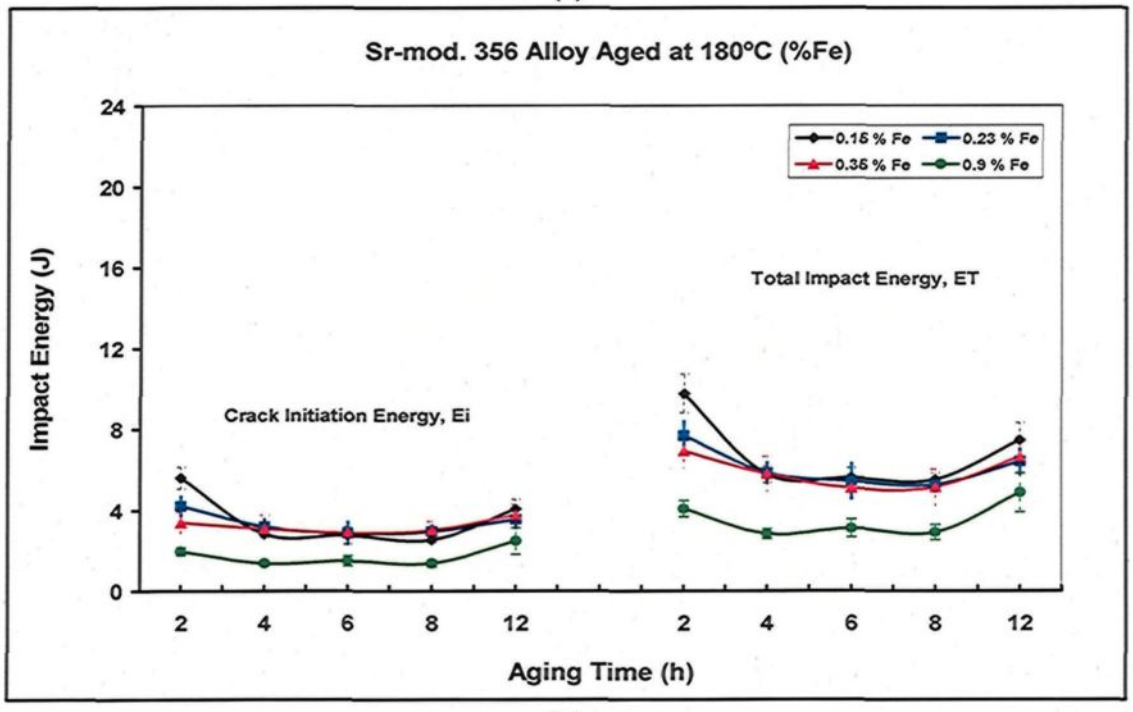

(b)

Figure 5.4 Impact energy as a function of aging time for 356 alloys containing four levels of Fe, and aged at 180°C: (a) non-modified alloys, and (b) Sr-modified alloys.

conditions. The lowest impact energy values were obtained from the 356 alloys containing 0.87 wt% iron in both cases.

5.2.1.2 Effects of Aging Time at 220°C

Aging at such a high temperature results in the softening of the alloys; this fact is evident from the higher impact energy values listed in Table 8 (see Appendix 2) which were obtained in the case of both non-modified and Sr-modified alloys compared to those obtained at an aging temperature of 180°C. The effects of matrix-softening on the impact values is more pronounced particularly after 12 hrs of aging when the highest impact energy values are obtained, as may be seen in Figure 5.5. The coarsening of the Mg_2Si phase at this over-aging stage facilitates the motion of dislocations and hence eliminates the tendency towards dislocation pile-ups at the interface between the precipitated-phase particles and the matrix. The possibility of the initiation of microcracks will thus diminish and the resistance of the matrix would certainly be improved as a result. Furthermore, the microstructural changes occurring after the application of solution treatment to the Sr-modified alloys also enhance the improvements to be observed in both the crack initiation and the crack propagation resistance of the matrix.

All of the above facts contribute significantly to the large impact energy values of about 20 J for the Sr-modified 356 alloy containing 0.1 wt% Fe after 12 hrs of aging at 220°C. Such a considerable improvement in the impact energy values appears superior not only to the corresponding values in the as-cast condition but also to those of the entire range of 356 alloys investigated. It will also be observed from Figure 5.5 that the behavior

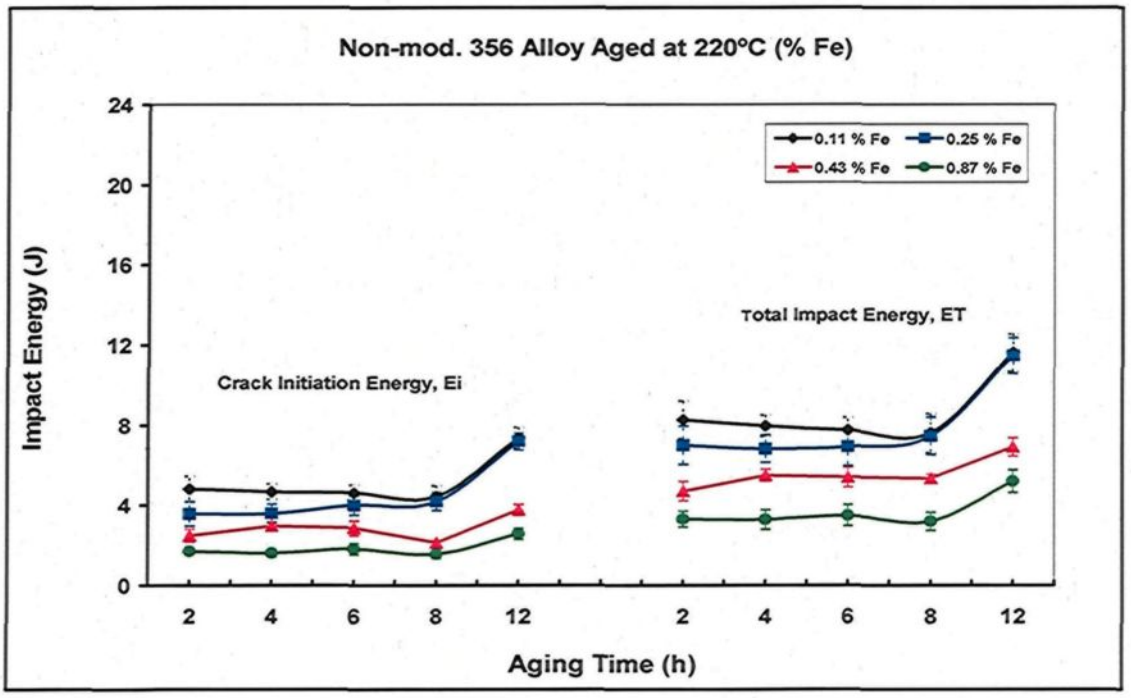

(a)

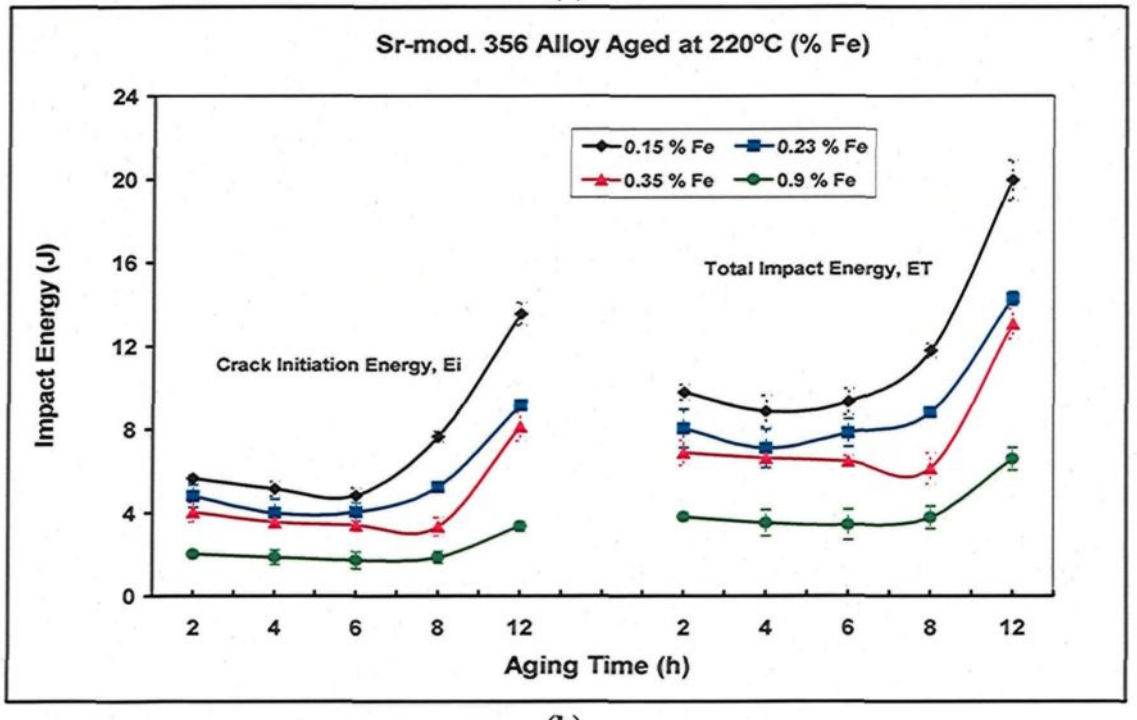

(b)

Figure 5.5 Impact energy as a function of aging time for 356 alloys containing different additions of Fe, and aged at 220°C: (a) non-modified alloys, and (b) Sr-modified alloys.

of crack initiation energy displays the same tendency as that of the total impact energy. This observation indicates that all the microstructural changes taking place as a result of the application of Sr-modification together with a T7 temper are more effective and pronounced in improving the crack initiation resistance (CIR) of the matrix than they are in conditions of solution treatment and aging at a temperature of 180°C.

5.2.2 Effects of Combined Additions of Fe and Mn

A number of approaches have been widely reported upon and recommended in previous studies either to balance or to level off the deleterious effects of iron-bearing intermetallic phases such as the β-Fe platelet phas on the mechanical properties of cast Al-Si alloys.[14, 71, 73, 74] One of these approaches involves the addition of neutralizing elements such as Mn and Cr where these elements tend to tie up with Al and Fe so as to form the more compact α-Fe intermetallic phase.[72] The average values of different impact parameters and their standard deviations for 356 alloys are summarized in Table 6. Also, it is obvious from Figure 5.6 that addition of Sr enhances the impact energy values of non-modified alloys as a result of the morphological changes occurring in the eutectic Si phase. This improvement may be ascribed to an increase in the matrix resistance to microcrack initiation as well as to an increase in the proportion of the ductile α-Al phase in the matrix. Applying the T4 treatment appears to develop the impact energy values to a noticeable degree, particularly for 356 alloys containing 0.22 wt% Fe and 0.1 wt% Mn, as shown in Figure 5.6.

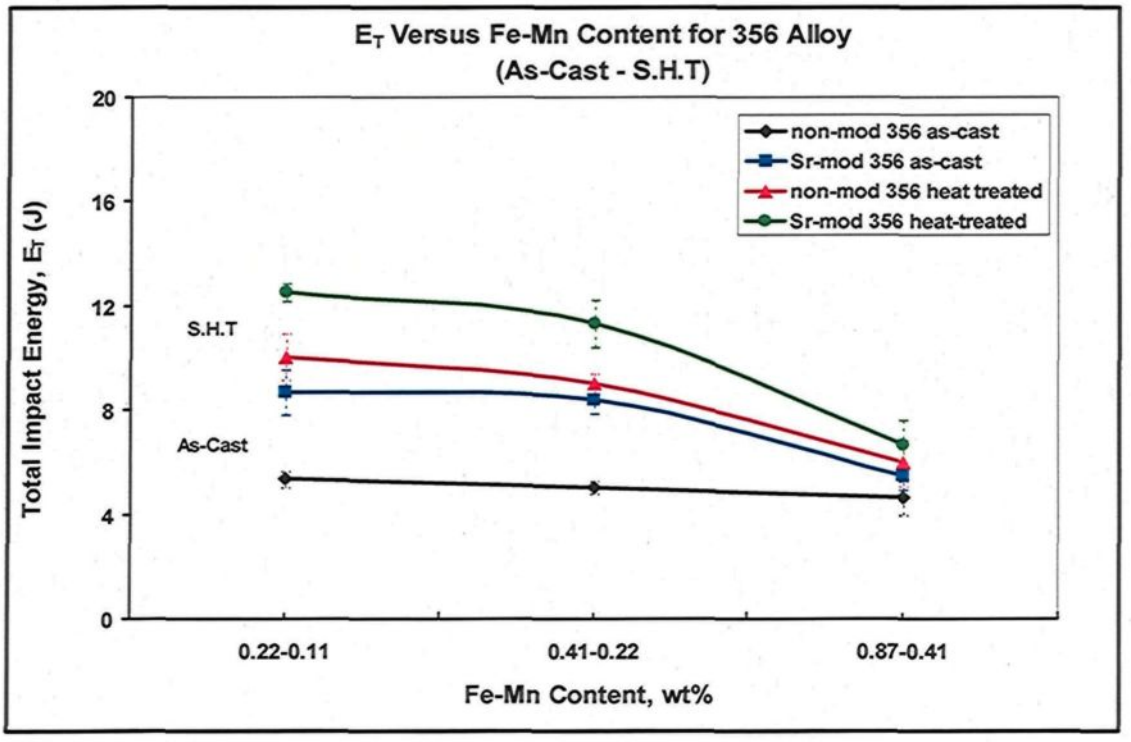

Figure 5.6 Total impact energy plotted against Fe-Mn content in non-modified and Sr-modified 356 alloys for the as-cast and solution heat-treated conditions.

The accelerated spheroidization and coarsening rates of the eutectic Si particles during solution treatment increase the inter-particle spacing and thus, also increase the proportion of ductile α-Al dendrites which separate the eutectic Si phase particles in the matrix. Such changes in the features of the microstructural constituents lead to a significant improvement in the resistance of the matrix to the crack propagation.[5] The dissolution of the brittle Mg_2Si particles after the application of a T4 temper also increases this improvement. The T4 treatment process thus succeeds in cutting down on as many sources for crack initiation in the matrix as is possible.

It is also worth noting from Figure 5.6 that the addition of 0.1 wt% Mn to non-modified as-cast 356 alloys seems to have no observable effect on the impact energy values as expected, when they are compared to those obtained for the same alloys containing only iron. The precipitation of iron as α-Fe Chinese-script particles within α-Al dendrites in this case results in diminishing the amounts of detrimental β-iron platelets, thereby leading to a certain amount of improvement in the resistance of the matrix to crack initiation (CIR). On the other hand, the strengthening effect resulting from the precipitation of α-Fe particles within the dendrites decreases the ductility of the matrix and hence weakens the resistance of the matrix to crack propagation (CPR). It appears that the increase in the CIR values may be negated by the decrease in those for CPR and this balance between the two components of total impact energy may explain the insignificant influence of the addition of 0.1 wt% Mn on the impact energy values of 356 alloys. Increasing the level of Mn addition up to 0.4 wt%, however, is observed to slightly improve the impact energy values for both non-modified and Sr-modified alloys compared to those containing only iron under the same conditions.

Kumari *et al.* [14] carried out an investigation on the effects of Mn addition with other elements on the mechanical properties of Al-7Si-0.3Mg-0.8Fe alloy. Their results indicate that an addition of 0.4 wt% Mn promotes the formation of the Chinese script α-Fe phase. No observable improvement in the impact strength values, however, was obtained for non-modified alloys containing 0.4 wt% Mn; it should be noted that these values appear to be less than those obtained for the as-cast non-modified alloy without any additives, as shown in Figure 5.7.

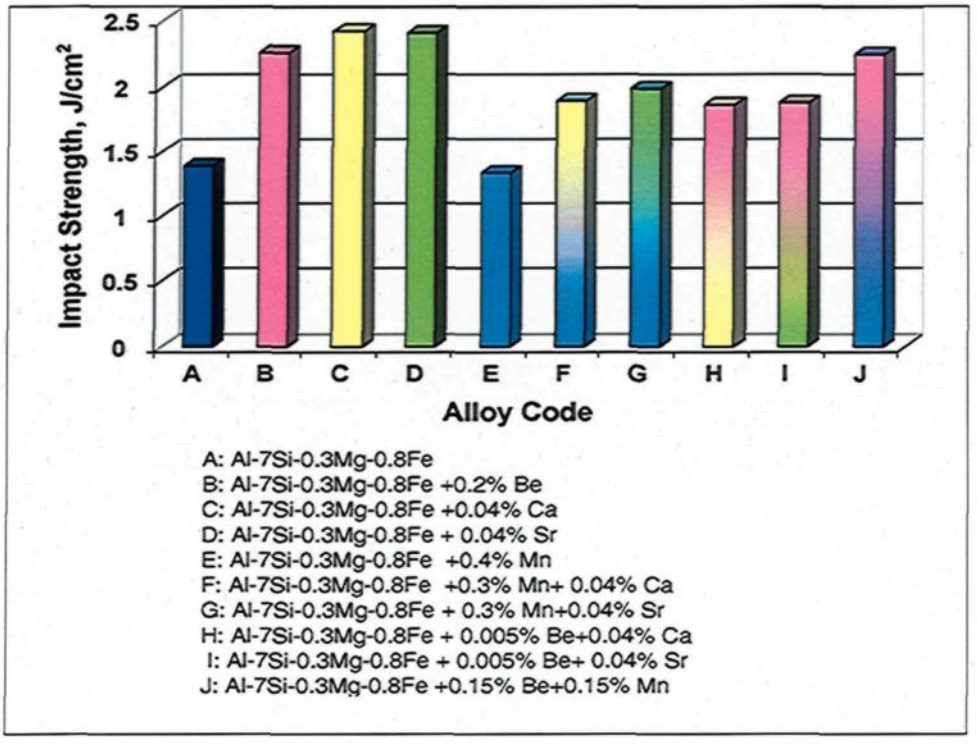

Figure 5.7 Effects of the addition of Be, Mn, Ca and Sr individual and in combination on the impact strength of Al–7Si–0.3Mg–0.8Fe alloy.[14]

5.2.2.1 Effects of Aging Time at 180°C

The addition of Mn to 356 alloys is well known to have no observable influence either on their response to the aging process or on the subsequent precipitation-hardening reactions. Table 9 provides the average values with their standard deviations for the different parameters which were determined from the instrumented impact test for non-modified and Sr-modified 356 alloys containing various levels of Fe and Mn additions. It will be observed, from Figure 5.8, that the impact energy displays virtually the same type of behavior as that observed in the alloys containing only iron, as shown in Figure 5.4. A

noticeable improvement in the impact energy values may be obtained after only 2 hrs of aging compared to those obtained in the as-cast condition for the alloys containing 0.1 wt% Fe. This improvement is to be expected since, in this case, the alloys are in the under-aged stage. The impact energy values, thereafter, decline over time to reach a minimum after 8 hrs of aging in view of the maximum hardness attained during the peak-aging stage.

Furthermore, increasing the aging time results in a noticeable recovery in the impact energy values for Sr-modified 356 alloys, particularly after the combined addition of 0.24 wt% Fe and 0.14 wt% Mn, as may be seen clearly in Figure 5.8(b) which shows the over-aging stage. The preceding changes in the shape of the hardening Mg_2Si phase during the different stages of the aging process thus significantly affect the impact behavior of these alloys. It may be concluded that a third parameter, which is the morphology of the Mg_2Si phase, controls the impact energy values mutually with the eutectic Si and iron-containing intermetallic phases in these conditions.

As mentioned previously, relatively higher impact values are frequently obtained for Sr-modified alloys containing 0.24 wt% Fe and 0.14 wt% Mn. The beneficial changes in the morphology and size of both eutectic Si and iron-based intermetallic phases associated with the addition of Sr and solution treatment may explain the incidence of these higher values. The influence of the aging process on the impact energies of the alloys containing combined additions of 0.9 wt% Fe and 0.4 wt% Mn is not apparent since these alloys possess a higher volume fraction of iron-bearing intermetallic compounds. Consequently, from Figure 5.8, it may be assumed that both the size and morphology of the

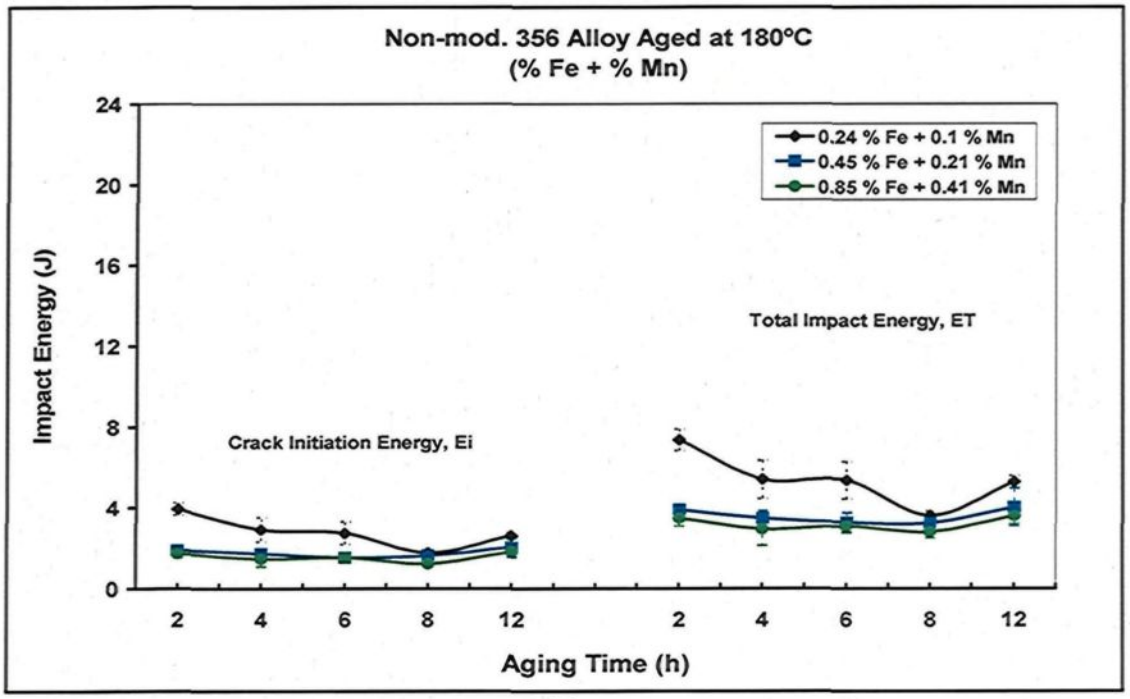

(a)

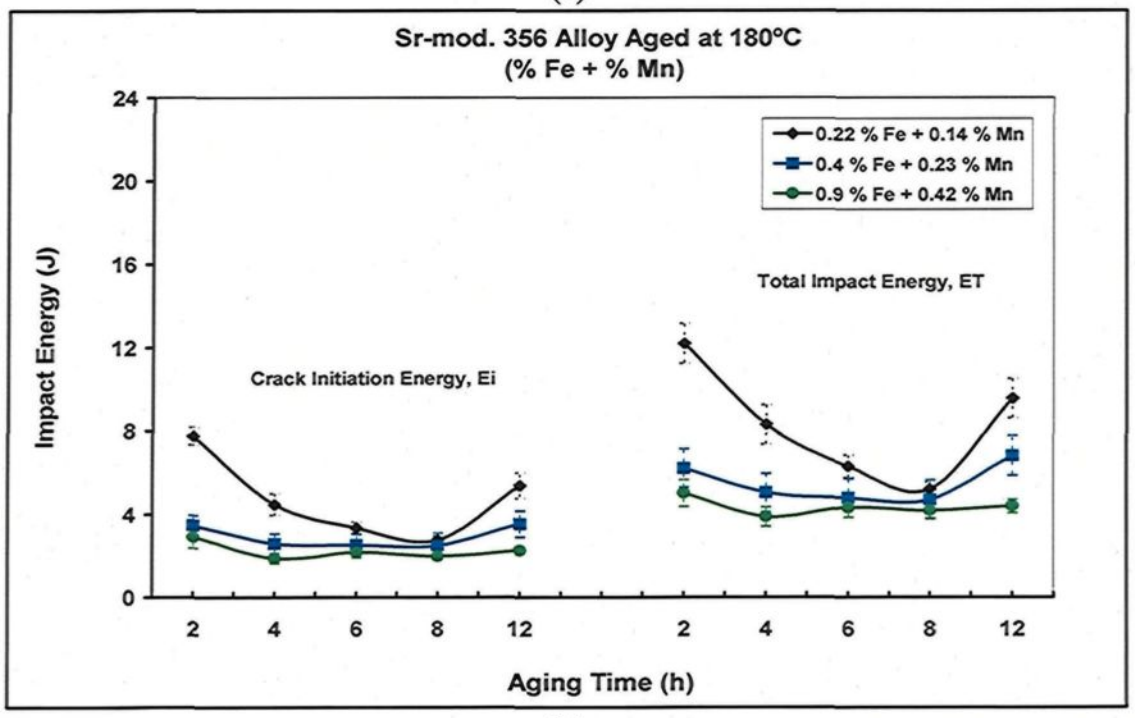

(b)

Figure 5.8 Impact energy as a function of aging time for 356 alloys containing different combined additions of Fe-Mn, and aged at 180°C: (a) non-modified alloys, and (b) Sr-modified alloys.

iron-based intermetallic phases are the predominant factors controlling the impact behavior in these alloys. It should also be noted here that the behavior of the crack initiation energy values (E_i) displays the same tendency as that of the total impact energy values (E_T).

5.2.2.2 Effects of Aging Time at 220°C

Table 10 lists the average values for impact energy with their standard deviations, as well as a variety of other parameters relating to 356 alloys containing three levels of combined Fe and Mn addition, and aged at 220°C for various aging times. The response of these alloys to the expected softening effect at such high aging temperatures is evident from the impact behavior shown in Figure 5.9. The impact energy values are seen to increase in a virtually linear manner with further aging times of up to 12 hrs for the non-modified alloys, particularly for those containing low levels of Fe-Mn, as shown in Figure 5.9(a). The impact behavior of Sr-modified alloys shows the same tendency as that obtained in non-modified alloys, although they display considerable improvement beyond 12 hrs of aging in the over-aging stage. The same significant improvement may also be observed in the crack initiation energy values in that they confirm the softening effect occurring in these alloys upon application of the T7 temper.

It may be concluded from the above mentioned results that the aging process in terms of temperatures and times appears to contribute significantly to either improving or reducing the matrix resistance to crack initiation by also controlling the number of stress concentration sites at the interface between the particles of the precipitated-phases and the matrix. The strength and ductility of the α-aluminum phase which affected by the aging process will also govern the propagation of the cracks in the matrix.

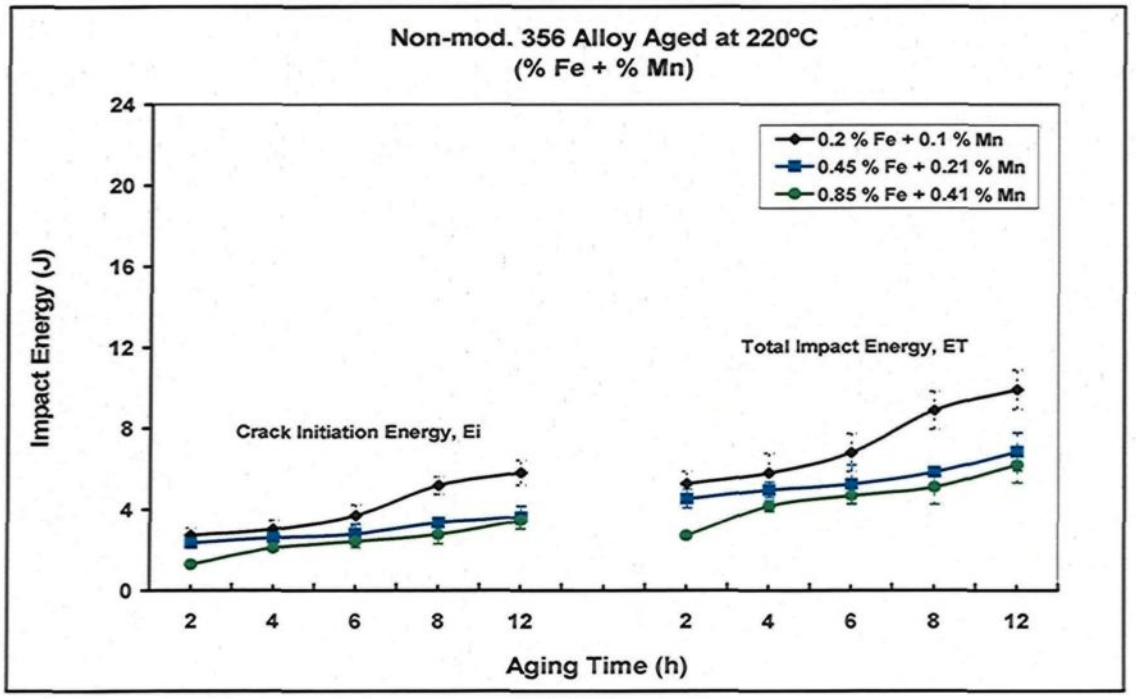

(a)

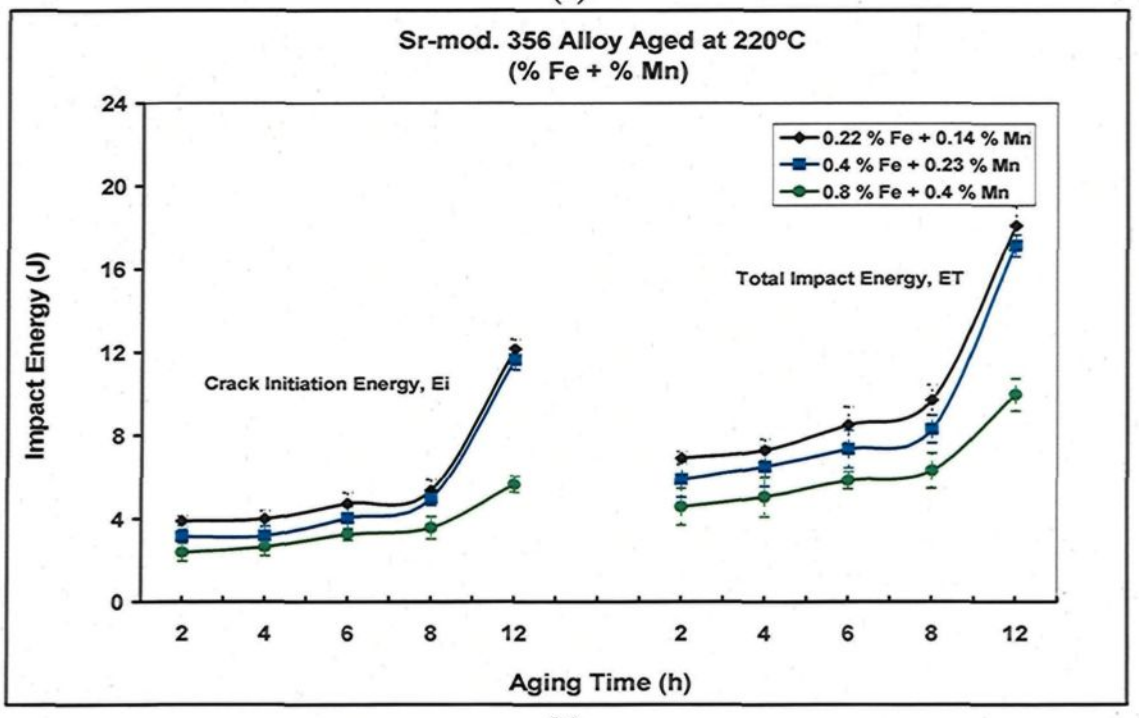

(b)

Figure 5.9 Impact energy as a function of aging time for 356 alloys containing different additions of Fe-Mn, and aged at 220°C: (a) non-modified alloys, and (b) Sr-modified alloys.

The design of certain critical components to meet specific requirements is of importance in the automobile industry. Impact toughness is one of the main requirements which should be taken into account in the design of such automobile components. In this way, sudden failure resulting from weakened impact toughness may be circumvented through the selection of the proper alloy composition and the appropriate casting and heat treatment conditions. The high impact energies obtained through the application of a T7 treatment in the case of Sr-modified 356 alloys containing either 0.15 wt% Fe addition or a combined addition of 0.2 wt% Fe and 0.1 wt% Mn may be the most appropriate solution for avoiding any unexpected breakdown occurring in components made from cast 356 alloys.

5.3 319 ALLOYS

The as-cast microstructure of the 319-type alloy usually comprises soft α-Al dendrites, a hard eutectic Si phase, and numerous intermetallic phases such as Al_2Cu and Fe-containing phases. Strontium-modification as a melt treatment process is frequently applied to 319 alloys to convert the acicular Si particles into fine fibrous ones. Subjecting these alloys to a solution heat treatment also causes significant changes in the characteristics of the as-cast microstructural constituents, which together with Sr-modification, would result in acquiring reasonable strength and ductility values.

Moreover, by applying aging treatment to such alloys it becomes possible to obtain the precipitation of the hardening Al_2Cu phase which contributes to the nucleation and formation of microcracks at the interface between the matrix and the precipitated-phases.[44] Consequently, the various stages of precipitation-hardening which occur during the

artificial aging of 319 alloys, will affect the impact toughness of such alloys to a large degree.

The following subsections will discuss the effects of the various constituents of the microstructure, including eutectic Si, Al_2Cu, and iron-based intermetallic phases in conjunction with the effects of aging conditions on the impact behavior of 319 alloys. The impact toughness of hypoeutectic 319 alloys is relatively lower than that reported previously for 356 alloys. The energy scale thus will be varied in the following subsections to clarify and emphasize on the changes in the impact energy values as a function of the studied parameters.

5.3.1 Effects of the Addition of Fe

As may be clearly observed in 356 alloys, the impact energy values of 319 alloys are also expected to vary as a function of the structural fineness, as well as of the morphology and the size of the microstructural constituents, particularly the eutectic Si, Al_2Cu and Fe-containing intermetallic phases. The application of aging treatments is also reported to influence the microstructure to a large degree.

Table 11 summarizes the average values and the standard deviation of impact properties obtained for non-modified and Sr-modified 319 alloys containing various addition levels of Fe and Mn for as-cast and solution-treated conditions. This table and Figure 5.10 represent the effects of various levels of iron content, solution heat treatment, and Sr-modification on the impact energy values of 319 alloys. As similarly observed for the 356 alloys, the impact energy values diminish noticeably with an increase in iron content from 0.2 wt% to 1 wt% for all the conditions involved. This reduction may be

attributed mainly to the formation of detrimental plate-like β-phase particles which become increasingly more susceptible to fracture, particularly in the as-cast non-modified alloys. This result is in good agreement with the generally accepted fact that increasing the size and aspect ratio of the β-phase needles enhances the probability of particle fracture to a great extent. [18] Thus, the lower impact energy values obtained may be explained by the considerable contribution of the β-Fe platelet phase to increasing the potential for crack initiation at the sharp edges of β-platelets and in the regions containing porosity.

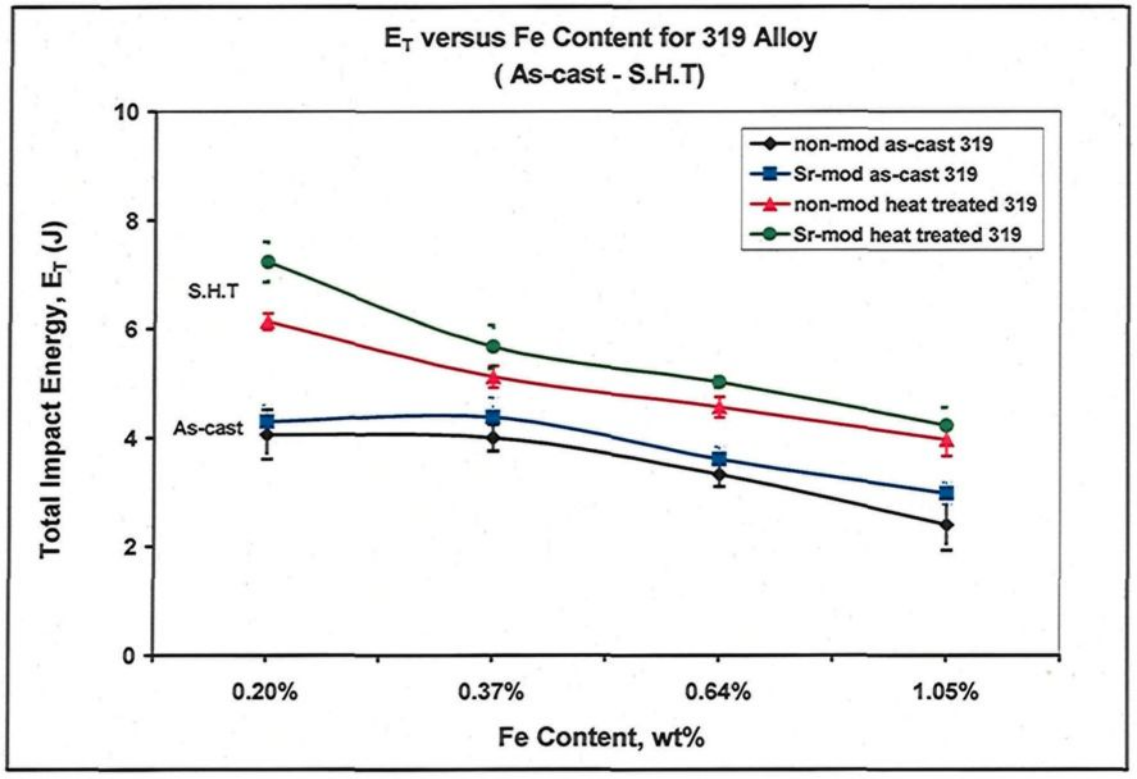

Figure 5.10 Relationship between total impact energy and iron content in non-modified and Sr-modified 319 alloys for as-cast and solution heat-treated conditions.

These observations are in accordance with the results obtained from work carried out by Li *et al.* [8] They found that addition of Fe up to 1.2 wt% leads to an increase in the precipitation of β-Al_5FeSi platelets, which increases crack initiation sites in addition to the those provided by the brittle eutectic Si particles. The presence of both microstructural constituents at 1.2 wt% Fe has been observed to reduce considerably the impact energy values of both non-modified and Sr-modified 319 alloys, *i.e.* by 47% and 56%, respectively, at an SDAS of about 47 μm.

The addition of Sr to the as-cast alloys increases the energy E_i required to initiate the cracks. Such an observation seems to concur with the results obtained in a study carried out by Shivkumar *et al.*, [19] who found that the addition of Sr not only refines the eutectic Si particles but also the Cu- and Fe-bearing intermetallic phases. The authors, however, did not discuss the effects of Sr on the segregation of the Al_2Cu phase and its subsequent affinity for forming acicular blocklike particles instead of fine eutectic ones, as has been reported by other researchers.[2, 4, 10, 114] Such an effect is thought not to be beneficial to impact properties, since the coarser brittle block-like Al_2Cu particles are hard to be completely dissolved after the application of solution heat treatment. These particles provide more stress concentration sites which, in sequence, facilitate the initiation of microcracks in the matrix. For this reason, a low degree of improvement is observed in the impact energy values of Sr-modified 319 alloys.

Solution treatment at 495°C for 8 hrs greatly enhances the total absorbed impact energy (E_T) of both non-modified and Sr-modified 319 alloys compared to the values obtained in the as-cast condition, as was observed previously for the 356 alloys. Applying

the solution heat treatment to Sr-modified alloys increases the energy required for both crack initiation (E_i) and crack propagation (E_p). [116] In addition, both the dissolution of the hard, brittle Al_2Cu phase and the fragmentation of platelike β-iron particles in this case contribute strongly in improving the resistance of the matrix to both crack initiation and crack propagation. Since the solution treatment temperature is not high, Shivkumar *et al.* [19] proposed that commercial 319 sand castings should be solution-treated for extended periods in order to obtain a significant improvement in the impact properties of the Sr-modified alloys.

It is clear that the 319 alloys show lower impact properties than 356 alloys, as may be deduced from a comparison between the impact energy values in Figures 5.10 and 5.2. The above conclusion appears to be in a good conformity with the results of Paray *et al.* [2] These researchers revealed that no evidence of plastic deformation may be detected from the load-time curves obtained for 319 alloys and thus this type of alloys seems to be brittle and displays poor impact properties. This conclusion is further supported by Shivkumar *et al.* [19] who reported that the impact values for Sr-modified 319 and A356 alloys in the T6 condition are on the order of 1.8 and 13.1 J, respectively, for metallic mold castings.

5.3.1.1 Effects of Aging Time at 180°C

In general, Sr-modified 319 alloys display somewhat higher impact energy values than the non-modified alloys after aging at 180°C for different aging times, as may be observed in Table 12. A sharp decrease in the impact values is evident with increasing levels of iron content of up to 1 wt% for both non-modified and Sr-modified alloys for all aging times, as may clearly be seen in Figure 5.11.

It is possible to observe from Figure 5.11 that a slight increase in the impact energy values is obtained after 2 hrs of aging at 180°C for both non-modified and Sr-modified 319 alloys containing 0.2 and 0.4 wt% Fe; thereafter the impact values are seen to decrease with increasing aging time. Nevertheless, a considerable recovery in impact energy values may be observed after 12 hrs of aging.

The impact toughness of 319 alloys depends strongly on the proportion of the ductile α-Al phase and on the morphology of the eutectic Si particles, as well as on that of brittle Al_2Cu particles present in the matrix. [20, 21] The aging process of the 319 alloy at 180°C proceeds with increasing aging times, resulting in the subsequent precipitation of the Al_2Cu second phase particles. Precipitation-hardening begins with the formation of GP (I) zones which hinder the dislocation movement slightly during the under-aging stage. [44] In view of the preceding data and from Figure 5.11, a slight increase may be observed in the impact energy values of non-modified and Sr-modified 319 alloys after 2 hrs of aging compared to those obtained for the as-cast condition. Further aging leads to the precipitation of coherent Al_2Cu particles which then provide the maximum resistance to dislocation motion during the peak-aging stage. This increase in the strength involves a decrease in the overall ductility of the alloy, and thus a gradual reduction in the impact properties may be observed after 6 hrs of aging for the case of non-modified alloys, and after 8 hrs for the Sr-modified alloys. In the final stage of age-hardening, or the

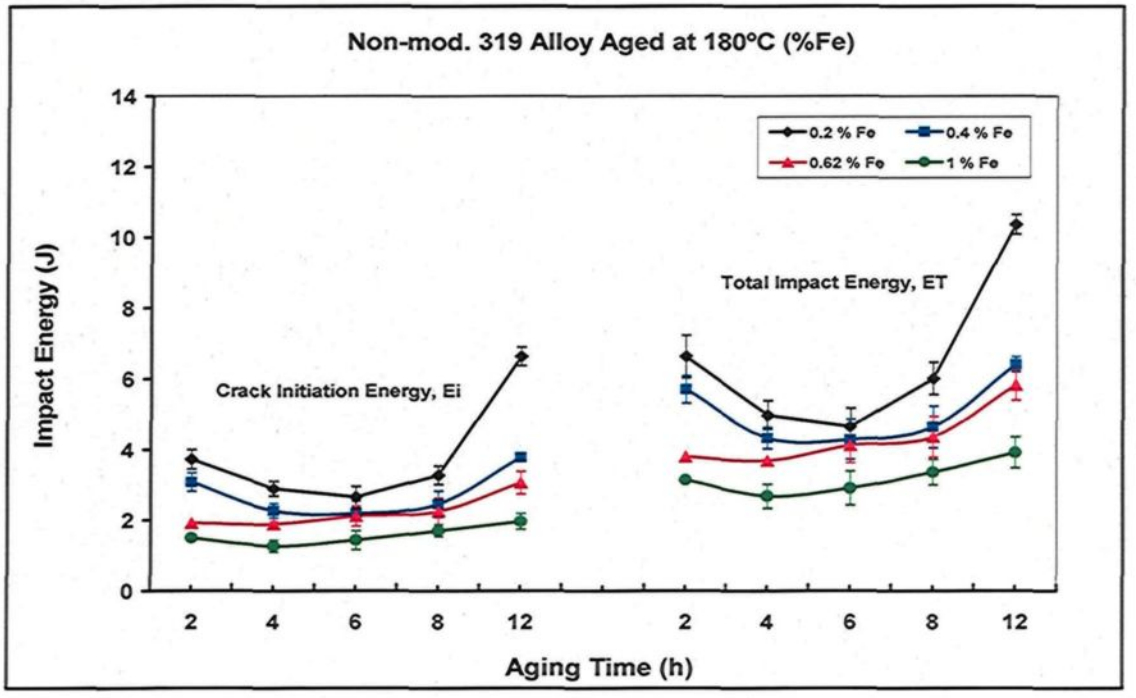

(a)

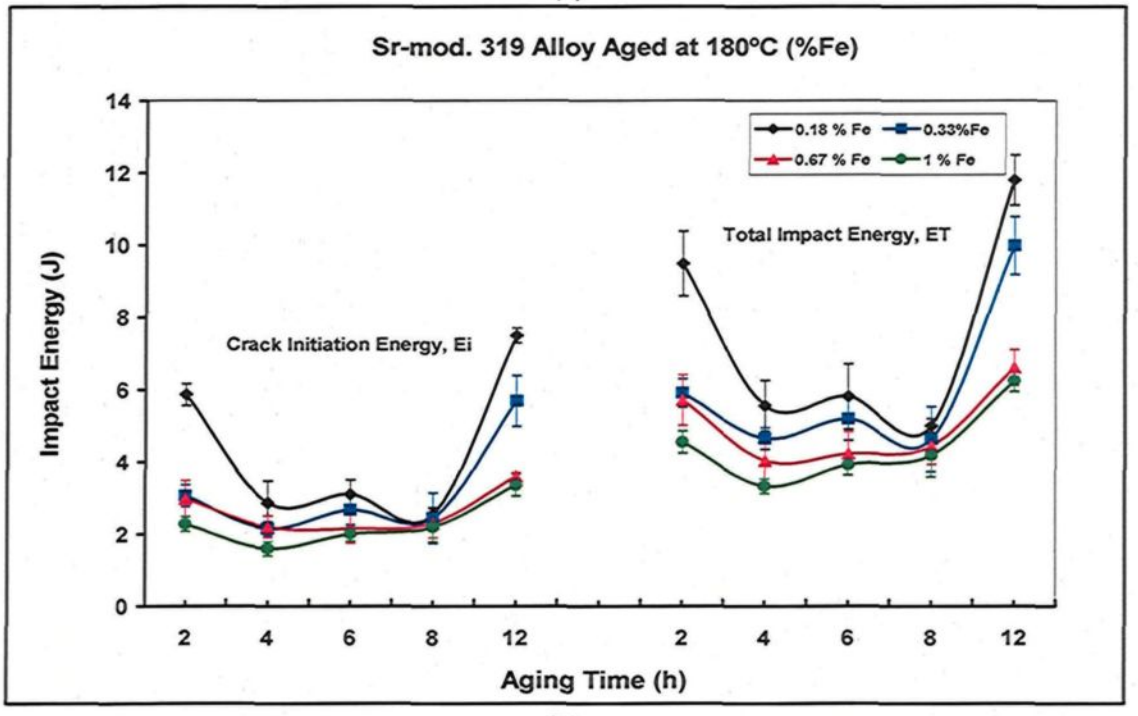

(b)

Figure 5.11 Effects of aging time on impact energy of 319 alloys containing various levels of Fe, and aged at 180°C: (a) non-modified alloys, and (b) Sr-modified alloys.

over-aging stage, the brittle Al_2Cu phase particles coarsen with extended aging time, leading to a softening of the alloy matrix. As a result, a significant improvement in the impact values is to be observed at aging conditions of 180°C/12h. The highest impact energy value obtained is 12 J for the Sr-modified 319 alloy containing 0.18 wt% Fe aged at 180°C for 12 hrs.

The preceding results reveal that the only major changes occurring during aging treatment are in the size and the morphology of the Al_2Cu phase particles and no observable changes take place either in the size or in the shape for the eutectic Si particles and Fe-based intermetallics. It may thus be concluded that the impact energy values of aged 319 alloys seem to be regulated, to a large extent, by the size, morphology, and distribution of the hard, brittle Al_2Cu phase than the eutectic Si phase. This conclusion is supported by the greater improvement to be observed in the impact values of both non-modified and Sr modified 319 alloys subjected to 12 hrs of aging at 180°C (*i.e.* in the case of over-aging) compared to the values obtained for the same alloys under solution heat-treated conditions. Paray *et al.* [2] suggested that the morphology of Al_2Cu phase has a strong influence on the impact values of such alloys as 319 and 332 which contain copper as the main alloying element.

5.3.1.2 Effects of Aging Time at 220°C

In view of the fact that the precipitation-hardening process is considered to be a diffusion-controlled process, the aging of 319 alloys at high temperatures, such as 220°C, will tend to accelerate the precipitation of the coherent Al_2Cu phase, which will then lead to the hardening of the matrix, and ultimately to a decrease in alloy ductility. There is, thus, a

distinct relationship between the age-hardening of these alloys and their ductility. Since the impact toughness of an alloy is a strong function of its ductility, the impact behavior may then be explained on the basis of the age-hardening response, particularly for 319 alloys containing low levels of iron. Table 13 summarizes the average values and standard deviation of the impact properties of 319 alloys aged at 220°C for different aging times. In the early stages of the precipitation process, *i.e.* in the under-aging stage, the motion of dislocations is obstructed to a slight degree by the precipitated particles of Al_2Cu. Consequently, the impact energy values of alloys containing 0.2 wt% Fe will display a noticeable increase after 2 hrs aging time, as shown in Figure 5.12.

Increasing aging time results in the precipitation of a coherent Al_2Cu phase which hinders the motion of dislocations to a great degree, ultimately leading to an increase in the strength of the matrix during the peak-aging stage. As a result, a continuous decrease in the impact energy values may be observed after aging times of up to 8 hrs, as shown in Figure 5.12(a). The recovery in the impact energy values observed after 12 hrs of aging time, particularly for low Fe-containing alloys, may be attributed to the softening of the alloy as a result of the coarsening of Al_2Cu particles during the over-aging stage which occurs at the end of the aging process. Also, one significant aspect to note here is that, due to the presence of undissolved blocklike Al_2Cu particles in 319 alloys, the recovery in the impact energy values obtained at such high aging temperatures is lower than that obtained for the 356 alloys shown in Figure 5.5.

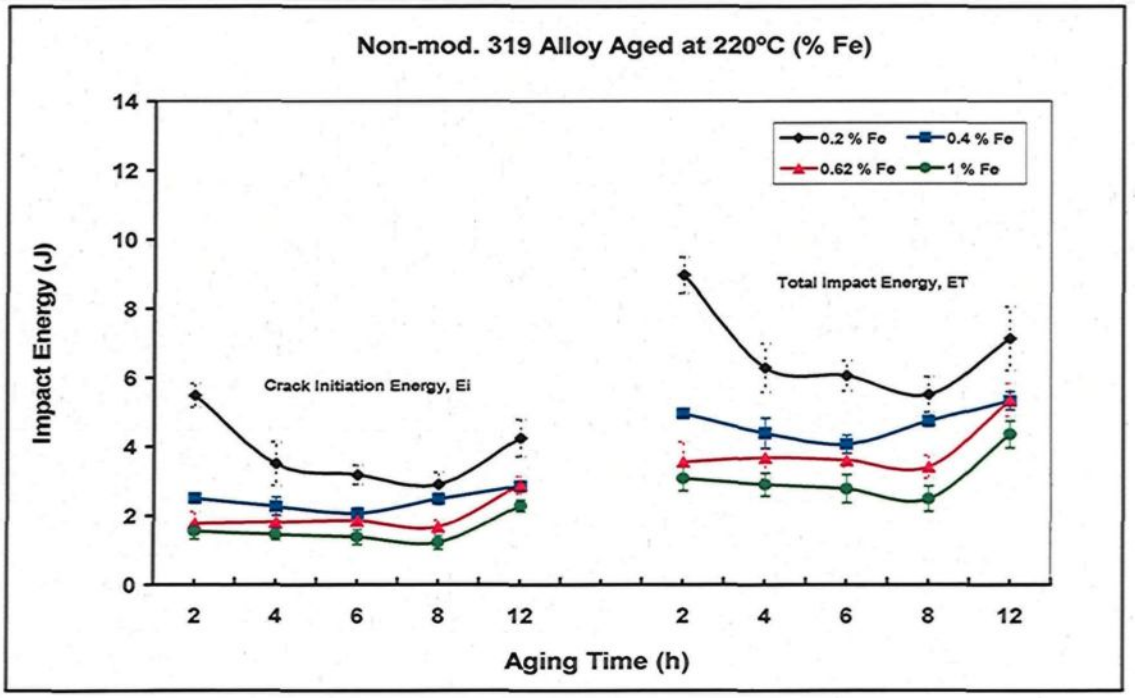

(a)

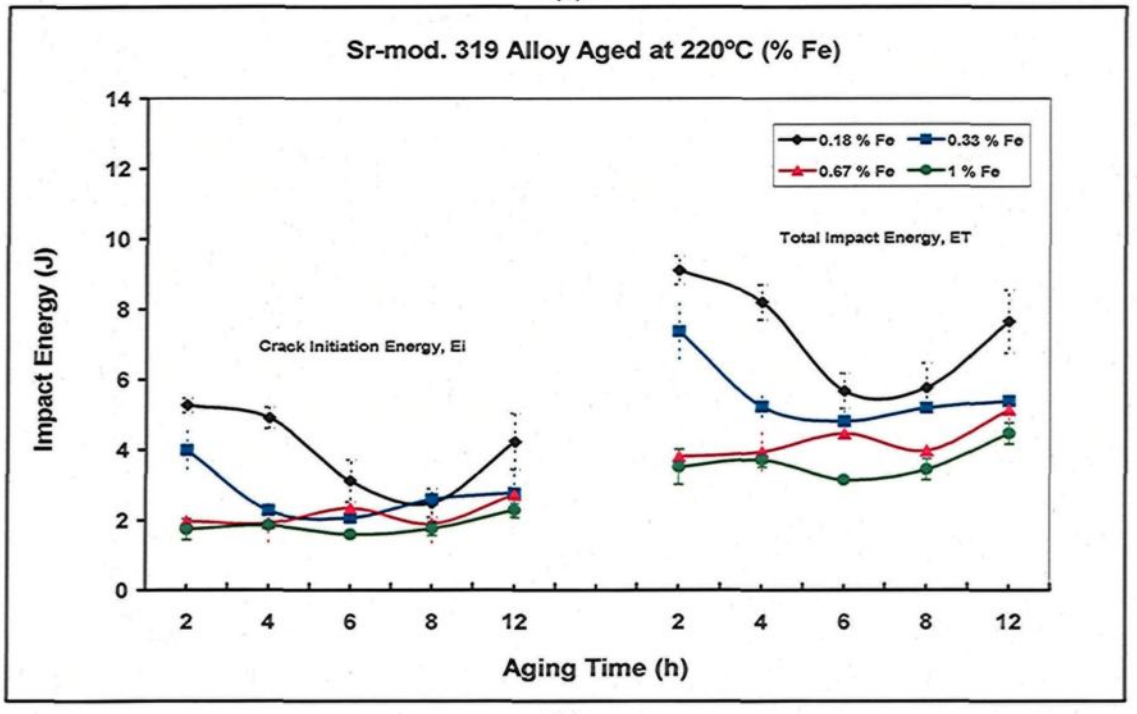

(b)

Figure 5.12 Effects of aging time on impact energy of 319 alloys containing different levels of Fe, and aged at 220°C: (a) non-modified alloys, and (b) Sr-modified alloys.

It will also be observed from Figure 5.12 that the aged Sr-modified alloys exhibit slightly higher impact energies than the non-modified ones. Both non-modified and Sr-modified alloys containing higher levels of iron, ~ 1 wt%, display the lowest impact energy values for all conditions, regardless of aging time.

5.3.2 Effects of Combined Additions of Fe and Mn

Manganese is usually added to Al-Si alloys in certain fixed amounts to reduce the detrimental effects of the β-iron platelike phase through the precipitation of iron in the form of the compact α-Fe Chinese-script particles. [25] The average impact test results are presented in Table 11, while Figure 5.13 shows the behavior of the impact energy of non-modified and Sr-modified 319 alloys containing different levels of combined Fe-Mn additions, for the as-cast and solution heat-treated conditions. At the 0.1 wt% level of Mn addition, the impact energy values of non-modified and Sr-modified alloys remain almost the same as they do for the as-cast alloys containing only iron, as shown in Figure 5.10. As a result of increasing the levels of Mn addition up to about 0.38 wt%, a high proportion of the α-iron Chinese-script particles are formed, reducing the number of potential crack initiation sites. Such reduction in the probability of crack initiation implies an increase in the energy required for triggering the cracks and for this reason, an improvement in the impact energy values of non-modified and Sr-modified alloys is obtained for both as-cast and solution heat-treated conditions.

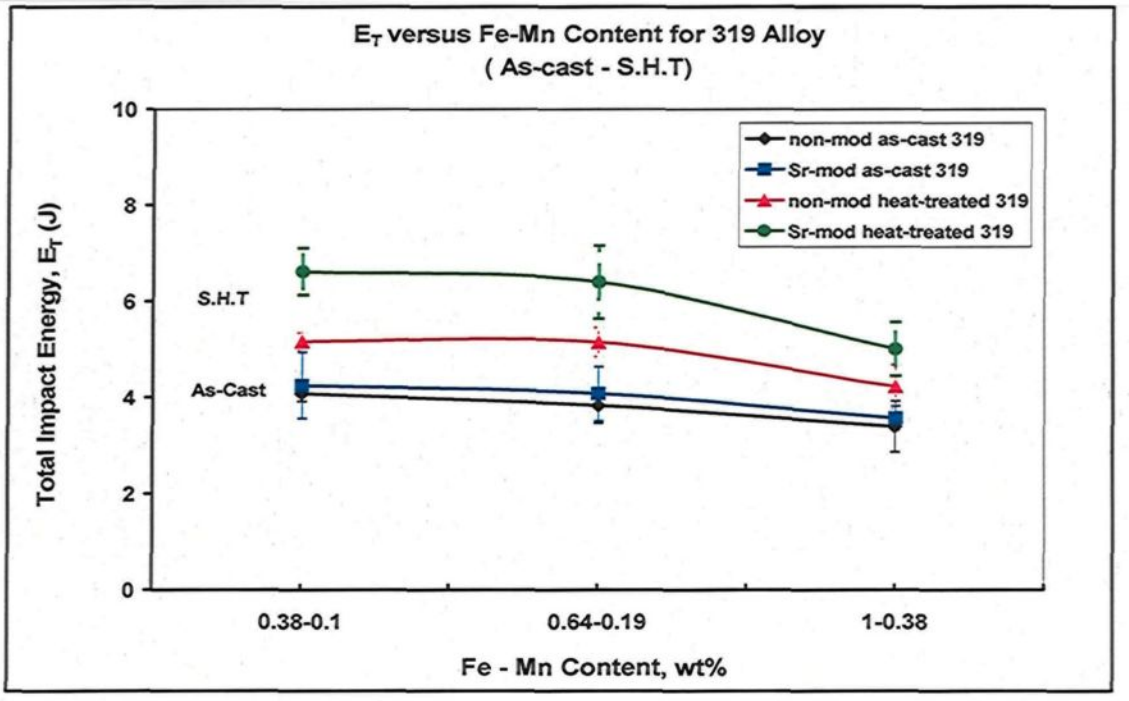

Figure 5.13 Relationship between total impact energy and Fe-Mn content in non-modified and Sr-modified 319 alloys for the as-cast and solution heat-treated conditions.

Higher impact energy values are observed for Sr-modified solution-treated 319 alloys containing a 1 wt% Fe-0.38% Mn combined addition level compared to those obtained for alloys containing only 1 wt% Fe addition shown in Figure 5.10. These slightly higher impact energy values may be ascribed to the preceding effects concomitantly with the contribution of both Sr and solution heat treatment to the fragmentation and dissolution of any remaining β-iron platelets, the spheroidization of eutectic Si particles, and the dissolution of the brittle acicular Al_2Cu particles.

5.3.2.1 Effects of Aging Time at 180°C

Table 13 and Figure 5.14 reveal the effects of aging time at 180°C on the impact energy values of 319 alloys containing various levels of combined Fe and Mn additions. The addition of Mn has no effect on the formation of Al_2Cu phase particles during the aging process. As a result, the impact behavior of 319 alloys containing these combined additions appears to be governed to a large extent by their aging response. It is also obvious from the same figure that this behavior is similar to that of the alloys containing only iron, as shown in Figure 5.11. A slight increase in the impact energy values of non-modified alloys is observed after 2 hrs of aging, followed by decrease in these values with increasing aging times of up to 8 hrs. A significant recovery in the impact energy values is also to be observed with extended aging times of up to 12 hrs.

The Sr-modified alloys show a significant improvement in impact energy after 2 hrs of aging at 180°C, as shown in Figure 5.14(b), compared to the same alloys in both as-cast and solution heat-treated conditions. The initial modified microstructure makes the Sr-modified alloys display higher levels of impact energy than non-modified ones.

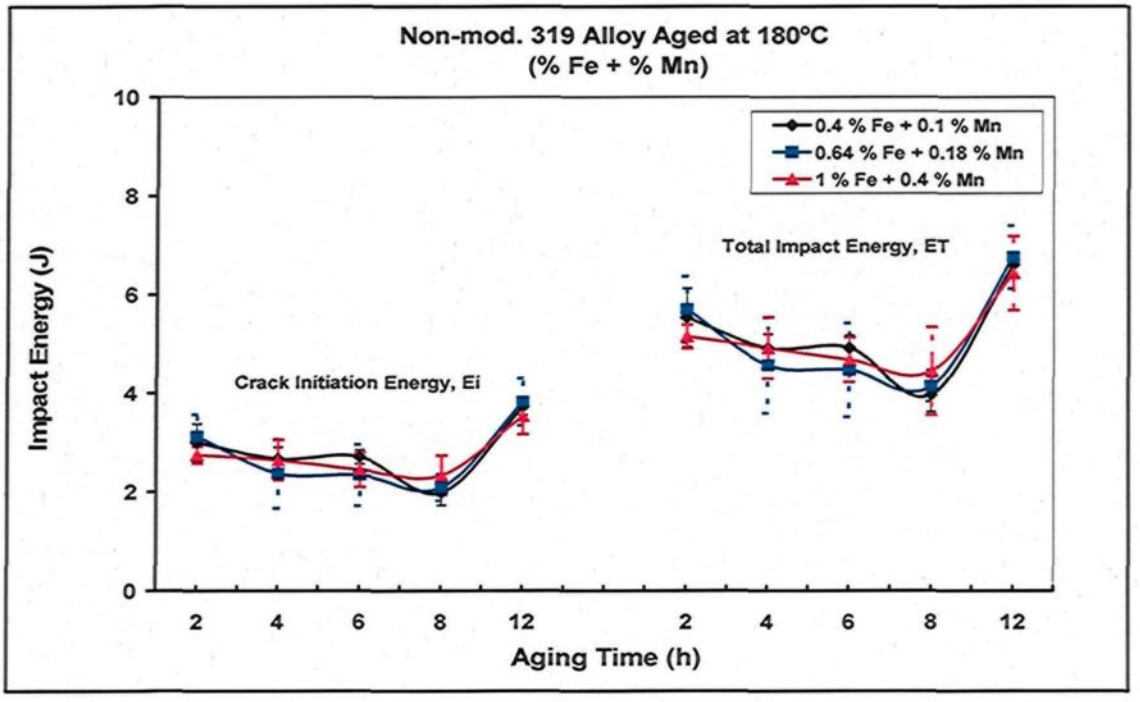

(a)

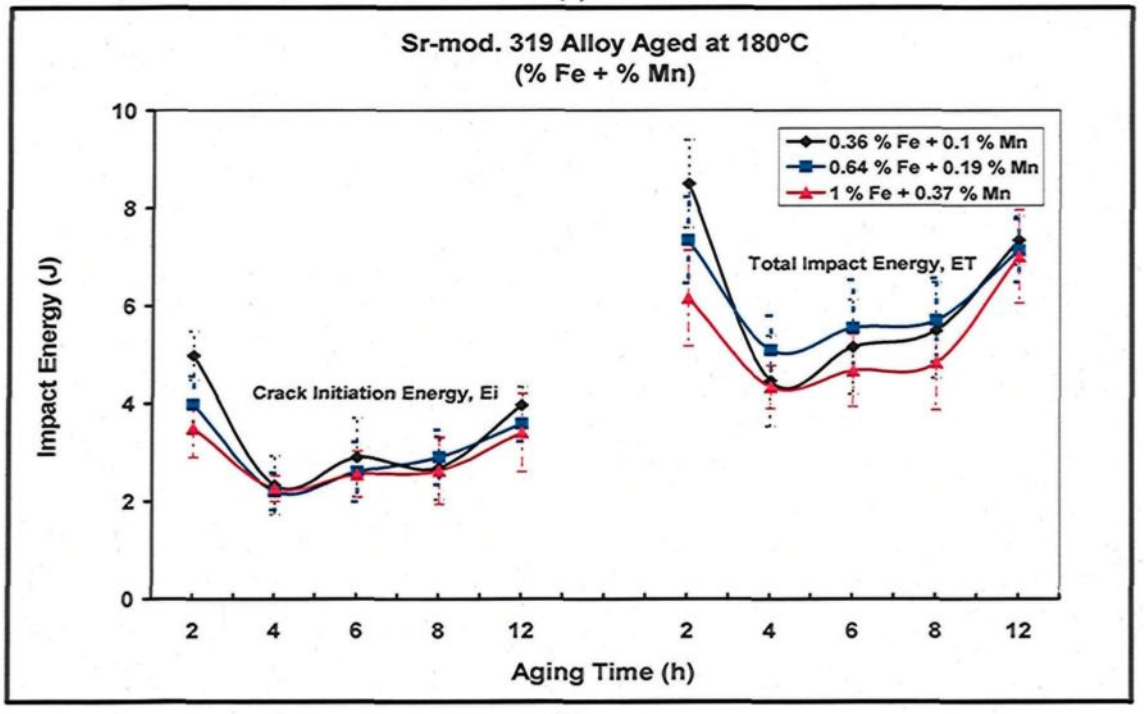

(b)

Figure 5.14 Effects of aging time on impact energy of 319 alloys containing different levels of Fe-Mn, and aged at 180°C: (a) non-modified alloys, and (b) Sr-modified alloys.

5.3.2.2 Effects of Aging Time at 220°C

Table 15 lists the impact energy values of 319 alloys containing various levels of Fe and Mn, and aged at 220°C. Figure 5.15 shows that the variation of impact energy values with aging time displays the same behavior as that obtained after aging at 180°C, as shown in Figure 5.14. From these figures, it is clear that the impact energies decrease upon going from the 2 hr-aging condition, which represents the under-aging stage, to the peak-aging stage, attained after 8 hrs of aging; beyond this, the impact energies increase with 12 hrs of aging time in the over-aging stage. This type of variation in the impact energy values will be observed for both non-modified and Sr-modified alloys. It may thus be concluded that the changes which occur in the morphology and size of the Al_2Cu phase particles during aging regulate the impact properties to a great extent. Furthermore, higher impact energy values are obtained in the Sr-modified alloys than those obtained for the non-modified alloys, as was observed in the case of the previous conditions.

5.3.3 Effects of Combined Additions of Fe and Mg

Table 16 summarizes the averages and standard deviation of the total impact energy valuesof 319 alloys containing various levels of Fe and Mg additions. Figure 5.16 shows the influence of various levels of combined additions of Fe and Mg, as well as of solution heat treatment and Sr-modification on the impact energy of 319 alloys. It will be observed that increasing the levels of combined additions of Fe and Mg decreases the impact energy values for all the conditions involved as a result of increasing the volume fraction of intermetallic phases.

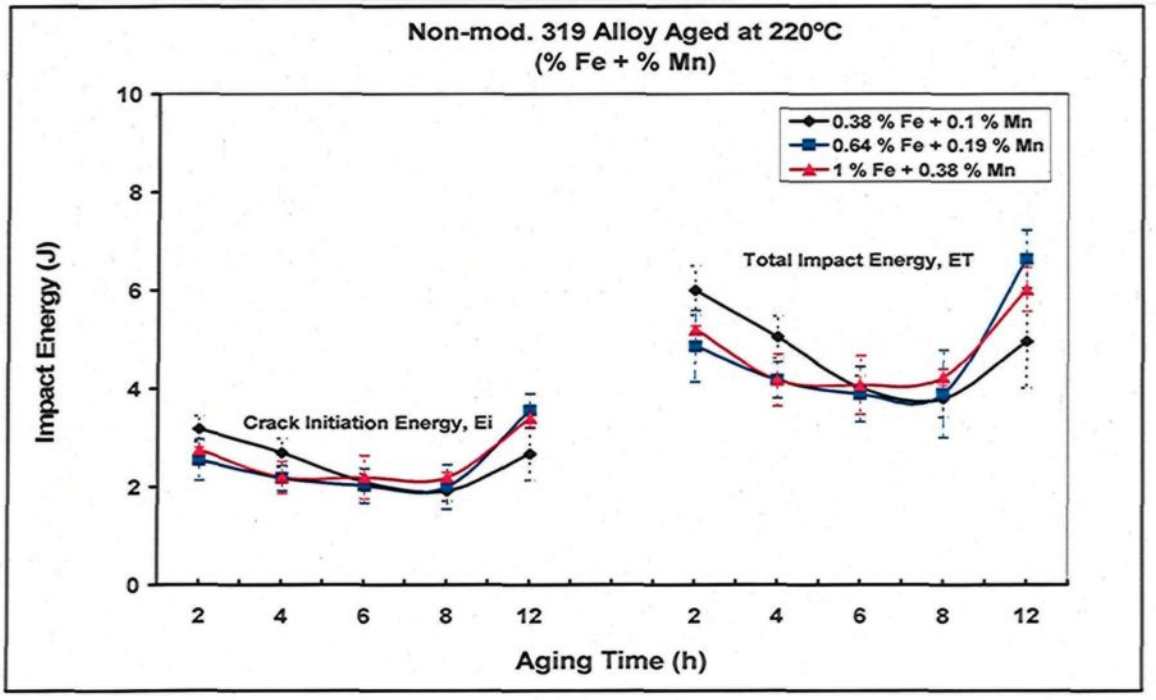

(a)

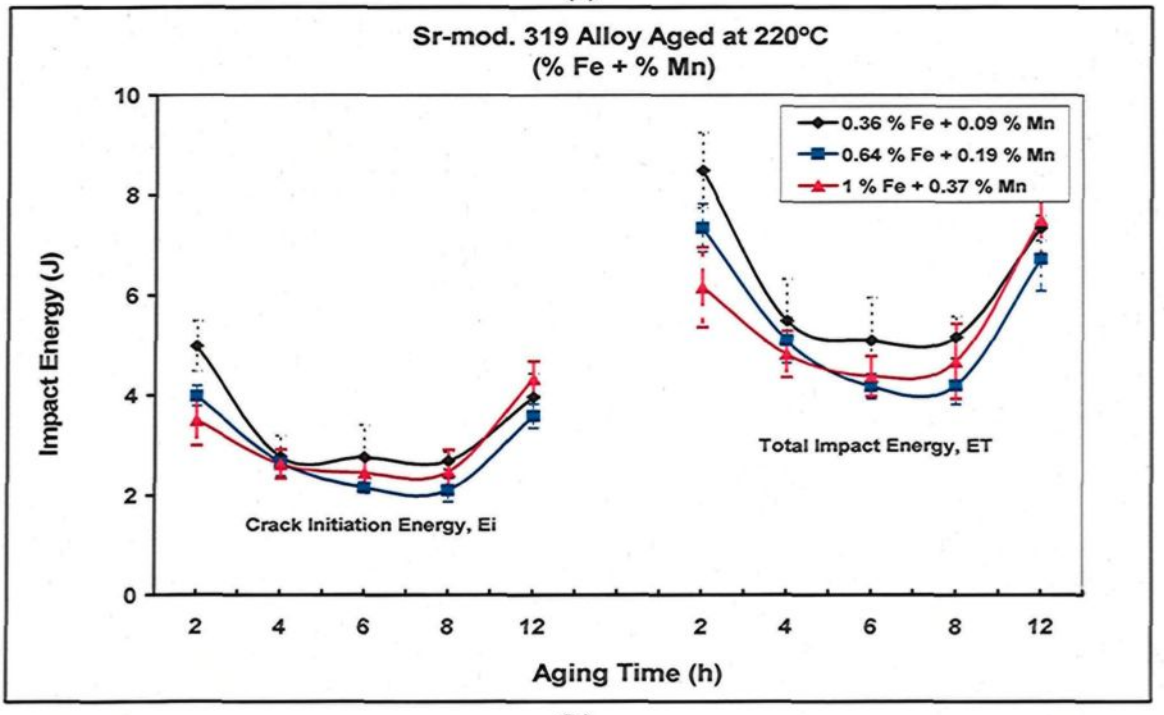

(b)

Figure 5.15 Effects of aging time on impact energy of 319 alloys containing different levels of Fe-Mn, and aged at 220°C: (a) non-modified alloys, and (b) Sr-modified alloys.

Magnesium has been reported to negate the modifying effects of Sr in that it forms a number of intermetallic phases in alloys containing Sr, leading to a decrease in the amount of Sr available to complete the modifying action. Also, the presence of Sr together with Mg promotes the segregation of the Al_2Cu phase in areas away from the eutectic Si regions in the form of blocklike particles. [114, 117] The changes in the morphology of the microstructural constituents may contribute significantly to increasing the number of stress concentration sites in the matrix, thereby lessening the energy required for crack initiation and providing an additional means to diminish the impact energy values of these alloys.

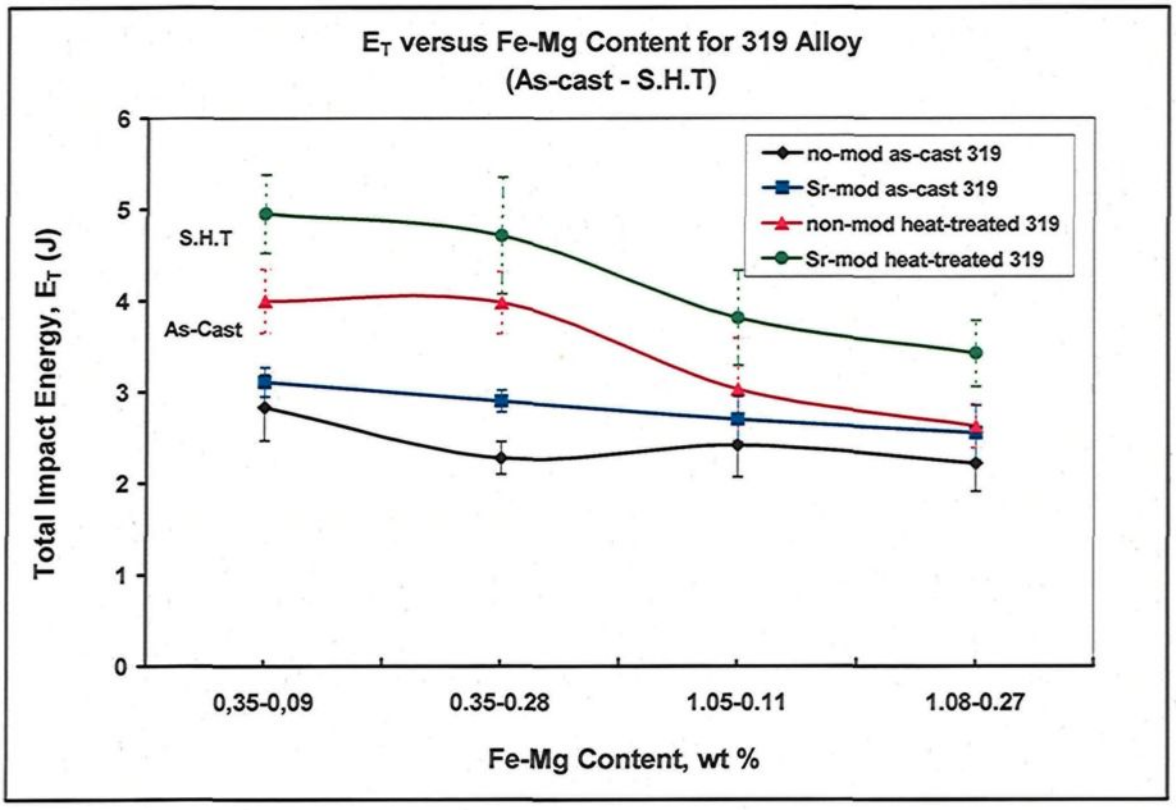

Figure 5.16 Relationship between total impact energy and Fe-Mg content in non-modified and Sr-modified 319 alloys for the as-cast and solution heat-treated conditions.

The application of solution heat treatment in conjunction with Sr modification improves the impact energy to a noticeable degree as was reported in the previous section, particularly for alloys containing 0.35 wt% Fe and 0.1 wt% Mg, as shown in Figure 5.16. The significant increase in impact energy values in this case may be ascribed to the dissolution of the hard phases such as the Al_2Cu phase in low Fe- and Mg-containing alloys and both the Al_2Cu and Mg_2Si phases in high Fe- and Mg-containing alloys. The spheroidization of the eutectic Si particles and the fragmentation of β-iron platelets also contribute to such improvement.

It should also be observed from Figure 5.16 that increasing the combined Fe-Mg additions diminishes the impact properties of 319 alloys considerably. This reduction in impact properties is more pronounced for all alloy conditions involved compared to the impact energies obtained for both alloys containing additions of only iron, and those containing combined additions of Fe and Mn, under the same conditions. This observation makes it possible to conclude that an addition of 0.3 wt% Mg reduces the impact properties of 319 alloys to a large degree. For the most part, these findings are consistent with those reported in the study carried out by Komatsu *et al.*, [54] who reported that increasing the addition of Mg to Al-Si-Cu alloys results in the precipitation of the Mg_2Si phase and the increase in the length of the β-iron phase platelets which consequently causes a decline in their impact energies for the as-cast, solution heat-treated, and aged conditions, as shown in Figure 5.17.

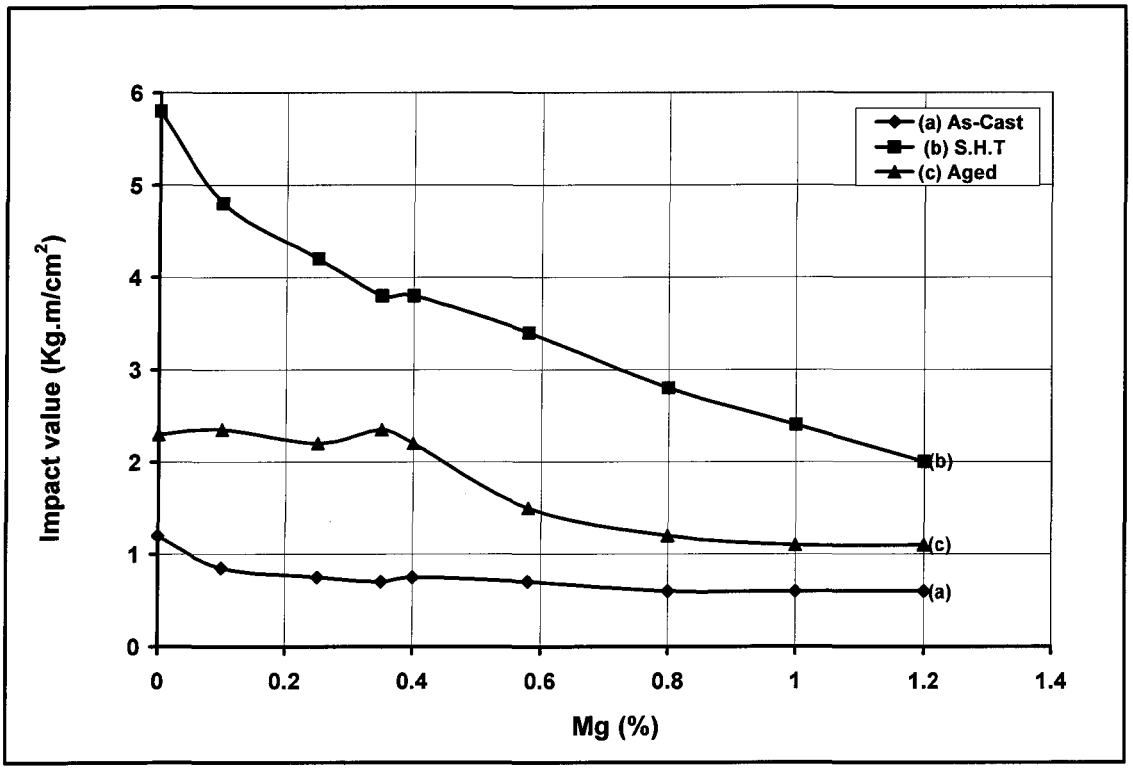

Figure 5.17 Charpy impact energy of Al-6.1% Si-4.5% Cu alloys as a function of Mg content corresponding to (a) as-cast, (b) solution heat-treated at 500°C/4h, and (c) aged at 160°C/5h conditions.[54]

5.3.3.1 Effects of Aging Time at 180°C

The impact energy values for 319 alloys containing Fe and Mg aged at 180°C are listed in Table 17. The effects of various aging times on the impact values of 319 alloys at 180°C are shown in Figure 5.18. A slight increase in the impact energy values will be observed after a 2 hrs-aging period which may be attributed to the fact that the formation of the Cu- and Mg-rich GP zones in the under-aging stage is not enough to allow for sufficient precipitation-hardening of the alloys. A gradual drop in impact energies is to be observed

with increasing aging times of up to 8 hrs resulting from the formation of coherent precipitates during the peak-aging stage.[48] These precipitates tend to hinder dislocation movement and to promote crack initiation in the matrix.[44] The drop in impact energy values may be observed clearly in the Sr-modified alloys containing low levels of Fe and Mg. Once again, a significant restoration in the impact energies will be observed after 12 hrs of aging, corresponding to the over-aging stage.[48] It will also be observed, from Figure 5.18, that both non-modified and modified 319 alloys containing high levels of Fe and Mg addition exhibit somewhat lower impact energy values than do those containing low levels of Fe and Mg. The precipitation of both the Al_2Cu and Mg_2Si hardening phases during aging, together with the high volume fraction of iron-based intermetallic phases in these alloys, particularly in the Sr-modified case, may explain the lower impact energy values more fully.

From Figure 5.18, it may be concluded that the impact energy values of the 319 alloys depend to a great extent on the ductility of the matrix which is governed by the aging response of these alloys where level of Cu and the presence of Mg addition as well as the aging temperature and time strongly regulate the size, morphogy, and the distribution of the hradening phases which control the aging response of these alloys.

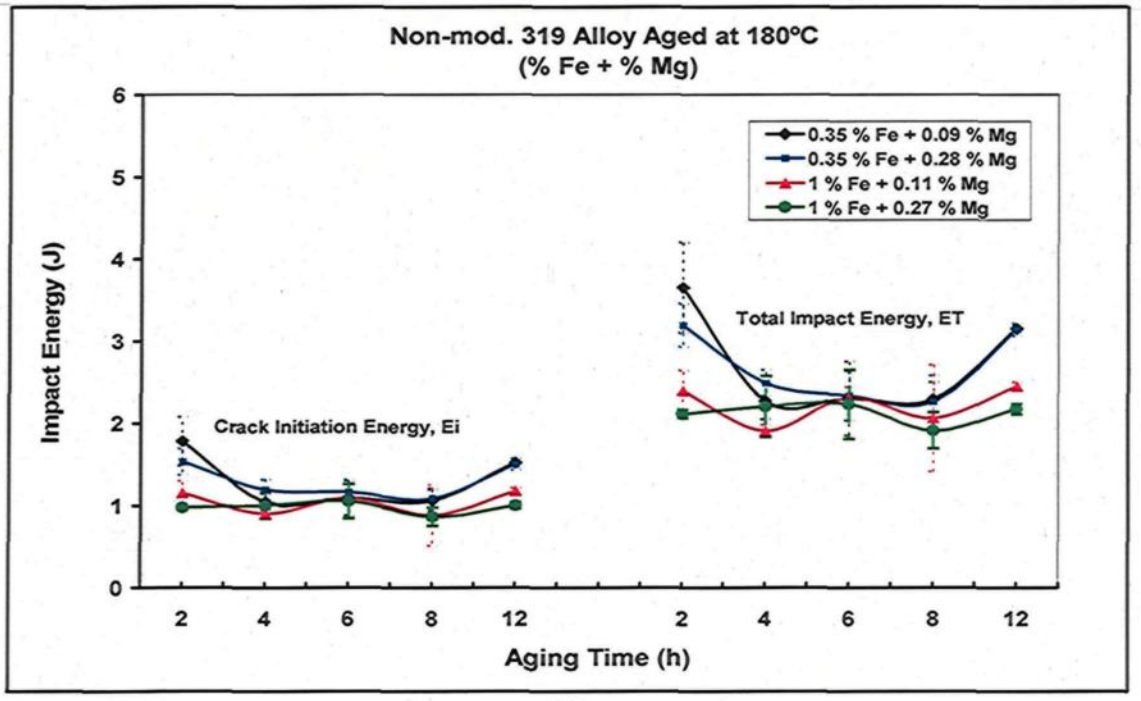

(a)

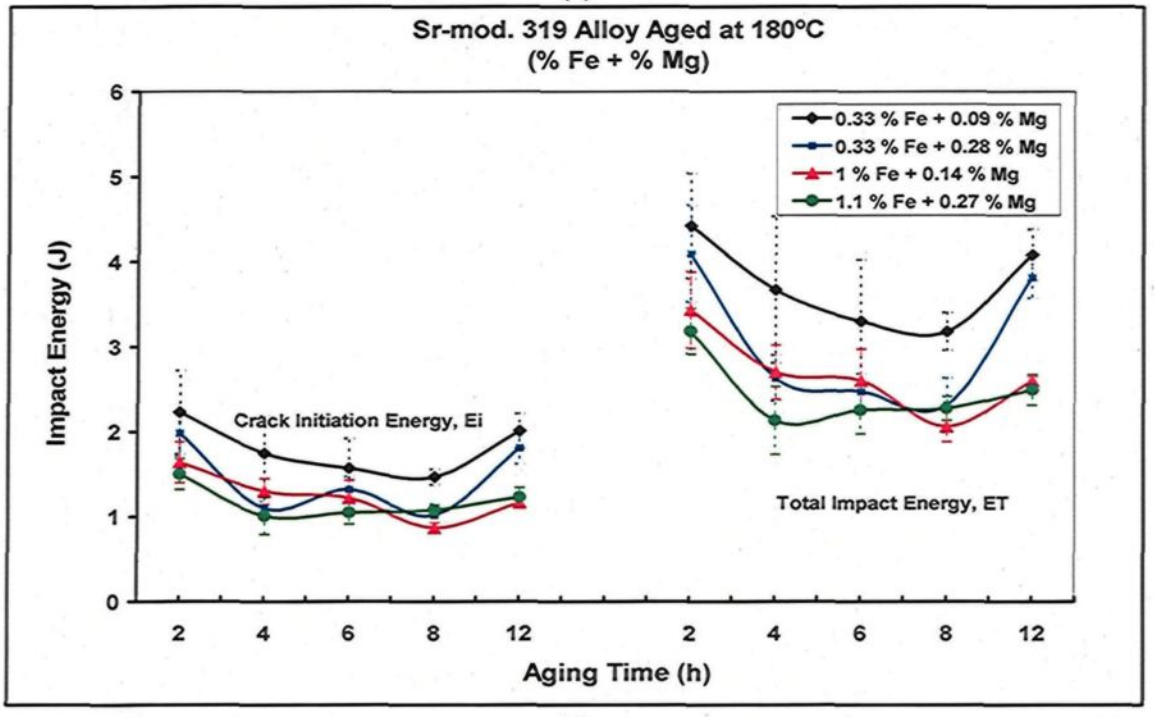

(b)

Figure 5.18 Effects of aging time on impact energy of 319 alloys containing different levels of Fe-Mg, and aged at 180°C: (a) non-modified alloys, and (b) Sr-modified alloys.

5.3.3.2 Effects of Aging Time at 220°C

It will be observed from Table 18 and Figure 5.19 that the impact energy values of 319 alloys show a similar tendency after aging at 220°C for various time durations, as that observed in the aging cycle at 180°C, shown in Figure 5.18. The impact energy values decrease gradually with increasing aging times of up to 6 hrs, as the peak-aging stage is reached, where maximum strengthening of the matrix is obtained. The impact behavior thus depends strongly on the ductility of the alloys which is controlled, to a large degree, by the shape and distribution of the hardening Al_2Cu and/or Mg_2Si precipitates during the aging process. The coarsening of both Al_2Cu and Mg_2Si precipitates after aging at 220°C for a relatively long period of 12 hrs (over-aging stage) tends to soften the matrix so that a significant increase in the impact energy values is observed in Figure 5.19. Likewise, Sr-modified alloys show higher impact energies than non-modified alloys.

The strengthening of the matrix through precipitation of both the Al_2Cu and Mg_2Si phases during the various stages of artificial aging explains the lowest impact energies obtained for the alloys containing 1 wt% Fe and 0.3 wt% Mg of all the alloys investigated. This observation emphasizes the conclusion that the alloy composition and aging conditions play a significant role in regulating the impact behavior of the aged 319 alloys, as well as both the shape and size of the eutectic Si particles and iron-bearing intermetallic compounds.

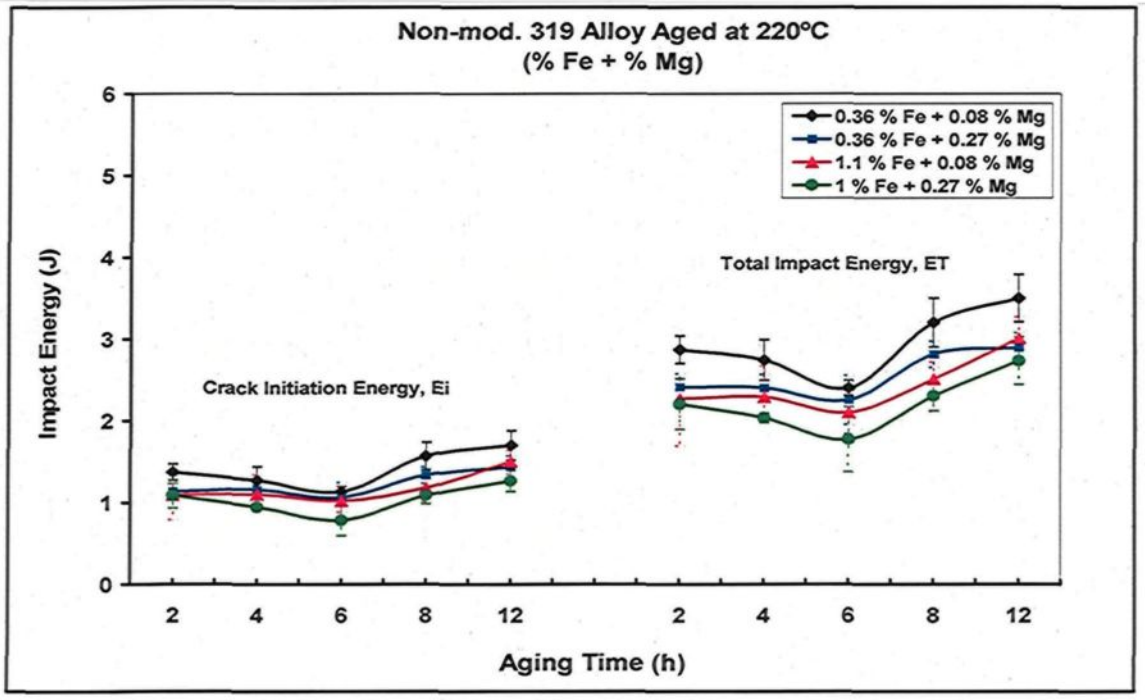

(a)

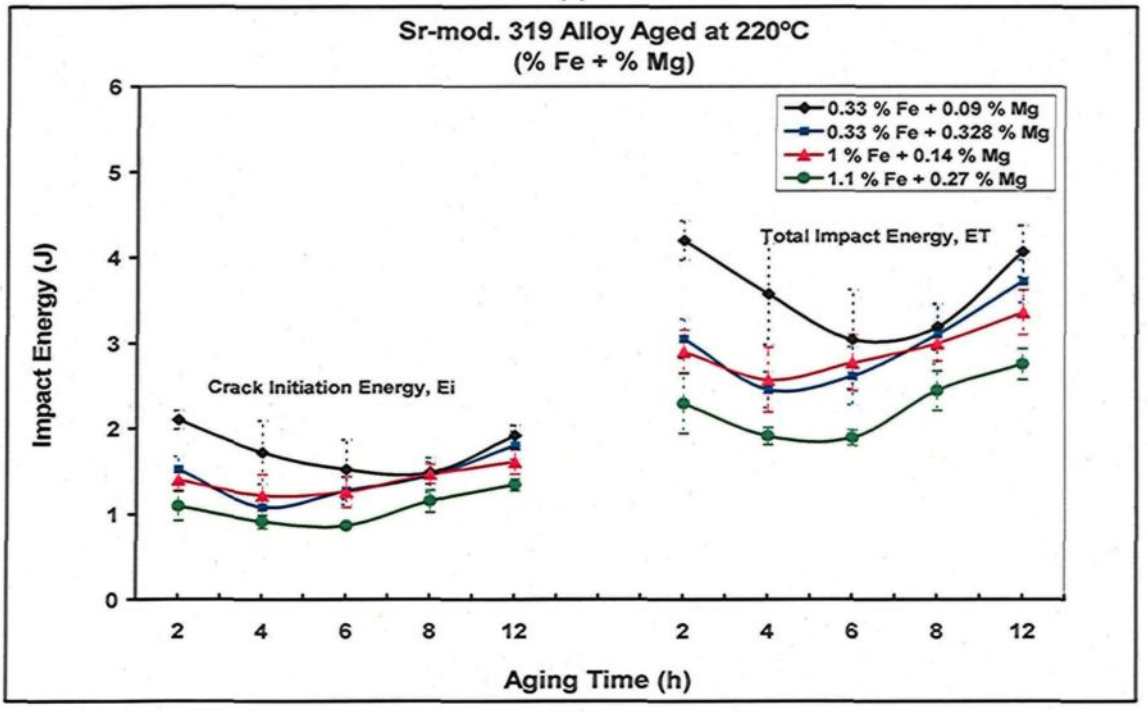

(b)

Figure 5.19 Effects of aging time on impact energy of 319 alloys containing different levels of Fe-Mg, and aged at 220°C: (a) non-modified alloys, and (b) Sr-modified alloys.

5.3.4 Effects of Combined Additions of Fe, Mn, and Mg

Table 16 and Figure 5.20 show the variation in impact energy values for the 319 alloys containing combined additions of Fe, Mn, and Mg after Sr modification and solution heat treatment. As expected, the impact energies are slightly improved by modification of the eutectic Si particles. Solution heat treatment also enhances the impact energy values of the non-modified alloys. The rate of improvement, however, is not the same as the one which was obtained for the other alloys investigated.

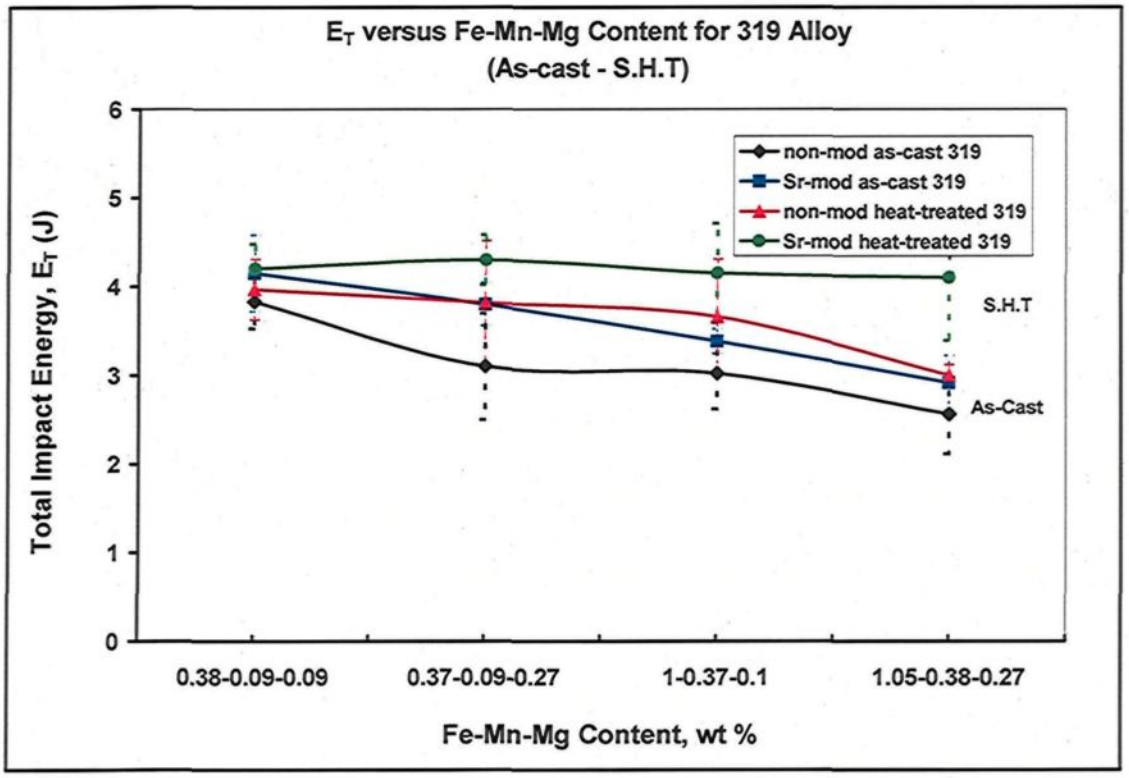

Figure 5.20 Relationship between total impact energy and Fe-Mn-Mg content in non-modified and Sr-modified 319 alloys for as-cast and solution heat-treated conditions.

A noticeable enhancement in the impact energy values of 319 alloys may be obtained by applying Sr-modification in conjunction with solution treatment, irrespective of the level of Fe, Mn, and Mg additions. Such an improvement may clearly be seen in the case of alloys containing high levels of this type of addition, and results from the morphological changes in their microstructural constituents under the modified and solution heat-treated conditions. The complex chemistry of the alloys in this case and the various types of intermetallic phases subsequently formed may explain the lower impact energies of these alloys when compared with those containing either Fe and/or combined Fe and Mn additions.

5.3.4.1 Effects of Aging Time at 180°C

From Table 19 and Figure 5.21, it appears that the impact energy values of the non-modified 319 alloys remain almost unaffected after aging at 180°C for various times, compared to the values obtained after solution heat treatment, as shown in Figure 5.20. It will be observed, however, that an aging time of only 2 hrs is capable of producing a slight increase in the impact energy values. As the aging time increases, the impact energy of non-modified alloys displays lower values than those obtained for the same alloys in the solution heat-treated condition, as shown in Figure 5.20. It is reasonable to deduce that no observable improvement in the impact energy would obtained with a further increase in aging time at 180°C for the non-modified alloys. The precipitation of Al_2Cu and Mg_2Si hardening phases provides more stress concentration sites and one more possibility for reducing the resistance of the matrix to crack initiation.

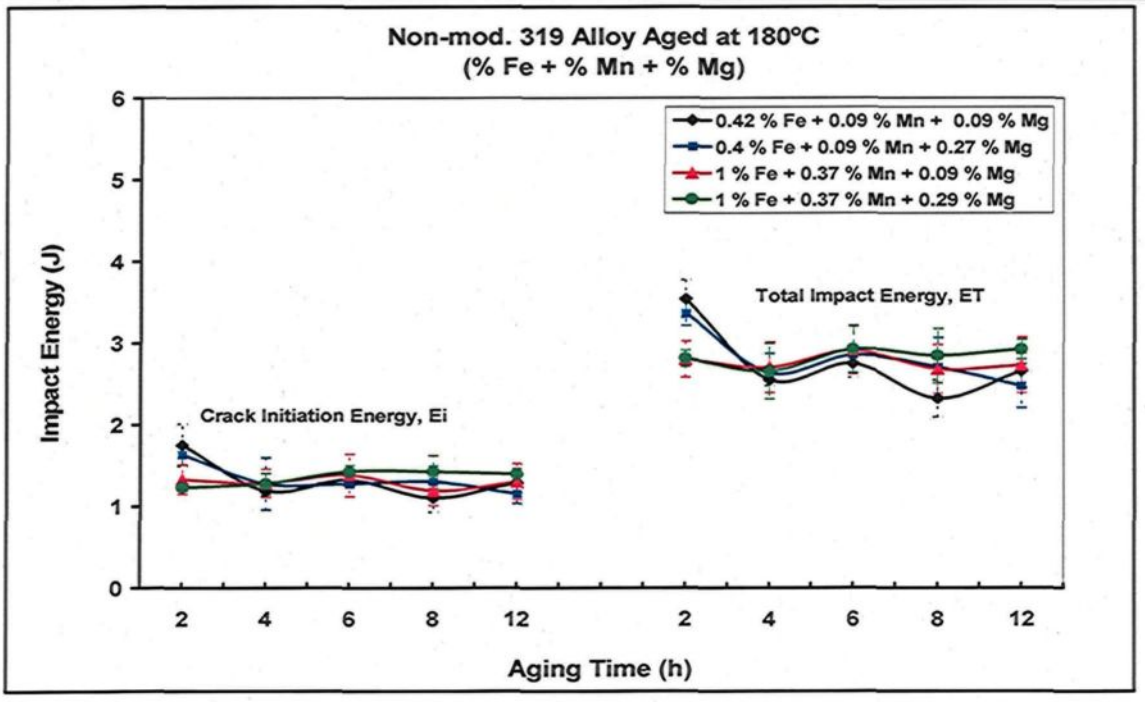

(a)

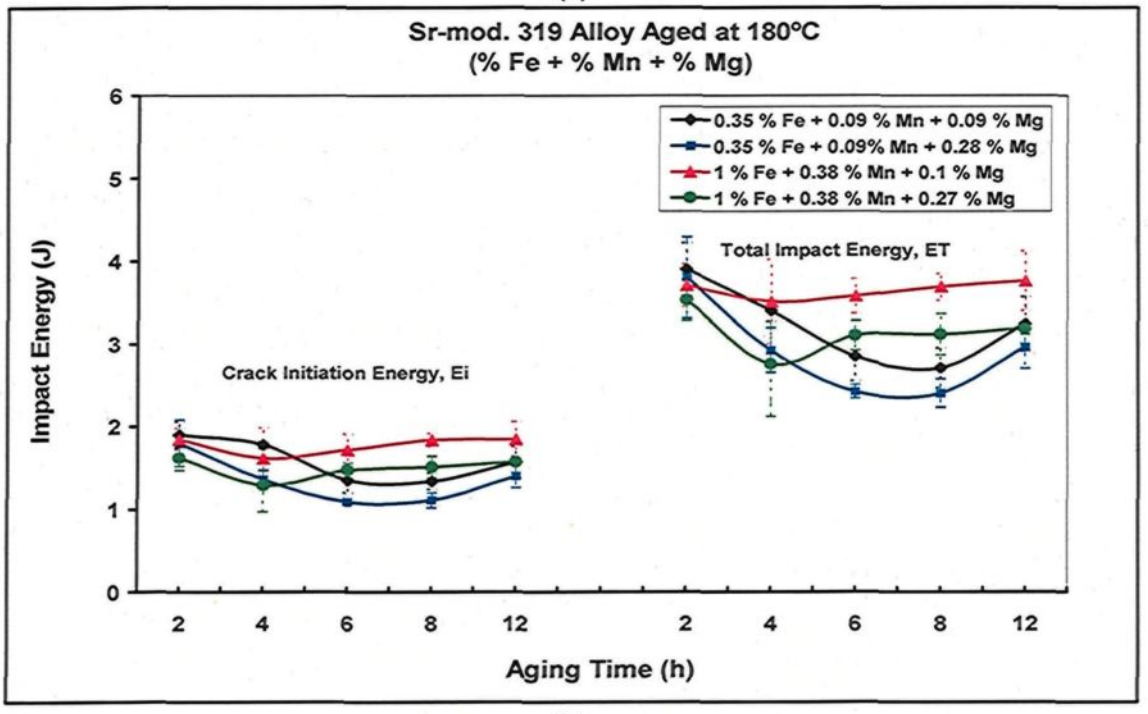

(b)

Figure 5.21 Effects of aging time on impact energy of 319 alloys containing different levels of Fe-Mn-Mg, and aged at 180°C: (a) non-modified alloys, and (b) Sr-modified alloys.

Artificial aging of the Sr-modified alloys at 180°C for 2 hrs produces almost the same level of impact energy values as that obtained in the solution heat-treated condition. These energy values decrease gradually, thereafter, with increasing aging times of up to 8 hrs. Beyond that, the values show a slight recovery when exposed to more extended aging times, *e.g.* 12 hrs, as shown in Figure 5.21(b).

5.3.4.2 Effects of Aging Time at 220°C

Table 20 together with Figure 5.22 illustrate the changes in the impact energy values for the 319 alloys containing various levels of Fe, Mn, and Mg additions after aging at 220°C for various aging times. It will be observed that these values remain virtually unchanged for both non-modified and Sr-modified alloys, and no improvement is seen to be obtained in the under-aging stage. A slight increase in the impact energy values, however, may be observed after 12 hrs of aging for the non-modified alloys containing low levels of Fe, Mn, and Mg additions.

It is worth noting that the Sr-modified 319 alloy containing an addition of 0.3 wt% Fe-0.09 wt% Mn-0.09 wt% Mg displays higher impact energy values for all aging times than those obtained for the same alloys in the solution heat-treated condition, as may been seen in Figure 5.22(b). Such improvements may be ascribed to the high aging temperature (220°C) which results in the softening of the matrix, and also to the low Fe-based intermetallic content of this alloy. All these changes lead to increases in the energy required for both crack initiation and propagation and hence to predominantly improved total impact energy values.

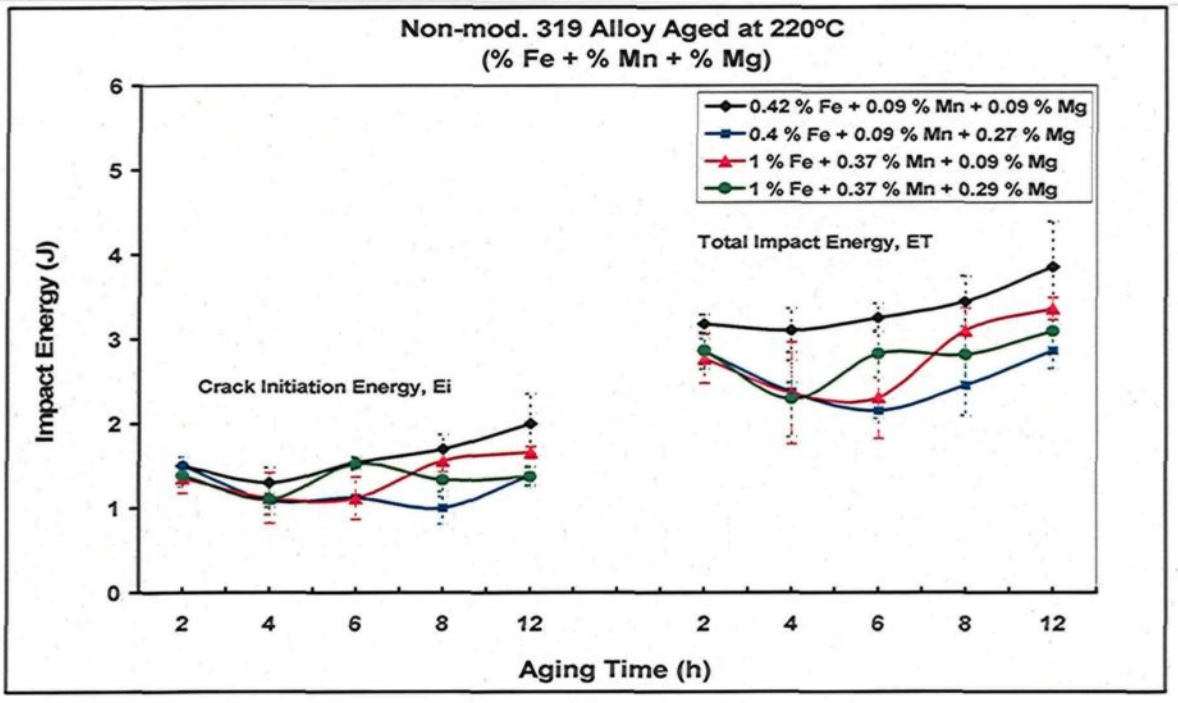

(a)

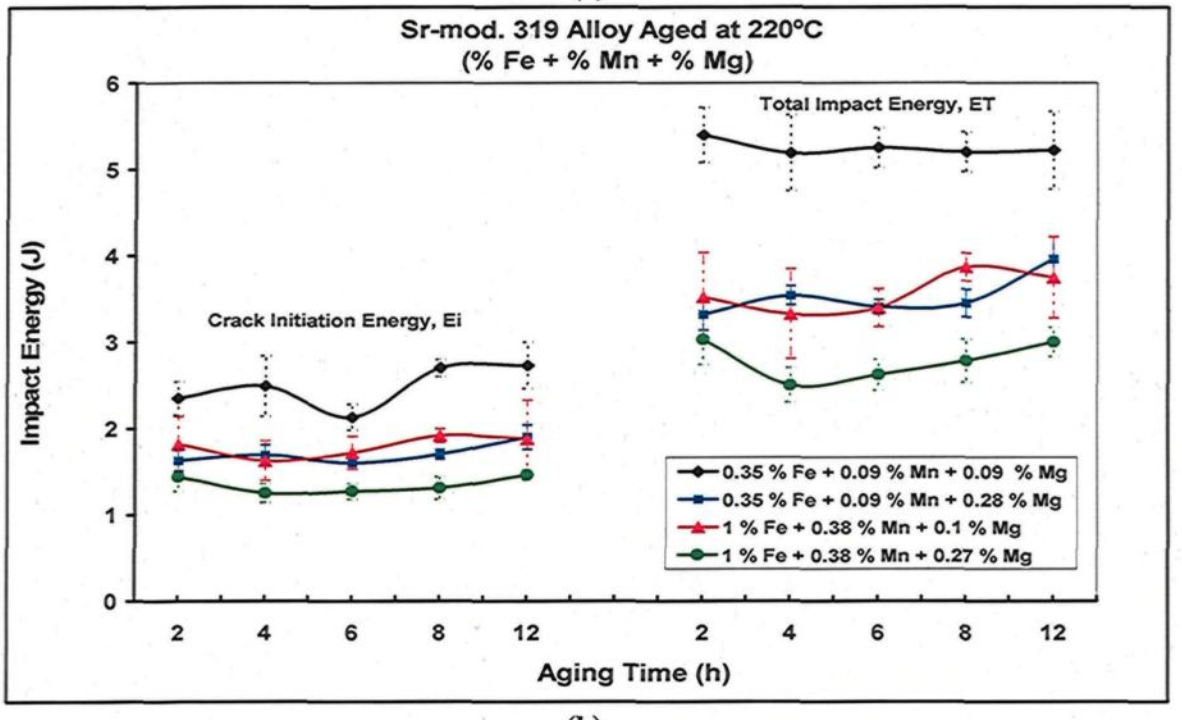

(b)

Figure 5.22 Effects of aging time on impact energy of 319 alloys containing different levels of Fe-Mn-Mg, and aged at 220°C: (a) non-modified alloys, and (b) Sr-modified alloys.

Increasing the level of Mg addition to 0.37 wt% makes it possible for the Mg_2Si phase to precipitate, which, together with the Al_2Cu phase, increases the strength of the matrix at the expense of alloy ductility. The impact energy values thus drop to lower levels, as may be observed for the Sr-modified 319 alloy containing 1 wt% Fe-0.37 wt% Mn-0.29 wt% Mg shown in Figure 5.22(b).

5.4 FRACTOGRAPHY

The fracture surface of selected impact-tested samples of 319 alloys was examined using a scanning electron microscope. Backscattered and secondary electron images were taken from the central region of the fracture surface and the crack initiation edge, accompanied by EDX analysis, all of which was carried out with a view to investigating the role of the Al_2Cu phase in the fracture process of 319 alloys.

Figure 5.23 shows the fracture surface of a non-modified solution-treated 319 alloy containing 0.1 wt% Fe. The presence of acicular eutectic Si particles in both the backscattered and the secondary electron images tends to highlight the role of these particles in the crack initiation and propagation processes in the matrix, as may be seen in Figure 5.23(a) and (c). The Al_2Cu phase is usually to be observed in this alloy in both fine eutectic and blocklike forms. The application of solution heat treatment will dissolve both types of Al_2Cu up to a certain extent; however, the dissolution of the blocklike Al_2Cu phase is more sluggish. The presence of undissolved brittle Al_2Cu is also known to promote crack initiation and facilitate crack propagation. The EDX ray spectrum, corresponding to the bright phase observed in Figure 5.23(a), indicates the presence of Cu and Al peaks;

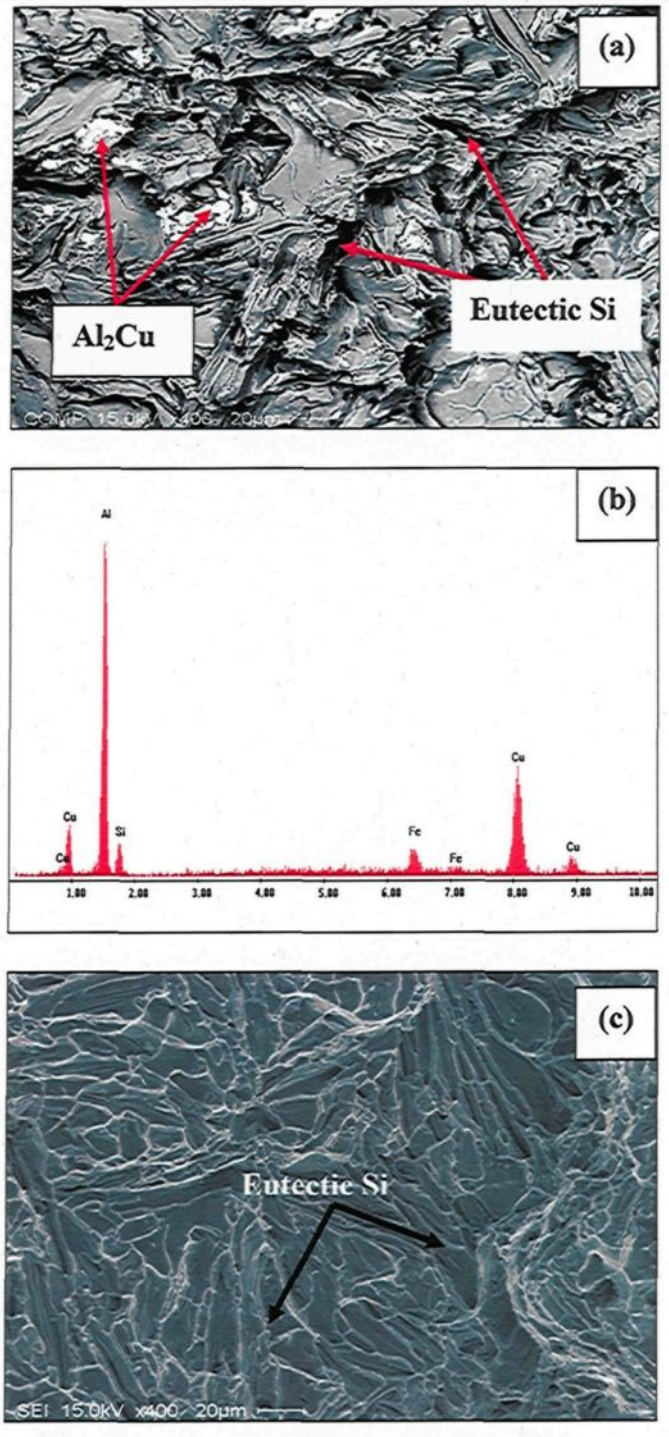

Figure 5.23 The fracture surface of the non-modified 319 alloy: (a) backscattered image, (b) corresponding EDX-ray spectrum of the arrowd phase in (a), and (c) secondary electron images near the crack initiation region shwoing the acicular eutectic Si partcles,

this confirms the fact that the blocklike Al_2Cu phase still persists in the matrix even after solution treatment.

The addition of Sr to non-modified 319 alloys causes the segregation of the Al_2Cu phase in areas away from the eutectic Si regions in the form of block-like particles which are increasingly sluggish in dissolving during solution treatment. The large bright areas present in Figure 5.24(a) show the undissolved block-like particles (arrowed). The secondary electron image taken near the crack initiation region shows the presence of spheroidized eutectic Si particles and dimples indicative of ductile fracture, as indicated by the arrows and circled area in Figure 5.24(c). An analysis of the EDX-ray spectrum of the bright phase/region in (a) shows high-intensity peaks for both Cu and Al elements, Figure 5.24(b), emphasizing the presence of high amounts of undissolved block-like Al_2Cu phase after the application of solution heat treatment. This observation explains why the impact energy values obtained for this alloy are lower than would be expected with the combined application of Sr-modification and solution heat treatment.

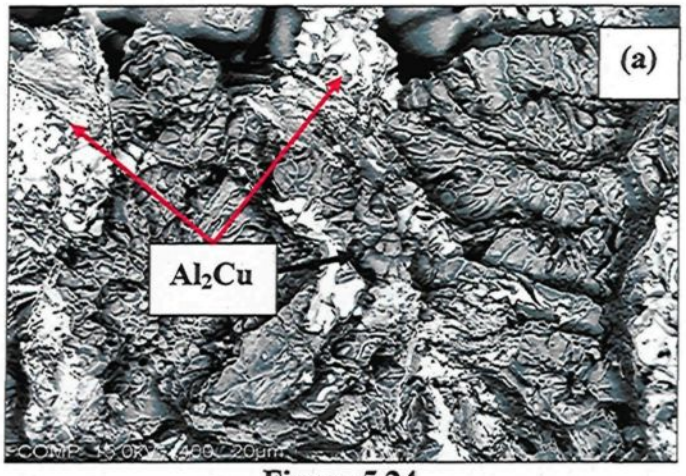

Figure 5.24

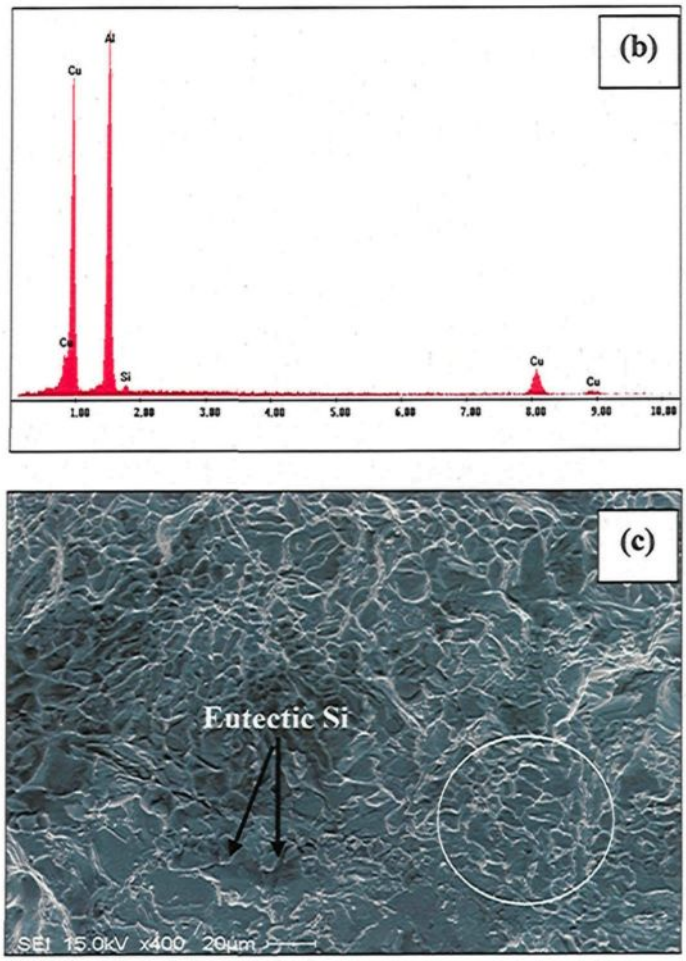

Figure 5.24 The fracture surface of Sr-modified 319 alloy: (a) backscattered image, (b) corresponding EDX-ray spectrum of Al_2Cu phase arrowed in (a), and (c) secondary electron image of the crack initiation region showing modified eutectic Si particles and dimpled area.

5.5 MICROSTRUCTURAL PROFILE BENEATH THE FRACTURE SURFACE

A number of longitudinal sections was extracted perpendicular to the fracture surface from selected impact-tested samples of both 356 and 319 alloys to examine the fracture profile beneath the fracture surface using an optical microscope. This examination was carried out with a view to determining the microstructural constituents which cause

and/or contribute strongly to either the crack initiation or crack propagation processes, these being the two main components of the fracture mechanism.

5.5.1 Effects of Eutectic Si Phase Morphology

Figure 5.25 shows optical micrographs of the longitudinal sections below the fracture surface of non-modified 356 alloy samples containing 0.1 wt% Fe, and aged for 12 hrs at 180°C. It will be observed from these micrographs that the formation of microcracks begins with the cracking of the brittle eutectic Si particles. During the impact testing, rapid non-homogeneous deformation induces internal stresses on the eutectic Si particles and Fe-based intermetallics which start to crack once such internal stresses reach the level of the fracture stress of these particles. [92, 93] In Figure 5.25(a), a secondary microcrack is also observed in the β-iron platelet in the microstructure under the fracture surface. Such an observation confirms the lower impact energy values of about 5.5 J obtained for non-modified 356 alloys under the same aging conditions. Once a large number of eutectic Si particles crack, the microcracks start to grow by linking with adjacent microcracks formed by fracture of other particles so as to form one principal crack. The crack then continues to propagate through the cleavage of other acicular Si particles along the direction shown in Figure 5.25(b), where the fracture appears to display a mainly brittle mode.

The fracture profile beneath the fracture surface of Sr-modified 356 alloys aged for 12 h at 180°C is shown in Figure 5.26. The edge of the sample indicated by the arrow at the left seems to be more curved or rounded than the same area observed in the non-modified alloys (Figure 5.25 (a)). The surface also shows separation of the α-Al dendrites

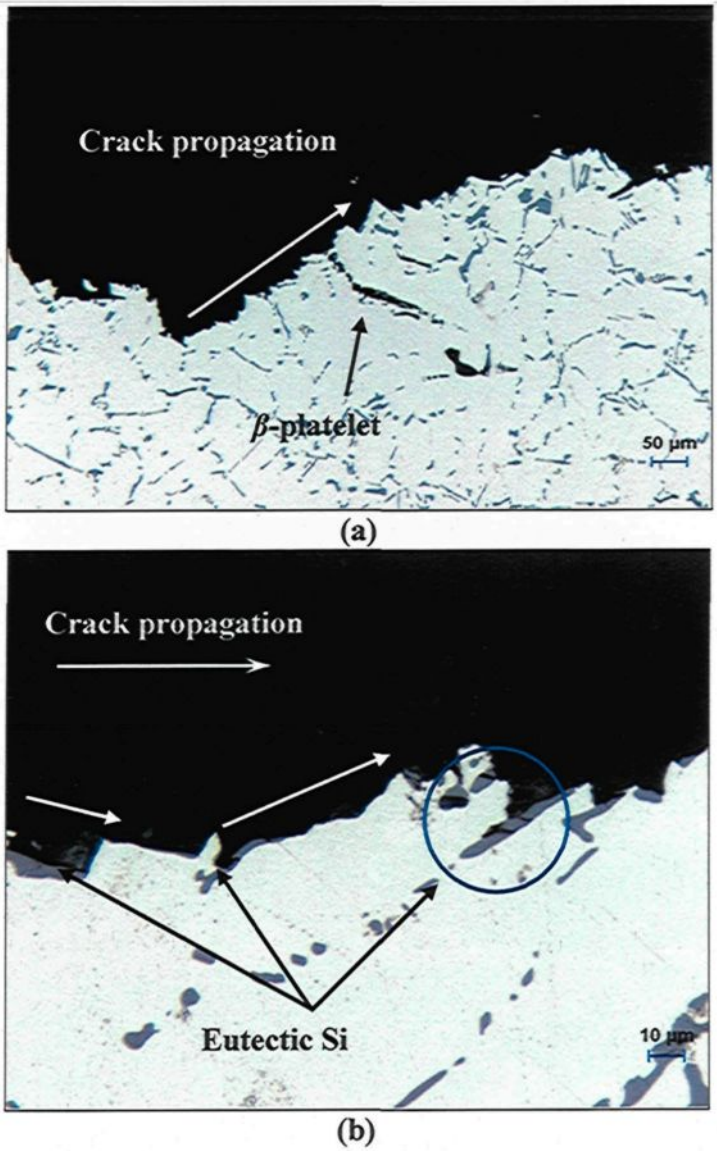

Figure 5.25 Optical micrographs obtained from longitudinal sections below the fracture surface of non-modified 356 alloy samples containing 0.1 wt% Fe, and aged for 12 hrs at 180°C showing the brittle fracture by cleavage of (a) a β-iron platelet, and (b) cracking of eutectic Si particles.

indicating that the fracture occurs primarily in a ductile mode, as may be seen clearly in Figure 5.26(a). The principal crack is then formed by the local linkage of adjacent microcracks. The crack subsequently propagates via further cleavage of iron-based

intermetallics and the fracture path goes mainly through the interdenritic regions, as shown by the arrows in Figure 5.26(b), displaying an intergranular fracture mode.

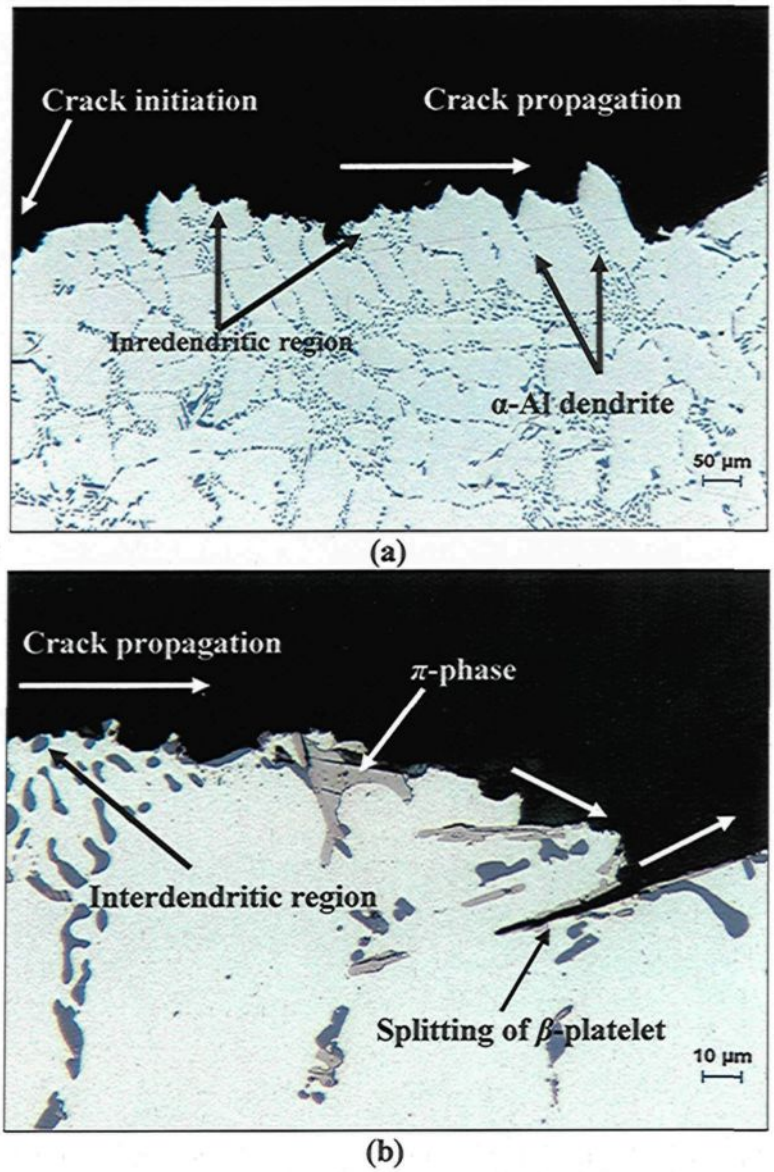

Figure 5.26 Optical micrographs of Sr-modified 356 alloy containing 0.1 wt% Fe showing crack propagation: (a) through interdendritic regions, and (b) via cracking of β-iron platelets and π-iron phase particles.

5.5.2 Effects of Iron-Based Intermetallic Phases

Figure 5.27 presents optical micrographs of the fracture profile beneath the fracture surface, obtained from longitudinal sections of impact-tested 356 alloy samples. This figure shows the role of iron-based intermetallic phases in the fracture process of 356 alloys containing 0.8 wt% Fe and combined additions of 0.8 wt% Fe and 0.4 wt% Mn. It is apparent that the fracture profile is mainly flat and straight, indicating a brittle fracture mode. The fracture of long β-iron platelets contributes strongly to the initiation of microcracks, as shown in Figure 5.27(b) which is a high magnification view of the encircled area shown in Figure 5.27(a). Also, secondary microcracks may form by the splitting of the β-iron platelet into two halves through the middle. The stresses located at the front of this crack are relaxed by local plastic flow into the surrounding ductile α-Al matrix, halting the propagation of the crack. This observation confirms the fact that β-iron platelet are increasingly susceptible to fracture because of their high aspect ratio; it is also in agreement with the approach that larger and elongated particles are more likely to crack than smaller and more rounded ones. Such a fact may also be attributed to the presence of higher internal stresses generated around the elongated particles, thus leading to the probability that cracking will be intensified.[118]

The α-iron Chinese-script phase, on the other hand, undergoes fracture through its arms, the fracture occurring in a direction parallel to the direction of the striking load during the impact test, as shown in Figure 5.27(c) and (d), for Sr-modified 356 alloy containing 0.8 wt% Fe and 0.4 wt% Mn. The platelet β-iron particles appear to be present in these alloys in low amount, however, they were also observed to undergo cracking inside

the microstructure near the fracture surface, as shown in Figure 5.27(b), contributing indirectly to the fracture process.

The role of iron-based intermetallic phases in the fracture process of 319 alloys aged at 180°C for 12 hrs was also examined and is presented in the optical micrographs of Figure 5.28. The β-iron platelets undergo fracture during the Charpy impact test causing either a primary microcrack at the fracture surface or a secondary microcrack beneath the fracture surface inside the matrix, as shown in Figure 5.28(a) and (b). This eventuality emphasizes the significant contribution of β-iron platelets to crack initiation and propagation, confirming the reason for the low impact values obtained for these alloys (~ 2.7 J).

Conversely, the 319 alloys containing combined additions of 0.8 wt% Fe and 0.4 wt% Mn display different fracture mechanisms. It is apparent from Figure 5.28(c) that the α-iron Chinese-script particle fractured through the centerline in the direction of the impact load for the non-modified alloy. The Chinese-script α-iron particles may also undergo fracture by cracking through the arms, as shown in Figure 5.28(d). It should be noted here that the principal crack continues to propagate by the fracture of further α-iron particles through the centerline. This observation supports the findings reported in the preceding sections that the addition of Mn to 319 alloys did not improve the impact energy to any large extent, as had been expected, particularly when compared with the values obtained for the same alloys containing only iron additions

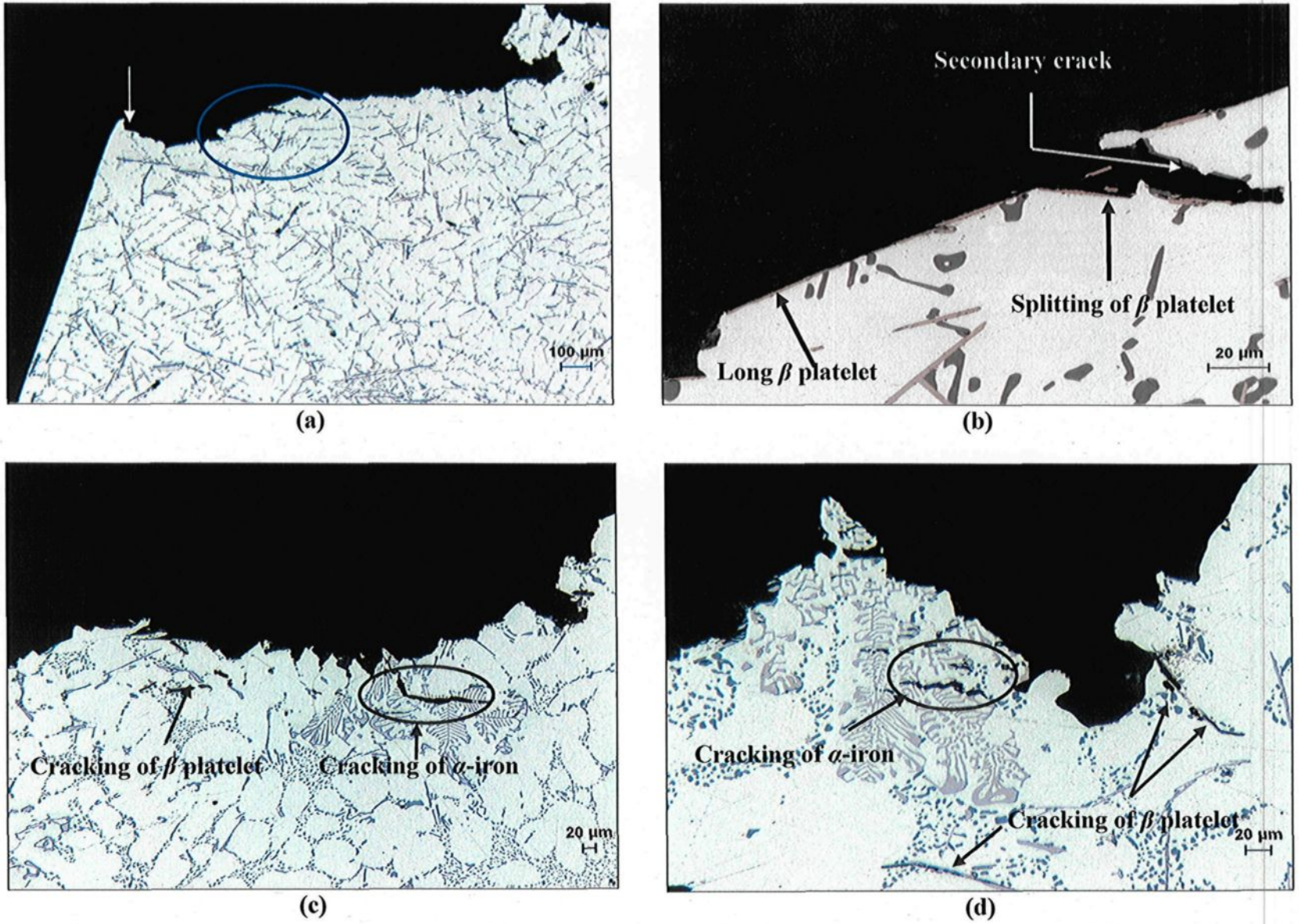

Figure 5.27 Optical micrographs showing the effects of iron-based intermetallics on the fracture behavior of 356 alloys: (a) and (b) non-modified alloy containing 0.8 wt% Fe; (c) and (d) Sr-modified alloy containing 0.8 wt% Fe-0.4 wt % Mn.

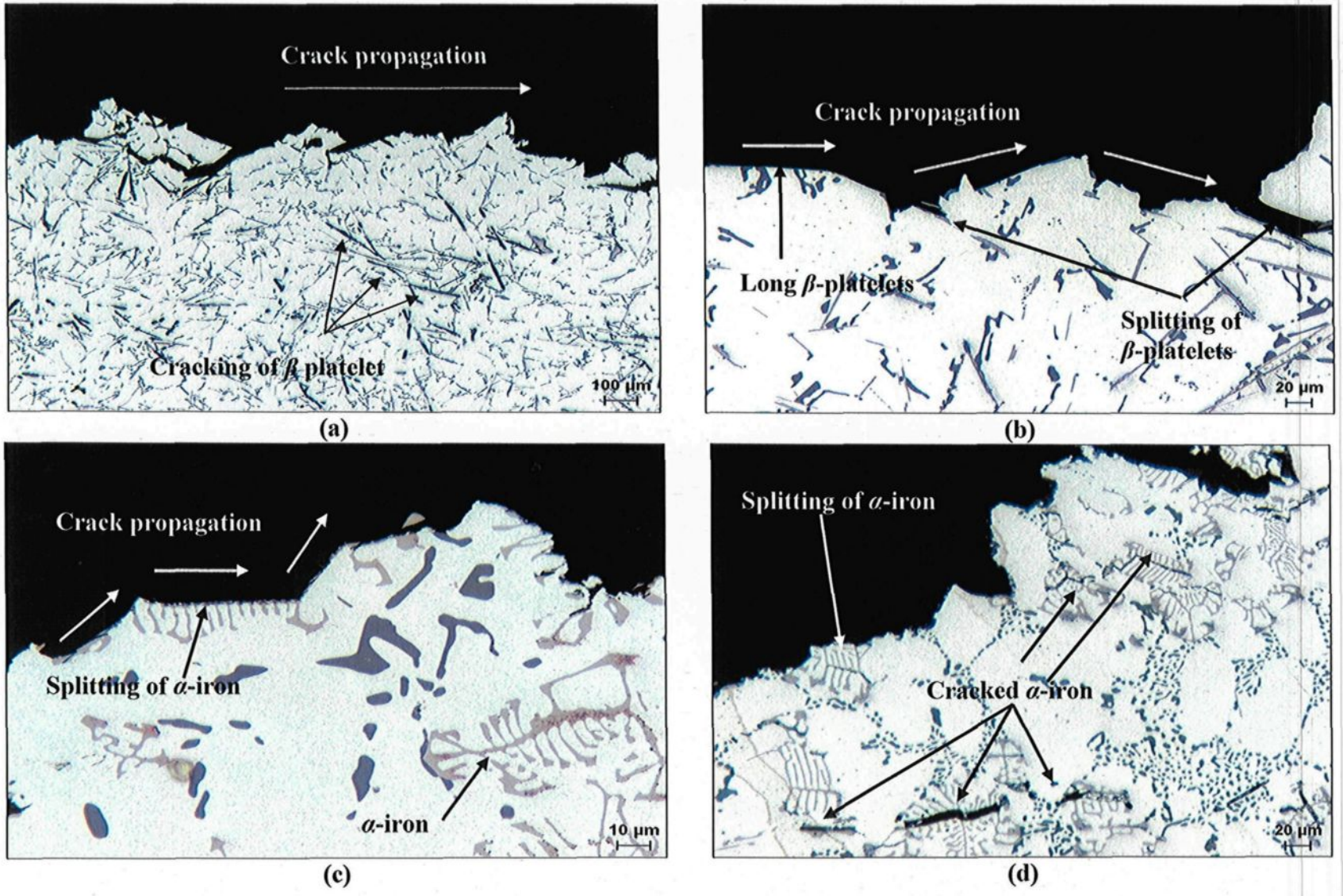

Figure 5.28 Optical micrographs showing the effects of iron-based intermetallic phases on the fracture behavior of 319 alloys: (a) and (b) non-modified alloy containing 0.8 wt% Fe-0.3 wt% Mg; (c) non-modified, and (d) Sr-modified alloys containing 0.8 wt% Fe-0.4 wt% Mn.

CHAPTER 6

IMPACT TOUGHNESS OF NEAR-EUTECTIC ALLOYS

CHAPTER 6

IMPACT TOUGHNESS OF NEAR EUETCTIC ALLOYS

6.1 INTRODUCTION

The current chapter evaluates the effects of cooling rate, additives, and melt treatment as well as of aging conditions on the impact behavior of a newly developed 396 alloy as part of a research project conducted with a view to characterizing and developing a new alloy for automotive applications. The discussion and the interpretation of certain aspects of the impact behavior of the widely-used 356 and 319 hypoeutectic Al-Si alloys in the preceding chapter makes it possible to elaborate on these approaches to arrive at an understanding of the behavior of the new 396 alloy under impact testing conditions.

This near-eutectic 396 alloy was designed to combine upgraded casting characteristics with improved strength and toughness properties to replace ordinary alloys so as to produce thin complex cast components for automotive applications. In order to obtain these design requirements, a Si content having a near-eutectic composition of about 11 wt% in conjunction with specifically controlled amounts of Cu and Mg were selected to form the chemical composition of the new alloy.

The microstructure of these 396 alloys containing various addition levels of Mn and Sr, and obtained under two cooling rate conditions, were discussed in an in-depth study

carried out by Ma *et al.* [119] The main significant conclusions obtained from their study may be summarized as follows:

1) The volume fractions of intermetallic phases are generally much higher in air-cooled samples (high cooling rate) than in furnace-cooled samples (slow cooling rate). Iron-based sludge particles were observed in almost all of the air-cooled alloys with sludge factors of between 1.4 and 1.9; they were not, however, observed in the furnace-cooled alloys having similar sludge factors.
2) Solution heat treatment coarsens the Si particles in the non-modified alloys for both of the cooling rates investigated. In the Sr-modified alloys, solution heat treatment has different effects depending on the cooling rate and Mn level, while it increases the Si-particle area slightly in the air-cooled samples. In the furnace-cooled samples, however, solution treatment decreases the Si-particle area significantly in alloys containing 0.45 wt% Mn whereas it increases it in those containing 0.65 wt% Mn, compared to as-cast conditions.
3) In the air-cooled alloys, solution heat treatment increases the particle roundness of the Sr-modified samples but has no effect on the non-modified ones. In the furnace-cooled samples, solution treatment increases the roundness of the particles in the low-Mn alloys containing 0.45% Mn. This effect decreases with an increase in the Sr level in the high-Mn alloys containing 0.65% Mn so that the roundness begins to diminish at 300 ppm Sr.

4) The length of the Si particles is generally greater and less homogeneous in the furnace-cooled samples than it is in the air-cooled ones. Solution treatment spheroidizes these particles and ultimately leads to coarsening.

6.2 Effect of High Cooling Rate

It has frequently been reported that cooling rate affects the size and morphology of the microstructural constituents of Al-Si alloys to a great extent.[5, 120] The ductility of Al-Si alloys is known to be sensitive, in varying degrees, to dendrite arm spacing, to the eutectic Si phase, to Cu and Mg content, and to the iron-based intermetallics present in the alloy, as well as to the aging conditions. The ductile α-Al dendrites present in the matrix impart toughness to the Al-Si alloy. The composition and morphology of the iron-based intermetallic phases depend not only on alloy composition but also on solidification conditions. The morphology of the iron-containing intermetallic phases is often the main cause of their detrimental effects on alloy quality and on mechanical properties. These phases have a partiality for selective precipitation in the form of α-iron Chinese-script particles under high and low cooling rate conditions of ~ 5-20°C/sec and ~ 0.2°C/sec, respectively, whereas the β-iron platelets tend to be more stable at intermediate cooling rates of 0.6-5°C/sec.[3, 16] Also, the Al_2Cu phase tends to precipitate in the form of fine eutectic Al-Al_2Cu particles at a high cooling rate, whereas it is more likely to be found precipitated in the form of blocklike particles at a low cooling rate.[10] All of these microstructural constituents consequently affect the behavior of the 396 alloys during impact testing.

The total absorbed impact energy, E_T, will be used to discuss the impact behavior of the newly developed 396 alloy from the point of view of additive types and aging conditions, for alloy samples obtained under the two cooling rate conditions. The impact properties and hardness values were determined from the same samples having an identical microstructure, as mentioned previously in Chapter 3; it is thus of interest to interpret the impact behavior in terms of the aging response which may be deduced from the graphs of hardness values plotted against aging temperature as reported in an earlier study. [121]

6.2.1 Effects of Mn Additions

Table 21 gives the average values and standard deviation for the impact properties of 396 alloys containing different addition levels of Mn and Sr for the as-cast and solution heat-treated conditions. It will be observed from Figure 6.1 that the non-modified E1 and E4 alloys display the lowest impact energy values in the as-cast condition as a result of the presence of a number of brittle acicular microstructural constituents acting as crack initiators in the matrix. An addition of 200 ppm of Sr brings about a slight improvement in the impact energy values of the E2 and E5 alloys by about 21% and 39%, respectively, as was to be expected based on the results of the improvements obtained in both crack initiation and propagation energies. The addition of Sr results in the formation of massive particles of the Al_2Cu phase which together with iron-sludge particles serve as stress concentration sites leading to a decrease in crack initiation energy while also facilitating the propagation of cracks. The presence of these microstructural constituents may thus explain such a slight improvement in the impact energy values obtained in this case.

The over-modified E3 and E6 alloys show somewhat lower impact energies compared to those obtained in the modified E2 and E5 alloys, as seen in Figure 6.1. This observation may be explained by the fact that increasing the Sr level up to 350 ppm reduces the degree of modification; thus the eutectic Al-Si structure remains partially modified. The reason for this partial modification is the tendency of Sr to form less-common intermetallic phases such as Al_2SrSi_2 or Al_4SrSi_2, leading to a reduction in the amount of Sr required to obtain full modification.[122, 123] The increased amount of blocklike Al_2Cu particles and their segregation associated with addition of both Sr and Mg may explain the lower impact energy values obtained. These findings are in good agreement with the results obtained in a study carried out by Hafiz *et al.* [83] The researchers found that Sr-modification improves the impact energy values of high purity Al-8Si alloy from 3.9 J to 21 J. Increasing the level of Sr addition by up to 300 ppm, however, reduces the impact energy by about 19%, as shown in Figure 2.28. This study did not, however, discuss the role of iron-intermetallic phases as a parameter with control over the impact behavior of Al-Si alloys. This parameter is of great interest from the design-requirement point of view, particularly in commercially produced castings where iron exists naturally.

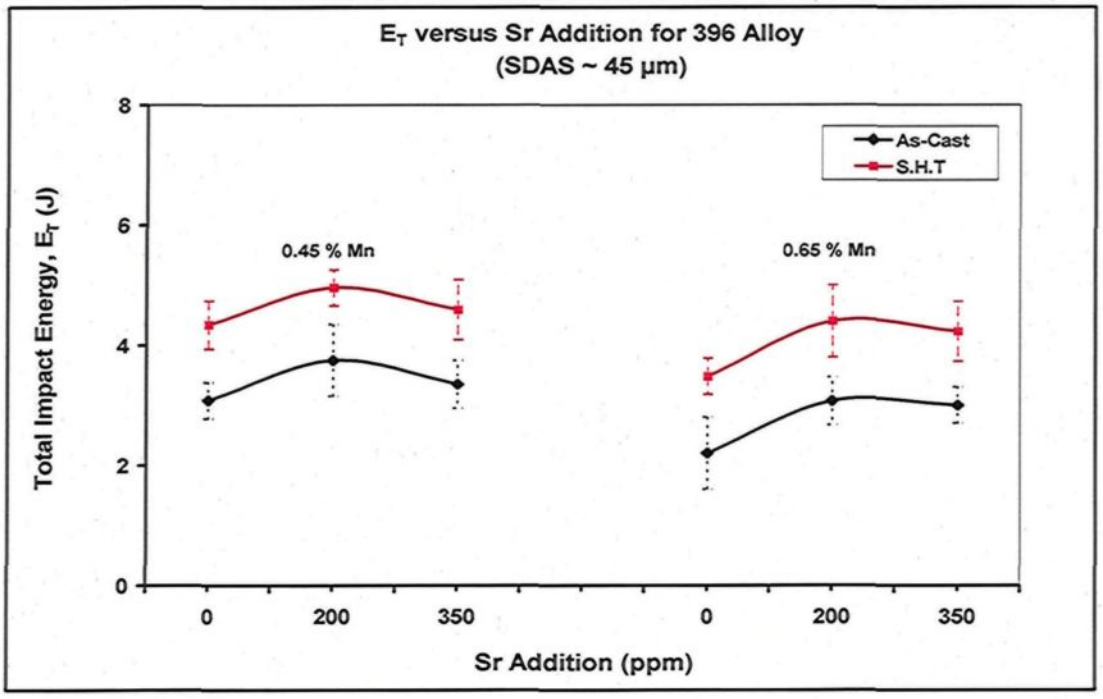

Figure 6.1 Total impact energy versus Sr addition level in 396 alloys containing 0.45 wt% and 0.65 wt% Mn, in the as-cast and solution heat-treated conditions.

It is worth noting that solution treatment at 495°C for 8 hrs appears to improve the impact energy values to a significant degree, regardless of alloy composition. For example, the impact energy of the E1 alloy increases by about 41% which is approximately twice the improvement obtained by Sr-modification which is about 21%. Solution heat treatment is thus generally deemed to be more effective in improving the impact energy than Sr-modification alone. It should also be noted here that a considerable improvement of about 62% in the impact energy values may be observed in the E1 alloy when Sr-modification is combined with solution heat treatment. Such an improvement reflects the beneficial changes occurring in the microstructural constituents associated with the application of both Sr-modification and solution heat treatment. Increasing the level of Mn addition to

0.65 wt%, results in an increase in the volume fraction of α-iron intermetallics and in the proportion of sludge particles, thereby also increasing the brittleness of the high-Mn content alloys, namely E4, E5, and E6. For this reason, the impact energy values obtained for these alloys were lower than those obtained for the alloys containing low levels of Mn, regardless of the alloy condition.

It will be apparent from Figure 6.1 that the 396 alloys display the same behavior as was observed for both the 356 and 319 alloys in the preceding chapter; these values, however, are not so high as those obtained for the 356 alloys. This observation may be attributed to the microstructural differences existing between the 396 alloys and the 356 and 319 alloys in terms of the increase in either the proportion of the eutectic Si phase or in the volume fraction of the intermetallic phases. Another significant reason for such distinct behavior is that the high Mn/Fe ratio of ~ 1.1 to 1.5 in 396 alloys leads to the precipitation of iron-based intermetallic compounds mainly in the form of the Chinese-script α-iron intermetallic phase together with sludge particles; this was reported in an earlier microstructural investigation carried out by Ma *et al.*[119] on the same alloys from which the impact-test specimens were extracted. Since the sludge phase mentioned above consists of hard brittle particles which provide another source for crack initiation and thus have a detrimental effect on the impact energy of the alloys.[124]

6.2.1.1 Effects of Aging Conditions

The aging response to be observed in the 396 alloys depends mainly on the alloying additives and the prevailing aging conditions. Interpreting the aging response based on the hardness plots would promote an understanding of the impact toughness behavior of these

new alloys since both impact energy and hardness values were determined from exactly the same samples i.e. with identical microstructures. The hardness values of the 396 alloys investigated were discussed in detail in a study carried out by Ma *et al.*[121] Analyzing the hardness results of aged alloys yielded the following conclusions:

1. The highest hardness levels to be found among the artificially-aged samples were observed in the non-modified, air-cooled alloys having an SDAS of ~45 μm.
2. The highest hardness levels were obtained by aging for longer times at lower temperatures, as for example at 155°C. At shorter aging times of 5 to 10 hrs, it is possible to obtain high hardness values by aging at 180°C.
3. The alloys studied did not display any softening after 44 hrs at 155°C. At 180°C, however, a slght softening was easily observed after 10-15 h. At aging temperatures of 200°C, 220°C, and 240°C, softening started immediately after a 2 hrs-period of aging.
4. The θ′(Al_2Cu) and S′(Al_2CuMg) second phase precipitates are likely to be responsible for the age hardening in the 396 alloys investigated.

It has been frequently reported that the main changes taking place in the microstructural constituents during the artificial aging process will be noticeable in the size, shape, and distribution of the hardening phases. Such changes are responsible for the artificial aging response of these alloys to a significant degree, depending on the aging temperature and time. Table 22 summarizes the average values and standard deviation for the impact properties of 396 alloys containing 0.45 wt% Mn, aged at different temperatures. Figure 6.2 shows the effects of aging temperature, at certain selected aging times, on the impact behavior of the 396 alloy containing 0.45 wt% Mn, for samples

obtained under high cooling rate conditions. It is apparent that the impact behavior of these alloys is governed to a significant degree by the aging response in which they display minimum impact energy values during the peak-aging stage of 4 hrs at 180°C, regardless of the degree of modification, as shown in Figure 6.2(a). A significant restoration in impact energy may be obtained after aging at 240°C for the Sr-modified E2 alloy. This observation may be attributed to the precipitation of both θ′(Al_2Cu) and S′(Al_2CuMg), leading to a significant increase in the matrix strength at the expense of ductility.[121] It should be noted here that although the E1 and E3 alloys possess different initial eutectic Si strcture, they show a similar impact behavior after aging for 4 hrs at different aging temperature, displaying with lower impact energy values compared to those obtained for the E2 alloy. These findings are in good agreement with those reported in the work of Mohamed *et el.* [125] The researchers observed that the impact energy of near-eutectic Al-10.8% Si alloys containing 0.47% Mn showed minimum values at 180°C which then recovered by about 30 %, as the aging temperature was further increased to 240°C.

The effects of aging temperature on impact behavior may be quite different over relatively large periods of time, as for example after 16 and 44 hrs of aging, as shown in Figures 6.2(b) and (c), respectively. It is evident that increasing the aging time up to 16 hrs and/or 44 hrs results in the expected alloy softening which is reflected by a gradual increase in the impact energy for all the alloys investigated, however, at different rates. It is believed that the improvement observed in crack propagation energy (Ep) is a direct response to the increase in the matrix ductility associated with the softening, ultimately leading to an increase in the overall impact energy (E_T).

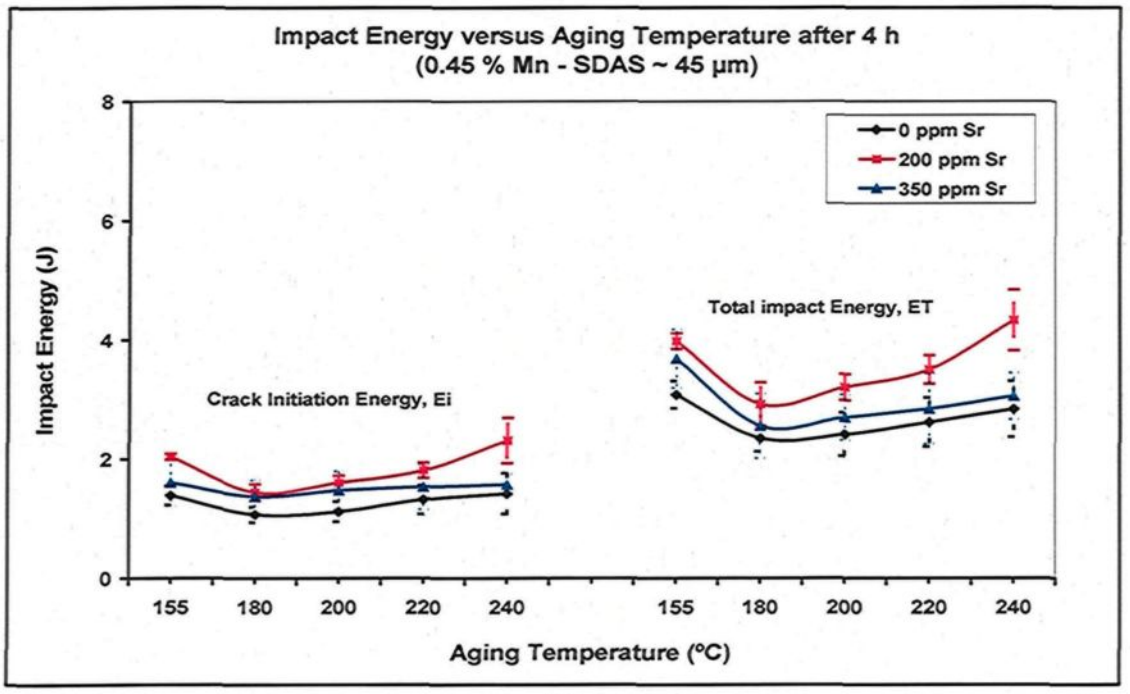
Impact Energy versus Aging Temperature after 4 h
(0.45 % Mn - SDAS ~ 45 µm)
0 ppm Sr
200 ppm Sr
350 ppm Sr
Total impact Energy, ET
Crack Initiation Energy, Ei
Impact Energy (J)
Aging Temperature (°C)
0
2
4
6
8
155
180
200
220
240

(a)

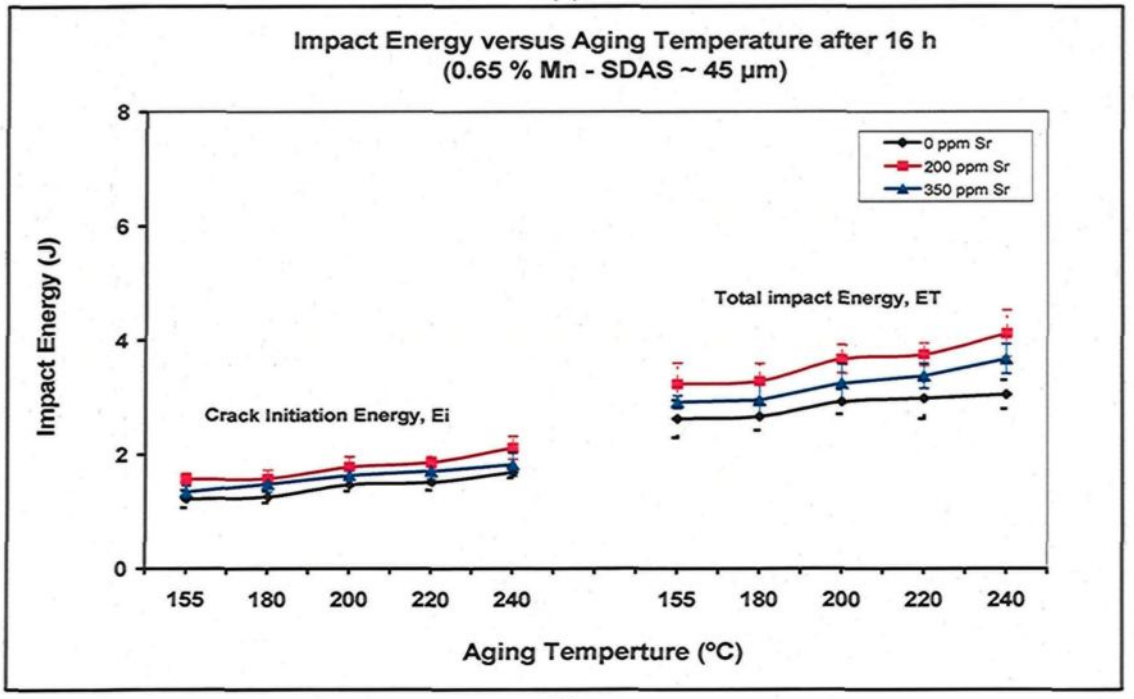
Impact Energy versus Aging Temperature after 16 h
(0.65 % Mn - SDAS ~ 45 µm)
0 ppm Sr
200 ppm Sr
350 ppm Sr
Total impact Energy, ET
Crack Initiation Energy, Ei
Impact Energy (J)
Aging Temperture (°C)
0
2
4
6
8
155
180
200
220
240

(b)

Figure 6.2

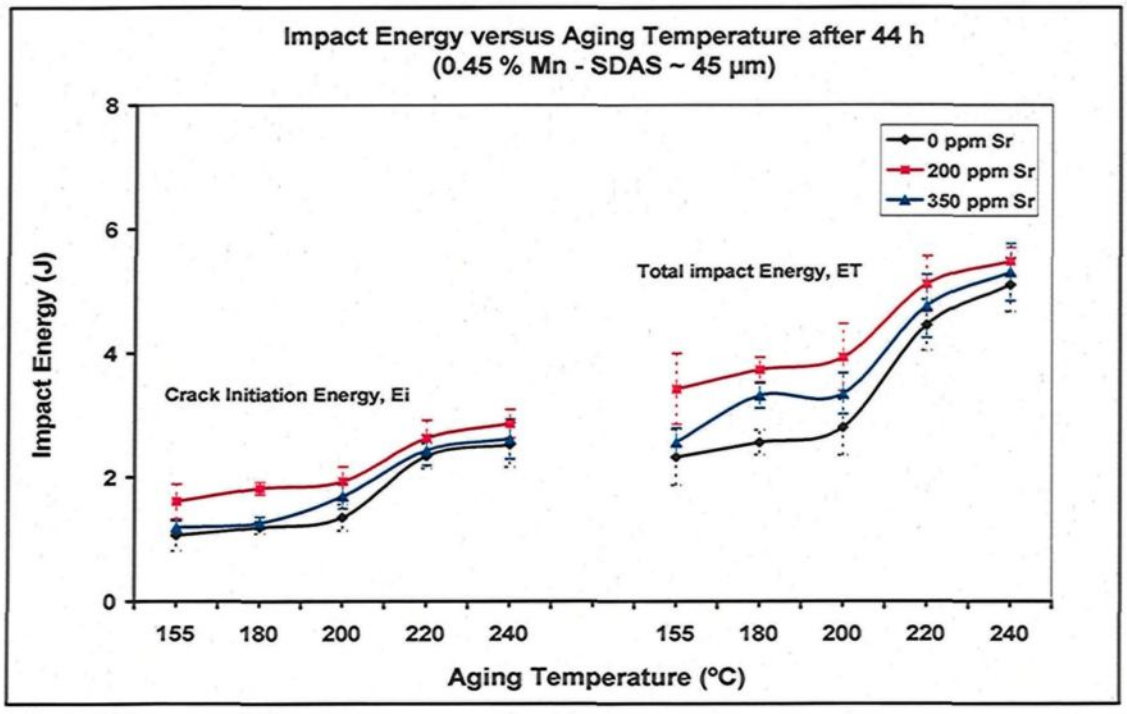

(c)

Figure 6.2 Effects of aging temperature on impact energy of 396 alloys containing 0.45 wt% Mn after aging for: (a) 4, (b) 16, and (c) 44 hrs (SDAS ~45 µm).

It is also interesting to note that the 396 alloys show lower impact energies than those obtained for hypoeutectic 356 and 319 alloys for the same aging conditions. The reason for such behavior may be based on the fact that alloys with different microstructural constituents and aging responses will behave in a distinct way under impact testing or rapid loading conditions. In addition, the presence of hard sludge particles may further contribute to decreasing the crack initiation energy of these alloys.

The effects of aging time on the impact energies of E1, E2, and E3 alloys were analyzed by plotting the total absorbed impact energy as a function of aging time at temperatures of 180°C and 240°C, as shown in Figure 6.3; the average values obtained are

listed in Table 23. These aging temperatures were selected to represent the peak-aging and over-aging stages, respectively, as was reported in the hardness study.[121] The impact energy values appear to change slightly with different aging times at 180°C where, for example, a slight decrease of about 12% is observed for the E2 alloys after 12 hrs of aging, followed by a gradual increase up to 44 hrs. The softening of the alloys results in a slight improvement in the impact energy for all the alloys investigated. Such an observation emphasizes the fact that aging temperature is an essential parameter and that increasing the aging time further does not produce much improvement in impact energy values; this is in good accordance with the findings reported in an earlier study.[121] This negligible improvement is mainly a result of non-significant softening which may occur at peak-aging temperatures with further aging times.

The impact energy values of E1, E2, and E3 alloys after aging at 240°C show a different behavior from the one observed at 180°C, as may be seen in Figure 6.3(b). It is clear that impact energy values increase at a faster rate after 4 hrs for all the alloys because of the softening effect which occurs rapidly at such high aging temperatures. This observation is further confirmed by the decrease in the hardness values in the over-aging stage which is reached in these conditions.[121]

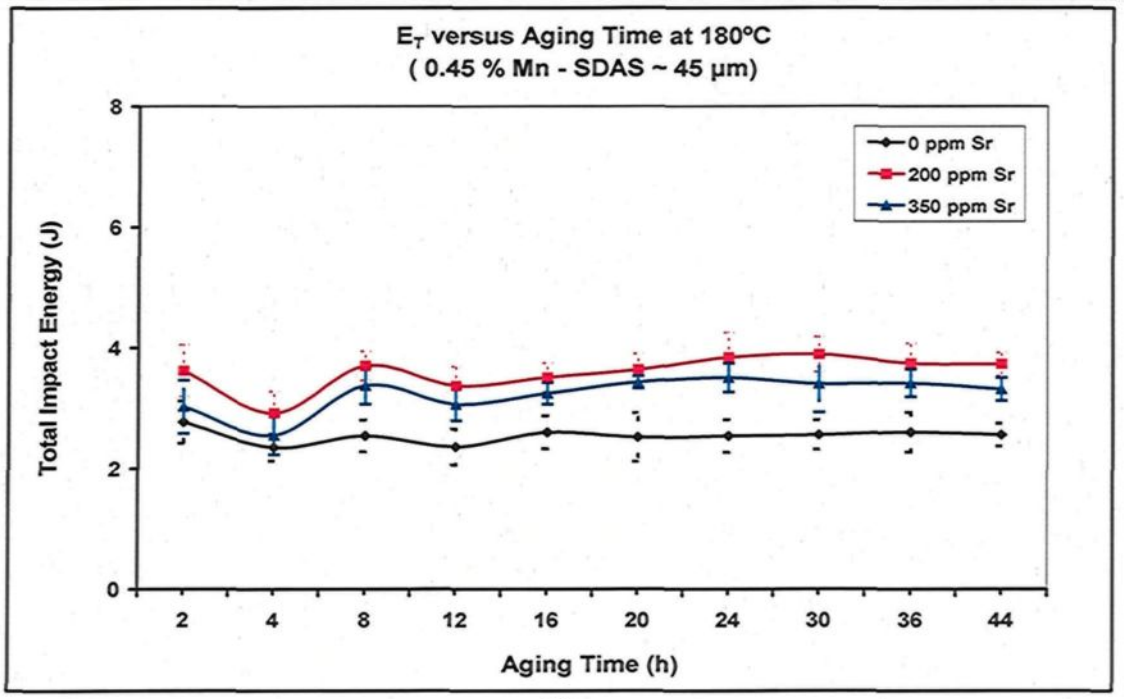

(a)

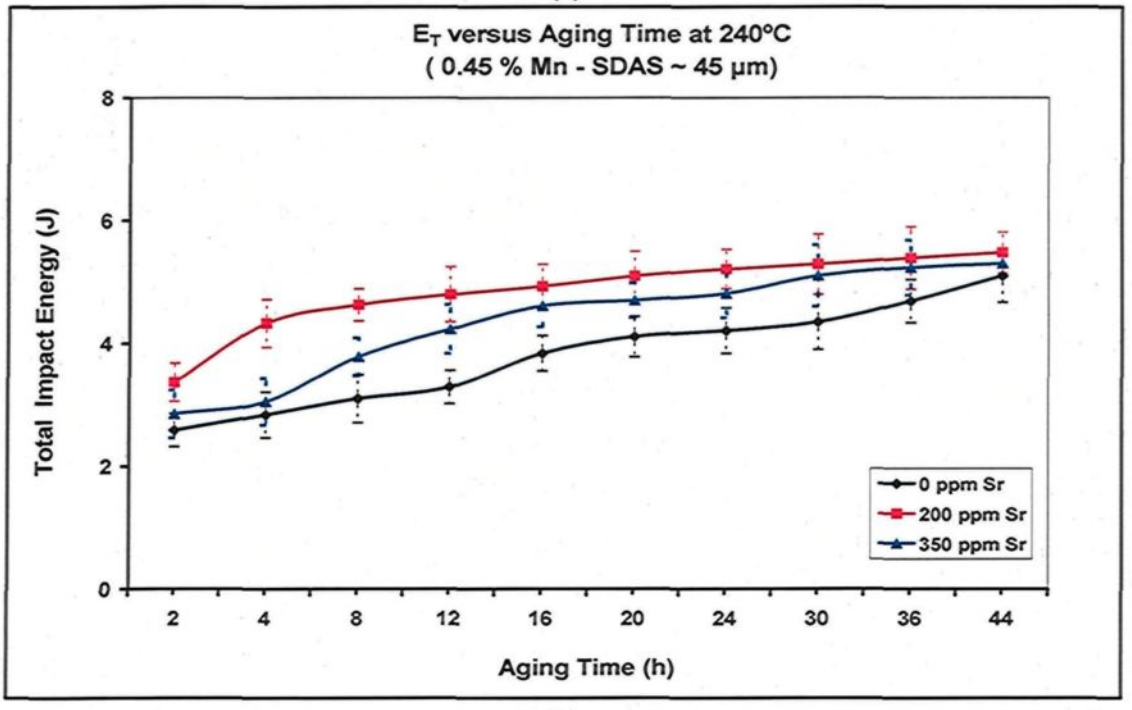

(b)

Figure 6.3 Effects of aging time on impact energy of 396 alloys containing 0.45 wt% Mn, and aged at: (a) 180°C, (b) 240°C, for three different modification levels (SDAS ~45 µm).

Table 24 gives the average values and standard deviation of high-Mn content 396 alloys aged at selected times. The influence of aging temperature on E4, E5, and E6 alloys containing 0.65 wt% Mn is shown in Figure 6.4 where the total impact energy was plotted as a function of aging temperature at 4, 16, and 44 hrs of aging time. The impact energy values of all the alloys decrease with an increase in the aging temperature from 155°C to 180°C after aging for 4 hrs, as shown in Figure 6.4(a). This reduction in impact energy values is thought to be a result of the formation of the peak-aging stage at 180°C which increases the strength of the matrix at the expense of a decrease in the matrix ductility, and which may also promote the possibility of crack formation.

Increasing the aging temperature further from 180°C to 240°C for the same aging time of 4 hrs leads to a recovery in the impact energy by about 45-50%. The alloy softening which takes place at higher aging temperatures explains the recovery in impact properties obtained at 240°C. This behavior is similar to that observed for E1, E2, and E3 alloys, as shown in Figure 6.2(a), although the alloys containing 0.65 wt% Mn appear to display lower impact energies because of the increase in the volume fraction of iron-based intermetallic compounds to 4.4 vol% which consequently decreases matrix ductility and facilitates crack propagation.

Increasing the aging time up to 16 hrs at the same temperatures appears to gradually increase the impact energy values, as shown in Figure 6.4(b). This increase may be explained in terms of the softening which occurs in all alloys being investigated, particularly at aging temperatures of 220°C and 240°C. Artificial aging of high Mn-content

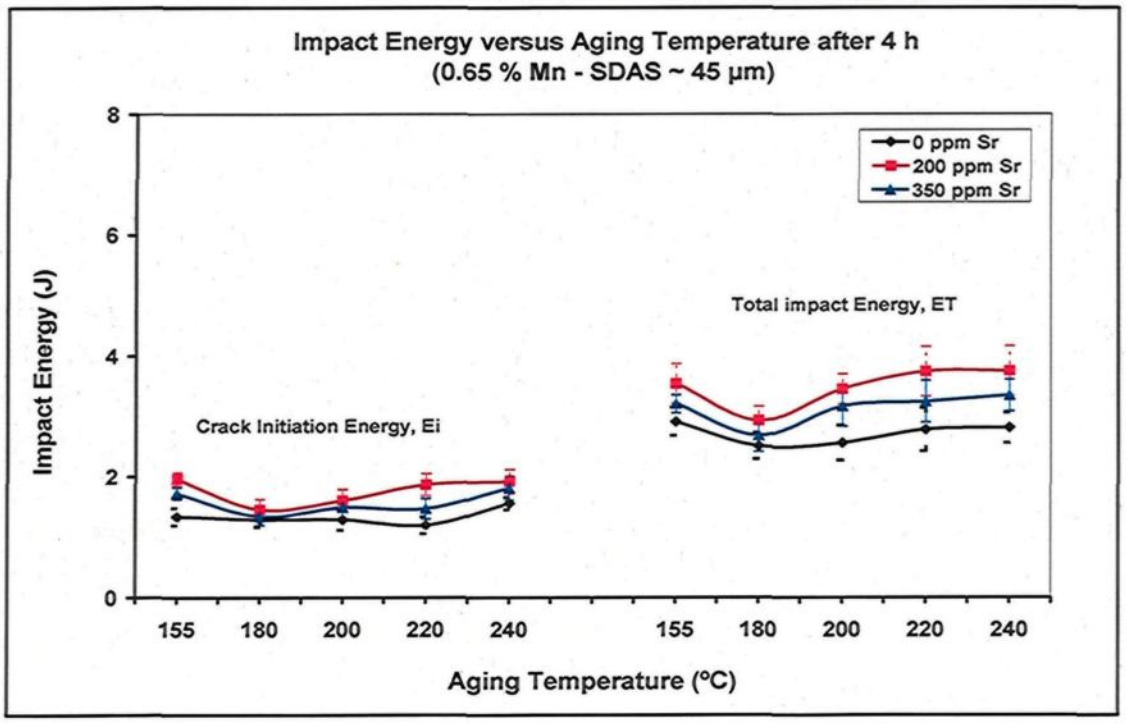
Impact Energy versus Aging Temperature after 4 h
(0.65 % Mn - SDAS ~ 45 µm)
0 ppm Sr
200 ppm Sr
350 ppm Sr
Total impact Energy, ET
Crack Initiation Energy, Ei
Impact Energy (J)
Aging Temperature (°C)
0
2
4
6
8
155
180
200
220
240

(a)

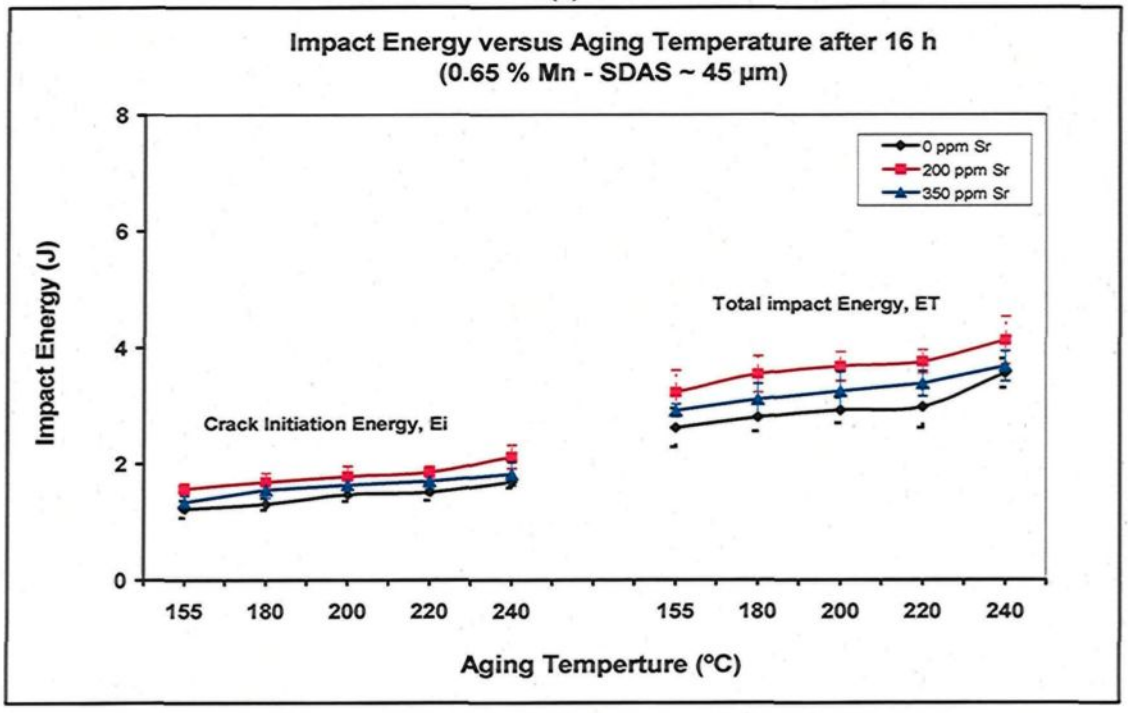
Impact Energy versus Aging Temperature after 16 h
(0.65 % Mn - SDAS ~ 45 µm)
0 ppm Sr
200 ppm Sr
350 ppm Sr
Total impact Energy, ET
Crack Initiation Energy, Ei
Impact Energy (J)
Aging Temperture (°C)
0
2
4
6
8
155
180
200
220
240

(b)

Figure 6.4

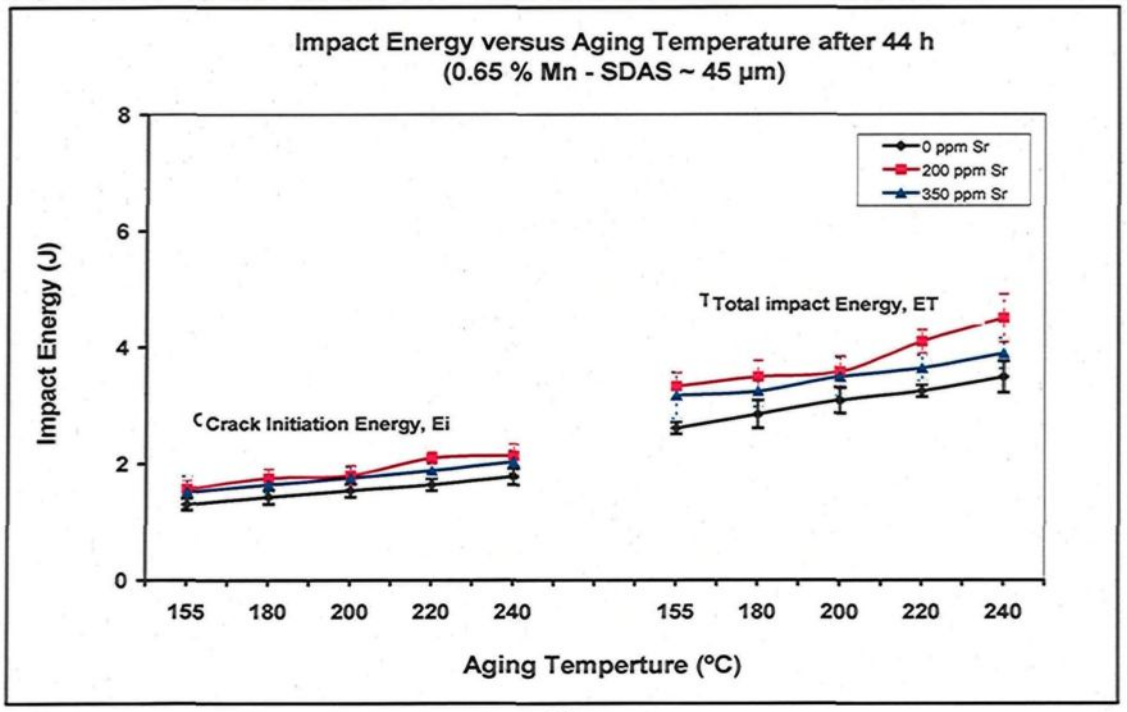

(c)

Figure 6.4 Effects of aging temperature on impact energy of 396 alloys containing 0.65 wt% Mn after aging for: (a) 4, (b) 16, and (c) 44 hrs (SDAS of ~45 µm).

alloys for 44 hrs results in alloy softening which is obvious from the continuous increase in the impact energy values with further aging temperatures, as shown in Figure 6.4(c). For example, the impact energy values show an improvement of about 30%, as the aging temperature is increased from 155°C to 240°C, going from 3.33 J to 4.3 J for the E5 alloy.

Table 25 presents the impact test results of high-Mn content 396 alloys aged at 180°C and 240°C for various aging times. Figure 6.5 shows the dependence of the impact energies of the E4, E5, and E6 alloys containing 0.65 wt% Mn on aging time during aging at both the peak-aging temperature of 180°C and the over-aging temperature of 240°C. It will be observed that the impact behavior follows an opposite tendency to that of hardness

behavior reported elsewhere.[121] This observation once again emphasizes the fact that there is a significant interrelationship between Charpy impact energy and the hardness of Al-Si alloys. It should also be noted that the alloys containing 0.65 wt% Mn show slightly lower impact values than those obtained in alloys containing 45 wt% Mn, as shown in Figure 6.3.

Aging at 240°C for aging times ranging from 2 hrs up to 44 hrs results in an increase in the impact energy values for high-Mn content alloys, representing an improvement of about 62-74%, as shown in Figure 6.5(b). Although the impact behavior of the E4, E5, and E6 alloys displays the same tendency with increasing aging times of up to 44 hrs as a result of undergoing softening at such high aging conditions, they show some variation in their impact energies. The differences in the microstructural constituents of these alloys may be the reason for such variations.

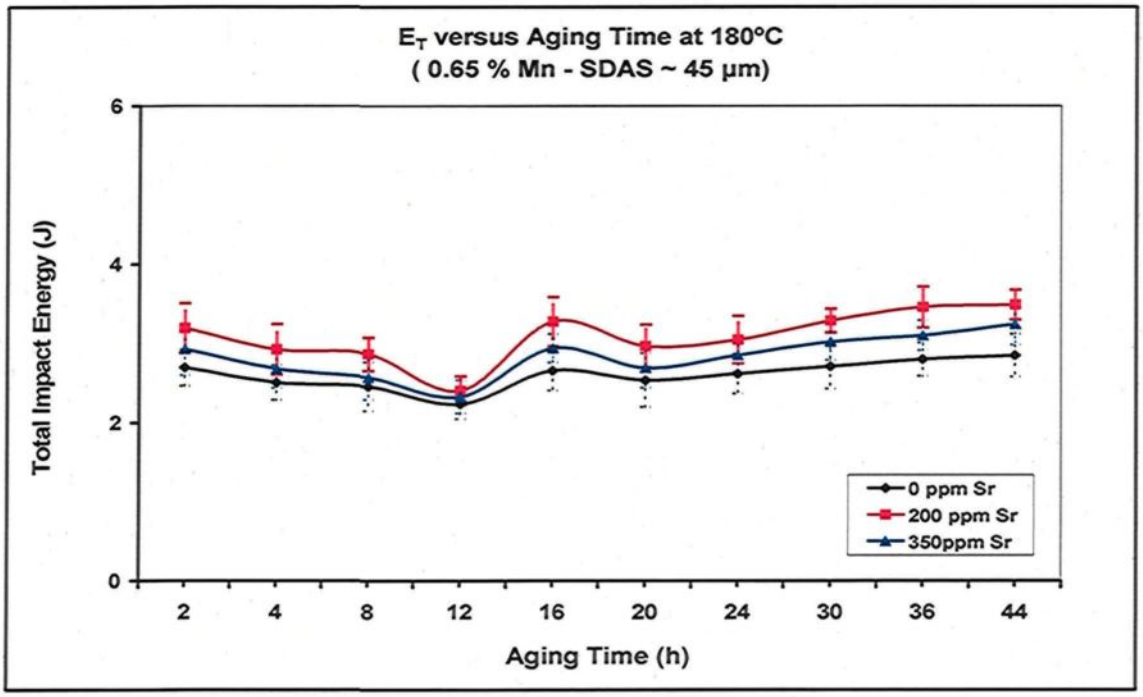

(a)

Figure 6.5

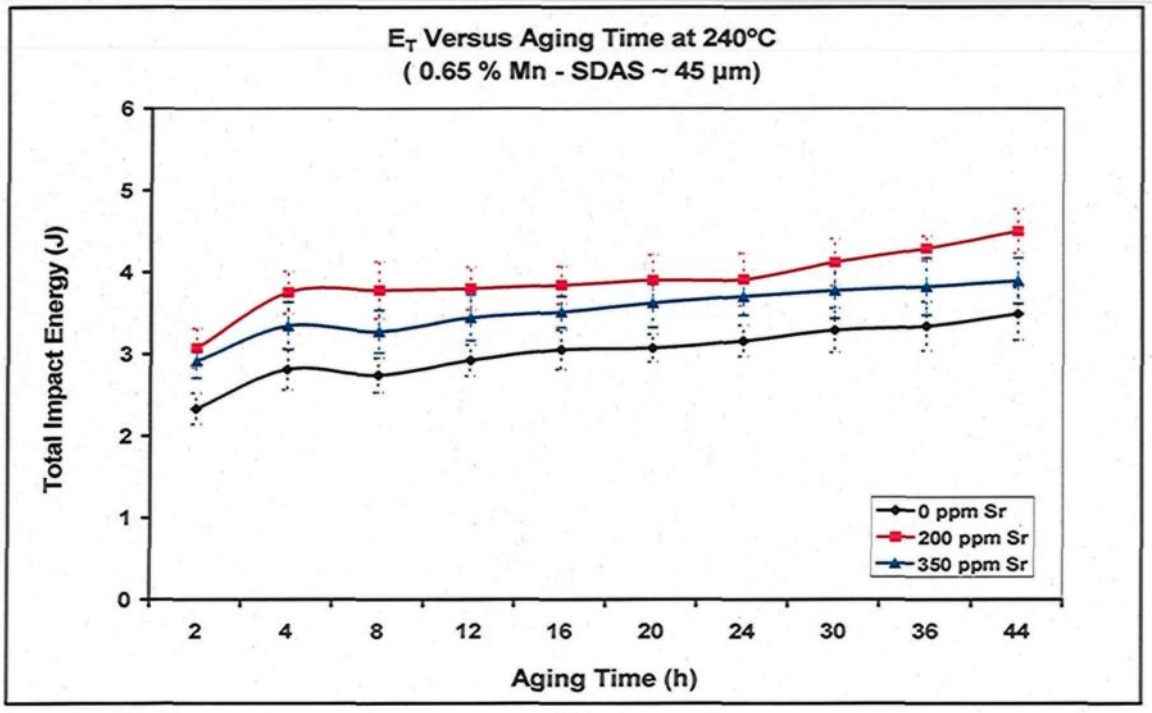

(b)

Figure 6.5 Effects of aging time on impact energy of 396 alloys containing 0.65 wt% Mn, and aged at: (a) 180°C, (b) 240°C, for three different modification levels (SDAS ~45 µm).

6.3 Effect of Low Cooling Rate

It has frequently been reported that a low cooling rate results in non-uniform and large-sized microconstituents in the microstructure of Al-Si alloys. In the present section, decreasing the cooling rate gradually through solidification of the castings inside the furnace increases the dendrite arm spacing to ~ 120 µm and produces large-sized eutectic Si particles having an average particle area of ~ 48 μm^2, accompanied by an increased interparticle spacing of 16 µm in the non-modified HE1 alloy, as reported recently in a study carried out on the microstructure of 396 alloys.[119] The importance of the interparticle

spacing, λ, lies in the fact that it is the ductile matrix distance between the eutectic Si particles which strongly affects the alloy mechanical properties.

6.3.1 Effects of Mn Additions

The total impact energy was plotted as a function of Sr addition for both low- and high-Mn content alloy samples obtained under slow cooling rate conditions, as shown in Figure 6.6; the related averge values are given in Table 21.The scale will be observed to vary with respect to the previous section in order to clarify the changes taking place in the impact energy values upon decreasing the cooling rate. The non-modified HE1 and HE4 alloys show the lowest impact energy values because of the presence of large acicular eutectic Si and primary Si particles, as well as iron-based intermetallic compounds.

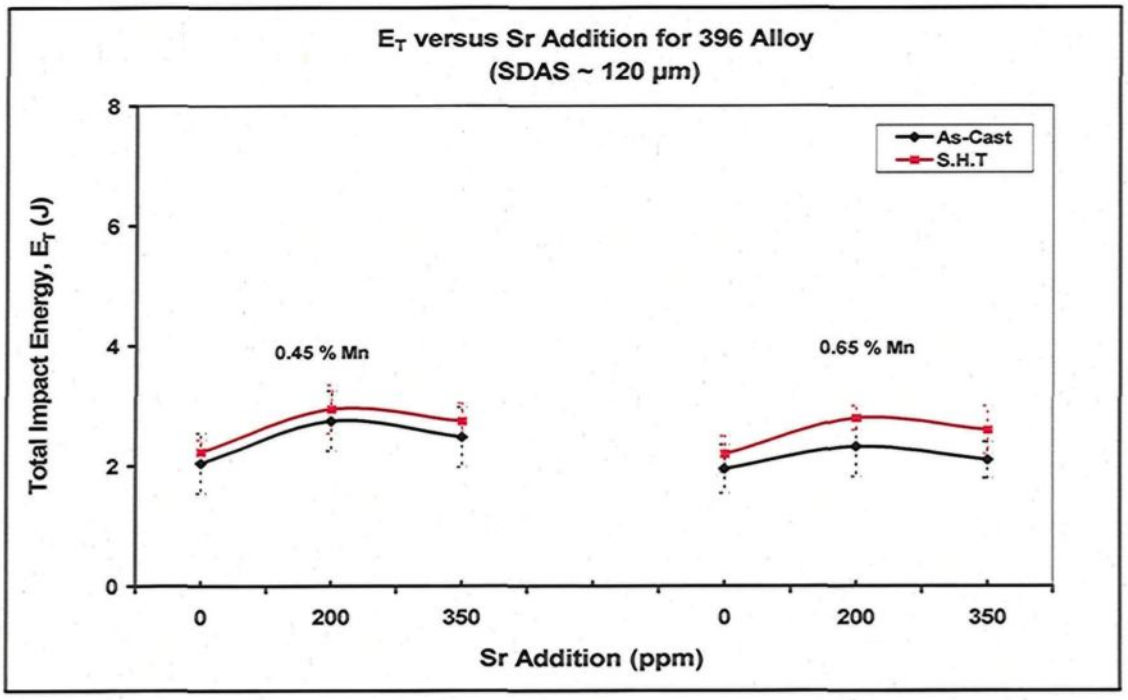

Figure 6.6 Total impact energy versus Sr addition level in 396 alloys containing 0.45 wt% and 0.65 wt% Mn, for the as-cast and solution heat-treated conditions.

Introducing 200 ppm Sr into the non-modified HE1 alloy changes the morphology of the eutectic Si phase and thus improves the resistance to both crack initiation and crack propagation. This improvement, however, is non-significant due to the presence of primary Si particles, massive particles of Al_2Cu phase, and large branched α-Fe phase particles. Although furnace-cooled alloys with both high- and low-Mn content show lower impact energies than those obtained for air-cooled alloys upon the application of Sr addition and solution treatment, these alloys display similar impact behavior for each of the two cooling rates. The increased size of the eutectic Si particles and intermetallics is mainly responsible for these lower impact energies, as will clearly be seen in the backscattered images of Figure 6.19 and Figure 6.20 provided further in section 6.4 of this chapter. These findings are in good agreement with results obtained from the research carried out by Hafiz *et al.*[126] on the role of microstructure in controlling the impact toughness of Al-Si alloys. Their results revealed that the decrease in the impact energy is concurrent with the increase in both dendrite arm spacing and the mean free path across the dendrite or, in other words the interdendritic region, particularly for non-modified alloys, as shown in Figure 6.7.

It is thus reasonable to conclude that impact toughness appears to be more susceptible to minimal variations in the characteristics of the microstructural constituents brought about by the different cooling rates and Sr-modification.

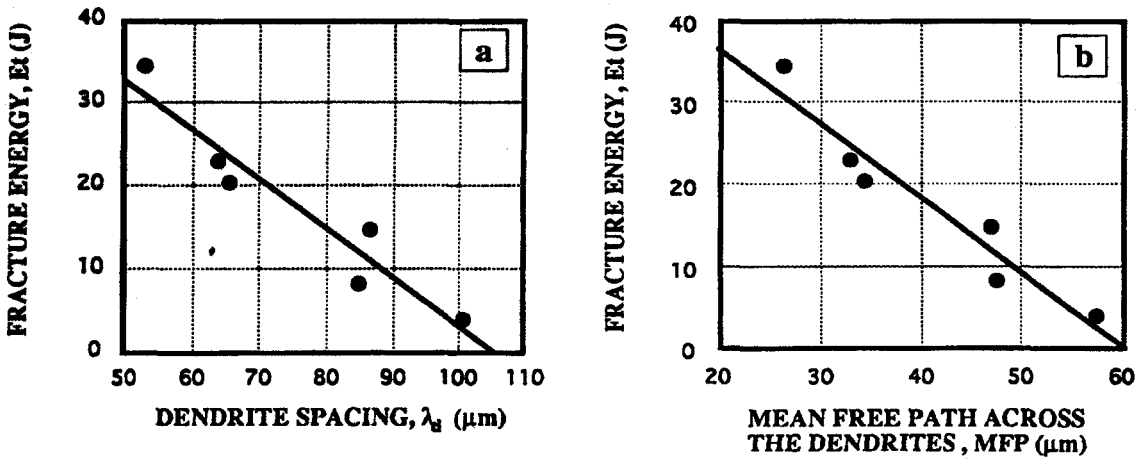

Figure 6.7 Fracture energy as a function of the dendrite spacing and the mean free path across the dendrites.[126]

6.3.1.1 Effects of Aging Conditions

Table 26 lists the average values and standard deviation for low-Mn content 396 alloys. Figure 6.8 shows the effects of aging temperature on the impact energy of 396 alloy samples obtained under low cooling rate conditions, and aged for 4, 16, and 44 hrs, respectively. The important finding here is that although the impact behavior of furnace-cooled alloys shows the same tendency as that observed in the air-cooled alloys with changing aging temperatures, they tend to display lower impact energy values. Decreasing the cooling rate enhances the precipitation of the Al_2Cu phase in the form of blocklike particles which are more difficult to dissolve completely after solution heat treatment and consequently reduce the crack initiation energy. Aging for 4 hrs at different aging temperature results in impact behavior which is opposite to that revealed by the hardness behavior mentioned in an earlier study.[121] The impact energy values decrease until they

reach the peak-aging temperature of 180°C and then they recover again slightly with an increase in aging temperature to 240°C. On the other hand, extending the aging time, for example, either to16 hrs or to 44 hrs, will tend to cause a slight increase of ~ 21% in the impact energy values as a result of alloy softening, which may be clearly seen in Figures 6.8(b) and (c) compared to those shown in Figure 6.8(a). The softening of the alloys, however, appears not to have any effect in raising the impact energy to the level of values expected with an increase in the aging temperature and time, in this case 240°C/44 h. Again, such non-significant effect may be attributed to the fact that the initial microstructure of these alloys contains large sized-particles of iron-based intermetallics, undissolved Al_2Cu phase particles, as well as Si particles, all of which promote crack formation and propagation.

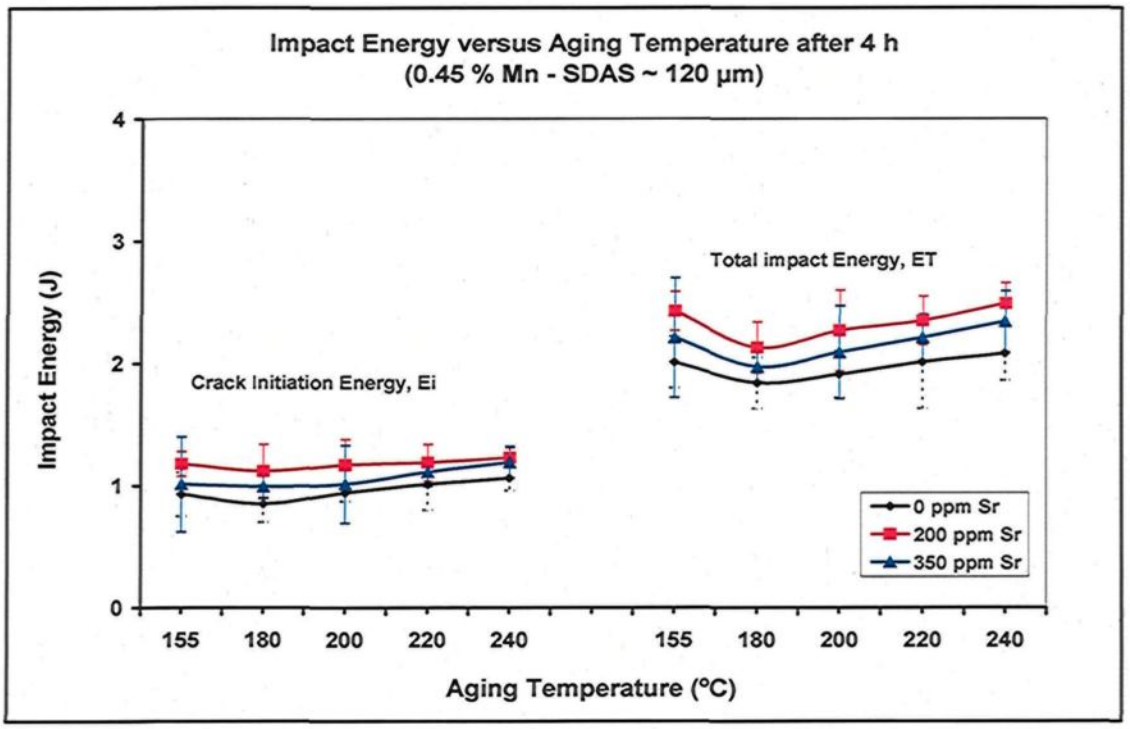

(a)

Figure 6.8

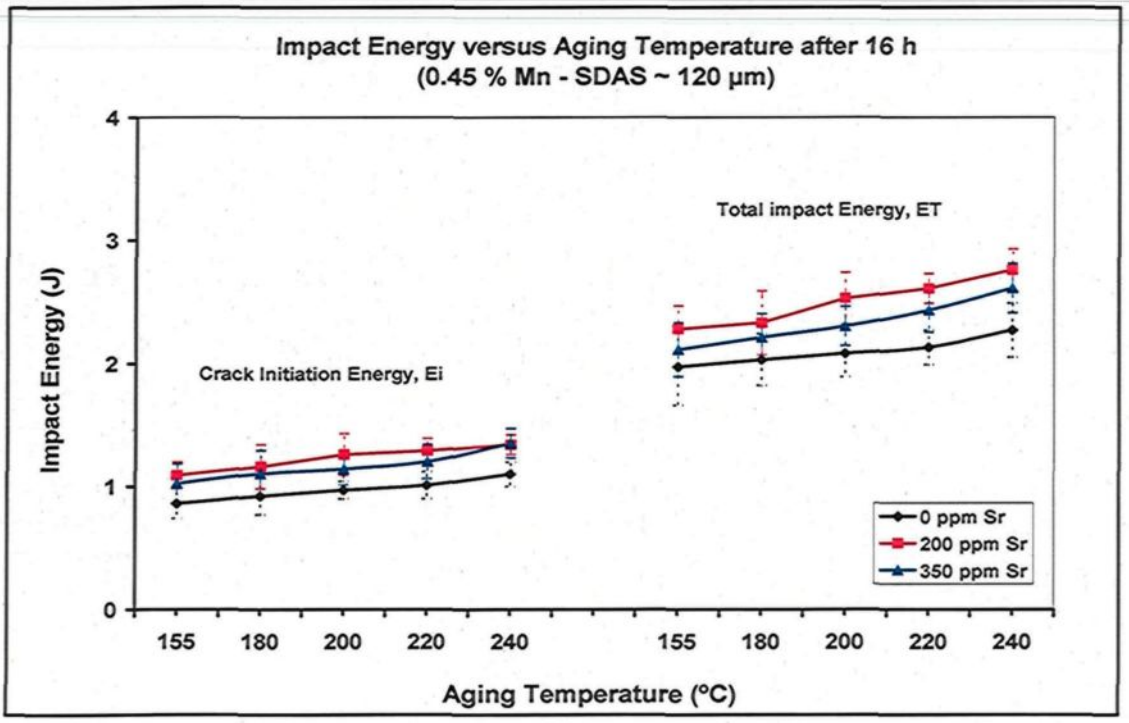

(b)

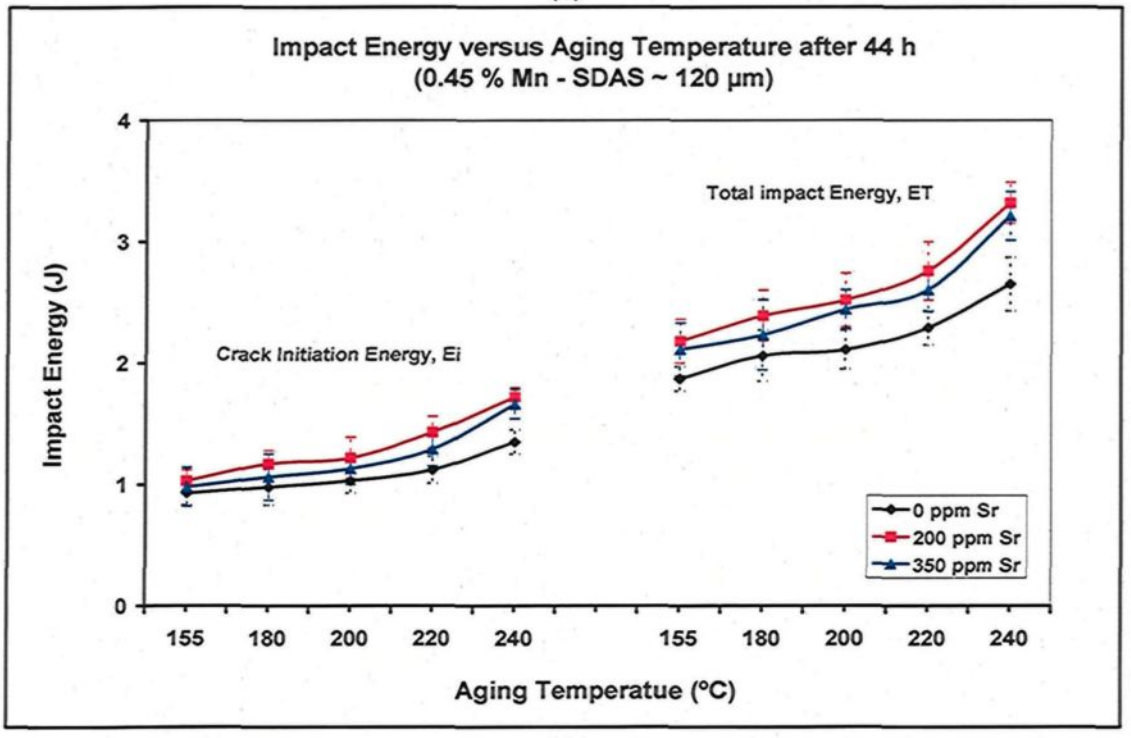

(c)

Figure 6.8 Effects of aging temperature on impact energy of 396 alloys containing 0.45 wt% Mn after aging for: (a) 4, (b) 16, and (c) 44 hrs (SDAS ~120 µm).

It will also be observed that the non-modified HE1 alloy always displays the lowest impact energy of all the alloys investigated as a result of the presence of numerous acicular microconstituents as well as of primary silicon particles, regardless of the aging conditions, as shown in Figure 6.35 under section 6.4.2.

Table 27 summarizes the average impact energy values and standard deviation obtained at both 180°C and 240°C for 396 alloys containing 0.45 wt% Mn, while Figure 6.9 illustrates the effects of aging time on the impact energy of these low-Mn content alloys aged at the two temperatures. It should be noted that the impact energy values of the HE2 alloy show a slight reduction with an increase in aging time of up to 12 hrs and then remain unchanged, whereas the impact values of the HE1 and HE3 alloys remain virtually constant, as shown in Figure 6.9(a). This impact behavior is similar to that observed previously in the air-cooled alloys shown in Figure 6.3. The initial microstructure of furnace-cooled alloys contains large size eutectic Si and intermetallic phase particles, as well as primary silicon which should also be considered when discussing the impact behavior.

Artificial aging at high temperatures of 240°C, on the other hand, results in an increase in the impact energy values with further aging time up to 44 hrs, as shown in Figure 6.9(b). The improvement observed may be ascribed to the alloy softening which occurs at such high aging temperatures. It is also worth noting that the impact energies obtained in this case are lower than those obtained for air-cooled alloys under the same conditions. These results lead to the same conclusions, namely that the impact energy values of aged alloys depend strongly on the changes occurring in the characteristics of the

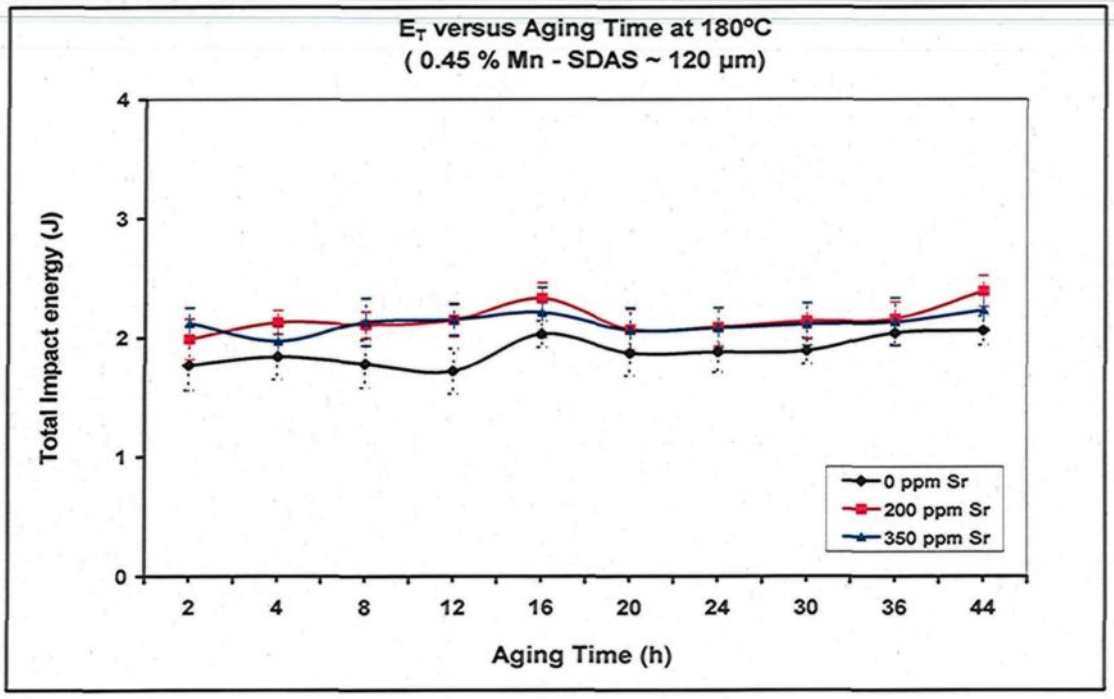

(a)

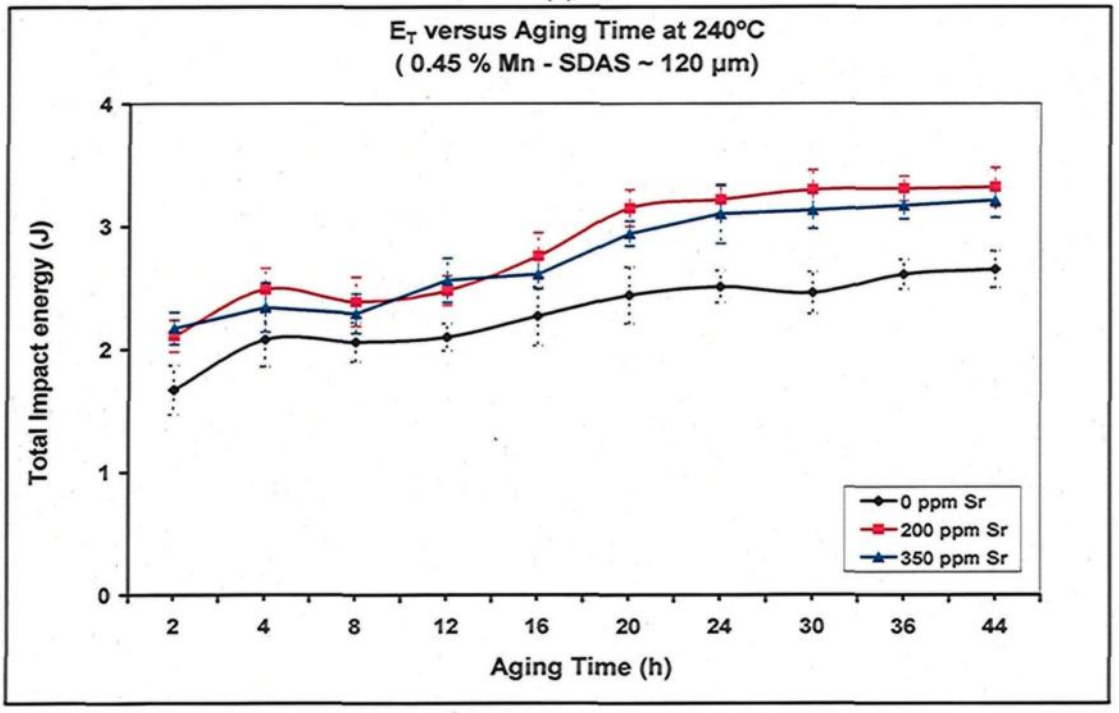

(b)

Figure 6.9 Effects of aging time on impact energy of 396 alloys containing 0.45 wt% Mn, and aged at: (a) 180°C, (b) 240°C, for three different modification levels (SDAS of ~ 120 µm).

hardening phases as well as on the characteristics of the initial microstructural constituents in the as-cast condition.

The influence of aging temperature on the impact energy values of high-Mn content alloy samples obtained under low cooling rate conditions, and aged for 4, 16, and 44 hrs is shown in Figure 6.10 and the average values are listed in Table 28. It will be observed that the variation in impact energy is relatively small between the different alloys investigated. Increasing the aging time to 16 hrs and 44 hrs leads to a softening of the alloys, as deduced by the obvious increase in impact energy values seen in Figures 6.10(b) and (c). These observations are similar to the previous findings on low-Mn content alloys displayed in Figure 6.8. Another observation which may be made from Figure 6.10 is that the crack initiation energy behavior also displays a tendency similar to that of the total impact energy

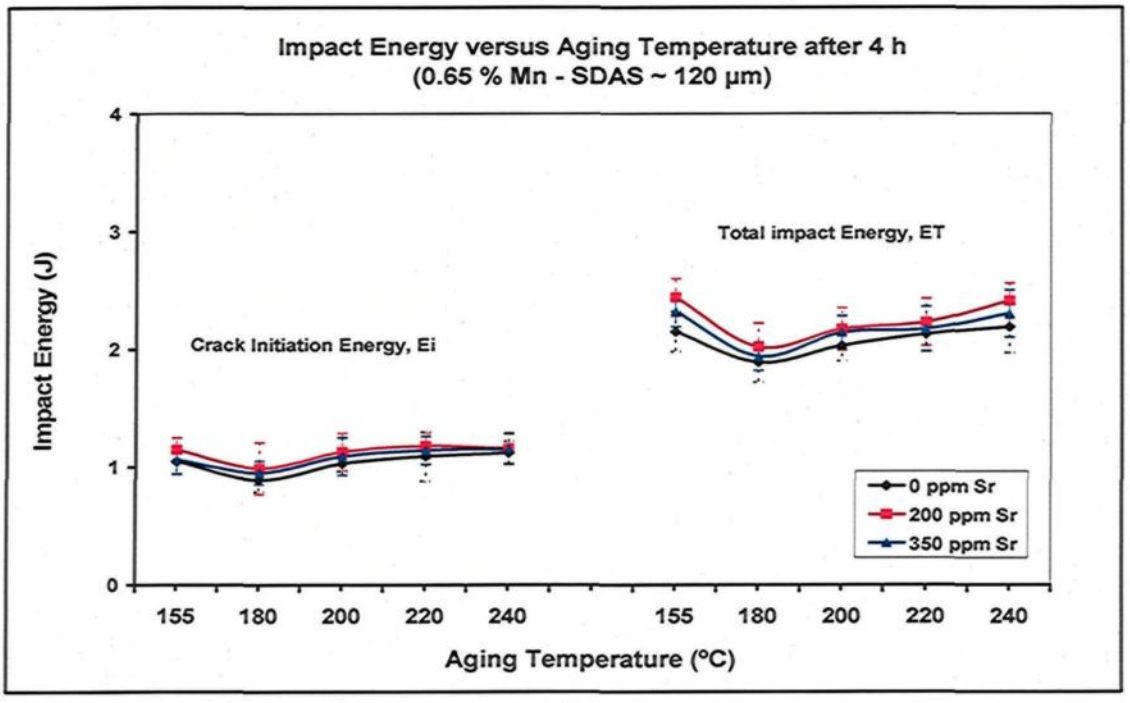

(a)

Figure 6.10

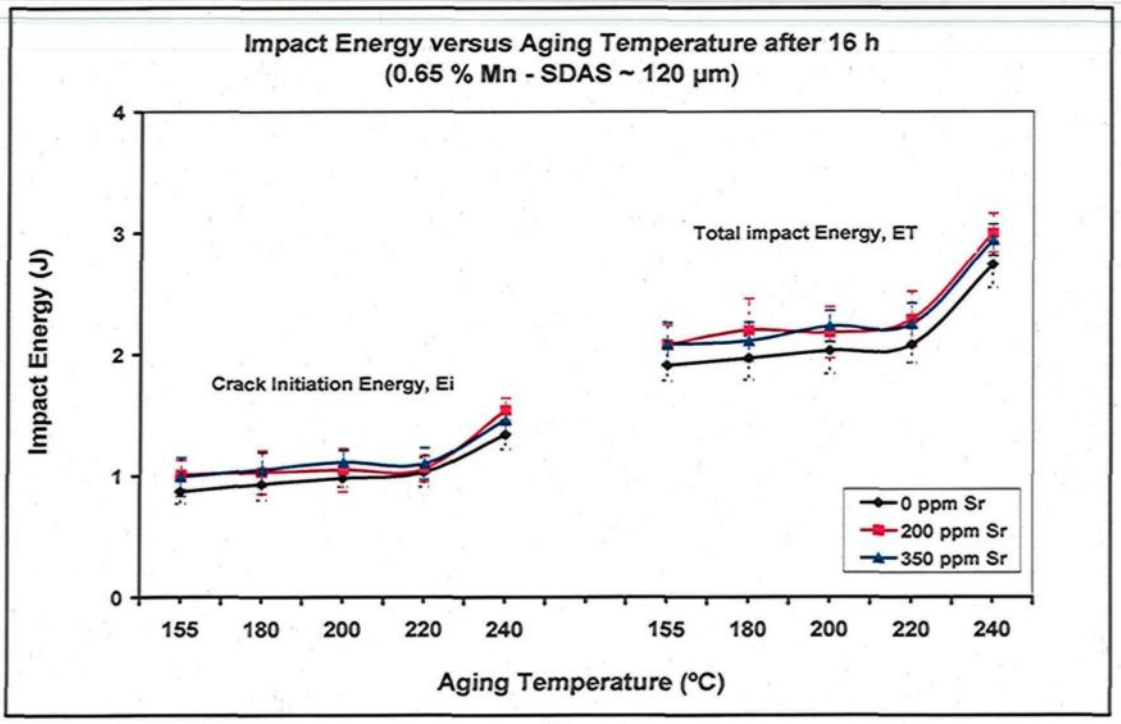

(b)

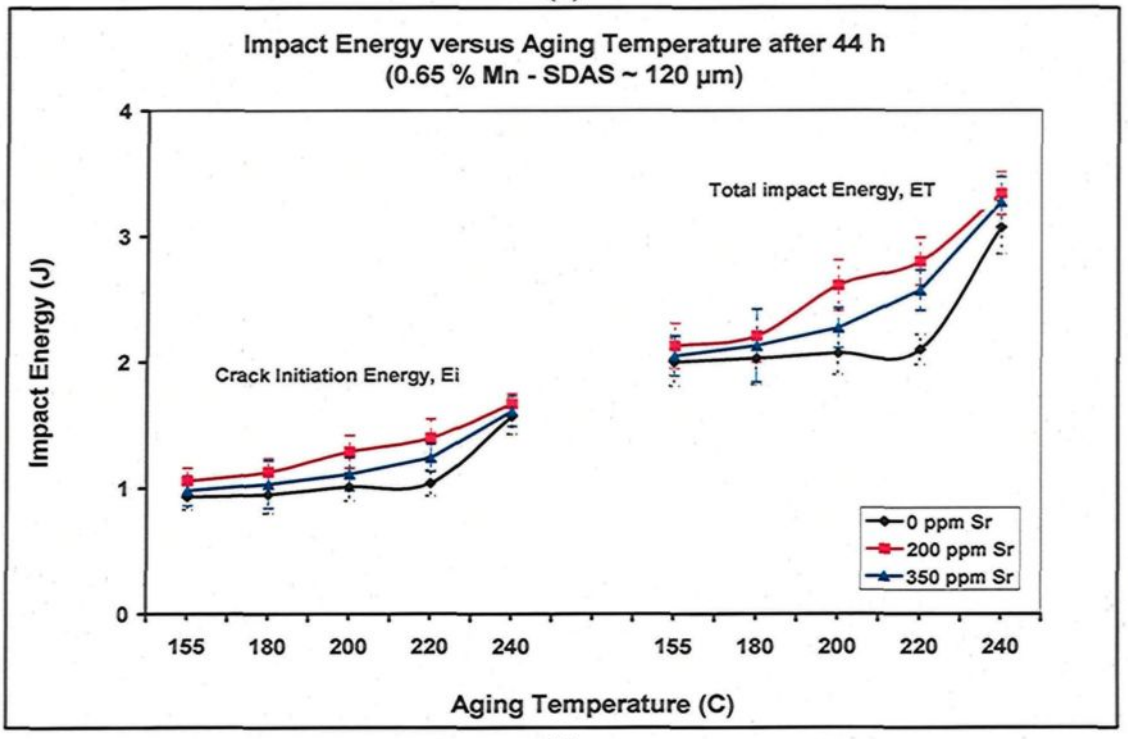

(c)

Figure 6.10 Effects of aging temperature on impact energy of 396 alloys containing 0.65 wt% Mn, after aging for: (a) 4, (b) 16, and (c) 44 hrs (SDAS ~120 µm).

for all the alloy conditions studied. It would be reasonable to conclude, therefore, that the initial microstructure plays an important role in regulating the impact behavior of these alloys.

Table 29 presents the average values and standard deviation of impact energy parameters for 396 alloys. Figure 6.11 draws the comparison between the effects of aging time on the impact energy values of high-Mn content alloys at the peak-aging temperature of 180°C and those prevailing at the over-aging temperature of 240°C. The variation in impact energy values is only slightly discernible, or else it remains virtually unchanged with different aging times at 180°C, as shown in Figure 6.11(a). This result was previously observed for the low-Mn content alloys shown in Figure 6.9 under the same conditions, emphasizing the aspect that increasing the aging temperature is more effective in improving the impact energy values than the aging time. Such an aspect is further clarified in Figure 6.11(b), where the impact energies are seen to improve significantly after aging at 240°C for various times up to 44 hrs, as, for example, the increase of ~39% observed for the HE5 alloy. The softening which occurs at during over aging appears to improve both crack propagation and crack initiation energy values, although the large-sized undissolved Al_2Cu particles and iron-based intermetallics cause this improvement not to be as large as that obtained in the case of the air-cooled alloys, as observed in Figure 6.5. The preceding results emphasize the fact that, even in the aged condition, the features of the initial microstructural constituents are a significant parameter should be considered in the interpretation of the impact behavior, particularly for alloys cast under low cooling rate conditions.

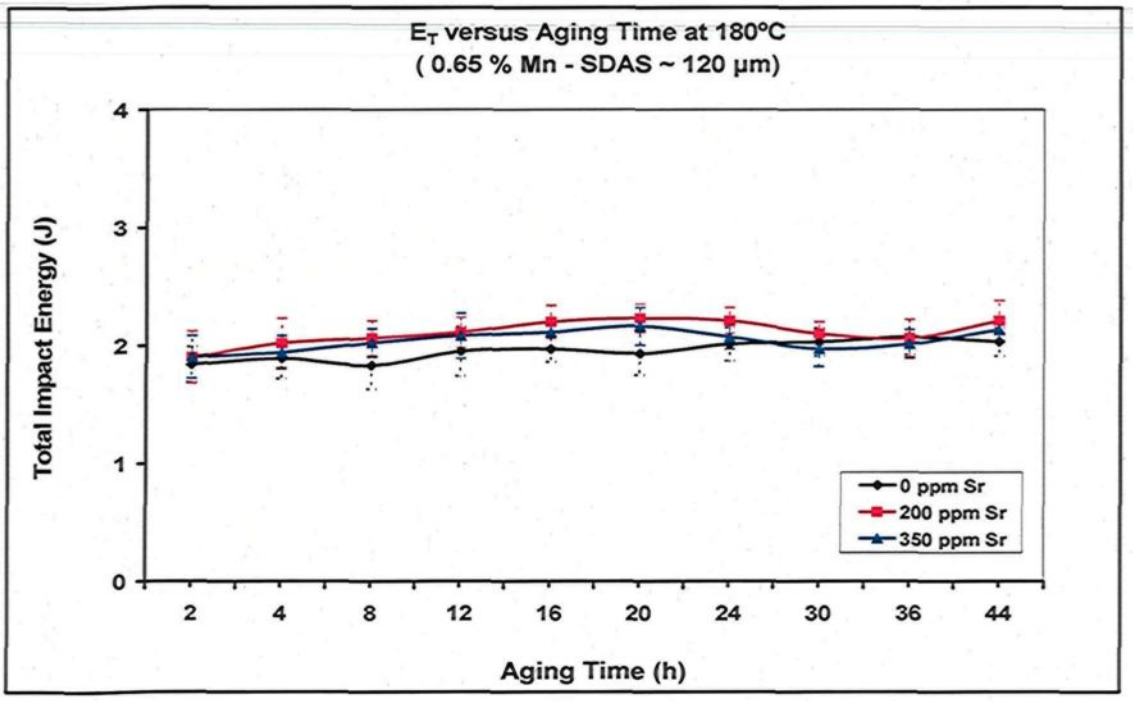

(a)

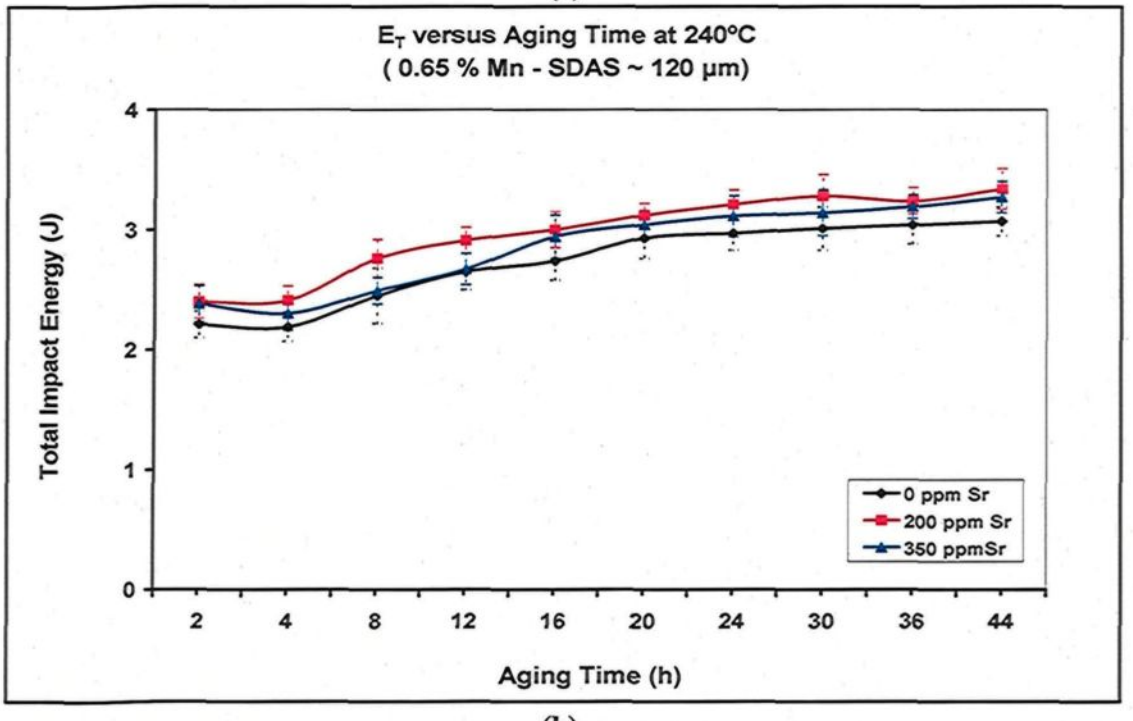

(b)

Figure 6.11 Effects of aging time on impact energy of 396 alloys containing 0.65 wt% Mn, and aged at: (a) 180°C, (b) 240°C, for three different modification levels (SDAS ~120 µm).

6.4 FRACTOGRAPHY

In order to arrive at a better understanding of the impact toughness results, the fracture surfaces of selected impact-tested alloy samples were examined using scanning electron microscopy (SEM) to determine the nature of crack initiation and crack propagation. This understanding would be based on the features observed on the fracture surfaces in relation to the iron- and copper-containing intermetallic phases present in the alloys being investigated. For the purposes of examining the crack propagation behavior beneath the fracture surface, longitudinal samples were sectioned from the impact-tested samples, perpendicular to the fracture surface. These sections were then mounted and polished for further examination by means of optical microscopy.

Table 30 in Appendix 3 shows the chemical composition, cooling rates, and heat treatment conditions of the samples which were examined for this part of the study, while Table 31 documents the volume fractions of the Al_2Cu and Fe-based intermetallic phases (mainly α-Fe) observed in each alloy sample.

6.4.1 SEM Examination – Analysis of Crack Initiation and Propagation

6.4.1.1 As-Cast Alloys

Figure 6.12(a) displays the fracture surface characteristics of the as-cast E1 alloy sample containing 0.45 wt% Mn, obtained under high cooling rate conditions. Since the alloy was not modified with Sr, the Al_2Cu phase appears in the form of scattered blocklike particles shown in Figure 6.12(b), or in the form of the Al-Al_2Cu eutectic shown in Figure 6.12(d), indicating that the crack passed through the Cu-containing phase, as was confirmed

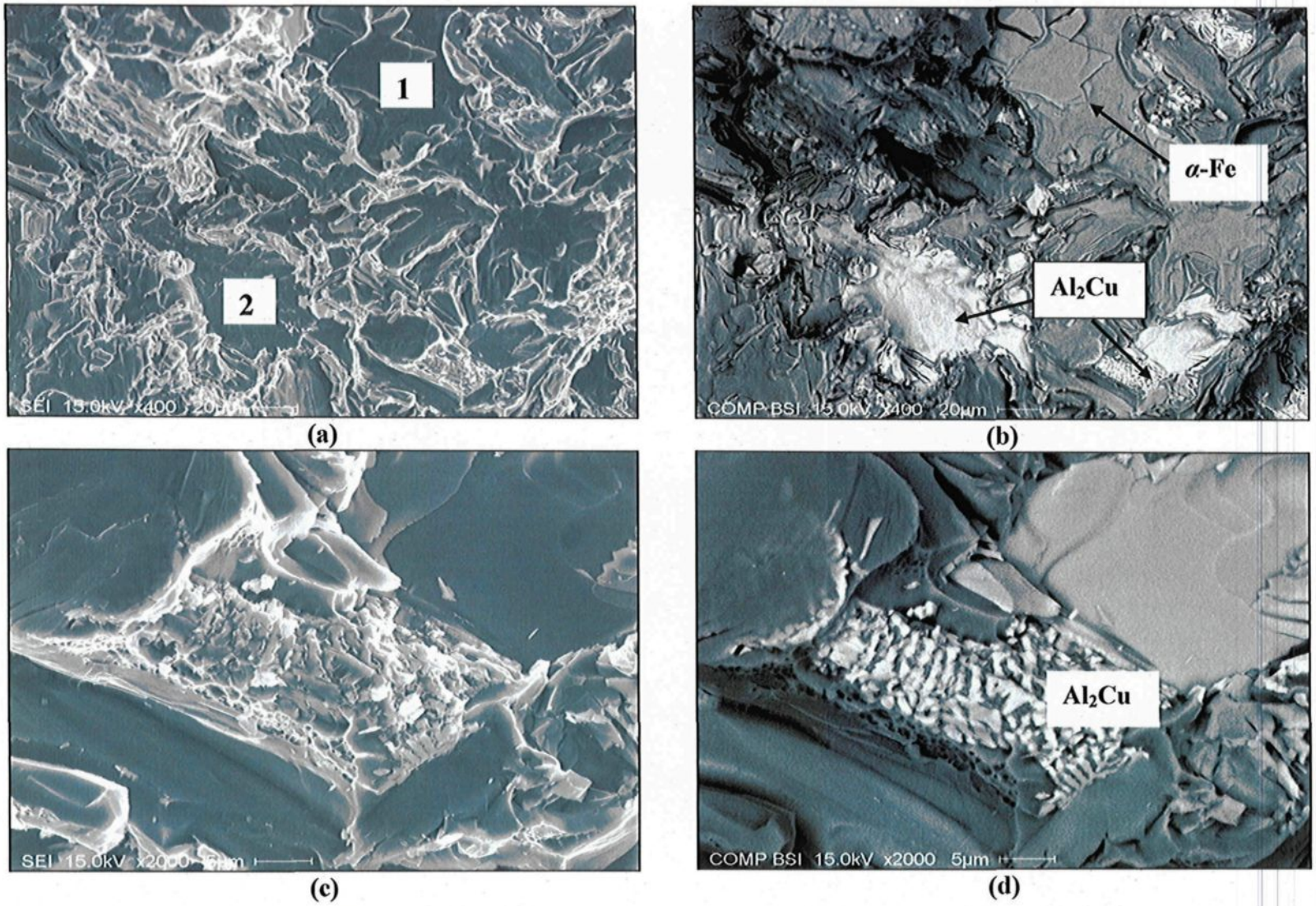

Figure 6.12 Fracture surface of as-cast E1 alloy showing the role of α-Fe and Al_2Cu intermetallics in the fracture process: (a) secondary electron image, and (b) backscattered image corresponding to (a); (c) secondary electron image; and (d) backscattered image corresponding to (c) obtained at high magnification.

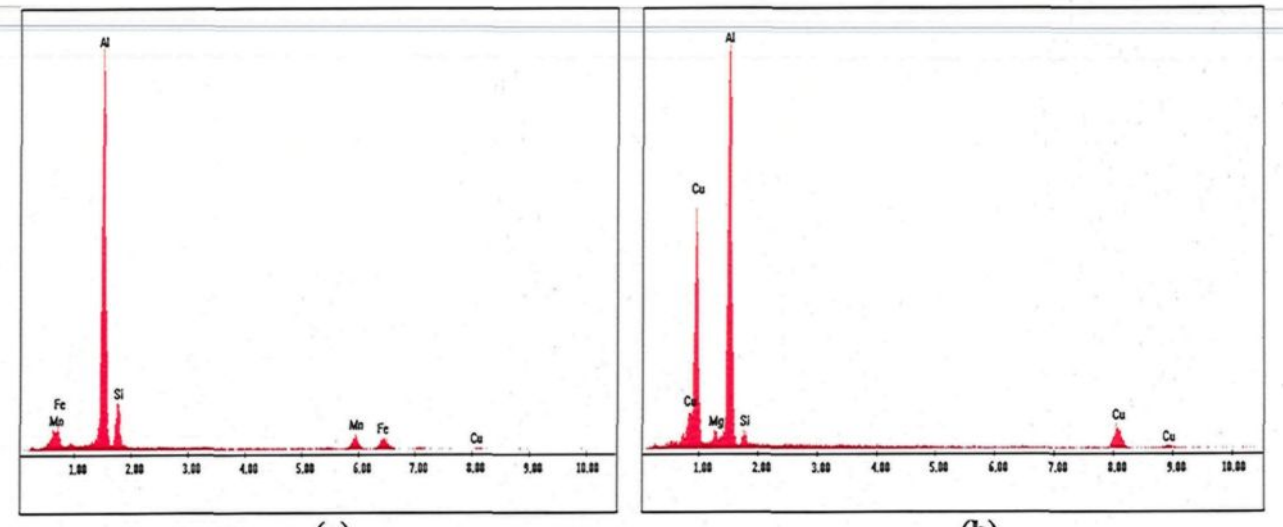

(a) (b)

Figure 6.13 EDX-ray spectra obtained from as-cast E1 alloy corresponding to areas (1) and (2) in Figure 6.12(a), confirming precipitation of (a) α-Fe phase; and (b) Al_2Cu phase, respectively.

by the corresponding EDX-ray spectrum illustrated in Figure 6.13. The addition of 200 ppm Sr to the E1 alloy, thereby creating the E2 alloy, resulted in a massive segregation of Al_2Cu phase particles as is clearly evident from Figure 6.14 which shows the presence of large blocklike Al_2Cu particles situated ahead of the moving crack. Such segregation is expected to lead to generally low levels of impact energy, 3.1 J in the case of the E2 alloy sample. The corresponding EDX-ray spectrum, presented in Figure 6.14(d), reveals strong Cu reflections. A small peak related to the presence of Mg may also be seen, indicating the possible concurrent precipitation of the Mg-containing Q-$Al_5Mg_8Cu_2Si_6$ phase. [7]

Increasing the Mn level from 0.45 wt% to 0.65 wt%, thereby producing E4 alloy, was found to cause no significant change in the morphology of the Al_2Cu phase, as shown in Figure 6.15. Large amounts of the α-$Al_{15}(Mn,Fe)_3Si_2$ phase, however, were observed on

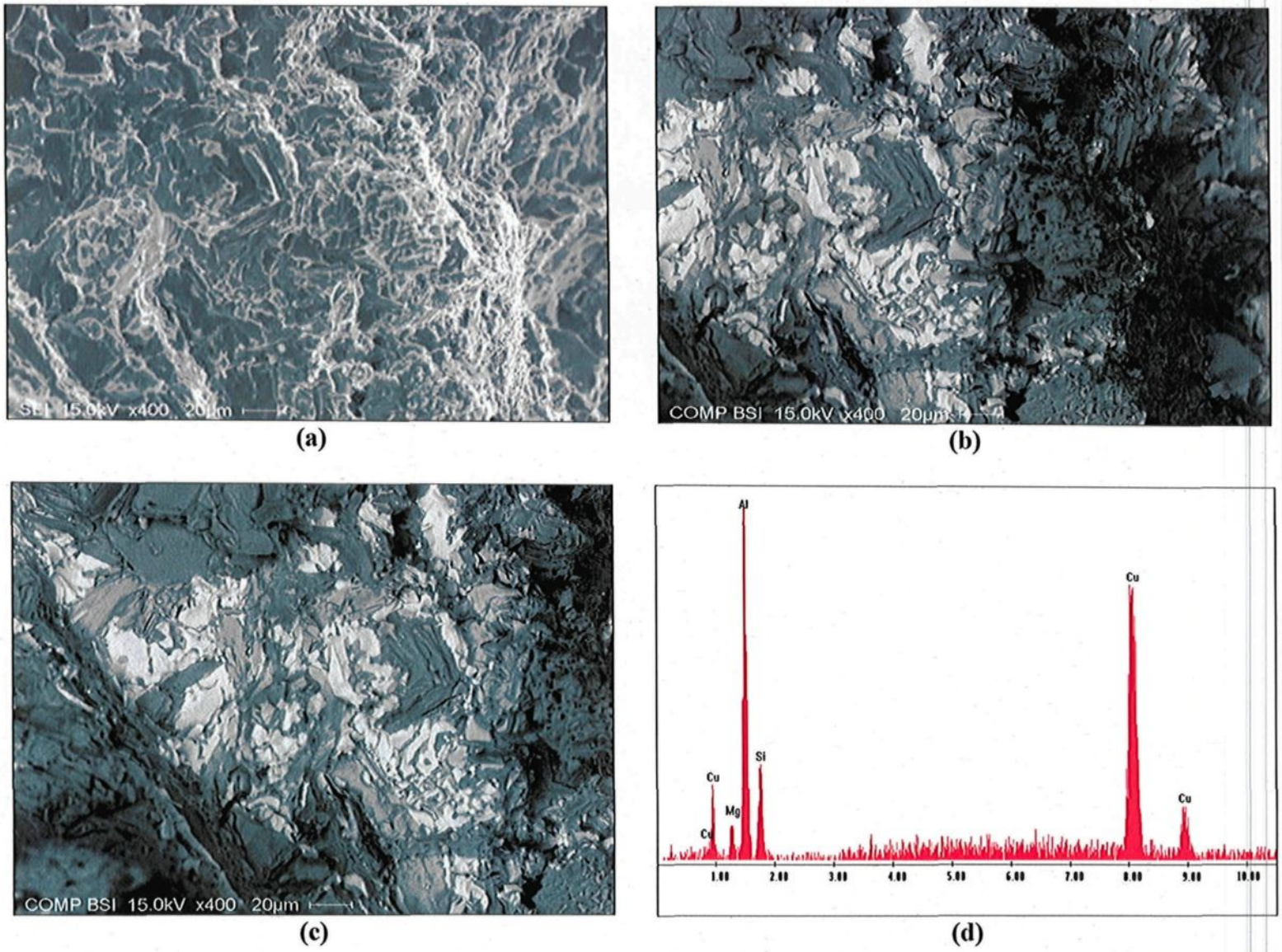

Figure 6.14 Fracture surface of as-cast E2 alloy: (a) secondary electron image, and (b) backscattered image corresponding to (a); (c) backscattered image taken from another area of the same sample; and (d) EDX-ray spectrum revealing the precipitation of Al_2Cu and *Q*-phase in (c).

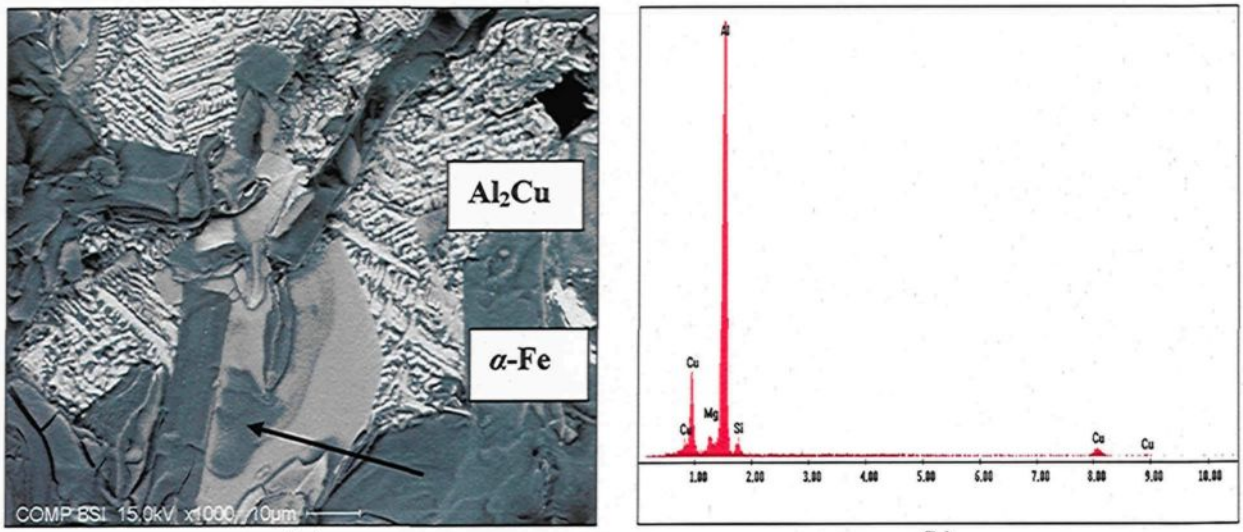

(a) (b)

Figure 6.15 Fracture surface of as-cast E4 alloy: (a) backsacttered image showing the presence of Cu- and Fe-intermetallic, and (b) EDX-ray spectrum confirming the precipitation of the *Q*-phase as indicated by the solid arrow in (a).

the fracture surface of the E4 sample, as revealed by the backscattered image shown in Figure 6.15(a). Due to the high Mg content of 0.37 wt% in this alloy, the *Q*-$Al_5Mg_8Cu_2Si_6$ phase was frequently observed in the microstructure, as indicated by the solid arrow in Figure 6.15(a); this phase was confirmed by the corresponding EDX-ray spectrum as shown in Figure 6.15(b).

Figure 6.16 presents further views of the fracture surface of the alloy mentioned, showing the presence of α-$Al_{15}(Mn,Fe)_3Si_2$ phase particles appearing in Chinese-script form, as shown in Figure 6.16(b); the presence of areas containing Al_2Cu phase particles in the form of Al-Al_2Cu eutectic will also be observed in the figure. Figure 6.17 shows the fracture surface of E5 alloy in the as-cast condition. The predominant feature of the images

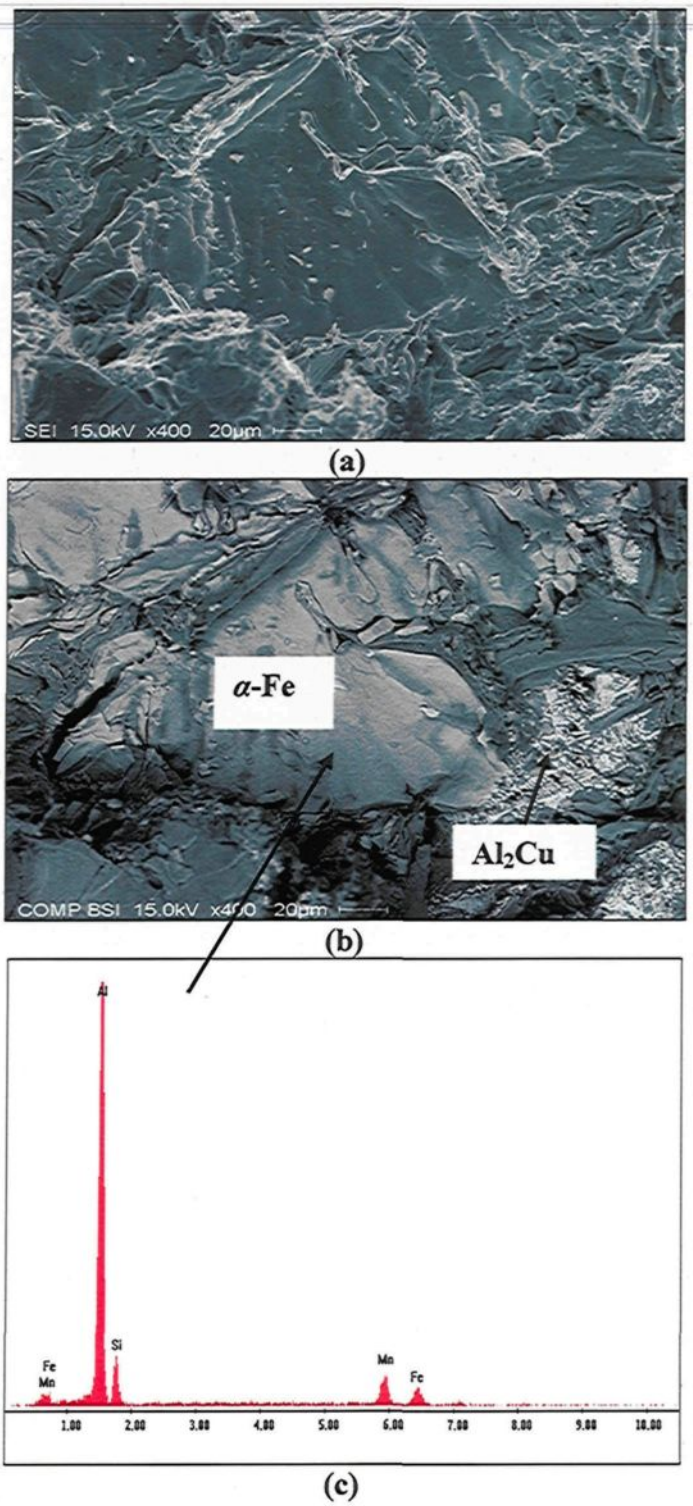

Figure 6.16 Fracture surface of as-cast E4 alloy: (a) secondary electron image; (b) backscattered image of (a); and (c) EDX-ray spectrum corresponding to the α-Fe phase in (b).

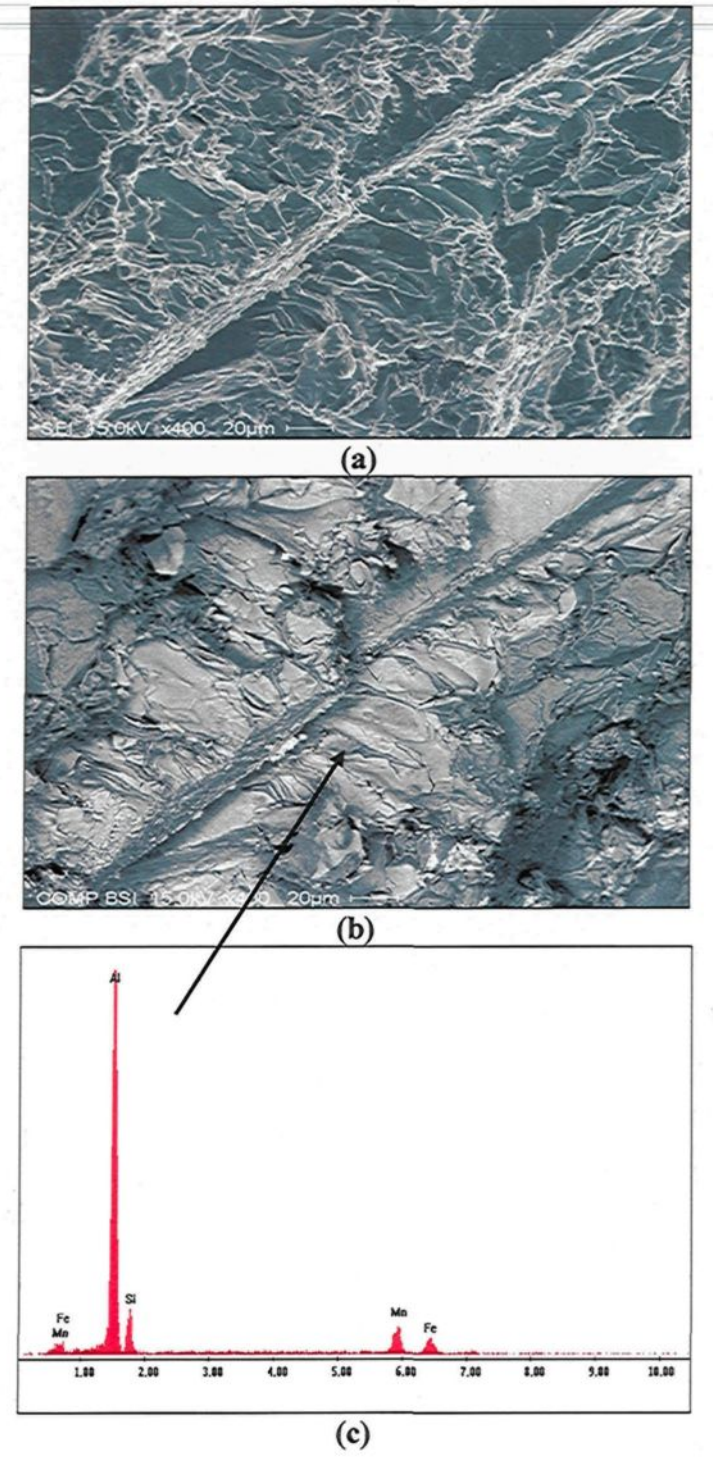

Figure 6.17 Fracture surface of as-cast E5 alloy showing the precipitation of a large α-Fe phase particle: (a) secondary electron image, (b) backscattered image of (a); (c) corresponding EDX-ray of the α-Fe phase arrowd in (b).

show in (a) and (b) is the presence of a large branched α-$Al_{15}(Mn,Fe)_3Si_2$ phase particle almost 2000 μm in length. It would appear that the presence of Sr in this alloy does not produce any fragmentation of the α-Fe intermetallic phase, as is known to be the case for the β-Al_5FeSi phase. Figure 6.18, however, reveals the existence of massive Al_2Cu particles throughout the matrix, as a result of the segregation of the copper phase upon the addition of Sr.

Fairly coarse microconstituents were obtained using a slow cooling rate by allowing the casting in the mold to cool inside the furnace (the corresponding samples displaying an SDAS of ~120 μm), compared to those reported for the air-cooled alloy castings which solidified at a relatively high rate (exhibiting an SDAS of ~ 45 μm). Figure 6.19 shows the fracture surface of the HE1 alloy in the as-cast condition, where iron-based intermetallics are observed to dominate the matrix, even at a concentration of 0.45 wt% Mn. Although the HE1 alloy was not modified with Sr, the amount of precipitated Al_2Cu phase accompanied by the *Q*-phase as shown in Figure 6.20 is still clearly greater than the amount observed in the E1 alloy. As expected, the introduction of 200 ppm Sr to the HE1 alloy, thereby creating HE2 alloy, led to the precipitation of massive amounts of the Al_2Cu phase, as displayed in Figure 6.21; occasionally, β-Al_5FeSi iron intermetallic phase platelets were also observed. Figure 6.22, which displays the fracture surface of the HE4 alloy in the as-cast condition, reveals the precipitation of three intermetallic phases in the backscattered image shown in (b). The EDX-ray spectrum of these intermetallics, shown in Figure 6.22(c), reflects the presence of α-iron, Al_2Cu, and the *Q*-$Al_5Mg_8Cu_2Si_6$ phases. [7, 16]

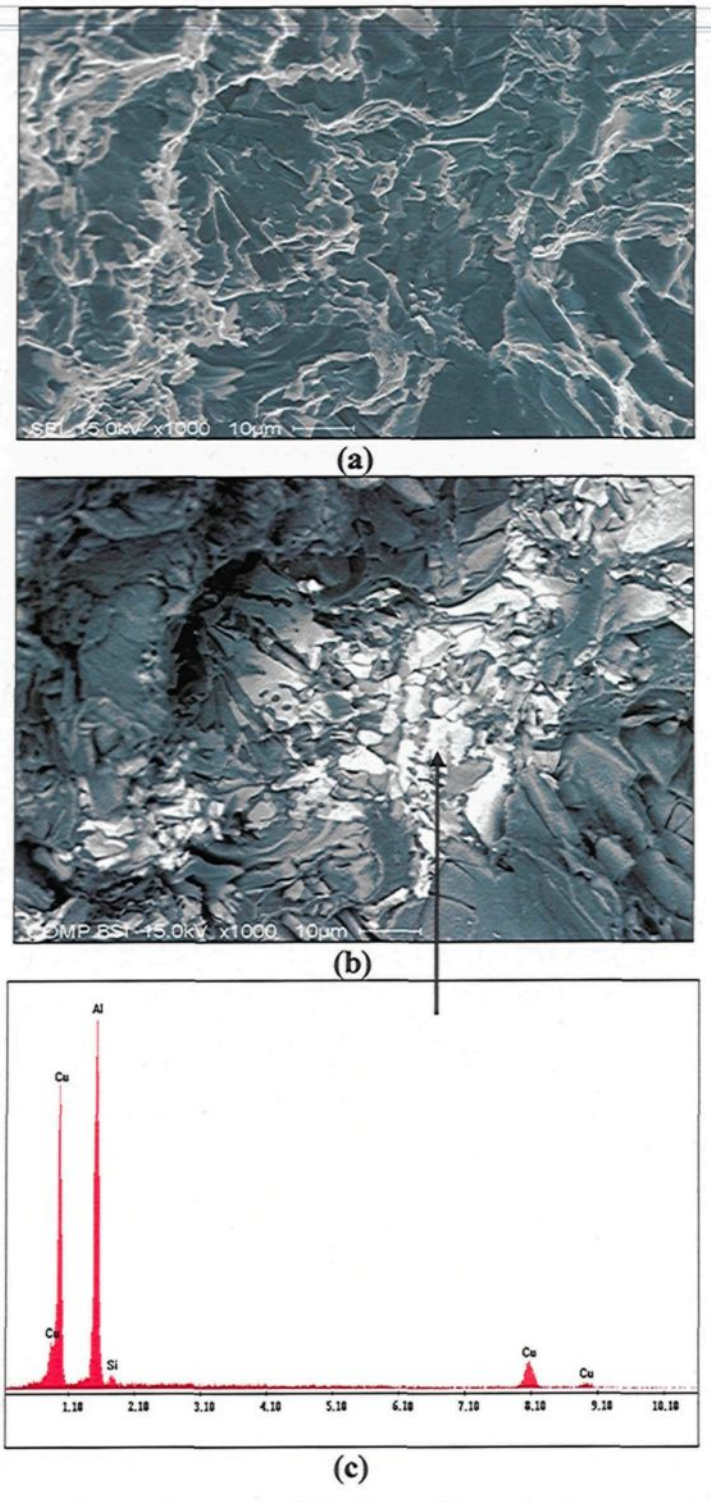

Figure 6.18 Fracture surface of as-cast E5 alloy: (a) secondary electron image, (b) backscattered image of (a); (c) EDX-ray spectrum corresponding to the Al_2Cu phase region arrowed in (b).

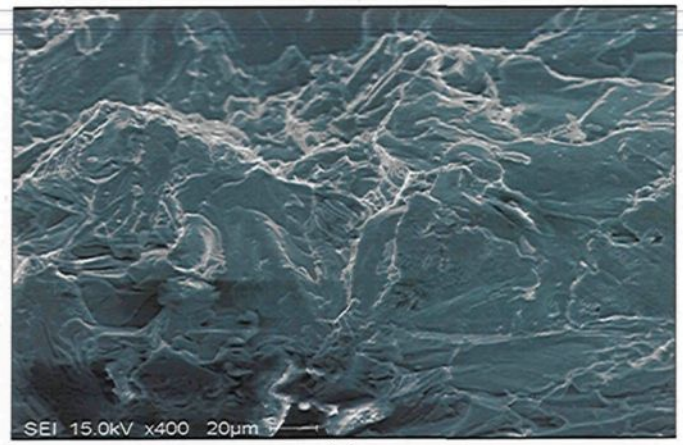

(a)

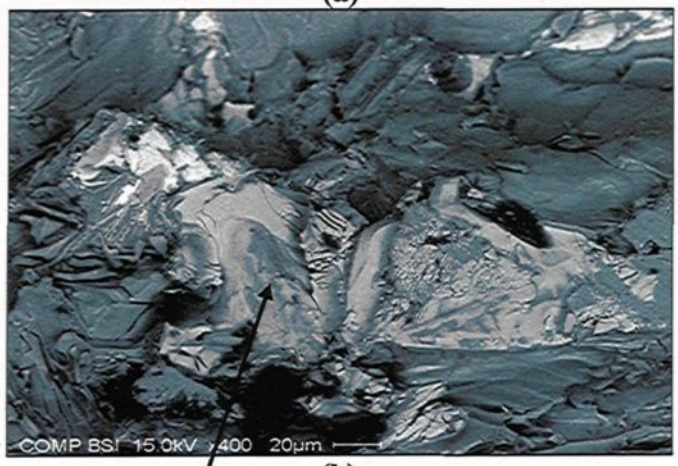

(b)

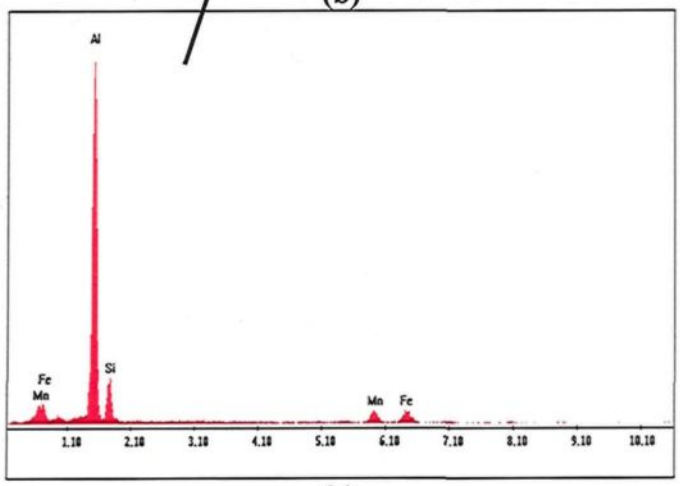

(c)

Figure 6.19 Fracture surface of as-cast HE1 alloy: (a) secondary electron image, and (b) backscattered image of (a); (c) EDX-ray spectrum corresponding to the α-Fe phase arrowed in (b).

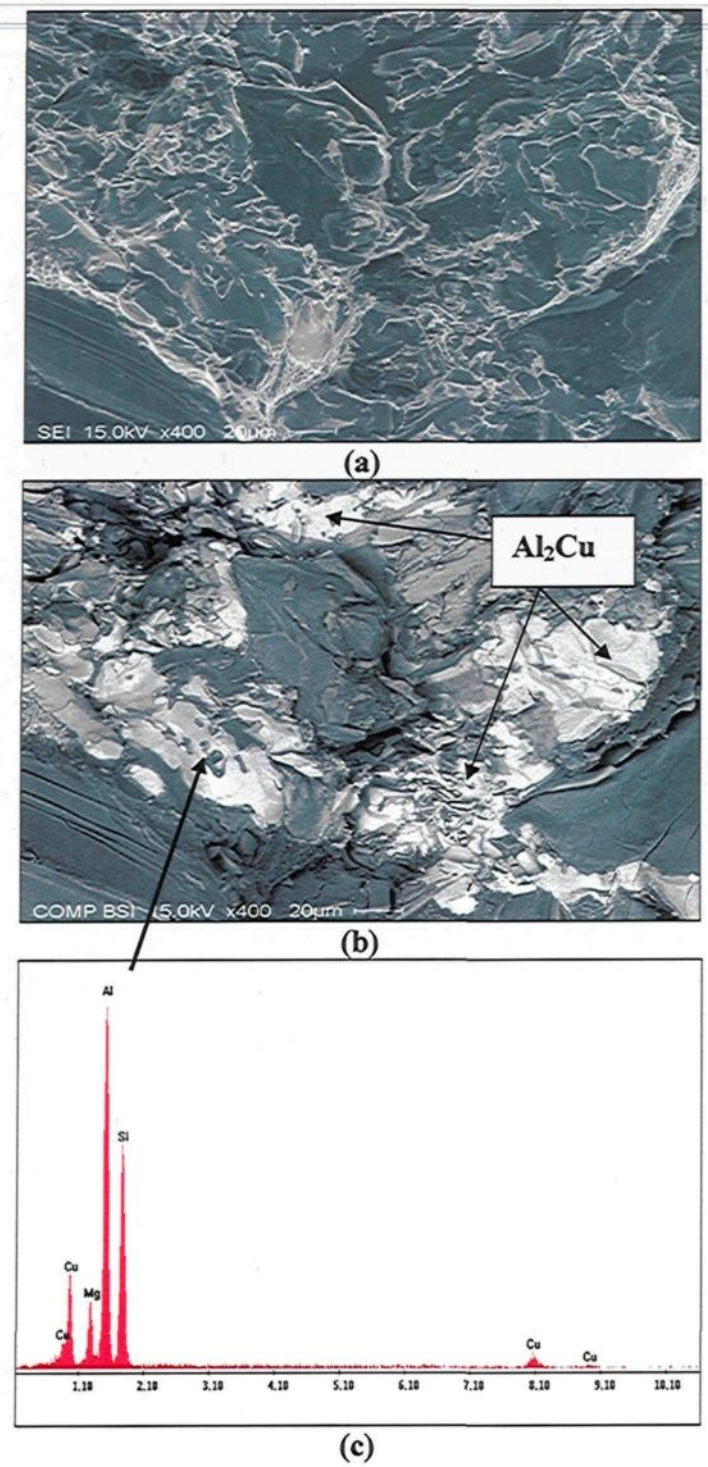

Figure 6.20 Fracture surface of as-cast HE1 alloy: (a) secondary electron image, and (b) backscattered image of (a); (c) EDX-ray spectrum corresponding to the *Q*-phase arrowed in (b).

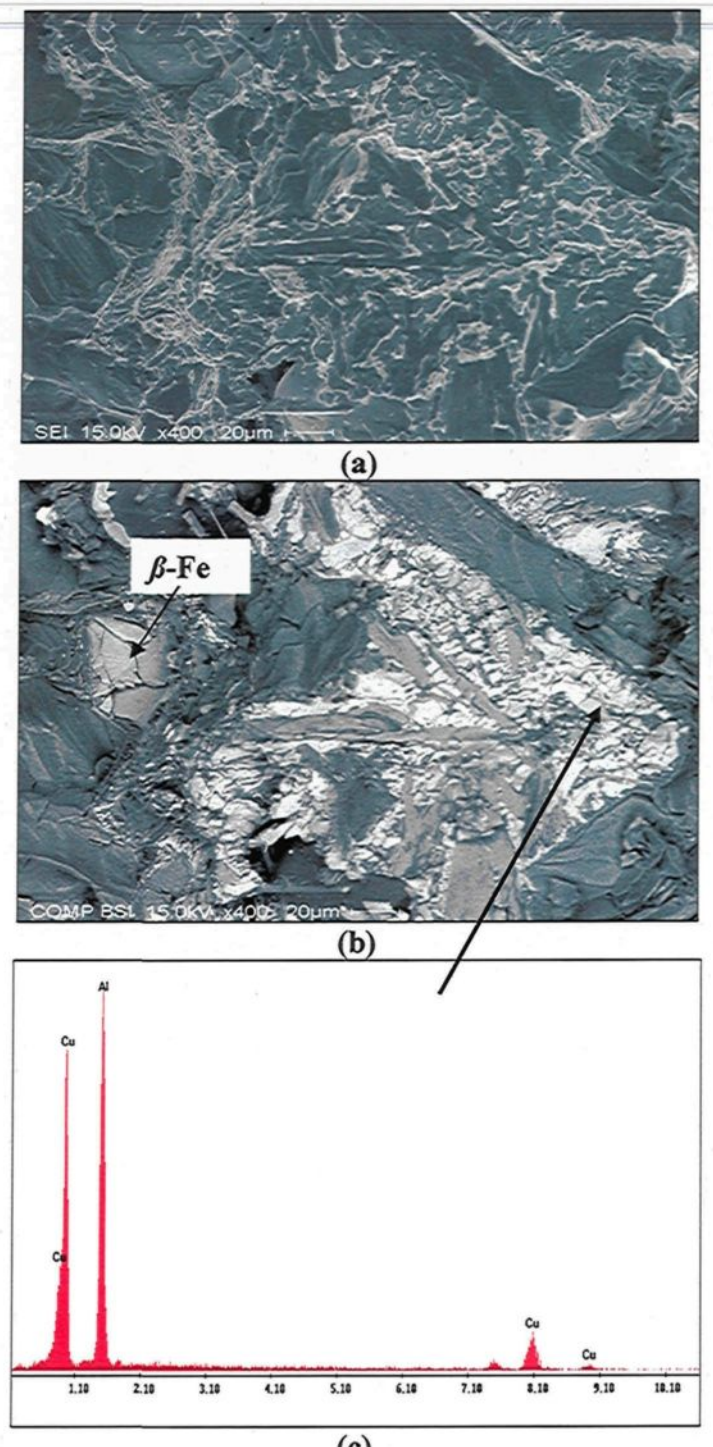

Figure 6.21 Fracture surface of as-cast HE2 alloy: (a) secondary electron image, and (b) backscattered image of (a); (c) EDX-ray spectrum corresponding to the Al_2Cu phase arrowed in (b).

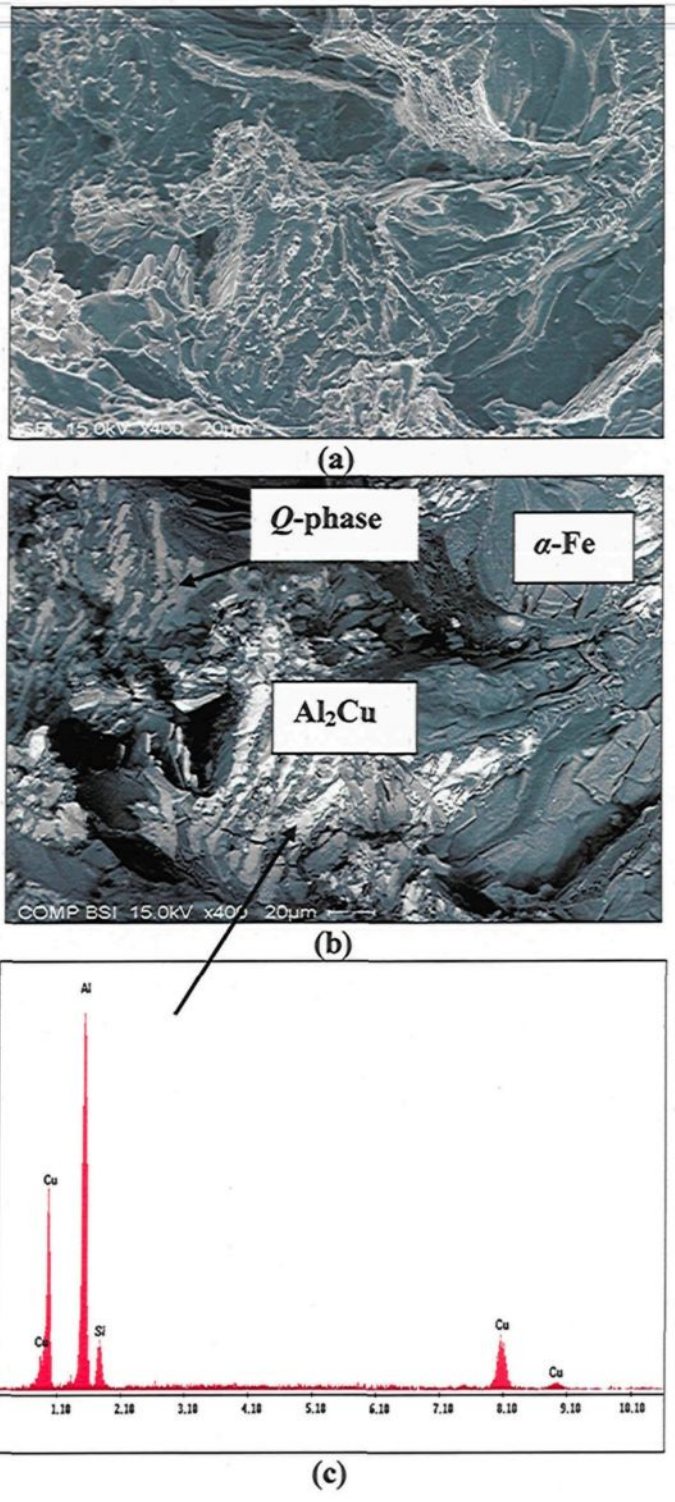

Figure 6.22 Fracture surface of as-cast HE4 alloy: (a) secondary electron image, and (b) backscattered image of (a); (c) EDX-ray spectrum corresponding to the Al_2Cu phase arrowed in (b).

Modification of the HE4 alloy with 200 ppm Sr, thereby creating the HE5 alloy, resulted in large areas of Al_2Cu particles having blocklike morphology, as observed clearly in Figure 6.23, in the backscattered image of the fracture surface of the as-cast HE5 alloy sample shown in (b), and corresponding to the secondary electron image shown in (a). This observation is confirmed by the strong Cu reflection in the corresponding EDX ray spectrum shown in Figure 6.23(d). The α-iron intermetallic phase appears in the form of broken fragments, as evident in the backscattered image shown in Figure 6.23(b), the EDX ray spectrum for which is shown in Figure 6.23(c).

6.4.1.2 Solution Heat-Treated Alloys

The fracture surface of the solution heat-treated E1 alloy sample, as displayed in Figure 6.24, shows a good example of the existence of α-Al_{15} $(Mn,Fe)_3Si_2$ in its script form, as described by Bäckerud *et al.*,[16] even after solution heat treatment at 495°C for 8 hrs, indicating its insoluble nature. The fracture surface of the Sr-modified version of the alloy, namely the E2 alloy, as seen in Figure 6.25, reveals the persistence of the Al_2Cu phase. Such an observation confirms the fact that this phase is not completely dissolved in the matrix after solution heat treatment, which increases the brittleness of the alloy, ultimately resulting in its lower impact energy compared to that obtained for the Sr-modified solution-treated 356 alloy.

Increasing the Mn content to 0.65 wt%, thereby creating the E4 alloy, led to the precipitation of the α-$Al_{15}(Mn,Fe)_3Si_2$ iron intermetallic phase in a blocklike form, as shown in Figure 6.26, rather than in the classic Chinese-script form observed previously in

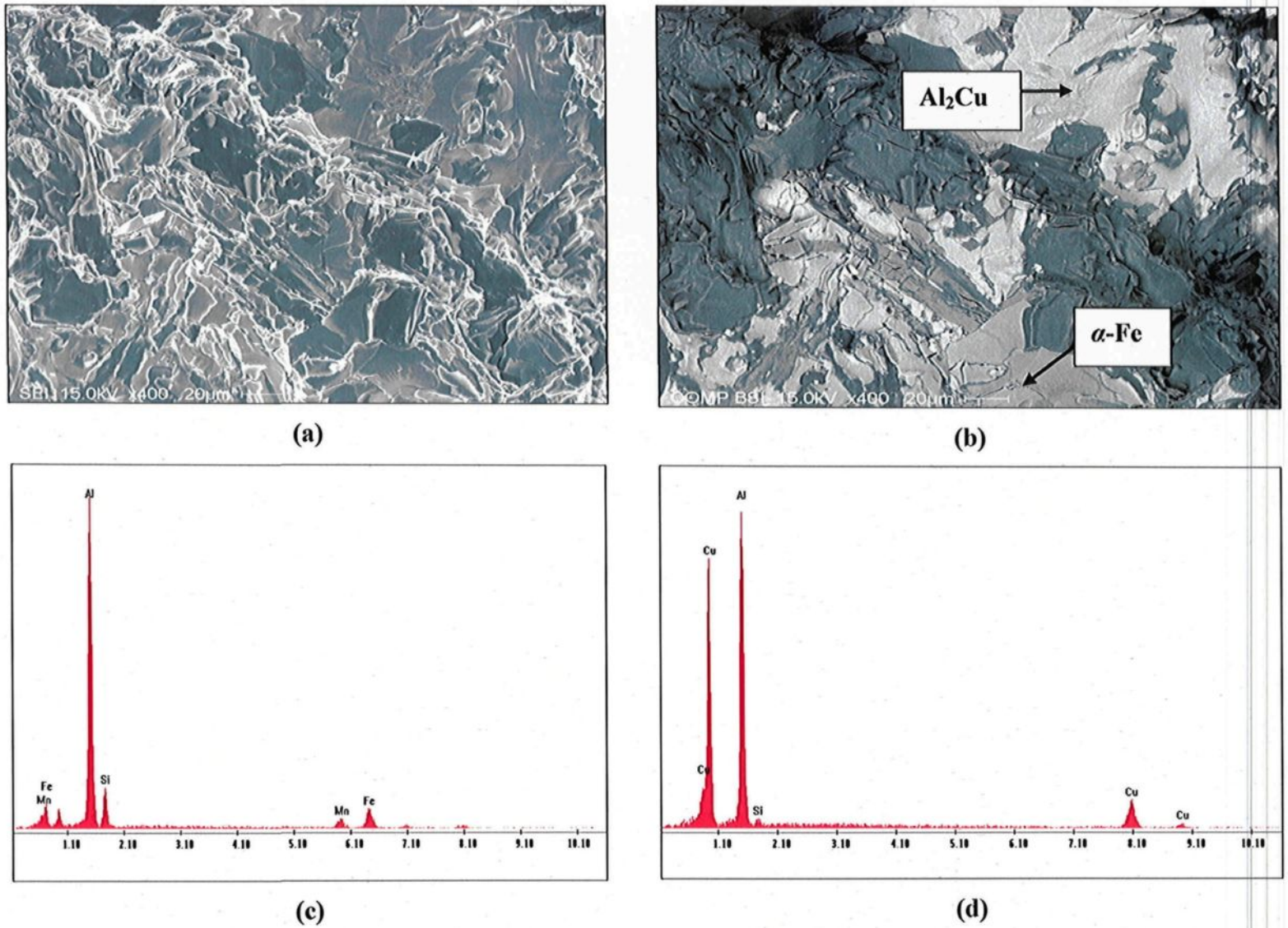

Figure 6.23 Fracture surface of as-cast HE5 alloy: (a) secondary electron image, and (b) backscattered image of (a); (c) & (d) EDX-ray spectra corresponding to the α-Fe and Al_2Cu phases shown in (b).

the low-Mn content alloys. Due to the massive nature of these α-iron intermetallic particles, neither the addition of 200 ppm Sr nor solutionizing at 495°C for 8 hrs could succeed in causing any noticeable fragmentation of these particles. With respect to the backscattered image of the E5 alloy sample shown in Figure 6.27(b), it seems reasonable to conclude that the crack passed through the α-Fe phase particle by shattering it into two halves, *i.e.* creating a transverse fracture, without altering its morphology. Another feature to be considered in regulating alloy toughness is the amount of undissolved Al_2Cu phase remaining in the sample, as revealed by the backscattered image of the E5 alloy sample displayed in Figure 6.28(b), where, as Table 31 in Appendix in 3 shows, this sample is seen to contain 0.27 vol% of undissolved Al_2Cu phase after solution heat treatment.

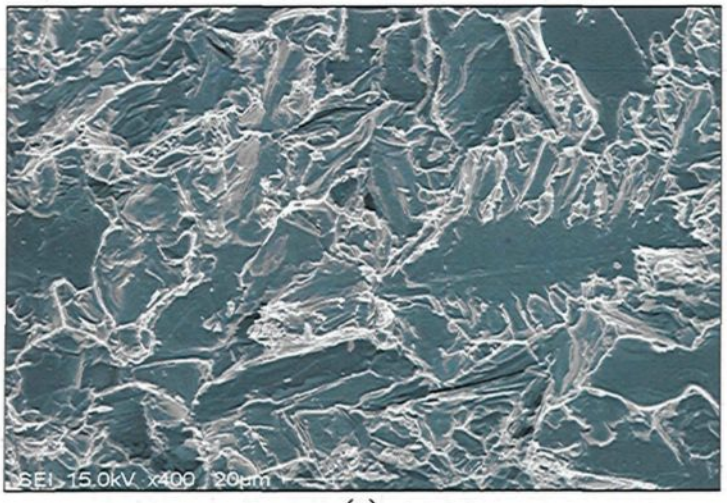

(a)

Figure 6.24

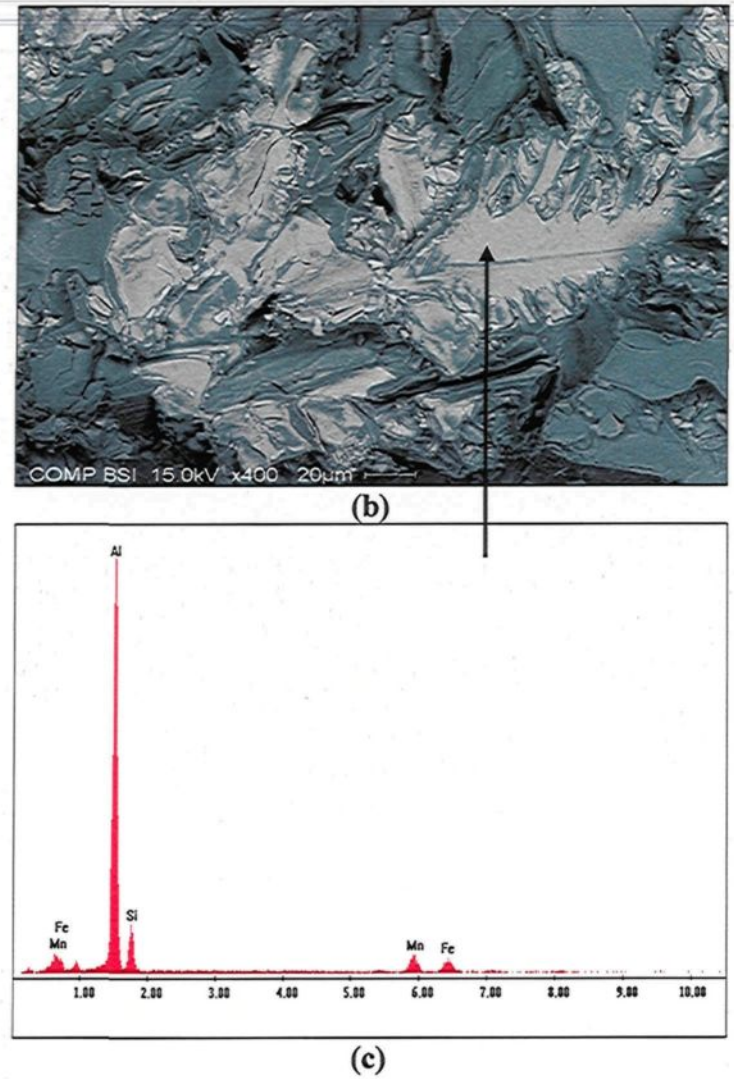

Figure 6.24 Fracture surface of solution heat-treated E1 alloy: (a) secondary electron image, and (b) backscattered image of (a); (c) EDX-ray spectrum corresponding to the α-Fe phase arrowed in (b).

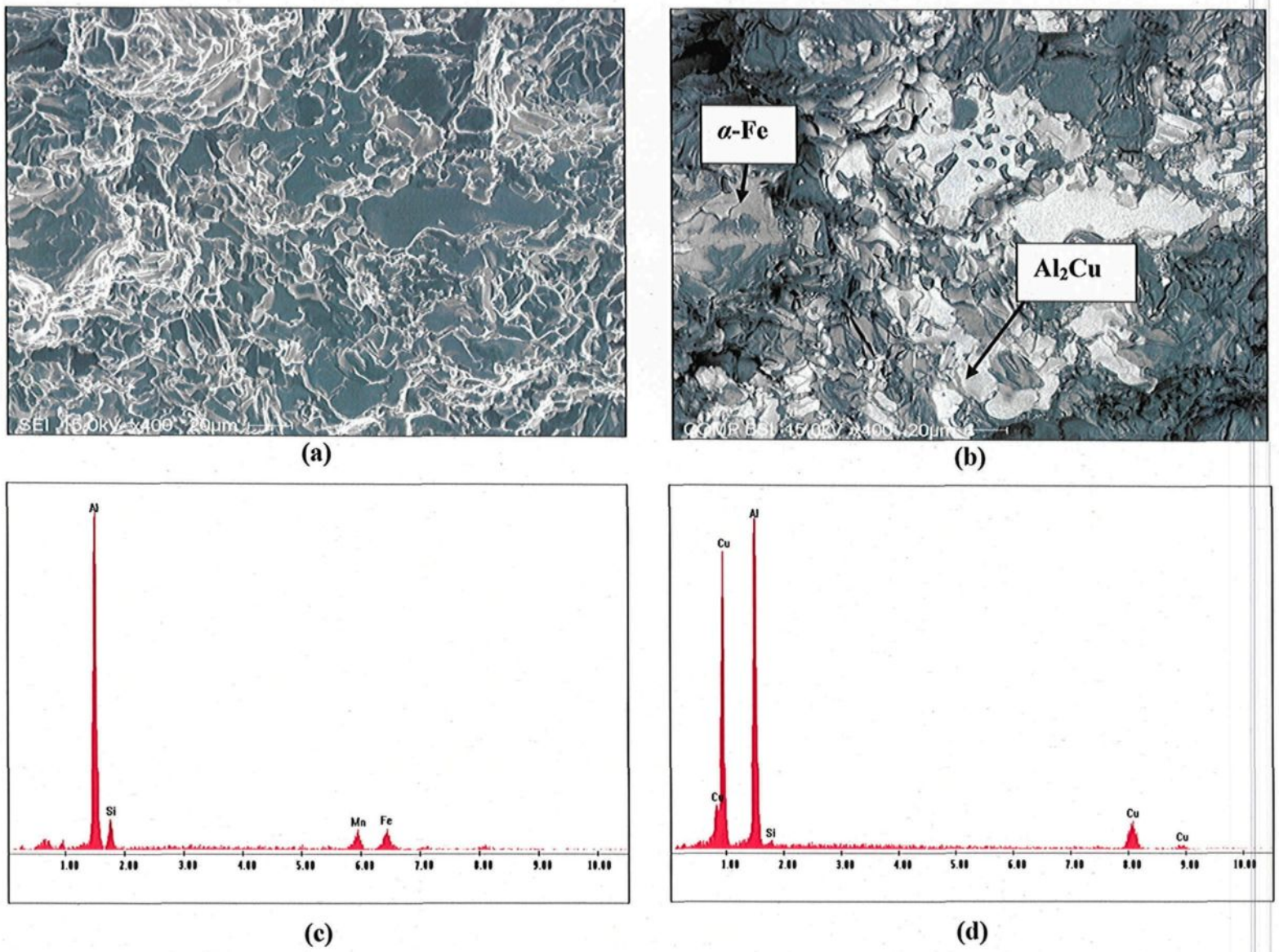

Figure 6.25 Fracture surface of solution heat-treated E2 alloy: (a) secondary electron image, and (b) backscattered image of (a); (c) & (d) EDX-ray spectra corresponding to the α-Fe and Al_2Cu phases shown in (b).

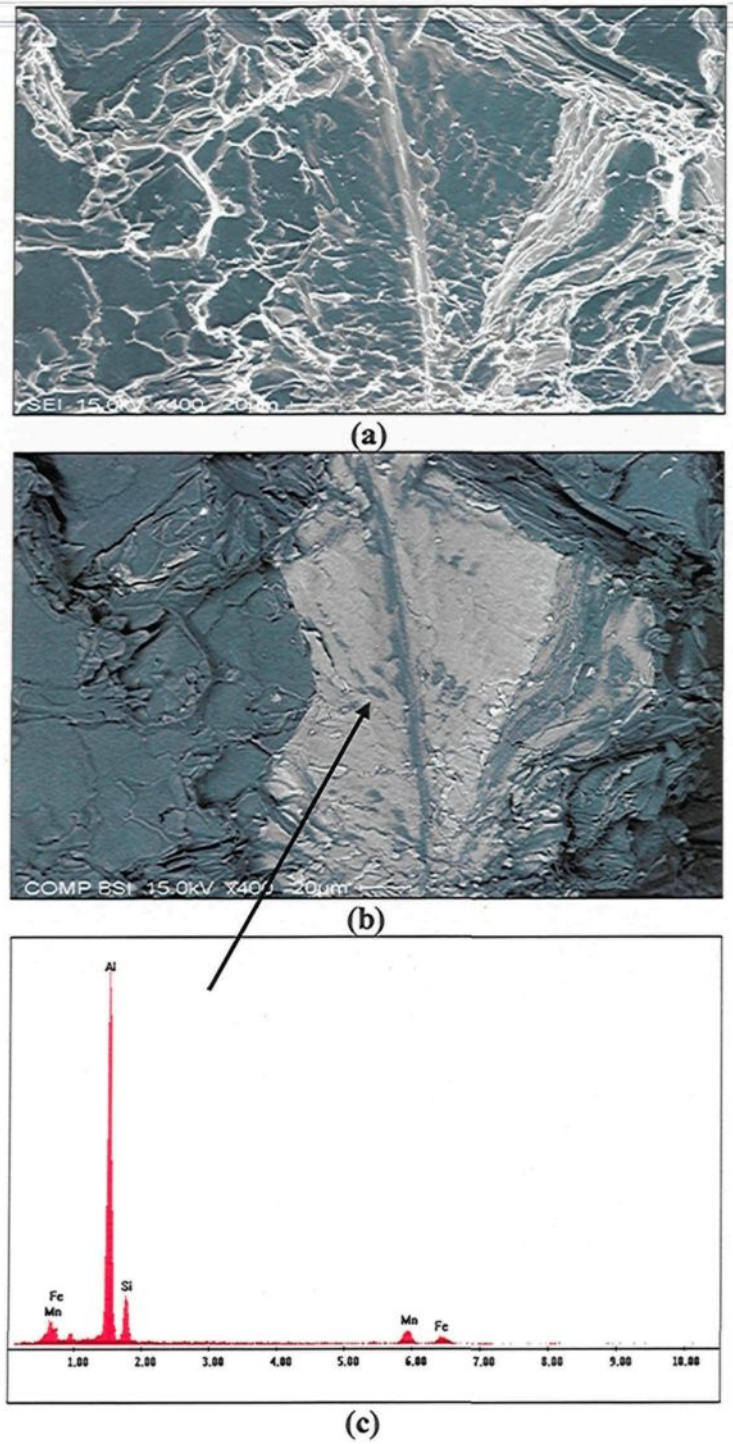

Figure 6.26 Fracture surface of solution heat-treated E4 alloy: (a) secondary electron image, and (b) backscattered image of (a); (c) EDX-ray spectrum corresponding to the α-Fe phase arrowed in (b).

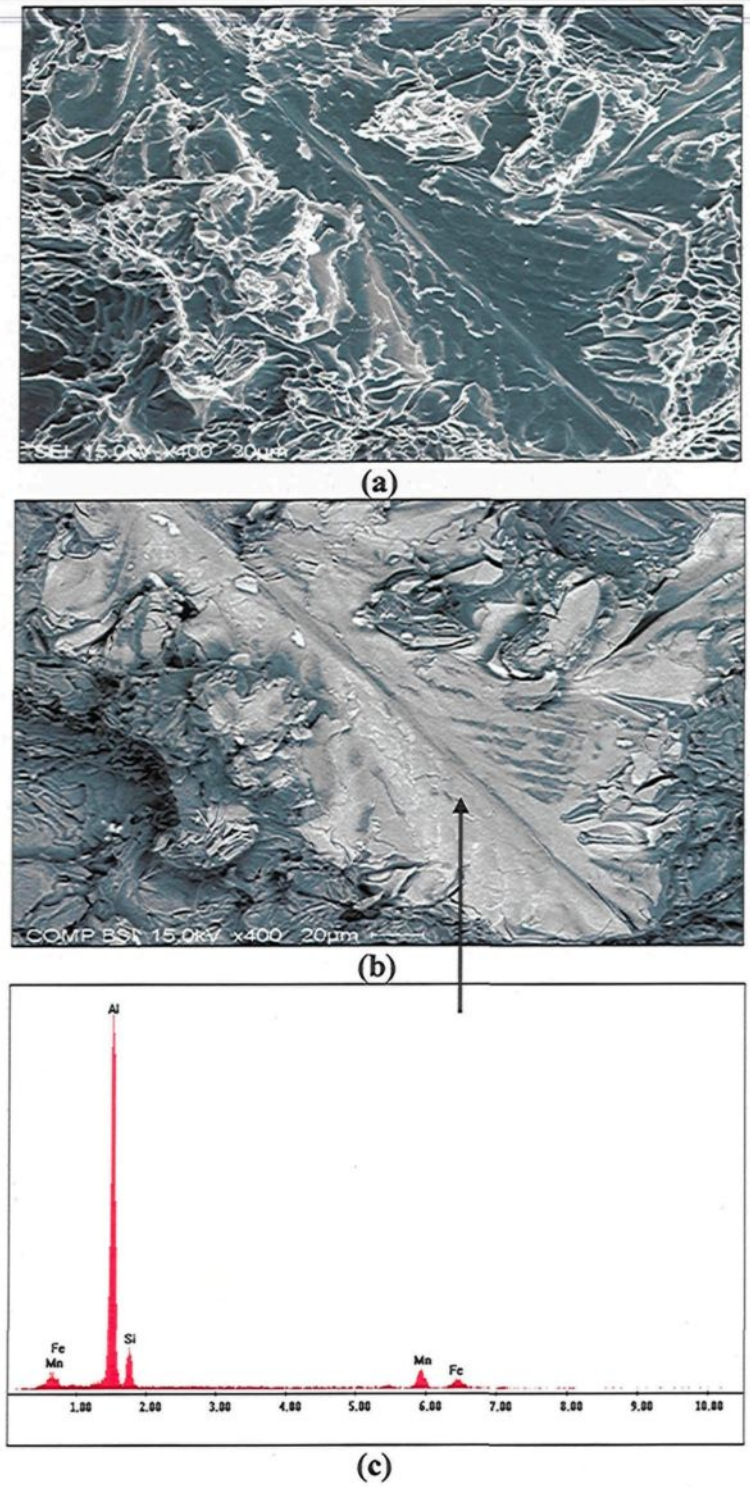

Figure 6.27 Fracture surface of solution heat-treated E5 alloy: (a) secondary electron image, and (b) backscattered image of (a); (c) EDX-ray spectrum corresponding to the α-Fe phase arrowed in (b).

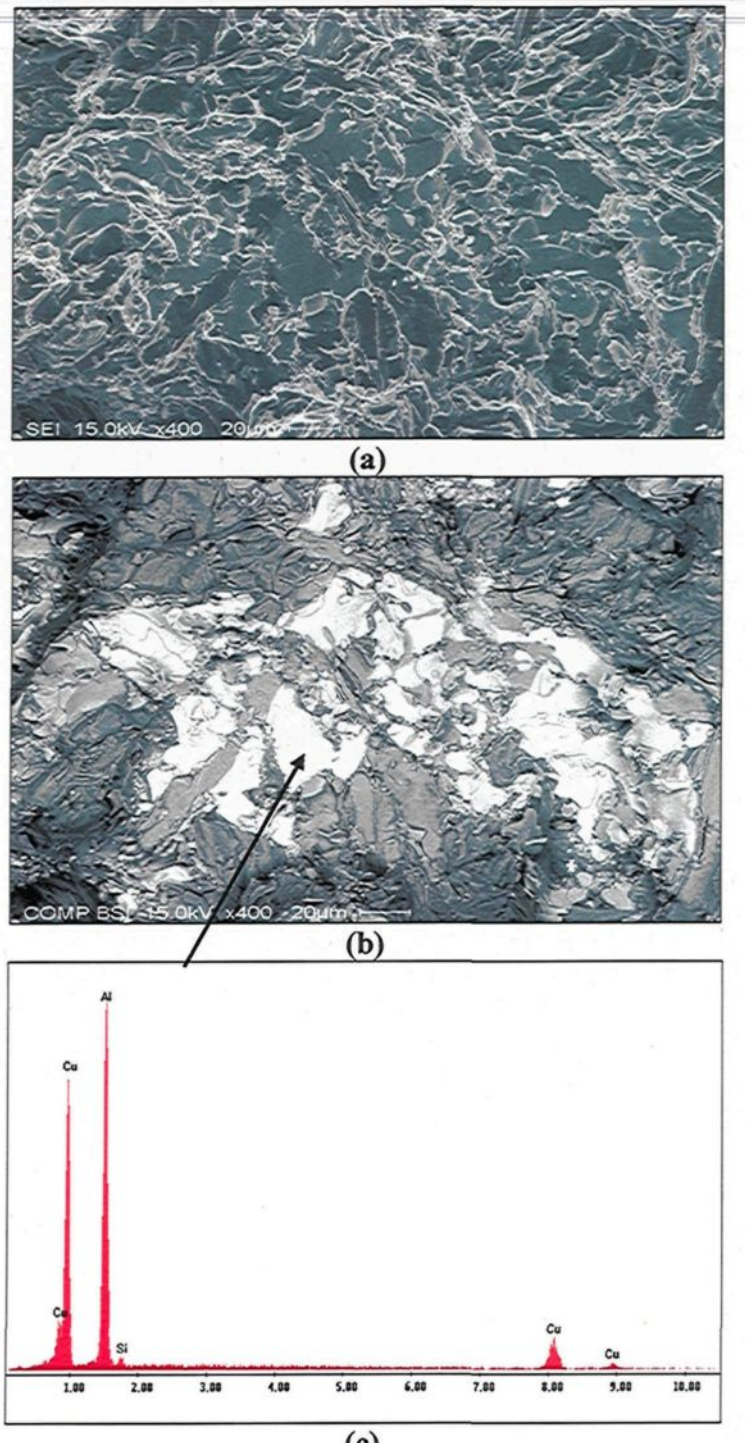

Figure 6.28 Fracture surface of solution heat-treated E5 alloy: (a) secondary electron image, and (b) backscattered image of (a); (c) EDX-ray spectrum corresponding the Al_2Cu phase arrowed in (b).

The abovementioned observations indicate that solution heat treatment has no significant effect on changing the size of the α-iron phase particles; the crack passes through these particles, causing them to fracture into fragments depending upon their initial size, as may be observed from Figures 6.29 and 6.30 which show the fracture surface of the HE1 alloy. Modification with Sr and applying a low cooling rate, as in the case of the HE2 alloy, will tend to worsen the situation due to the presence of an extensive amount of undissolved Al_2Cu phase, in addition to the presence of iron-based intermetallics, as revealed by the fracture surface of the alloy shown in Figure 6.31.

Figure 6.32, corresponding to the solution-treated HE4 alloy, clearly shows the co-existence of the two main types of intermetallics. As reported in Table 31 (Appendix 3), increasing the Mn content in this alloy increases the volume fraction of both the Al_2Cu and α-iron intermetallic phases. Solution heat treatment results in dissolving more or less half of the Al_2Cu phase formed in the as-cast condition, with no noticeable change in the volume fraction of the iron-based intermetallic phases. This statement is supported by the strong Cu reflection observed in the corresponding EDX-ray spectrum taken from the solution heat-treated HE5 alloy sample, shown in Figure 6.33.

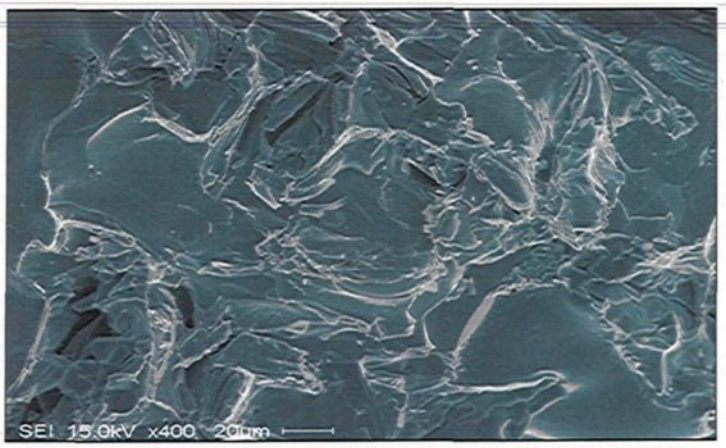

(a)

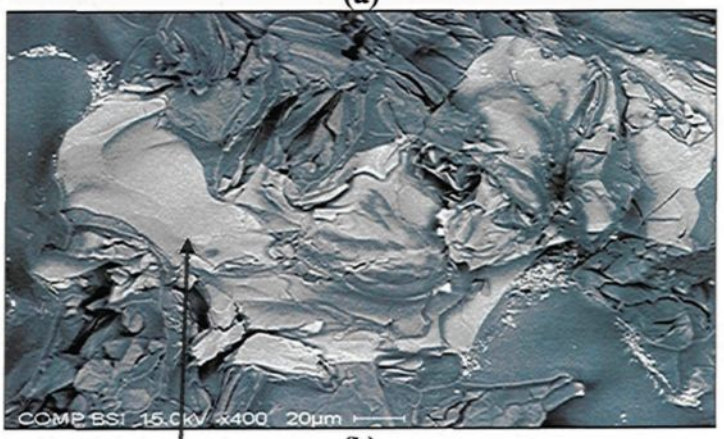

(b)

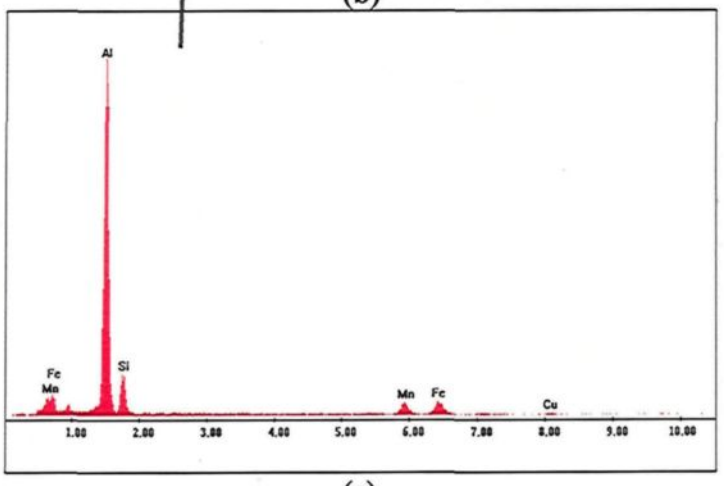

(c)

Figure 6.29 Fracture surface of solution heat-treated HE1 alloy: (a) secondary electron image, and (b) backscattered image of (a); (c) EDX-ray spectrum corresponding to the α-Fe phase arrowed in (b).

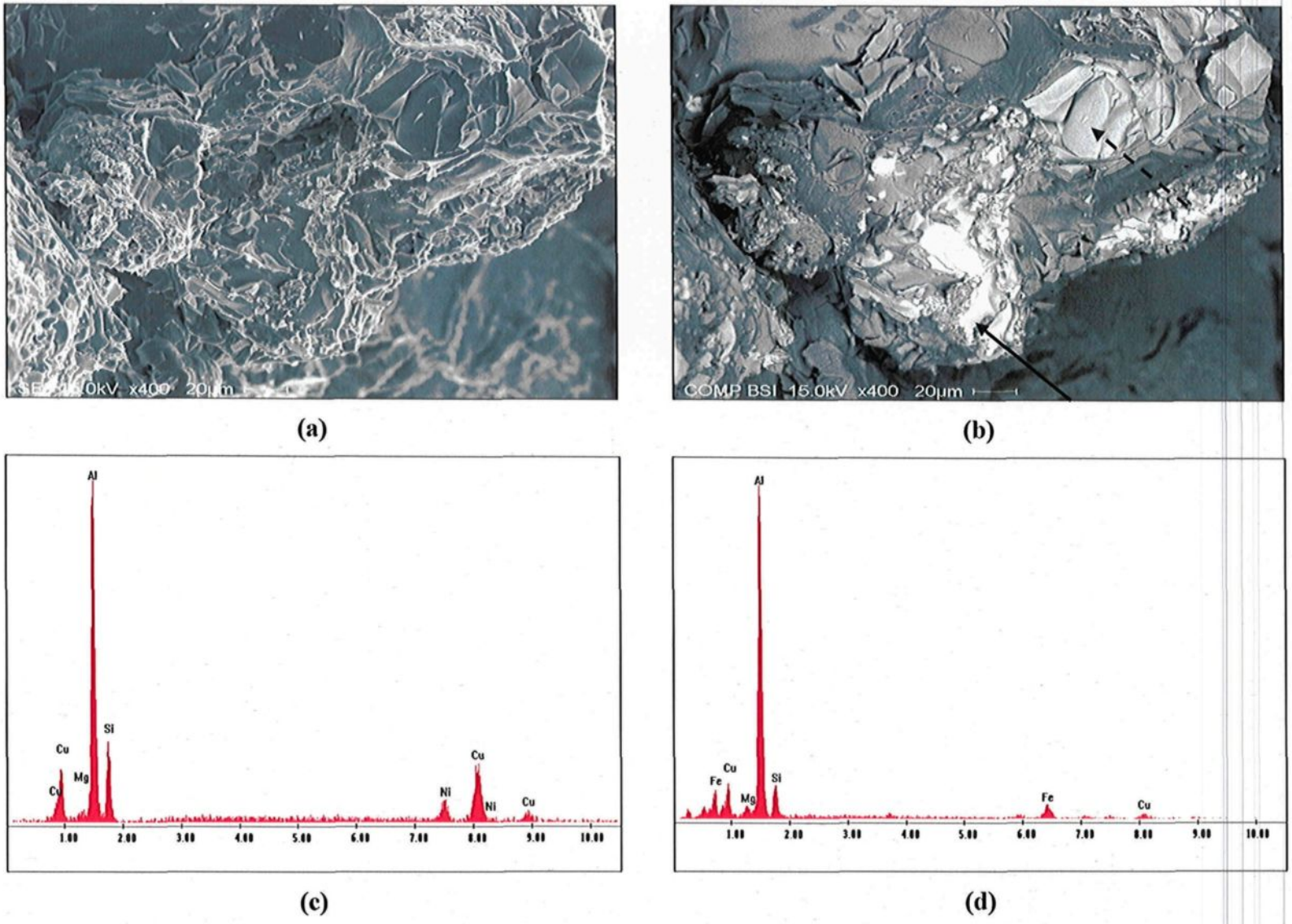

Figure 6.30 Fracture surface of solution heat-treated HE1 alloy: (a) secondary electron image, and (b) backscattered image of (a); (c) & (d) EDX-ray spectra corresponding to the Al_6Cu_3Ni (solid arrow) and Al_7Cu_2Fe (broken arrow) phases shown in (b).

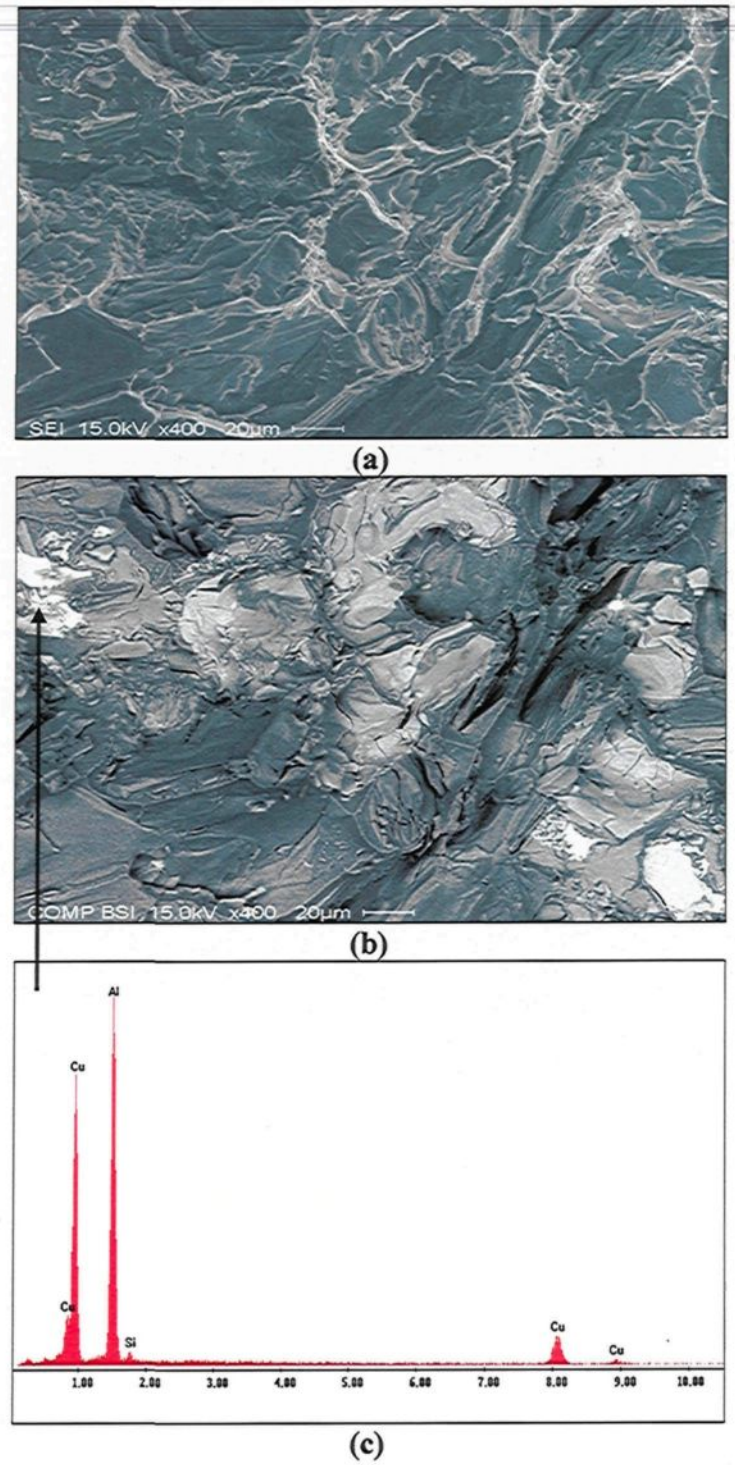

Figure 6.31 Fracture surface of solution heat-treated HE2 alloy: (a) secondary electron image, and (b) backscattered image of (a); (c) EDX-ray spectrum corresponding to the Al_2Cu phase arrowed in (b).

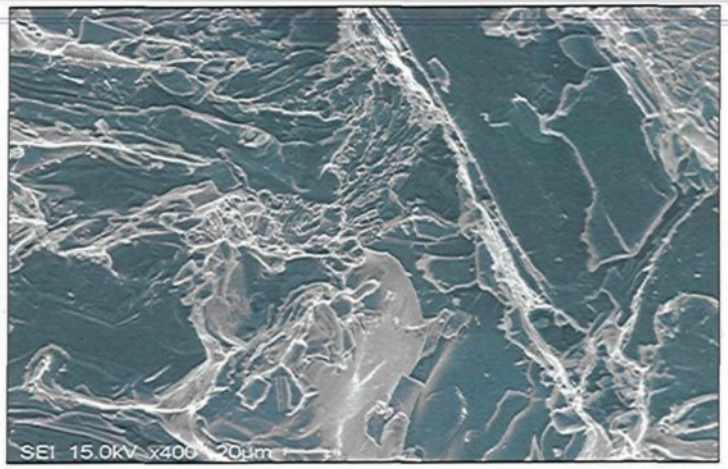

(a)

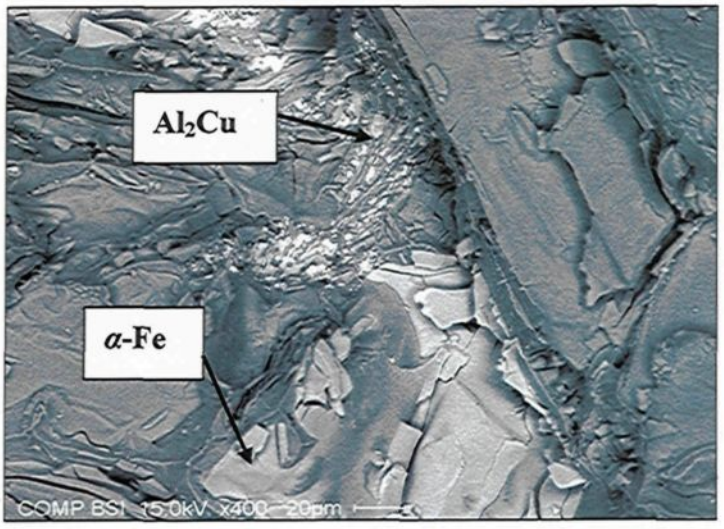

(b)

Figure 6.32 Fracture surface of solution heat-treated HE4 alloy: (a) secondary electron image, and (b) backscattered image of (a), showing the dissolution of Al_2Cu phase and the persistence of the α-Fe phase.

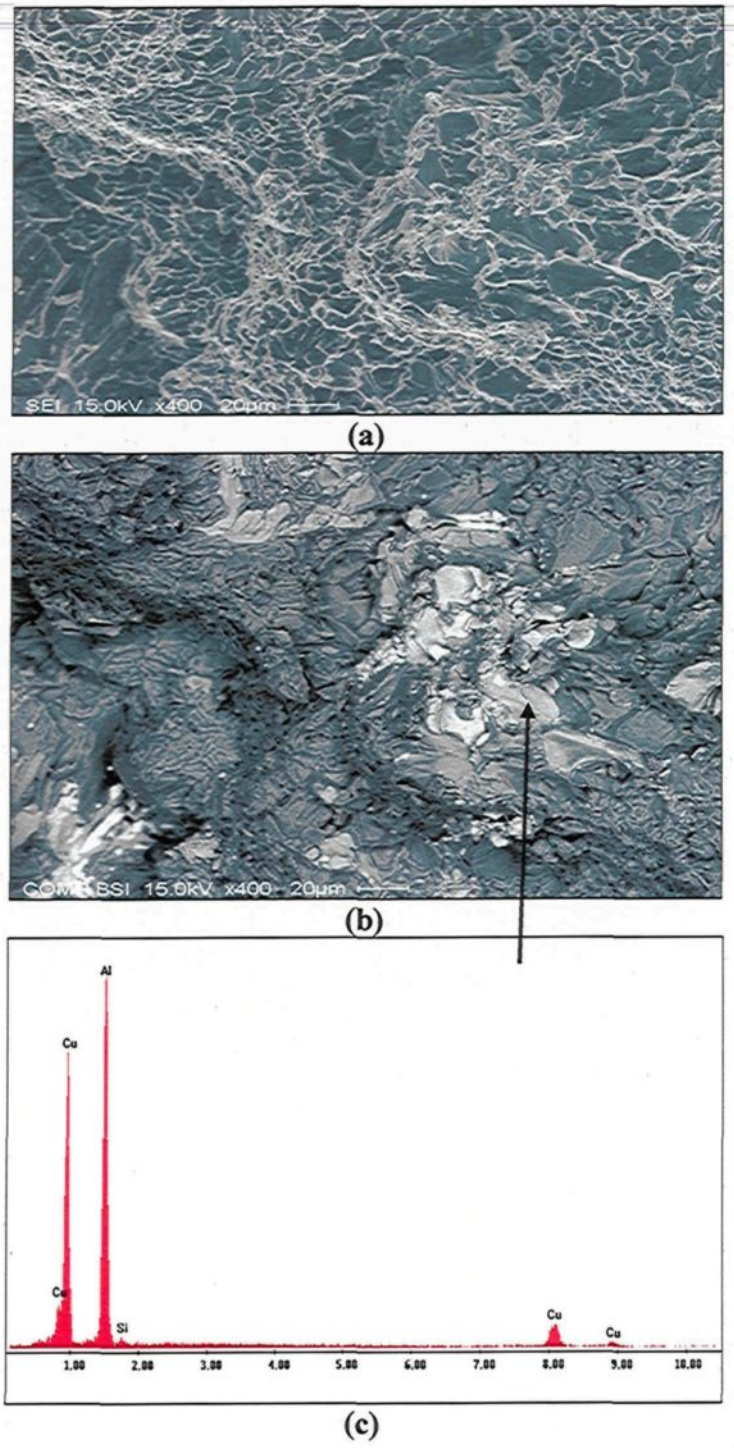

Figure 6.33 Fracture surface of solution heat-treated HE5 alloy: (a) secondary electron image, and (b) backscattered image of (a); (c) EDX-ray spectrum corresponding to the α-Fe phase arrowed in (b).

6.4.2 Analysis of the Microstructure beneath the Fracture Surface

Table 32 (Appendix 3) documents the eutectic Si particle characteristics for the samples which were specifically examined for this part of the study. As can be seen from the average values listed in the table for the as-cast alloy samples having an (SDAS of ~45 μm), the average eutectic Si particle area was reduced from 37 μm^2 in the non-modified E1 alloy to 5.3 μm^2 in the Sr-modified version, namely the E2 alloy. Due to the initially large size of the non-modified Si particles, solution heat treatment at 495°C for 8 hrs has seemingly no effect on the fragmentation of these particles, as may be inferred from the measurements. The particle density, however, as measured by the number of Si particles/mm^2, is significantly increased in the case of Sr-modified alloys, that is to say from 14574 particles/mm^2 in the as-cast condition to 36840 particles/mm^2 after solution treatment. Similar observations were made for the furnace-cooled alloy samples with an SDAS of ~ 120 μm.

The optical micrographs seen in Figure 6.34 show the microstructure beneath the fracture surface of the as-cast E1 alloy sample. It is evident from Figure 6.34(a) that the long acicular Si particles act as crack initiation sites, as indicated by the white arrow at the top left. The black arrow indicates the presence of secondary cracks beneath the fracture surface. Although modification with Sr produces fine fibrous Si particles, severe segregation of the Al_2Cu phase is frequently reported, as illustrated by the black arrow in Figure 6.34(b). Figures 6.34(c) and (d) show the role of α-iron intermetallics in enhancing

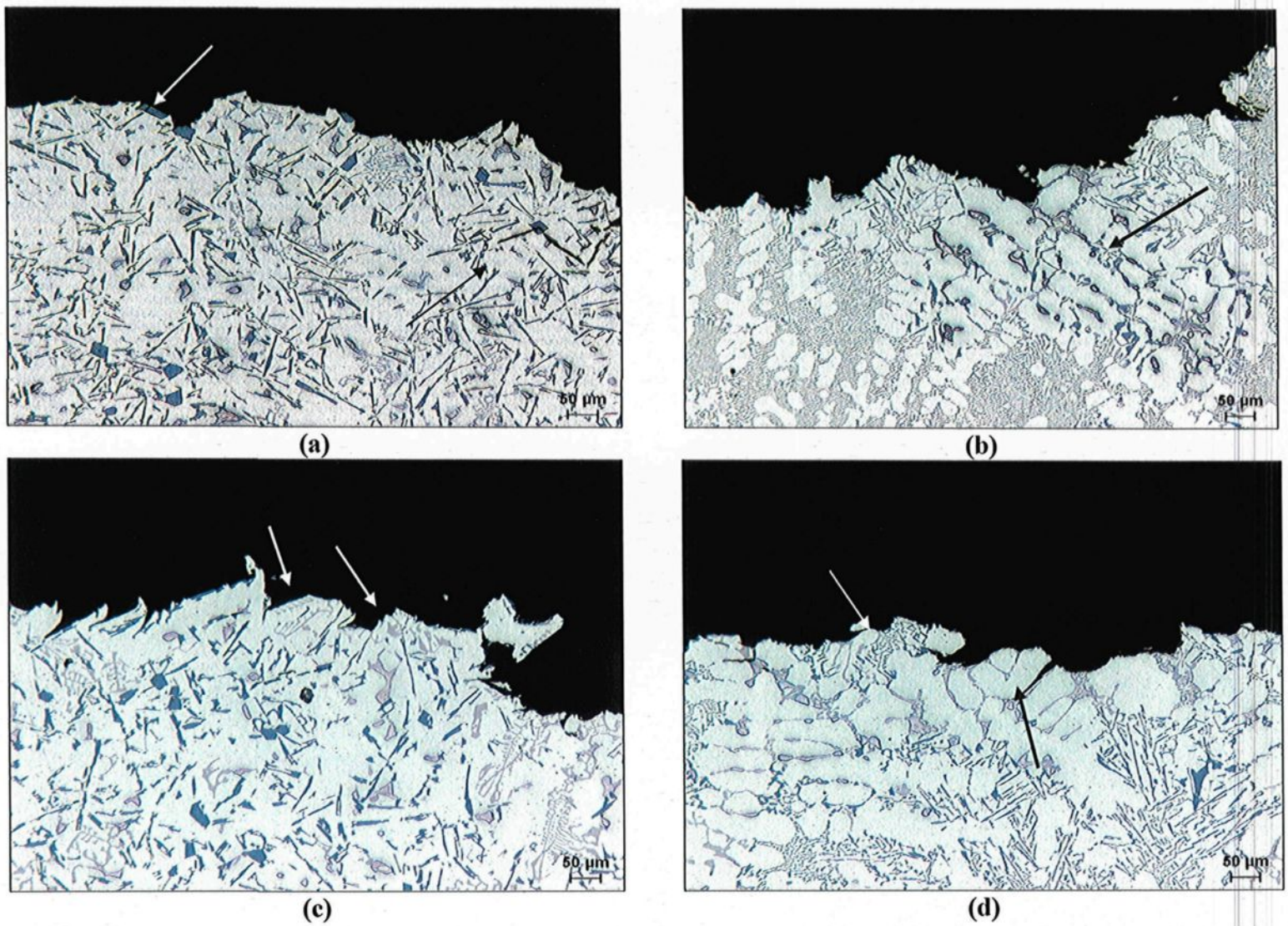

Figure 6.34 Optical micrographs showing the microstructure beneath the fracture surface of as-cast 396 alloy samples obtained under high cooling rate conditions (SDAS of ~45 µm): (a) E1 alloy, (0.45 wt% Mn), non-modified; (b) E2 alloy, (0.45 wt% Mn), Sr-modified; (c) E4 alloy, (0.65 wt% Mn), non-modified; and (d) E5 alloy, (0.65 wt% Mn), Sr-modified.

crack propagation in high Mn-containing alloys, as indicated by the white arrows. Figure 6.34(d) provides a good example of how the crack passes through an existing Al_2Cu particle without penetrating the elastic aluminum matrix.

A reduced cooling rate leads to an increase in the size of the eutectic Si particles as well as to the precipitation of primary Si particles, as may be seen in Figure 6.35(a). Both types of Si particles were found to contribute to crack initiation as marked by the white arrow for eutectic Si and the black arrow for primary Si in the micrograph. Under such low cooling rate conditions, addition of Sr was not sufficiently effective in producing fully modified Si particles which, in turn, helped to accelerate the crack initiation process, as shown by the solid white arrow in Figure 6.35(b). It should be mentioned here that the Cu-containing phase tends to precipitate in the Al-Al_2Cu eutectic form, an example of which is indicated by the broken white arrow. As may be seen, the latter was clearly fractured into two halves by the crack passing through.

The volume fraction of the insoluble α-$Al_{15}(Fe,Mn)_3Si_2$ increases with an increase in the Mn content to 0.65 wt%, as shown in Table 4. The white arrows in Figure 6.35(c) show the fracture of the α-iron intermetallic phase particles through the propagation of the primary crack, all of which is in good agreement with the fractographs presented in section 6.4.1. Similar observations were noted with respect to the fracture of the Al_2Cu phase in the Sr-modified HE5 alloy, as shown in Figure 6.35(d) by the white arrows. Likewise the balck arrows in (b) and (d) point to the presence of secondary cracks beneath the fracture surface.

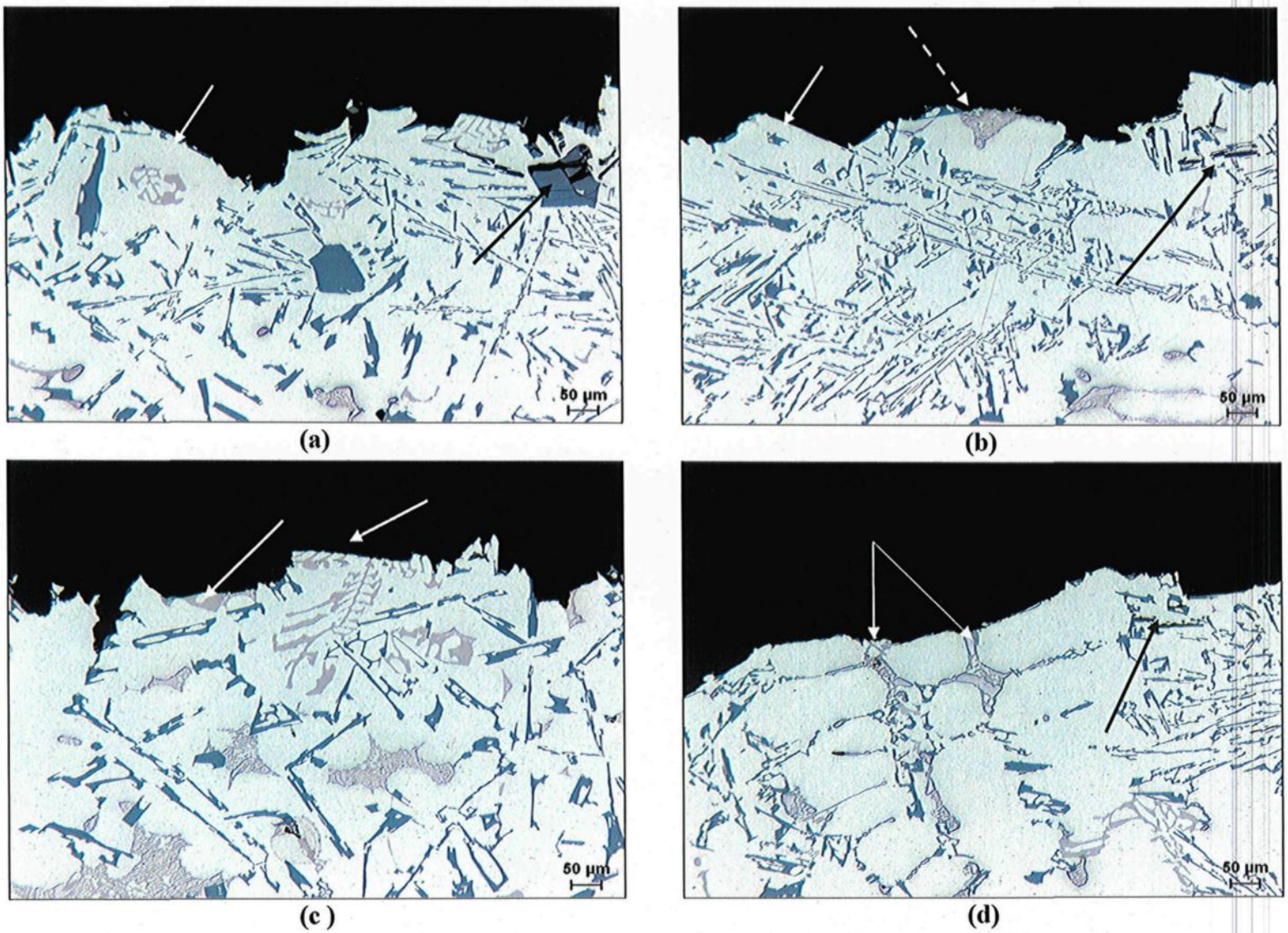

Figure 6.35 Optical micrographs showing the microstructure beneath the fracture surface of as-cast 396 alloy samples obtained under slow cooling rate conditions (SDAS of ~120 µm): (a) HE1 alloy, (0.45 wt% Mn), non-modified; (b) HE2 alloy, (0.45 wt% Mn), Sr-modified; (c) HE4 alloy, (0.65 wt% Mn), non-modified; and (d) HE5 alloy, (0.65 wt% Mn), Sr-modified.

The effects of solution heat treatment on the microstructural constituents of air-cooled samples having a SDAS of ~ 45 μm are shown in Figure 6.36. As will be observed, the fracture advances mainly through the acicular Si particles in the non-modified alloys, as shown in Figure 6.36(a), and (c), and also mainly by way of the α-$Al_{15}(Fe,Mn)_3Si_2$ phase in the Sr modified alloys, as shown in Figure 6.36(b) and (d).

The increase in the volume fraction of the α-iron intermetallic phase when the Mn content was increased to 0.65 wt% is evident from Figure 6.36(c). Figure 6.36(d) reveals that in the Sr-modified alloys, α-$Al_{15}(Fe,Mn)_3Si_2$ precipitates within the α-aluminum, as indicated by the black arrow in the micrograph.

In the furnace-cooled alloy samples, several interesting features were noted as displayed in Figure 6.37. These include the following:

(a) The eutectic Si particles formed are fairly large, at ~ 22 μm, making them good candidates for crack initiation, as may be seen in Figure 6.37(a), see the white arrow.

(b) The primary crack propagates within the α-$Al_{15}(Fe,Mn)_3Si_2$ phase as indicated by the white and black arrows in Figure 6.37(b).

(c) Many secondary cracks appear in the microstructure beneath the fracture surface as delineated by the black arrows in Figure 6.37(c) and the white arrow in (d).

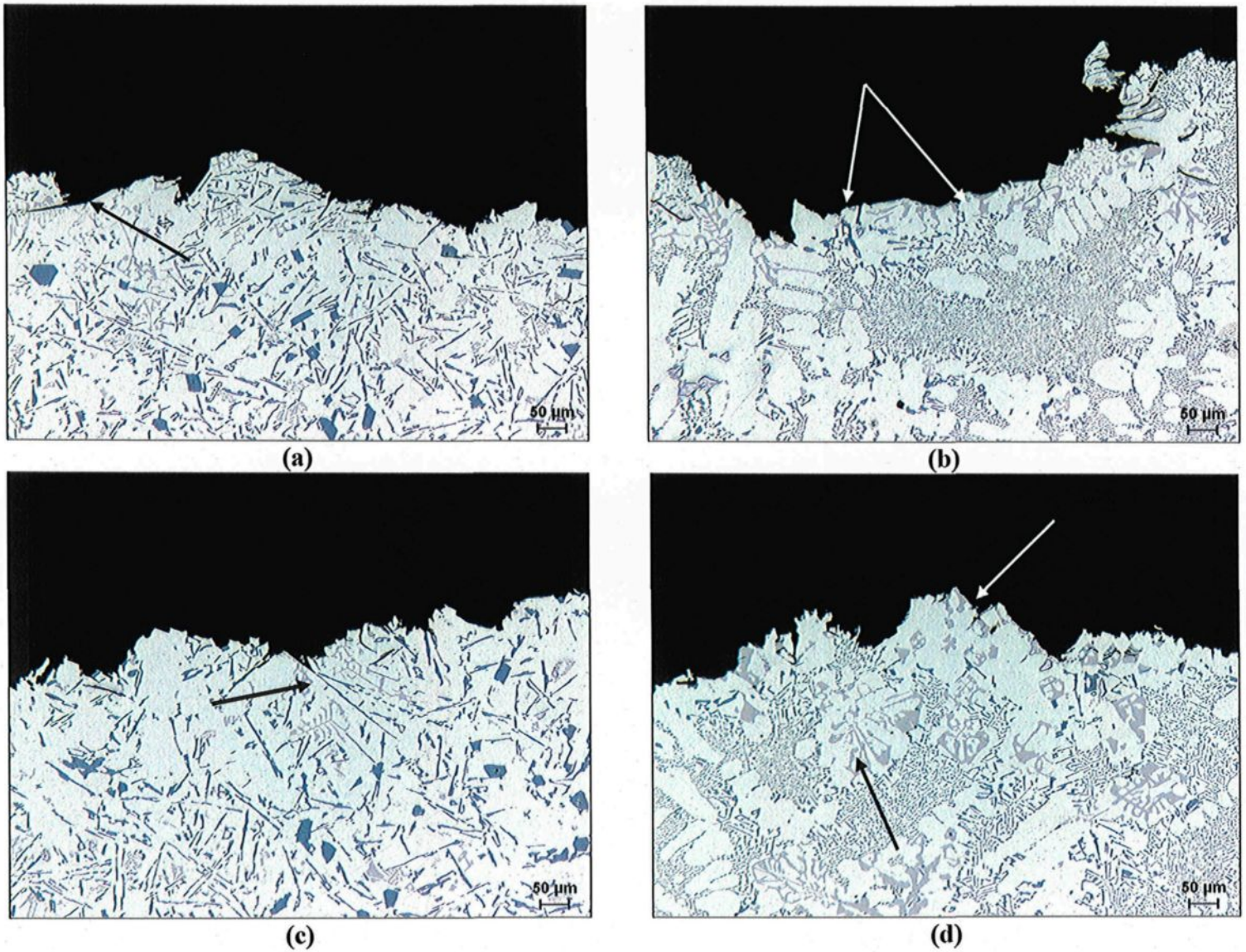

Figure 6.36 Optical micrographs showing the microstructure beneath the fracture surface of solution heat-treated 396 alloy samples obtained under high cooling rate cooling (SDAS ~45 µm): (a) E1 alloy, (0.45 wt% Mn), non-modified (b) E2 alloy, (0.45 wt% Mn), Sr-modified; (c) E4 alloy, (0.65 wt% Mn), non-modified; and (d) E5 alloy, (0.65 wt% Mn), Sr-modified.

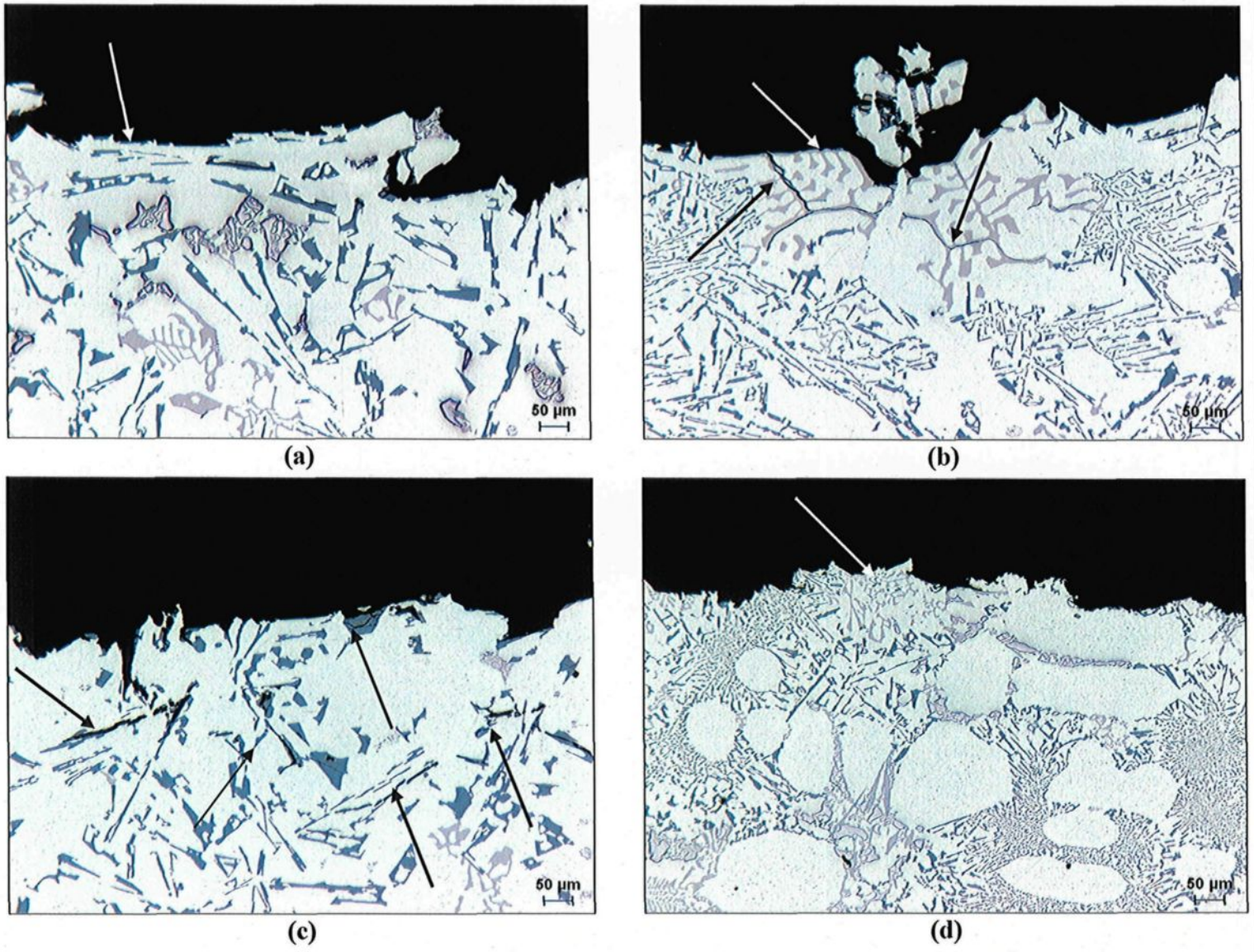

Figure 6.37 Optical micrographs showing the microstructure beneath the fracture surface of solution heat-treated 396 alloy samples obtained under low cooling rate conditions (SDAS ~120µm): (a) HE1 alloy, (0.45 wt% Mn), non-modified; (b) HE2 alloy, (0.45 wt% Mn), Sr-modified; (c) HE4 alloy, (0.65 wt% Mn), non-modified; and (d) HE5 alloy, (0.65 wt% Mn), Sr-modified

CHAPTER 7

CONCLUSIONS

CHAPTER 7

CONCLUSIONS

This study was directed towards the effects of Sr-modification, intermetallic phases and aging conditions on the impact behavior of 356, 319 and 396 type Al-Si alloys containing various levels of Fe, Mn and Mg additions. From the results obtained, the following conclusions may be drawn.

Microstructure of 356 Alloys

1. The as-cast non-modified 356 alloys display large acicular eutectic Si particles.
2. The π-$Al_8FeMg_3Si_6$ iron phase was found to precipitate either in close association with the β-Al_5FeSi platelet phase or else in the form of independent script-like particles in the case of as-cast 356 alloys.
3. Both β-iron needles and π-iron script-like particles appear to be segregated away from the modified eutectic Si colonies in the Sr-modified 356 alloys.
4. Solution heat treatment of 356 alloys at 540°C for 8 hrs results in:
   (i) Complete transformation of small-sized particles of the π-phase into small fragments of β-iron phase, particularly for the 356 alloys containing low levels of iron.
   (ii) Partial dissolution of large-size particles of π-phase into the matrix due to insufficient solution time to produce complete dissolution.
   (iii) Necking and fragmentation of thin β-needles into smaller segments.
   (iv) Fragmentation, spheroidization and coarsening of the eutectic Si particles.

Impact Toughness of 356 Alloys

1. Increasing the level of Fe additions diminishes the impact energy values of the 356 alloys to a noticeable degree (~ 35-57%), regardless of alloy condition.
2. Combination of Sr-modification and solution treatment significantly improves the total impact energy values (~ 110 %) of the as-cast 356 alloys, particularly at low level of iron.
3. With respect to aging treatment at 180°C:
   (i) Impact energy values increase by ~ 30% at 180°C/2h compared to those exhibited by the as-cast alloys;
   (ii) Subsequently, the impact energy decreases with aging times of up to 8 hrs;
   (iii) A slight recovery in impact energies is observed for the non-modified and Sr-modified alloys after 12 hours of aging.
4. The Sr-modified 356 alloys show higher impact energy values compared to non-modified alloys in the same conditions, regardless of the level of Fe addition or combined Fe-Mn additions.
5. The addition of 0.1 wt% Mn to non-modified 356 alloys seems to have no observable effect on the impact energy values, particularly when compared to the values obtained for the same alloys containing only Fe.
6. From the design and selection point of view, sudden failure may be circumvented through the application of a T7 treatment at 220°C for 12 hrs for Sr-modified 356 alloys containing 0.15 wt% Fe or a combined addition of 0.22 wt% Fe-0.14 wt% Mn, providing impact energy values of about 20 J and 18 J, respectively.

Impact Toughness of 319 Alloys

Effects of Fe Additions

1. Increasing the level of iron content decreases the impact energy values of 319 alloys considerably, regardless of the alloy conditions.
2. The combination of Sr modification and solution treatment increases the impact energy values of as-cast 319 alloys to a noticeable degree, particularly at a low level of iron content.
3. With respect to aging treatment at 180°C:
   (i) A slight increase in impact energy is obtained after 2 hrs of aging;
   (ii) Subsequently, the impact energy decreases with aging times up to 6 hrs.
   (iii) However, a remarkable recovery is observed in impact energy values after 12 hrs of aging.
4. The Sr-modified and non-modified 319 alloys aged at 180°C for 12 hrs display the highest impact energy values among all the alloys involved (*i.e.* ~10 to 12 J).
5. The impact energy of 319 alloys exhibits similar behavior at both 180°C and 220°C aging temperatures; however, the impact energy values obtained at 180°C are slightly higher than those obtained at 220°C.

Effects of Fe-Mn Additions

1. An addition of 0.1 wt% Mn has a negligible effect on the impact energy values of 319 alloys, while increasing the level of Mn addition up to 0.38 wt% appreciably improves the impact energy values for both non-modified and Sr-modified alloys compared to those containing only iron under the same as-cast and solution heat-treated conditions.

2. Artificial aging of 319 alloys at 180°C and 220°C temperatures for different times produces almost the same variation in the impact energy values. Also, the aged Sr-modified alloys exhibit higher impact energy values than those obtained for the non-modified alloys.

Effects of Fe-Mg Additions

1. Alloys containing various levels of combined Fe-Mg additions display lower impact energy values than those containing only iron. This reduction in the impact energy is more pronounced at a level of 0.28 wt% Mg addition.
2. A slight increase in the impact energy values of both non-modified and Sr-modified 319 alloys may be observed after aging at 180°C either for 2 hrs or 12 hrs compared to the values obtained for as-cast alloys at all levels of combined Fe-Mg additions.
3. The impact energy values of both non-modified and Sr-modified 319 alloys aged at 180°C and 220°C exhibit nearly a similar variation with aging time.

Effects of Fe-Mn-Mg additions

1. Increasing the level of combined Fe-Mn-Mg additions results in a remarkable reduction in the impact energy values of 319 alloys with the exception of the modified solution heat-treated alloys, where the impact energy remains almost unchanged.
2. A significant improvement in the impact energy may be achieved by applying Sr-modification in conjunction with solution heat treatment to 319 alloys, irrespective of the level of combined Fe-Mn-Mg additions.
3. Artificial aging at 180°C for various times has no observable effect on the improvement of the impact energy values of both non-modified and Sr-

modified alloys, however, an aging time of 2 hrs is capable of producing a slight recovery in the impact energy.

4. The Sr-modified 319 alloy containing 0.3 wt% Fe-0.09 wt% Mn-0.09 wt% Mg display slightly higher impact energy values for all aging times at 220°C than those obtained for the same alloys under solution heat-treated conditions.

5. In general, the impact toughness of aged 356 and 319 alloys depends to a great extent on their aging response at 180°C or 220°C aging temperatures. The degree of this dependence is strongly governed by the types and amounts of the alloying elements present in the alloy, as well as the aging temperature and time.

Impact Toughness of 396 Alloys

1. The impact energy values of the newly developed 396 alloys are, in general, lower than those obtained for 356 and 319 alloys.

2. The presence of undissolved intermetallic phases, mainly Al_2Cu and α-$Al_{15}(Mn,Fe)_3Si_2$, increases alloy brittleness and thus reduces the alloy impact toughness. The segregation of Al_2Cu caused by Sr addition is a parameter to be considered, especially for furnace-cooled alloys (SDAS ~ 120 μm).

3. Increasing the Mn content from 0.45 wt% to 0.65 wt% leads to an increase in the volume fraction of the α-$Al_{15}(Mn,Fe)_3Si_2$ phase, whereas a slow cooling rate increases the particle size of the phase significantly, in turn enhancing both crack initiation and crack propagation.

4. Increasing the aging time from 4 hrs up to 44 hrs at the peak-aging temperature of 180°C produces virtually no discernible change in the impact values of all the 396 alloys investigated.

5. Artificial aging at 240°C for different times of up to 44 hrs produces a significant increase in the impact energy values as a result of alloy softening, regardless of alloy composition.
6. Although the impact behavior of aged 396 alloys is similar under both cooling rate conditions, the air-cooled alloys (SDAS ~45 μm) display higher impact energy values than do furnace-cooled alloys (SDAS ~120 μm). The difference in impact energy values between the air-cooled and furnace-cooled alloys may be attributed to the microstructural differences resulting from the difference in cooling rates, regardless of alloy conditions.
7. The effects of the size and morphology of microstructural constituents on the impact behavior is more pronounced in the furnace-cooled alloys.

Fracture Behavior of 356 Alloys

1. The fracture behavior appears to be more controlled by the eutectic Si particles in the non-modified 356 alloys containing 0.15 wt% Fe.
2. The β-iron platelets undergo cracking in the non-modified 356 alloys containing 0.8 wt% Fe providing another source for microcrack initiation and further paths for crack propagation. The brittle nature of these platelets is evident from the optical micrographs showing the microstructure beneath the fracture surface.
3. Iron-bearing intermetallics contribute significantly to the nucleation and propagation of cracks in the Sr-modified 356 alloys containing 0.1 wt% Fe.

Fracture Behavior of 319 Alloys

1. The fracture of 319 alloys is governed to a large extent by the size and morphology of the Al_2Cu phase particles, particularly in the Sr-modified heat-treated alloys.

2. The α-iron Chinese-script particles and β-Fe platelets also undergo cracking, promoting crack propagation in non-modified and Sr-modified 319 alloys containing combined Fe-Mn additions; this cracking emphasizes on the role of such iron-based intermetallics in controlling the impact behavior of these alloys

Fracture Behavior of 396 Alloys

1. Crack propagation occurs mainly in the 396 alloys by passing through the Al_2Cu and/or α-iron intermetallic phases. In numerous cases, the morphology of the intermetallic phase is retained, indicating that the fracture is of the transverse type rather than a particle/matrix fracture.

RECOMMENDATIONS FOR FUTURE WORK

The results obtained from this portion of the current study underlined the role of a number of significant metallurgical parameters such as iron content, strontium modification, and heat treatment conditions on the impact toughness of the 356 319 and 396 alloys. The present study might be further elaborated by incorporating the following:-

1. Investigating the submicron phases present in the microstructure of 356 alloys such as Mg_2Si and Si precipitates by means of Transmission electron microscope (TEM)
2. Examining the role and contribution of these submicron phases on the impact fracture mechanism using Scanning electron microscope (SEM).
3. Modeling and simulating the internal stresses values and their distribution in the Charpy impact-tested specimen.
4. Finding a numerical correlation between the impact toughness and hardness values under different heat treatment conditions.

APPENDICES

Appendix 1

Chemical Composition of the Alloys Investigated in the Present Study

Table 3 Chemical composition of 356 alloys used in the present study

Alloy code	Elements (wt %)								
	Si	Mg	Cu	Fe	Mn	Ti	Sr	Mn/Fe	Bal.
1*	6.5	0.27	0.03	0.11	0.03	0.09	0.00	0.293	92.8
1S*	6.9	0.33	0.14	0.14	0.03	0.1	.017	0.246	92.1
2	6.7	0.25	.017	0.25	0.03	0.1	0.00	0.134	92.5
2S	7.08	0.34	0.17	0.23	0.04	0.11	.014	0.179	91.9
3	6.7	0.31	.017	0.43	0.03	0.1	0.00	0.081	92.2
3S	6.5	0.36	.06	0.35	.002	0.14	.014	0.007	92.5
4	6.8	0.3	.017	0.87	0.03	0.10	0.00	0.04	91.8
4S	6.8	0.35	.045	0.92	0.01	0.14	.016	0.12	91.6
5	6.4	0.33	.005	0.24	0.1	0.14	0.00	0.43	92.7
5S	7.6	0.36	.044	0.22	0.13	0.11	.017	0.62	91.3
6	6.5	0.31	.008	0.44	0.2	0.13	0.00	0.472	92.3
6S	7.1	0.35	.027	0.37	0.2	0.11	.017	0.614	91.6
7	6.5	0.3	.015	0.85	0.41	0.11	0.00	0.484	91.7
7S	6.9	0.32	.029	0.9	0.41	0.11	.018	0.465	91.1

*1: 356 base alloy; S: Sr-modified.

Table 4 Chemical composition of 319 alloys used in the present study

Alloy code	Elements (wt%)								
	Si	Cu	Mg	Fe	Mn	Ti	Sr	Mn/Fe	Bal.
22*	5.99	3.45	.014	0.22	.006	0.14	0.00	0.03	90.1
22S*	6.01	3.27	.016	0.18	.006	0.19	0.0248	0.03	90.2
8	6.12	3.33	.012	0.4	0.01	0.13	0.00	0.026	89.9
8S	6.03	3.18	.024	0.33	.008	0.12	0.016	0.023	90.2
9	5.85	3.34	.005	0.62	.002	0.14	0.00	0.003	90
9S	6.26	3.41	.02	0.67	.016	0.14	0.0118	0.0246	89.4
10	5.81	3.07	.012	1.03	.018	0.13	0.00	0.017	89.8
10S	6.03	3.32	.004	1.07	.003	0.13	0.015	0.003	89.4
11	5.85	3.32	.002	0.4	0.09	0.13	0.00	0.234	90.1
11S	6.24	3.6	.007	0.36	0.09	0.14	0.0158	0.256	89.6
12	5.79	3.35	.006	0.64	0.18	0.14	0.00	0.29	89.8

12S	5.80	3.24	.006	0.64	0.19	0.13	0.0165	0.3	89.9
13	5.66	3.2	.004	1.08	0.38	0.13	0.00	0.35	89.5
13S	5.99	3.23	.012	1.07	0.37	0.17	0.034	0.35	89
14	5.81	3.34	.088	0.37	.007	0.13	0.00	0.019	90.2
14S	5.87	3.22	.089	0.34	.008	0.13	0.0179	0.025	90.3
15	5.81	3.28	.086	1.1	.015	0.13	0.00	0.014	89.5
15S	6.75	2.9	0.14	1	.025	0.12	0.0131	0.026	86.8
16	5.81	3.3	0.27	0.36	.001	0.13	0.00	.003	90.1
16S	5.99	3.31	0.28	0.34	.002	0.13	0.0178	.007	89.9
17	5.61	3.2	0.27	1.05	.005	0.13	0.00	.004	89.7
17S	5.89	3.22	0.27	1.11	.007	0.13	0.0185	0.006	89.3
18	5.94	3.42	.09	0.42	.093	0.13	0.00	0.222	89.8
18S	6.01	3.3	.099	0.35	.09	0.14	0.0196	0.255	89.9
19	5.57	3.18	.089	1	0.37	0.13	0.00	0.364	89.6
19S	5.79	3.19	0.10	1.06	0.38	0.14	0.0193	0.363	89.2
20	6.00	3.4	0.27	0.4	.09	0.14	0.00	0.244	89.6
20S	6.05	3.35	0.28	0.35	.09	0.13	0.0209	0.278	89.6
21	5.42	3.06	0.28	1.04	0.37	0.16	0.00	0.36	89.6
21S	5.66	3.09	0.27	1.06	0.38	0.13	0.020	0.36	89.3

*22: 319 base alloy; S: Sr-modified.

Table 5 Chemical composition of 396 alloys used in the present study

Alloy Code	**Element (wt%)**								
	Si	**Cu**	**Mg**	**Fe**	**Mn**	**Cr**	**Sr**	**Mn/Fe**	**Bal.**
E1*	10.8	2.7	0.38	0.43	0.46	0.029	0.0001	1.06	85.2
E2	10.8	2.6	0.38	0.41	0.46	0.028	0.0167	1.11	85.3
E3	10.8	2.6	0.38	0.4	0.46	0.028	0.0272	1.15	85.3
E4	11.1	2.7	0.37	0.46	0.68	0.029	0.0004	1.49	84.4
E5	10.9	2.6	0.38	0.42	0.69	0.029	0.0163	1.67	85
E6	11.7	2.7	0.41	0.52	0.63	0.040	0.0301	1.23	83.4
HE1*	10.8	2.3	0.31	0.45	0.41	0.039	0.0004	0.91	85.7
HE2	11.1	2.5	0.37	0.46	0.47	0.039	0.0152	1.02	85
HE3	12.1	2.5	0.35	0.54	0.49	0.043	0.0407	0.91	84
HE4	11	2.5	0.33	0.44	0.7	0.040	0.0009	1.59	85
HE5	11	2.5	0.36	0.42	0.65	0.036	0.0132	1.55	85.02
HE6	10.7	2.5	0.36	0.36	0.63	0.030	0.0300	1.75	85.4

*E: 396 alloy; 1: 0 ppm Sr; 2: 200 ppm Sr; 3: 350 ppm Sr; H: low cooling rate alloy.

Appendix 2

Charpy Impact Properties of the Alloys Investigated

Table 6 Effects of Sr-modification and solution heat treatment on Charpy impact energy values of as-cast non-modified 356 alloys

Alloy Code	Alloy Condition	E_T (J)	E_I (J)	E_P (J)	Time to Failure (ms)	ACS (mm/ms)
1	A*	6.40 ± 0.6	3.83 ± 0.4	2.57 ± 0.2	0.35 ± .02	28.6 ± 1.4
(0.1Fe)	B*	12.48 ± 1	8.55 ± 0.8	3.93 ± 0.4	0.53 ± .06	18.8 ± 2.2
2	A	5.50 ± 0.5	3.09 ± 0.3	2.41 ± 0.1	0.34 ± .03	29.4 ± 2.2
(0.25Fe)	B	9.17 ± 0.9	5.63 ± 0.6	3.54 ± 0.3	0.42 ± .02	23.8 ± 1
3	A	4.56 ± 0.3	2.46 ± 0.1	2.10 ± 0.2	0.31 ± .01	32 ± 1.5
(0.43Fe)	B	6.13 ± 0.8	3.40 ± 0.5	2.73 ± 0.3	0.35 ± .04	28.6 ± 3.6
4	A	3.72 ± 0.2	1.95 ± 0.4	1.77 ± 0.3	0.28 ± .03	36 ± 3.3
(0.87Fe)	B	5.3 ± 0.8	2.78 ± 0.4	2.52 ± 0.3	0.29 ± .02	34.5 ± 2.4
5	A	5.35 ± 0.8	2.80 ± 0.3	2.55 ± 0.6	0.29 ± .03	34.5 ± 2.8
(0.2Fe-0.1Mn)	B	10.03 ± 0.9	6.20 ± 1	3.83 ± 0.1	0.45 ± .01	22.2 ± 1.1
6	A	5.05 ± 0.5	2.86 ± 0.1	2.19 ± 0.1	0.31 ± .02	32.2 ± 1.6
(0.4Fe-0.2Mn)	B	9.0 ± 0.4	5.0 ± 0.2	4 ± 0.1	0.42 ± .02	23.8 ± 1.6
7	A	4.63 ± 0.5	2.5 ± 0.6	2.13± 0.3	0.34 ± .03	29.4 ± 2.1
(0.8Fe-0.4Mn)	B	5.99 ± 0.9	3.0 ± 0.4	2.99 ± 0.4	0.33 ± .02	30.3 ± 2.4
1S*	A	7.00 ± 0.9	3.6 ± 0.5	3.4 ± 0.4	0.38 ± .02	26.3 ± 2.1
(0.14Fe)	B	13.9 ± 0.9	9.17 ± 0.9	4.73 ± 0.3	0.54 ± .04	18.5 ± 1.6
2S	A	5.77 ± 0.6	3.2 ± 0.4	2.57 ± 0.4	0.37 ± .02	27 ± 2.6
(0.23Fe)	B	13.7 ± 0.9	9.22 ± 1	4.48 ± 0.2	0.51 ± .03	19.6 ± 1.2
3S	A	5.57 ± 0.9	3.10 ± 0.6	2.47 ± 0.2	0.37 ± .01	27 ± 3.6
(0.35Fe)	B	11.97 ± 0.8	7.75 ± 0.8	4.22 ± 0.3	0.54 ± .05	18.5 ± 1.8
4S	A	4.53 ± 0.1	2.47 ± 0.2	2.06 ± .08	0.32 ± .02	31 ± 1.9
(0.92Fe)	B	7.22 ± 0.3	3.86 ± 0.3	3.36 ± .09	0.35 ± .01	28.5 ± 0.8
5S	A	8.69 ± 0.30	5.12 ± 0.9	3.57 ± 0.3	0.40 ± .06	25± 3.3
(0.2Fe-0.1Mn)	B	12.51 ± 0.3	6.64 ± 0.9	5.87 ± 0.3	0.54 ± .02	18.5 ± 1.3
6S	A	8.41 ± 0.2	4.93 ± 0.5	3.48 ± .09	0.46 ± .03	21 ± 1.7
(0.4Fe-0.2Mn)	B	11.31 ± 0.9	6.8 ± 0.6	4.51 ± 0.6	0.53 ± .04	18.8 ± 1.1
7S	A	5.45 ± 0.6	3.03 ± 0.3	2.42 ± 0.2	0.37 ± .04	27 ± 3
(0.9Fe-0.4Mn)	B	6.67 ± 0.9	3.62 ± 0.9	3.05 ± 0.4	0.34 ± .03	29.4 ± 3.2

*A: as-cast; B: solution heat-treated; S: Sr-modified; E_T: total impact energy; E_I: energy for crack initiation; Ep energy for crack propagation; and ACS: Average speed of crack propagation

Table 7 Effects of Sr-modification and aging times on Charpy impact energy values of 356 alloys containing four levels of Fe, and aged at 180°C

Alloy Code	Aging Time (h)	E_T (J)	E_I (J)	E_p (J)	Time to Failure (ms)	ACS (mm/ms)
1	2	8.35 ± 0.9	4.7 ± 0.6	3.65 ± 0.7	0.34 ± .02	29.4 ± 2
	4	7.4 ± 0.6	4.0 ± 0.4	3.4 ± 0.5	0.31 ± .02	32.2 ± 1.5
	6	6.1 ± 0.4	3.2 ± 0.3	2.9 ± 10.4	0.28 ± .01	35.7± 1.3
	8	4.9 ± 0.7	2.5 ± 0.4	2.4 ± 0.6	0.26 ± .02	40 ± 2.3
	12	5.5 ± 0.8	2.4 ± 0.5	3.1 ± 0.3	0.26 ± .03	38.5 ± 3.7
1S	2	9.7 ± 0.9	5.6 ± 0.5	4.1 ± 0.7	0.36 ± .03	27.7 ± 2
	4	5.7 ± 0.4	2.8 ± 0.2	2.9 ± 0.5	0.30 ± .01	33.3 ± 0.9
	6	5.6 ± 0.5	2.8 ± 0.4	2.8 ± 0.8	0.34 ± .03	29.4 ± 3.3
	8	5.5 ± 0.3	2.55 ± 0.1	2.95 ± 0.3	0.31 ± .02	32.2 ± 2.1
	12	7.5 ± 0.8	4.1 ± 0.4	3.4 ± 0.2	0.27 ± .02	37.1 ± 2.5
2	2	4.15 ± 0.6	2.08 ± 0.6	2.07 ± 0.7	0.26 ± .03	38.5 ± 4
	4	3.82 ± 0.3	1.90 ± 0.2	1.92 ± 0.5	0.24 ± .01	41.6 ± 1
	6	4.64 ± 0.3	2.28 ± 0.2	2.36 ± 0.6	0.26 ± .01	38.5 ± 0.9
	8	4.34 ± 0.6	2.24 ± 0.4	2.1 ± 0.4	0.26 ± .02	38.5 ± 2.7
	12	5.08 ± 0.9	3.76 ± 0.5	1.32 ± 0.3	0.27 ± .01	37 ± 0.7
2S	2	7.67 ± 0.7	4.2 ± 0.4	3.47 ± 0.1	0.31 ± .01	32.2 ± 1.6
	4	5.83 ± 0.5	3.18 ± 0.4	2.65 ± 0.3	0.30 ± .02	33.3 ± 2.3
	6	5.42 ± 0.9	2.86 ± 0.5	2.56 ± 0.5	0.29± .01	34.5 ± 1.8
	8	5.27 ± 0.3	2.95 ± 0.3	2.32 ± 0.8	0.29 ± .03	34.5 ± 3.4
	12	6.4 ± 0.6	3.55 ± 0.4	2.85 ± 0.4	0.28 ± .02	35.7 ± 2.14
3	2	3.44 ± 0.7	1.62 ± 0.3	1.82 ± 0.9	0.24 ± .01	41.6 ± 1.6
	4	3.05 ± 0.3	1.43 ± 0.1	1.62 ± 0.2	0.22 ± .01	45.5 ± 0.5
	6	3.04 ± 0.9	1.66 ± 0.3	1.38 ± 0.5	0.24 ±.02	41.6 ± 3.2
	8	2.74 ± 0.2	1.31 ± 0.1	1.43 ± 0.4	0.22 ± .01	45.5 ± 2
	12	4.76 ± 0.4	2.38 ± 0.1	2.38 ± 0.2	0.25 ± .01	40 ± 1.1
3S	2	6.24 ± 0.8	3.14 ± 0.5	3.10 ± 0.4	0.28 ± .02	35.7 ± 3
	4	5.8 ± 0.8	3.1 ± 0.6	2.7 ± 0.3	0.28 ± .02	35.7 ± 3.5
	6	5.1 ± 0.3	2.9 ± 0.2	2.2 ± 0.7	0.30 ±.01	33.3 ± 0.5
	8	5.15 ± 0.9	3.42 ± 0.4	1.73 ± 0.6	0.26 ± .02	38.5 ± 2.6
	12	6.65 ± 0.9	3.77 ± 0.5	2.88 ± 0.2	0.34 ± .03	29.4 ± 3.3
4	2	3.03 ± 0.3	1.5 ± 0.2	1.53 ± 0.7	0.22 ± .01	45.5 ± 0.6
	4	2.31 ± 0.2	1.2 ± 0.1	1.11 ± 0.8	0.24 ± .02	41.6 ± 3.5
	6	2.47 ± 0.5	1.14 ± 0.3	1.33 ± 0.3	0.22 ± .01	45.5 ± 2.4
	8	2.51 ± 0.3	1.8 ± 0.2	0.71 ± 0.5	0.22 ± .02	45.5 ± 2.6
	12	2.55 ± 0.7	1.2 ± 0.3	1.35 ± 0.4	0.23 ± .02	43.5 ± 3.4
4S	2	4.07 ± 0.4	1.95 ± 0.2	2.12 ± 0.3	0.25 ± .01	40 ± 2
	4	2.82 ± 0.2	1.36 ± 0.1	1.46 ± 0.4	0.26 ± .03	38.5 ± 3
	6	3.09 ± 0.4	1.48 ± 0.2	1.61 ± 0.5	0.24 ± .01	41.6 ± 2.3
	8	2.9 ± 0.3	1.36 ± 0.1	1.54 ± 0.1	0.25 ± .03	40 ± 3.5
	12	4.86 ± 0.9	2.47 ± 0.6	2.39 ± 0.8	0.23 ± .03	43.5 ± 2.3

Table 8 Effects of Sr-modification and aging times on Charpy impact energy values of 356 alloys containing four levels of Fe, and aged at 220°C

Alloy Code	Aging Time (h)	E_T (J)	E_I (J)	E_p (J)	Time to Failure (ms)	ACS (mm/ms)
1	2	8.26 ± 0.9	4.8 ± 0.6	3.46 ± 0.3	0.34 ± .02	29.4 ± 2
	4	7.96 ± 0.5	4.66 ± 0.4	3.3 ± 0.2	0.37 ± .03	27 ± 2.2
	6	7.5 ± 0.6	4.62 ± 0.4	2.88 ± 0.3	0.29 ± .01	25.6 ± 1.2
	8	7.6 ± 0.9	4.44 ± 0.5	3.27 ± 0.2	0.37 ± .01	27 ±1.3
	12	11.6 ± 0.9	7.36 ± 0.5	4.24 ± 0.1	0.5 ± .02	20 ±1.4
1S	2	9.78 ± 0.3	5.65 ± 0.2	4.13 ± 0.2	0.30 ± .01	33.3 ±1
	4	8.87 ± 0.7	5.14 ± 0.3	3.73 ± 0.4	0.33 ± .01	30.3 ±1.6
	6	9.32 ± 0.6	4.82 ± 0.3	4.5 ± 0.3	0.61 ± .01	16.4 ±1.3
	8	11.78 ± 0.3	7.7 ± 0.2	4.08 ± 0.1	0.5 ± .01	20 ± 1
	12	19.95 ± 0.9	13.55 ± 0.5	6.4 ±0.4	0.65 ± .03	15.4± 0.9
2	2	6.98 ± 0.9	3.56 ± 0.5	3.42 ± 0.2	0.38 ± .02	26.3 ± 1.7
	4	6.81 ± 0.9	5.14 ± 0.6	1.67 ± 0.3	0.36 ± .01	27 ± 1
	6	6.9 ± 0.9	3.98 ± 0.4	2.92 ± 0.3	0.36 ± .03	27.7 ± 2.1
	8	7.45 ± 0.9	4.18 ± 0.5	3.27 ± 0.4	0.37 ± .05	27 ± 1.5
	12	11.45 ± 0.8	7.17 ± 0.5	4.28 ± 0.3	0.5 ± .04	20 ± 1.5
2S	2	8.03 ± 0.9	4.8 ± 0.6	3.23 ± 0.4	0.41 ± .02	24.3 ± 1.8
	4	7.08 ± 0.6	3.58 ± 0.4	3.50 ± 0.2	0.39 ± .01	25.6 ± 1.3
	6	7.83 ± 0.6	4.03 ± 0.4	3.80 ± 0.2	0.33 ± .01	30 ± 1.6
	8	8.81 ± 0.2	5.23 ± 0.2	3.58 ± 0.7	0.39 ± .06	25.6 ± 2
	12	14.27 ± 0.3	9.14 ± 0.2	5.13 ± 0.2	0.51 ± .01	18.6 ± 0.8
3	2	4.7 ± 0.5	2.49 ± 0.3	2.0 ±0.2	0.25 ± .01	40 ±1.9
	4	5.48 ± 0.3	2.97 ± 0.2	2.51 ± 0.1	0.29 ± .01	34.5 ± 1.2
	6	5.4 ± 0.5	2.86 ± 0.3	2.54 ± 0.2	0.29 ± .01	34.4 ± 1.4
	8	5.34 ± 0.2	2.13 ± 0.1	3.21 ± 0.1	0.26 ± .01	38.5 ± 1.3
	12	6.9 ± 0.5	3.77 ± 0.3	3.2 ± 0.2	0.35 ± .01	28.6 ± 1.2
3S	2	6.88 ± 30.6	4.04 ± 0.4	2.84 ± 0.2	0.3 ± .01	33.3 ± 2
	4	6.63 ± 0.2	3.56 ± 0.1	3.07 ± 0.7	0.31 ± .04	32.2 ± 3
	6	6.47 ± 0.2	3.43 ± 0.2	3.05 ± 0.1	0.32 ± .01	31.25 ± 1.6
	8	6.13 ± 0.7	3.35 ± 0.4	2.78 ± 0.2	0.33 ± .01	30.3 ± 2.3
	12	13.06 ± 0.7	8.12 ± 0.7	4.94 ± 0.5	0.48 ± .01	20.8 ± 1.7
4	2	3.3 ± 0.4	1.71 ± 0.2	1.6 ± 0.2	0.22 ± .01	45.5 ± 1.7
	4	3.27 ± 0.5	1.6 ± 0.2	1.67 ± 0.3	0.23 ±.01	43.5 ± 2.5
	6	3.48 ± 0.5	1.8 ± 0.3	1.68 ± 0.2	0.24 ±.02	41.6 ± 1.9
	8	3.18 ± 0.4	1.55 ± 0.2	1.63 ± 03.2	0.24 ±.01	41.6 ± 2.3
	12	5.18 ± 0.6	2.56 ± 0.3	2.62 ±0.3	0.31 ±.01	32.2 ± 2.4
4S	2	3.80 ± 0.2	2.0± 0.1	1.2 ± 0.1	0.23 ± .01	43.5 ± 2
	4	3.50± 0.6	1.85 ± 0.3	1.65 ± 0.3	0.26 ± .02	38.5 ± 3
	6	3.42 ± 0.7	1.71 ± 0.4	1.71 ± 0.3	0.27 ± .01	37 ± 2.2
	8	3.76 ± 0.5	1.85 ± 0.3	1.91 ± 0.2	0.25 ± .01	40 ± 2.2
	12	6.57 ± 0.5	3.34 ± 0.2	3.23 ± 0.3	0.32 ± .01	31.2 ± 0.9

Table 9 Charpy impact properties of 356 alloys containing various levels of Fe-Mn, and aged at 180°C for different times

Alloy Code	Aging Time (h)	E_T (J)	E_I (J)	E_p (J)	Time to Failure (ms)	ACS (mm/ms)
5	2	7.35 ± 0.5	3.95 ± 0.3	3.4 ± 0.2	0.29 ± .01	34.5 ± 1.4
	4	5.4 ± 0.9	2.93 ± 0.6	2.3 ± 70.3	0.26 ± .04	38.5 ± 3
	6	5.35 ± 0.9	2.75 ± 0.5	2.6 ± 0.4	0.27 ± .01	37.0 ± 2.4
	8	3.61 ± 0.2	1.77 ± 0.1	1.84 ± 0.1	0.24 ± .01	41.6 ± 1.2
	12	5.28 ± 0.3	2.62 ± 0.2	2.66 ± 0.15	0.25 ± .01	40 ± 0.7
5S*	2	12.2 ± 0.3	7.75 ± 0.4	4.45 ± 0.2	0.47 ± .06	21.3 ± 2.8
	4	8.3 ± 0.5	4.47 ± 0.5	3.83 ± 0.5	0.30 ± .03	33.3 ± 3
	6	6.28 ± 0.8	3.35 ± 0.3	2.93 ± 0.2	0.31 ± .01	32.2 ± 1
	8	5.2 ± 0.7	2.75 ± 0.2	2.45 ± 0.1	0.27 ± .01	37 ± 2.1
	12	9.56 ± 0.9	5.37 ± 0.6	4.19 ± 0.1	0.32 ± .09	31.2 ± 3
6	2	3.9 ± 0.2	1.9 ± 0.1	1.9 ± 0.2	0.25 ± .07	40 ± 1.8
	4	3.47 ± 0.4	1.72 ± 0.2	1.75 ± 0.2	0.22 ± .02	45.5 ± 3
	6	3.27 ± 0.5	1.52 ± 0.3	1.75 ± 0.2	0.24 ± .01	41.6 ± 1.8
	8	3.24 ± 0.4	1.64 ± 0.3	1.6 ± 0.1	0.23 ± .01	43.5 ± 3
	12	4.03 ± 0.9	2.03 ± 0.5	2 ± 0.4	0.25 ± .01	40 ± 2.2
6S	2	6.20 ± 0.9	3.47 ± 0.5	2.73 ± 0.7	0.34 ± .03	29.4 ± 4
	4	5.02 ± 0.9	2.58 ± 0.5	2.44 ± 0.9	0.33 ± .05	30.3 ± 4
	6	4.76 ± 0.9	2.51 ± 0.5	2.25 ± 0.7	0.30 ± .02	33.3 ± 3
	8	4.7 ± 0.9	2.48 ± 0 6	2.22 ± 0.4	0.27 ± .01	37 ± 3
	12	6.8 ± 0.9	3.52 ± 0.6	3.28 ± 0.6	0.26 ± .02	38.5 ± 3
7	2	3.47 ± 0.4	1.73 ± 0.2	1.74 ± 0.2	0.23 ± .01	43.4 ± 2.5
	4	2.95 ± 0.8	1.45 ± 0.4	1.5 ± 0.5	0.23 ± .01	43.4 ± 1.6
	6	3.09 ± 0.3	1.52 ± 0.2	1.57 ± 0.1	0.22 ± .01	45.5 ± 1.4
	8	2.8 ± 0.3	1.23 ± 0.1	1.57 ± 0.2	0.24 ± .01	41.6 ± 2.5
	12	3.6 ± 0.4	1.82 ± 0.2	1.78 ± 0.2	0.24 ± .01	41.6 ± 1.4
7S	2	5.0 ± 0.6	2.9 ± 0.5	2.1 ± 0.1	0.29 ± .08	34.5 ± 4
	4	3.86 ± 0.5	1.86 ± 0.3	2.0 ± 0.2	0.25 ± .01	40 ± 2.1
	6	4.31 ± 0.5	2.15 ± 0.3	2.16 ± 0.1	0.26 ± .01	38.5 ± 1.14
	8	4.17 ± 0.4	1.96 ± 0.2	2.21 ± 0.2	0.25 ± .01	40 ± 1.6
	12	4.37 ± 0.3	2.24 ± 0.2	2.13 ± 0.1	0.24 ± .01	41.6 ± 1

*S: Sr-modified; see table 6 for alloy Fe-Mn levels

Table 10 Charpy impact properties of 356 alloys containing various levels of Fe-Mn, and aged at 220°C for different times

Alloy Code	Aging Time (h)	E_T (J)	E_I (J)	E_p (J)	Time to Failure (ms)	ACS (mm/ms)
5	2	5.27 ± 0.6	2.73 ± 0.3	2.54 ± 0.2	0.27 ± .01	37 ± 1.2
	4	5.8 ± 0.9	3.02 ± 0.4	2.78 ± 0.5	0.32 ± .02	31.2 ± 2.7
	6	6.8 ± 0.9	3.7 ± 0.5	3.1 ± 0.4	0.35 ± .03	28.5 ± 1
	8	8.89 ± 0.9	5.17 ± 0.4	3.72 ± 0.2	0.45 ± 0.1	22.2 ± 0.7
	12	9.92 ± 0.9	5.82 ± 0.6	4.1 ± 0.4	0.46 ± .03	21.7 ± 1.5
5S*	2	6.92 ± 0.3	3.9 ± 0.2	3.02 ± 0.1	0.35 ± .01	28.6 ± 0.8
	4	7.31 ± 0.5	4 ± 0.4	3.31 ± 0.1	0.39 ± .01	25.6 ± 1.7
	6	8.51 ± 0.8	4.73 ± 0.5	3.78 ± 0.3	0.43 ± 0.2	23.2 ± 2
	8	9.7 ± 0.7	5.36 ± 0.5	4.34 ± 0.3	0.42 ± .01	23.8 ± 0.8
	12	18.1 ± 0.9	12.15 ± 0.5	5.95 ± 0.4	0.65 ± .04	15.4 ± 0.1
6	2	4.51 ± 0.4	2.34 ± 0.2	2.17 ± 0.2	0.26 ± .01	38.5 ± 2.4
	4	4.95 ± 0.4	2.60 ± 0.2	2.35 ± 0.1	0.28 ± .01	35.7 ± 1.6
	6	5.23 ± 0.9	2.8 ± 0.5	2.43 ± 0.4	0.29 ± .03	34.5 ± 3
	8	5.83 ± 0.2	3.34 ± 0.4	2.49 ± 0.2	0.32 ± .01	31.2 ± 1.7
	12	6.84 ± 0.9	3.6 ± 0.6	3.24 ± 0.8	0.34 ± .07	29.4 ± 0.1
6S	2	5.88 ± 0.8	3.15 ± 0.3	2.73 ± 0.3	0.32 ± .04	31.2 ± 1.8
	4	6.5 ± 0.9	3.18 ± 0.5	3.32 ± 0.7	0.37 ± .03	27 ± 2.9
	6	7.3 ± 0.9	4.04 ± 0.5	3.26 ± 0.4	0.39 ± .02	25.6 ± 1.7
	8	8.3 ± 0.6	4.97 ± 0.3	3.33 ± 0.3	0.36 ± .01	27.7 ± 0.7
	12	17.1 ± 0.5	11.6 ± 0.5	5.46 ± 0.1	0.62 ± .02	16.1 ± 0.1
7	2	2.6 ± 0.1	1.21 ± .01	1.39 ± 0.1	0.22 ± .01	45.5 ± 1.6
	4	4.16 ± 0.3	2.09 ± 0.2	2.07 ± 0.1	0.25 ± .01	40 ± 1.2
	6	4.66 ± 0.4	2.42 ± 0.3	2.24 ± 0.1	0.27 ±.01	37 ± 2.2
	8	5.09 ± 0.8	2.76 ± 0.5	2.33 ± 0.4	0.26 ± .01	38.5 ± 0.6
	12	6.18 ± 0.8	3.44 ± 0.4	2.74 ± 0.8	0.33 ± .02	30.3 ± 2
7S	2	4.58 ± 0.9	2.38 ± 0.4	2.20 ± 0.5	0.26 ± .02	38.5 ± 4
	4	5.04 ± 0. 9	2.63 ± 0.4	2.68 ± 0.6	0.30 ± .02	33.3 ± 3
	6	5.84 ± 0.4	3.25 ± 0.3	2.59 ± 0.2	0.32 ± .02	31.2 ± 2.7
	8	6.31 ± 0.8	3.56 ± 0.5	2.75 ± 0.3	0.33 ± .024	30.3 ± 3
	12	9.95 ± 0.8	5.65 ± 0.4	4.3 ± 0.4	0.45 ± .04	22.2 ± 0.1

*S: Sr-modified; see table 6 for alloy Fe-Mn levels

Table 11 Charpy impact properties of 319 alloys containing different levels of Fe and Mn, in the as-cast and solution heat-treated conditions

Alloy Code	Alloy Condition	E_T (J)	E_I (J)	E_p (J)	Time to Failure (ms)	ACS (mm/ms))
22*	A*	4.06 ± 0.4	2.18 ± 0.3	1.88 ± 0.1	0.32 ± .02	30 ± 2.8
(0.2Fe)	B*	6.14 ± 0.1	3.21 ± 0.1	2.93 ± 0.1	34.4 ± .01	0.29 ± 0.5
8	A	4 ± 0.2	2.1 ± 0.2	1.99 ± 0.1	0.27 ± .01	37 ± 1.8
(0.37Fe)	B	5.12 ± 0.2	2.92 ± 0.5	2.20 ± 0.2	0.29 ± .01	34.5 ± 2.8
9	A	3.32 ± 0.2	1.75 ± 0.2	1.57 ± 0.2	0.26 ± .01	38.5 ± 2
(0.64Fe)	B	4.56 ± 0.2	2.27 ± 0.2	2.29 ± 0.1	0.27 ± .01	37 ± 1.2
10	A	2.4 ± 0.5	1.3 ± 0.3	1.1 ± 0.2	0.24 ± .05	41.6 ± 2
(1.0Fe)	B	3.96 ± 0.3	1.99 ± 0.4	1.97 ± 0.3	0.27 ± .02	37 ± 3
22S*	A	4.29 ± 0.3	2.23 ± 0.2	1.06 ± 0.2	0.32 ± .02	27 ± 2
(0.2Fe)	B	7.23 ± 0.4	4.03 ± 0.7	3.2 ± 0.4	0.33 ± .02	29.8 ± 2
8S	A	4.37 ± 0.4	3.0 ± 0.2	1.37 ± 0.2	0.29 ± .01	34.5 ± 0.7
(0.38Fe)	B	5.67 ± 0.4	2.76 ± 0.1	1.91 ± 0.3	0.30 ± .01	33.3 ± 1.5
9S	A	3.6 ± 0.2	1.74 ± 0.1	1.86 ± 0.1	0.26 ± .01	38.5 ± 2.8
(0.64Fe)	B	5.02 ± 0.1	2.77 ± 0.1	1.25 ± 0.1	0.31 ± .01	32.2 ± 2.2
10S	A	2.97 ± 0.2	1.51 ± 0.2	1.46 ± 0.3	0.26 ± .05	38.5 ± 3
(1.0Fe)	B	4.22 ± 0.3	2.06 ± 0.3	2.16 ± 0.3	0.27 ± .01	37 ± 1.5
11	A	4.08 ± 0.1	2.10 ± 0.1	1.98 ± 0.3	0.27 ± .01	37 ± 1.9
(0.4Fe-0.1Mn)	B	5.17 ± 0.2	2.71 ± 0.1	2.46 ± 0.1	0.28 ± .01	35.7 ± 0.9
12	A	3.84 ± 0.3	2.30 ± 0.2	1.54 ± 0.2	0.28 ± .01	35.7 ± 1.8
(0.6Fe-0.2Mn)	B	5.16 ± 0.3	2.91± 0.1	2.25 ± 0.2	0.30 ± .01	33.3 ± 1.5
13	A	3.4 ± 0.5	1.75 ± 0.3	1.65 ± 0.2	0.26 ± .01	38.5 ± 1.7
(1.0Fe-0.4Mn)	B	4.23 ± 0.5	2.28 ± 0.3	1.95 ± 0.2	0.27 ± .02	37 ± 2.9
11S	A	4.25 ± 0.7	2.45 ± 0.4	1.80 ± 0.2	0.27 ± .03	37 ± 2
(0.4Fe-0.1Mn)	B	6.62 ± 0.5	3.81 ± 0.4	2.81 ± 0.1	0.36 ± .02	27.7 ± 2
12S	A	4.08 ± 0.5	2.08± 0.3	2 ± 0.3	0.27 ± .01	37 ±2.3
(0.6Fe-0.2Mn)	B	6.40 ± 0.7	3.5± 0.7	2.9 ± 0.3	0.33 ± .03	30.3 ±3
13S	A	3.57 ± 0.2	1.86 ± 0.2	1.71 ± 0.1	0.26 ± .01	38.5 ± 1.4
(1.0Fe-0.4Mn)	B	5.01 ± 0.5	2.6 ± 0.3	2.41 ± 0.2	0.28 ± .01	35.7 ± 1.8

*22: Base 319 alloy; A: as-cast; B: solution heat-treated; and S: Sr-modified

Table 12 Charpy impact properties of 319 alloys containing various levels of Fe, and aged at 180°C for different times

Alloy Code	Aging Time (h)	E_T (J)	E_I (J)	E_p (J)	Time to Failure (ms)	ACS (mm/ms)
22*	2	6.63 ± 0.6	3.72 ± 0.3	2.91 ± 0.3	0.33 ± .01	30.3 ± 1.5
	4	4.97 ± 0.4	2.89 ± 0.2	2.08 ± 0.4	0.30 ± .02	33.3 ± 3
	6	4.64 ± 0.9	2.65 ± 0.9	1.99 ± 0.6	0.26 ± .01	38.5 ± 2.7
	8	6.01 ± 0.5	3.27 ± 0.3	2.74 ± 0.2	0.31 ± .01	32.2 ± 1.6
	12	10.37 ± 0.3	6.63 ± 0.3	3.74 ± 0.1	0.43 ± .07	23.3 ± 2
22S*	2	9.5 ± 0.8	5.86 ± 0.9	3.64 ±0.3	0.40 ± .02	25 ± 1.9
	4	5.56 ± 0.9	2.87 ± 0.7	2.69 ±0.6	0.32 ± .02	31.2 ± 2
	6	5.81 ± 0.8	3.1 ± 0.9	2.71 ±0.4	0.35 ± .02	28.6 ± 1.8
	8	5.0 ± 0.5	2.54 ± 0.2	2.46 ±0.2	0.30 ± .01	33.3 ± 1.5
	12	11.8 ± 0.7	7.5 ± 0.7	4.3 ±0.2	0.49 ± .01	20.4 ± 2.1
8	2	5.69 ± 0.4	3.07 ± 0.3	2.62 ± 0.1	0.29 ± .01	34.5 ± 1.1
	4	4.32 ± 0.3	2.26 ± 0.2	2.06 ± 0.1	0.28 ± .01	35.7 ± 1.1
	6	4.95 ± 0.5	2.59 ± 0.3	2.36 ± 0.2	0.28 ± .01	35.7 ± 1.8
	8	4.63 ± 0.6	2.45 ± 0.4	2.18 ± 0.2	0.27 ± .01	37 ± 1.5
	12	6.40 ± 0.2	3.78 ± 0.1	2.62 ± 0.5	0.39 ± .03	25.6 ± 2.1
8S	2	5.9 ± 0.4	3.06 ±0.3	2.84 ± 0.2	0.30 ± .01	33.3 ± 1
	4	4.64 ± 0.3	2.15 ± 0.2	2.49 ± 0.2	0.28± .01	35.7 ± 0.9
	6	5.19 ± 0.6	2.66 ± 0.4	2.53 ± 0.2	0.29 ± .02	34.5 ± 1.1
	8	4.62 ± 0.5	2.44 ± 0.7	2.18 ±0.5	0.29 ± .01	34.5 ± 1.5
	12	9.98 ± 0.4	5.68 ± 0.7	3.3 ± 0.1	0.42 ± .01	23.8 ± 1.1
9	2	3.8 ± .01	1.92 ± 0.1	1.88 ± 0.1	0.26± .01	38.5 ± 1.6
	4	3.68 ±.052	1.89 ± 0.3	1.79 ± 0.3	0.27± .01	37 ± 2
	6	4.36 ±.06	2.23 ± 0.4	2.13 ± 0.3	0.27± .01	37 ± 1.9
	8	4.23 ± 0.4	2.18 ± 0.3	2.05 ± 0.2	0.3±.04	33.3 ± 2
	12	5.82 ± 0.4	3.06 ± 0.2	2.76 ± 0.2	0.33±.01	30.3 ±1.3
9S	2	5.71 ± 0.7	2.98 ± 0.5	2.73 ± 0.2	0.30 ± .02	33.3 ± 2
	4	4.04 ± 0.6	2.2 ± 0.3	1.84 ± 0.7	0.28 ± .01	35.7 ± 1.7
	6	4.23 ± 0.6	2.15 ± 0.4	2.08 ± 0.3	0.27 ± .01	37 ± 2
	8	4.44 ± 0.5	2.3 ± 0.4	2.14 ± 0.2	0.29 ± .03	34.5 ± 3
	12	6.61 ± 0.5	3.6 ± 0.1	3.01 ± 0.2	0.30 ± .01	33.3 ± 1.3
10	2	3.13 ± 0.3	1.49 ± 0.2	1.64 ± 0.2	0.24 ± .01	41.6 ± 0.9
	4	2.67 ± 0.5	1.26 ± 0.3	1.41 ± 0.2	0.23 ± .01	43.5 ± 2
	6	2.9 ± 0.4	1.43 ± 0.2	1.47 ± 0.2	0.23 ± .01	43.5 ± 1.6
	8	3.35 ± 0.3	1.7 ± 0.2	1.65 ± 0.1	0.24 ± .01	41.6 ± 1
	12	3.91 ± 0.4	1.96 ± 0.3	1.95 ± 0.2	0.28 ± .01	35.7 ± 1.5
10S	2	4.54 ± 0.5	2.27 ± 0.3	2.27 ± 0.2	0.28 ± .01	35.7 ± 2.1
	4	3.32 ± 0.3	1.59 ± 0.2	1.73 ± 0.2	0.25 ± .01	40 ± 1.2
	6	3.92 ± 0.5	2.0 ± 0.3	1.92 ± 0.3	0.27 ± .01	37 ± 1.9
	8	4.18 ± 0.9	2.19 ± 0.6	1.99 ± 0.4	0.32 ± .04	31.2 ± 3
	12	6.24 ± 0.7	3.35 ± 0.3	2.89 ± 0.3	0.34 ± .02	29.4 ± 2

Table 13 Charpy impact properties of 319 alloys containing various levels of Fe additions, and aged at 220°C for different times

Alloy Code	Aging Time (h)	E_T (J)	E_I (J)	E_p (J)	Time to Failure (ms)	ACS (mm/ms)
22*	2	8.96 ± 0.5	5.48 ± 0.3	3.48 ± 0.2	0.37 ± .01	27 ± 1.2
	4	6.28 ± 0.7	3.5 ± 0.6	2.78 ± 0.1	0.33 ± .01	30 ± 1.3
	6	6.02 ± 0.4	3.18 ± 0.3	2.84 ± 0.3	0.32 ± .02	31 ± 2.7
	8	5.5 ± 0.5	2.9 ± 0.3	2.60 ± 0.2	0.29 ± .01	34.5 ± 1.7
	12	7.13 ± 0.9	4.25 ± 0.5	2.88 ± 0.4	0.37 ± .02	27 ± 1.5
22S*	2	9.11 ± 0.4	5.26 ± 0.2	3.85 ± 0.2	0.44 ± .01	22.7 ± 0.8
	4	8.20 ± 0.5	4.9 ± 0.3	3.3 ± 0.2	0.37 ± .01	27 ± 1.6
	6	5.67 ± 0.5	3.11 ± 0.6	3.56 ± 0.2	0.32 ± .01	31 ± 1.9
	8	5.76 ± 0.7	3.04 ± 0.4	2.72 ± 0.3	0.30 ±.01	33 ± 2
	12	7.65 ± 0.9	4.23 ± 0.8	3.42 ± 0.6	0.37 ±.01	27 ± 1.7
8	2	4.94 ± 0.1	2.5 ± 0.1	2.45 ± 0.1	0.27 ± .01	37 ± 0.5
	4	4.38 ± 0.4	2.26 ± 0.3	2.12 ± 0.2	0.26 ± .01	38.5 ± 1.8
	6	4.06 ± 0.3	2.06 ± 0.2	2 ± 0.7	0.26 ± .01	38.5 ± 0.8
	8	4.73 ± 0.3	2.48 ± 0.2	2.25 ± 0.1	0.30 ± .02	33 ± 2
	12	5.32 ± 0.3	2.85 ± 0.1	2.47 ± 0.1	0.29 ± .01	34.5 ±0.9
8S	2	7.36 ± 0.9	3.98 ± 0.7	3.37 ± 0.2	0.33 ± .01	30 ± 1.5
	4	5.22 ± 0.4	2.26 ± 0.2	2.96 ± 0.4	0.30 ± .01	33 ± 1.2
	6	4.8 ± 0.3	2.57 ± 0.2	2.23 ± 0.1	0.29 ± .01	34.5 ± 1
	8	5.18 ± 0.1	2.48 ± 0.2	2.7 ± 0.1	0.31 ± .01	32 ± 0.3
	12	5.38 ± 0.2	2.91 ± 0.1	2.47 ± 0.2	0.34 ± .01	29 ± 2
9	2	3.55 ± 0.6	1.78 ± 0.3	1.77 ± 0.3	0.26 ± .01	38.5 ± 2.5
	4	3.68 ± 0.6	1.81 ± 0.3	1.87 ± 0.3	0.25 ± .01	40 ± 1.7
	6	3.61 ± 0.2	1.86 ± 0.1	1.75 ± .01	0.25 ± .01	40 ± 1.4
	8	3.41 ± 0.3	1.68 ± 0.2	1.73 ± 0.2	0.24 ± .01	41.6 ± 1.6
	12	5.35 ± 0.5	2.88 ± 0.2	2.47 ± 0.2	0.29 ± .01	34.5 ± 1.1
9S	2	3.80 ± 0.1	1.96 ± 0.1	1.84 ± 0.1	0.26 ± .01	38.5 ± 0.6
	4	3.94 ± 0.7	1.91 ± 0.6	2.03 ± 0.2	0.26 ± .02	38.5 ± 0.9
	6	4.46 ± 0.2	2.34 ± 0.2	2.12 ± 0.1	0.28 ± .01	35.7 ± 0.8
	8	3.97 ± 0.1	1.89 ± 0.1	2.08 ± 0.1	0.27 ± .02	37 ± 1.4
	12	5.14 ± 0.4	2.72 ± 0.2	2.42 ± 0.2	0.28 ± .09	35.7 ± 0.7
10	2	3.07 ± 0.4	1.54 ± 0.2	1.53 ± 0.2	0.24 ± .01	41.6 ± 1.8
	4	2.89 ± 0.3	1.45 ± 0.2	1.44 ± 0.2	0.24 ± .01	41.6 ± 2.6
	6	2.77 ± 0.4	1.38 ± 0.2	1.39 ± 0.2	0.23 ± .01	43.5 ± 2
	8	2.48 ± 0.4	1.22 ± 0.2	1.26 ± 0.2	0.22 ± .01	45.5 ± 2.4
	12	4.35 ± 0.4	2.28 ± 0.2	2.07 ±0.2	0.28 ± .01	35.7 ± 1
10S	2	3.51 ± 0.5	1.73 ± 0.3	1.78 ± 0.2	0.25 ± .01	40 ± 2.1
	4	3.7 ± 0.2	1.84 ± 0.1	1.86 ± 0.1	0.25 ± .01	40 ± 2.6
	6	3.13 ± 0.1	1.58 ± 0.1	1.55 ± 0.1	0.25 ± .01	40 ± 2
	8	3.43 ± 0.3	1.75 ± 0.2	1.69 ± 0.2	0.25 ± .01	40 ± 1.3
	12	4.46 ± 0.3	2.27 ± 0.2	2.19 ± 0.1	0.29 ± .01	34.5 ± 1.8

*22: 319 base alloys; S: Sr-modified; see table 11 for alloy Fe levels

Table 14 Charpy impact energy properties of 319 alloys containing various levels of Fe-Mn additions, and aged at 180°C for different times

Alloy Code	Aging Time (h)	E_T (J)	E_I (J)	E_p (J)	Time to Failure (ms)	ACS (mm/ms)
11	2	5.53 ± 0.6	3.0 ± 0.3	2.53 ± 0.2	0.29 ± .01	34.5 ± 1.8
	4	4.91 ± 0.3	2.67 ± 0.2	2.24 ± 0.1	0.30 ± .02	33.3 ± 2
	6	4.92 ± 0.2	2.71 ± 0.1	2.21 ± 0.1	0.29 ± .01	34.5 ± 0.8
	8	3.97 ± 0.3	1.99 ± 0.2	1.98 ± 0.2	0.27 ± .01	37.0 ± 2
	12	6.6 ± 0.2	3.72 ± 0.1	2.88 ± 0.1	0.34 ± .01	29.4 ± 0.8
11S*	2	8.5 ± 0.9	4.98 ± 0.5	3.52 ± 0.4	0.39 ± .02	25.6 ± 1.4
	4	4.46 ± 0.9	2.33 ± 0.6	2.13 ± 0.3	0.29 ± .01	34.5 ± 1.4
	6	5.5 ± 0.9	2.9 ± 0.8	2.6 ± 0.6	0.33 ± .04	30.3 ± 2
	8	5.16 ± 0.9	2.69 ± 0.6	2.47 ± 0.5	0.32 ± .01	31.2 ± 2.5
	12	7.34 ± 0.5	3.96 ± 0.4	3.38 ± 0.2	0.38 ± .01	26.3 ± 0.9
12	2	6.49 ± 0.6	3.69 ± 0.4	2.80 ± 0.3	0.32 ± .02	31.2 ± 2.3
	4	4.14 ± 0.7	2.09 ± 0.7	2.05 ± 0.3	0.27 ± .02	37.0 ± 2
	6	4.56 ± 0.9	2.37 ± 0.6	2.19 ±0.4	0.30 ± .03	33.3 ± 2.1
	8	4.47 ± 0.8	2.34 ± 0.3	2.13 ± 0.3	0.30 ± .02	33.3 ± 2.5
	12	6.75 ± 0.6	3.82 ± 0.4	2.93 ± 0.3	0.35 ± .03	28.6 ± 0.6
12S	2	7.34 ± 0.8	3.98 ± 0.5	3.35 ± 0.3	0.35 ± .03	28.6 ± 1.9
	4	5.09 ± 0.7	2.66 ± 0.3	2.43 ± 0.3	0.30 ± .02	33.3 ± 2
	6	6.41 ± 0.9	3.44 ± 0.6	2.97 ± 0.4	0.32 ± .02	31.2 ± 1.9
	8	3.95 ± 0.8	2.2 ± 0.5	1.75 ± 0.3	0.30 ± .02	33.3 ± 2
	12	6.72 ± 0.6	3.58 ± 0.3	3.14 ± 0.3	0.36 ± .02	27.7 ± 2.4
13	2	5.15 ± 0.2	2.75 ± 0.1	2.40 ± 0.1	0.29 ± .01	34.5 ± 0.9
	4	4.48 ± 0.6	2.34 ± 0.4	2.14 ±0.2	0.28 ± .01	35.7 ± 1.8
	6	4.92 ± 0.4	2.65 ± 0.3	2.27 ± 0.1	0.30 ± .01	33.3 ± 1.5
	8	4.68 ± 0.8	2.45 ± 0.4	2.23 ± 0.4	0.29 ± .02	34.5 ± 2.5
	12	6.43 ± 0.7	3.54 ± 0.3	2.89 ± 0.3	0.34 ± .02	29.4 ± 1.8
13S	2	6.16 ± 0.9	3.50 ± 0.5	2.66 ± 0.4	0.34 ± .01	29.4 ± 1.4
	4	4.82 ± 0.4	2.63 ± 0.2	2.19 ± 0.3	0.30 ± .02	33.3 ± 2.3
	6	5.47 ± 0.7	2.92 ± 0.4	2.55 ± 0.3	0.31 ± .02	32.2 ± 2.4
	8	5.0 ± 0.9	2.68 ± 0.6	2.32 ± 0.4	0.31 ± .04	32.2 ± 2
	12	7.49 ± 0.9	4.33 ± 0.8	3.16 ± 0.4	0.40 ± .03	25 ± 2.6

S: Sr-modified; see table 11 for alloy Fe-Mn levels

Table 15 Charpy impact properties of 319 alloys containing various levels of Fe-Mn additions, and aged at 220°C for different times

Alloy Code	Aging Time (h)	E_T (J)	E_I (J)	E_p (J)	Time to Failure (ms)	ACS (mm/ms)
11	2	6 ± 0.5	3.18 ± 0.26	2.82 ± 0.24	0.30 ±.01	33 ± 1.1
	4	5.05 ± 0.34	2.69 ± 0.24	2.36 ± 0.15	0.27 ±.01	37 ± 1.4
	6	4.02 ± 0.24	2.09 ± 0.17	1.93 ±0.1	0.26 ± .01	38.5 ± 1.8
	8	3.79 ± 0.38	1.91 ± 0.2	1.88 ± 0.18	0.25 ± .007	40 ± 1.1
	12	4.96 ± 0.9	2.37 ± 0.54	2.17 ± 0.4	0.27 ± .02	37 ± 2.7
11S*	2	8.5 ± 0.75	4.98 ± 0.5	3.52 ± 0.3	0.34 ± .02	29 ± 1.8
	4	5.48 ± 0.84	2.77 ± 0.42	2.71 ± 0.5	0.33 ± .02	30 ± 2.7
	6	5.09 ± 0.86	2.76 ± 0.64	2.33 ± 0.7	0.30 ± .03	33 ± 1.8
	8	5.17 ± 0.42	2.69 ± 0.17	2.48 ± 0.28	0.29 ± .01	34.5 ± 1.2
	12	7.34 ± 0.25	3.96 ± 0.47	3.38 ± 0.17	0.43 ± .02	23 ± 1.1
12	2	4.86 ± 0.73	2.54 ± 0.42	2.32 ± 0.3	0.28 ± .02	35.7 ± 1.8
	4	4.17 ± 0.37	2.17 ± 0.26	2 ± 0.12	0.27 ± .02	37 ± 2.7
	6	3.88 ± 0.56	2.01 ± 0.35	1.87 ± 0.23	0.26 ± .03	38.5 ± 2
	8	3.89 ± 0.89	1.99 ± 0.45	1.90 ± 0.6	0.27 ± .03	37 ± 1.8
	12	6.63 ± 0.59	3.88 ± 0.34	3.18 ± 0.27	0.34 ± .02	29 ± 2.1
12S	2	7.34 ± 0.48	3.98 ± 0.2	3.36 ± 0.27	0.31 ± .01	32 ± 1.1
	4	5.09 ± 0.45	2.66 ± 0.27	2.43 ± 0.18	0.28 ± .005	35.7 ± 0.6
	6	4.17 ± 0.25	2.15 ± 0.11	2.02 ±0.15	0.27 ± .01	37 ± 1.7
	8	4.19 ± 0.38	2.1 ± 0.23	2.09 ± 0.17	0.27 ± .01	37 ± 2.2
	12	6.72 ± 0.64	3.58 ± 0.24	3.14 ± 0.4	0.35 ± .02	28.7 ± 2.5
13	2	5.2 ± 0.1	2.75 ± 0.05	2.45 ± .02	0.28 ± .01	35.7 ± 0.9
	4	4.17 ± 0.53	2.19 ± 0.33	1.98 ± 0.2	0.27 ± 0.1	37 ± 2.4
	6	4.07 ±0.6	2.19 ± 0.44	1.88 ± 0.2	0.29 ± .06	34.5 ± 2
	8	4.23 ± 0.17	2.19 ± 0.10	2.04 ± 0.1	0.26 ±. 003	38.5 ± 0.5
	12	6.02 ± 0.45	3.60 ± 0.31	2.96 ± 0.2	0.33 ± .01	30 ± 1.3
13S	2	6.16 ± 0.8	3.5 ± 0.5	2.66 ± 0.35	0.31 ± .02	32.2 ± 2
	4	4.82 ± 0.46	2.63 ± 0.29	2.19 ± 0.2	0.26 ± .03	38.5 ± 0.9
	6	4.38 ± 0.4	2.45 ± 0.28	1.93 ± 0.2	0.29 ± .04	34.5 ± 2
	8	4.68 ± 0.75	2.48 ± 0.43	2.2 ± 0.3	0.28 ± .01	35.7 ± 2
	12	7.5 ± 0.72	4.33 ± 0.35	3.17 ± 0.3	0.30 ± .02	33.3 ± 2.7

S: Sr-modified; see table 11 for alloy Fe-Mn levels

Table 16 Charpy impact properties of 319 alloys containing different levels of Fe, Mn, and Mg, in the as-cast and solution heat-treated conditions

Alloy Code	Alloy Condition	E_T (J)	E_I (J)	E_p (J)	Time to Failure (ms)	ACS (mm/ms)
14	A*	2.83 ± 0.3	1.45 ± 0.2	1.38 ± 0.1	0.24 ± .01	41.6 ± 2
(0.2Fe-0.1Mg)	B*	4.0 ± 0.3	2.08 ± 0.2	1.92 ± 0.1	0.27 ± .01	37 ± 2.5
16	A	2.28 ± 0.1	1.51 ± 0.1	1.39 ± 0.1	0.26 ± .02	38.5 ± 2
(0.2Fe-0.3Mg)	B	3.98 ± 0.3	1.98 ± 0.2	2 ± 0.1	0.26 ± .01	38.5 ± 2.
15	A	2.42 ± 0.3	1.16±0.2	1.26 ± 0.1	0.24 ±.02	41.6 ± 3
(0.8Fe-0.1Mg)	B	3.03 ± 0.5	1.98±0.4	2.2 ± 0.4	0.25 ±.01	40 ± 2.9
17	A	2.22 ± 0.3	1.05 ± 0.1	1.17 ± 0.1	0.22 ± .05	45.4 ± 1
(0.8Fe-0.3Mg)	B	2.63 ± 0.2	1.2 ± 0.1	1.43 ± 0.1	0.22 ± .01	45.4 ± 1
18	A	3.83 ± 0.3	1.93 ± 0.2	1.9 ± 0.1	0.26 ±.01	38.5 2.6±
(0.2Fe-0.1Mn0.1Mg)	B	3.97 ± 0.3	1.89 ± 0.2	1.98 ± 0.1	0.25 ± .01	40 ±1.3
20	A	3.1 ± 0.6	1.23 ± 0.3	1.48 ± 0.3	0.22 ± .01	45.4 ± 1
(0.2Fe-0.1Mn0.3Mg)	B	3.82 ± 0.7	2.03 ± 0.6	1.99 ± 0.6	0.26 ± .02	38.5 ± 2
19	A	3.58 ± 0.4	1.71 ±0.2	1.87 ± 0.2	0.25 ± .01	40 ± 1.2
(0.8Fe-0.4Mn0.1Mg)	B	4.16 ± 0.6	1.96 ±0.6	2.20 ± 0.4	0.24 ± .01	41.6 ± 2
21	A	2.56 ± 0.4	1.23 ±0.2	1.33 ±0.2	0.22 ± .01	45.4 ± 2
(0.8Fe-0.4Mn0.3Mg)	B	3 ± 0.1	1.4 ± 0.4	1.6 ± 0.1	0.25 ± .01	40 ± 2.1
14S	A	3.11 ± 0.1	1.45 ±0.2	1.38 ± 0.4	0.24 ± .02	41.6 ± 2
(0.2Fe-0.1Mg)	B	4.95 ± 0.4	2.50 ±0.1	2.45 ± 0.2	0.27 ± .05	37 ± 0.8
16S	A	2.9 ± 0.1	1.11 ± 0.4	1.17 ± 0.1	0.22 ± .01	45.4 ± 1
(0.2Fe-0.3Mg)	B	4.71 ± 0.6	2.38 ± 0.2	2.33 ± 0.2	0.27 ± .01	37 ± 2.4
15S	A	2.7 ± 0.2	1.34 ± 0.1	1.36 ± 0.1	0.25 ± .04	40 ± 2
(0.8Fe-0.1Mg)	B	3.81 ± 0.5	1.87 ± 0.4	1.94 ± 0.2	0.28 ± .02	35.7 ± 3
17S	A	2.55 ± 0.3	1.28 ± 0.2	1.27 ± 0.1	0.23 ± .01	43.5 ±2.2
(0.8Fe-0.3Mg)	B	3.42 ± 0.3	1.67 ± 0.3	1.75 ± 0.1	0.24 ± .01	41.6 ±2
18S	A	4.15 ± 0.4	2.05 ± 0.1	2.1 ± 0.2	0.27 ± .01	37 ± 0.5
(0.2Fe-0.1Mn0.1Mg)	B	4.2 ± 0.2	2.07 ± 0.2	2.13 ± 0.1	0.25 ± .01	40 ± 1
20S	A	3.8 ± 0.2	1.21 ± 0.2	1.29 ± 0.1	0.24 ± .01	41.6 ± 3
(0.2Fe-0.1Mn0.3Mg)	B	4.3 ± 0.2	1.75 ± 0.1	1.75 ± 0.2	0.23 ± .01	43.5 ± 1
19S	A	3.38 ± 0.1	1.8 ± 0.1	1.85 ± 0.1	0.26 ± .01	38.5 ± 1
(0.8Fe-0.4Mn0.1Mg)	B	4.15 ± 0.5	2.76 ± 0.3	2.64 ± 0.2	0.28 ± .01	35.7 ±1
21S	A	2.91 ± 0.3	1.40 ± 0.1	1.51 ± 0.1	0.24 ± .01	41.6 ± 2
(0.8Fe-0.4Mn0.3Mg)	B	4.13 ±0.7	1.9 ± 0.3	2.23 ± 0.4	0.25 ± .01	40 ± 2.6

*A: as-cast; B: solution heat-treated; and S: Sr-modified.

Table 17 Charpy impact properties of 319 alloys containing various levels of Fe-Mg content, and aged at 180°C for different times

Alloy Code	Aging Time (h)	E_T (J)	E_I (J)	E_p (J)	Time to Failure (ms)	ACS (mm/ms)
14	2	3.63 ± 0.5	1.78 ±0.3	1.85± 0.2	0.26±.01	38.5 ±1.3
	4	2.27 ± 0.2	1.04 ±0.1	1.23±0.1	0.20±.01	50 ±2.2
	6	2.3 ±0.4	1.09±0.2	1.21±0.2	0.21±.01	47.6 ±1.8
	8	2.29 ±0.2	1.06±0.1	1.23±0.1	0.22±.01	45.5±1.7
	12	3.15 ± 0.1	1.52±0.1	1.63±0.1	0.22±.01	45.5±1.2
14S	2	4.42 ± 0.6	2.23 ± 0.4	2.19 ± 0.2	0.27 ± .03	37 ± 4
	4	3.67 ± 0.8	1.75 ± 0.4	1.92 ± 0.4	0.26 ± .02	38.5 ± 4
	6	3.3 ± 0.7	1.57 ± 0.3	1.73 ± 0.3	0.24 ± .01	41.6 ± 2.8
	8	3.18 ± 0.2	1.47 ± 0.1	1.71 ± 0.2	0.23 ± .01	43.5 ± 2.7
	12	4.08 ± 0.3	2.01 ± 0.2	2.07 ± 0.1	0.25 ± .01	40 ± 2.8
16	2	3.19 ± 0.2	1.53 ± 0.2	1.66 ± 0.1	0.24 ± .01	41.6 ± 2.4
	4	2.49 ± 0.2	1.19 ± 0.1	1.3 ± 0.1	0.21 ± .01	47.6 ± 0.3
	6	2.33 ± 0.3	1.16 ± 0.2	1.17 ± 0.2	0.22 ± .01	45.5 ± 2.2
	8	2.26 ± 0.3	1.08 ± 0.1	1.18 ± 0.2	0.21 ± .01	47.6 ± 1.6
	12	3.14 ± 0.1	1.5 ± 0.1	1.64 ± 0.1	0.22 ± .01	45.5 ± 0.4
16S	2	4.09 ± 0.5	1.98 ± 0.2	2.11 ± 0.3	0.26 ± .03	38.5 ± 2.5
	4	2.63 ± 0.3	1.1 ± 0.2	1.53 ± 0.1	0.22 ± .01	45.5 ± 1.2
	6	2.47 ± 0.2	1.32 ± 0.1	1.15 ± 0.1	0.24 ± .01	41.6 ± 1.8
	8	2.31 ± 0.3	1.02 ± 0.1	1.29 ± 0.2	0.20 ± .01	50 ± 2.3
	12	3.81 ± 0.2	1.8 ± 10.2	2.0 ± 0.1	0.23 ± .01	43.5 ± 1.2
15	2	2.39 ± 0.3	1.15 ± 0.1	1.24 ± 0.2	0.24 ± .01	41.6 ± 3
	4	1.91 ± 0.1	0.9 ± 0.1	1.01 ± 0.1	0.20 ± .01	50 ± 0.8
	6	2.31 ± 0.1	1.09 ± 0.1	1.22 ± 0.1	0.21 ± .01	47.6 ± 1.3
	8	2.06 ± 0.6	0.88 ± 0.4	1.18 ± 0.3	0.21 ± .01	47.6 ± 1.9
	12	2.45 ± 0.1	1.17 ± 0.1	1.28 ± 0.1	0.21 ± .01	47.6 ± 2.5
15S	2	3.43 ± 0.4	1.64 ± 0.2	1.79 ± 0.2	0.24 ± .01	41.6 ± 1.8
	4	2.7 ± 0.3	1.3 ± 0.1	1.4 ± 0.2	0.23 ± .02	43.5 ± 2.1
	6	2.6 ± 0.3	1.22 ± 0.2	1.38 ± 0.2	0.22 ± .01	45.5 ± 1
	8	2.06 ± 0.2	0.87 ± 0.1	1.19 ± 0.2	0.21 ± .01	47.6 ± 2.4
	12	2.6 ± 0.1	1.17 ± 0.1	1.43 ± 0.1	0.21 ± .01	47.6 ± 1
17	2	2.11±0.1	0.97 ± 0.1	1.14 ± 0.1	0.21± .01	47.6 ± 0.2
	4	2.2±0.3	1.0 ± 0.1	1.2 ± 0.2	0.23 ± .02	43.5 ± 3.2
	6	2.23±0.4	1.05 ± 0.2	1.18 ± 0.2	0.21 ± .01	47.6 ± 2.3
	8	1.91±0.2	0.86 ± 0.1	1.05 ± 0.1	0.21 ± .01	47.6 ± 2.6
	12	2.17±0.1	1.0 ± 0.1	1.17 ± 0.1	0.21 ± .01	47.6 ± 2
17S	2	3.18 ± 0.2	1.50 ± 0.2	1.68 ± 0.1	0.23 ± .01	43.5 ± 3
	4	2.13 ± 0.4	1.01 ± 0.2	1.12 ± 0.2	0.21 ± .01	47.6 ± 0.7
	6	2.25 ± 0.3	1.05 ± 0.1	1.2 ± 0.1	0.22 ± .01	45.5 ± 0.8
	8	2.27 ± 0.1	1.08 ± 0.1	1.19 ± 0.1	0.21 ± .01	47.6 ± 1.9
	12	2.49 ± 0.2	1.23 ± 0.1	1.26 ± 0.1	0.21 ± .01	47.6 ± 1.6

Table 18 Charpy impact properties of 319 alloys containing various levels of Fe-Mg content, and aged at 220°C for different times

Alloy Code	Aging Time (h)	E_T (J)	E_I (J)	E_p (J)	Time to Failure (ms)	ACS (mm/ms)
14	2	2.87 ± 0.2	1.37 ± 0.1	1.50 ± 0.1	0.22 ± .01	45.5 ± 1.1
	4	2.74 ± 0.2	1.27 ± 0.2	1.47 ± 0.1	0.22 ± .01	45.5 ± 1.2
	6	2.40 ± 0.1	1.13 ± 0.1	1.27 ± 0.1	0.21± .01	47.6 ± 0.5
	8	3.2 ± 0.3	1.57 ± 0.2	1.63 ± 0.1	0.23 ± .01	43.5 ± 1
	12	3.5 ± 0.3	1.7 ± 0.2	1.8 ± 0.1	0.25 ± .01	40 ± 2.5
14S	2	4.2 ± 0.2	2.1 ± 0.1	2.1 ± 0.12	0.24 ± .01	41.6 ± 1.1
	4	3.57 ± 0.6	1.72 ± 0.4	1.85 ± 0.2	0.27 ± .01	37 ± 1.1
	6	3.04 ± 0.6	1.52 ± 0.3	1.52 ± 0.2	0.23 ± .01	43.5 ± 3
	8	3.19 ± 0.3	1.48 ± 0.1	1.71 ± 0 .2	0.25 ± .01	40 ± 1.9
	12	4.07 ± 0.3	1.92 ± 0.1	2.15 ± 0.2	0.26 ± .01	38.5 ± 1.5
16	2	2.41 ± 0.2	1.13 ± 0.1	1.28 ± 0.1	0.21 ± .01	47.6 ± 0.8
	4	2.4 ± 0.2	1.15 ± 0.1	1.25 ± 0.1	0.22 ± .01	45.5 ± 1
	6	2.25 ± 0.3	1.06 ± 0.1	1.19 ± 0.1	0.21 ± .01	47.6 ± 1.6
	8	2.81 ± 0.2	1.33 ± 0.1	1.48 ± 0.1	0.22 ± .01	45.5 ± 0.4
	12	2.89 ± 0.2	1.43 ± 0.1	1.46 ± 0.1	0.22 ± .01	45.5 ± 1.8
16S	2	3.05 ± 0.2	1.52 ± 0.1	1.53 ± 0.1	0.24 ± .01	41.6 ± 3.3
	4	2.45 ± 0.2	1.08 ± 0.1	1.37 ± 0.1	0.22 ± .01	45.5 ± 1.3
	6	2.61 ± 0.3	1.27 ± 0.2	1.34 ± 0.2	0.22 ± .01	45.5 ± 1.8
	8	3.10 ± 0.3	1.45 ± 0.2	1.65 ± 0.2	0.25 ± .01	40 ± 1.9
	12	2.84 ± 0.2	1.43 ± 0.2	1.41 ± 0.1	0.24 ± .01	41.6 ± 3
15	2	2.27 ± 0.6	1.09 ± 0.1	1.18 ± 0.1	0.22 ± .01	45.5 ± 3.3
	4	2.29 ± 0.3	1.10 ± 0.2	1.19 ± 0.2	0.22 ± .01	45.5 ± 1.8
	6	2.10 ± 0.2	1.02 ± 0.2	1.08 ± 0.1	0.21 ± .01	47.6 ± 2.7
	8	2.51 ± 0.4	1.18 ± 0.1	1.33 ± 0.1	0.22 ± .01	45.5 ± 3.7
	12	3.01 ± 0.3	1.51 ± 0.1	1.50 ± 0.1	0.23 ± .01	43.5 ± 1.6
15S	2	2.9 ± 0.2	1.4 ± 0.1	1.5 ± 0.1	0.20 ± .01	50 ± 1.5
	4	2.57 ± 0.4	1.22 ± 0.2	1.35 ± 0.2	0.25 ± .01	40 ±3
	6	2.73 ± 0.3	1.26 ± 0.2	1.47 ± 0.1	0.22 ±.01	45.5 ±1.8
	8	3 ± 0.2	1.57 ± 0.1	1.43 ± 0.1	0.21 ± .01	47.6 ±0.8
	12	3.36 ± 0.3	1.61 ± 0.1	1.75 ± 0.1	0.24 ± .01	41.6 ±1.5
17	2	2.2 ± 0.3	1.08 ± 0.2	1.12 ± 0.1	0.22 ± .01	45.5 ± 2.9
	4	2.03 ± 0.1	0.94 ± 0.1	1.99 ± 0.1	0.20 ± .01	50 ± 0.7
	6	1.77 ± 0.4	0.78 ± 0.2	0.99 ± 0.2	0.21 ± .01	47.6 ± 3.2
	8	2.3 ± 0.2	1.08 ± 0.1	1.22 ± 0.1	0.21 ± .01	47.6 ± 1.5
	12	2.73 ± 0.3	1.26 ± 0.1	1.47 ± 0.1	0.22 ± .01	45.5 ± 0.9
17S	2	2.29 ± 0.3	1.05 ± 0.2	1.24 ± 0.2	0.22 ± .01	45.5 ± 3.2
	4	1.91 ± 0.1	0.91 ± 0.1	1.00 ± 0.1	0.20 ± .01	50 ± 1
	6	1.89 ± 0.1	0.86 ± 0.1	1.03 ± 0.1	0.21 ± .01	47.6 ± 1.3
	8	2.44 ± 0.2	1.15 ± 0.1	1.29 ± 0.1	0.21 ± .01	47.6 ± 1
	12	2.75 ± 0.2	1.34 ±0.1	1.41 ± 0.1	0.21 ± .01	47.6 ± 0.9

Table 19 Charpy impact properties of 319 alloys containing different levels of combined Fe-Mn-Mg additions, and aged at 180°C for different times

Alloy Code	Aging Time (h)	E_T (J)	E_I (J)	E_p (J)	Time to Failure (ms)	ACS (mm/ms)
18	2	3.54 ± 0.2	1.75 ± 0.2	1.79 ± 0.2	0.24 ± .01	41.6 ± 2.5
	4	2.55 ± 0.1	1.19 ± 0.1	1.36 ± 0.1	0.21 ± .01	47.6 ± 0.3
	6	2.75 ± 0.2	1.32 ± 0.1	1.43 ± 0.1	0.22 ± .01	45.5 ± 1.7
	8	2.32 ± 0.2	1.1 ± 0.2	1.22 ± 0.2	0.22 ± .03	45.5 ± 2
	12	2.66 ± 0.2	1.29 ± 0.1	1.37 ± 0.3	0.24 ± .01	41.6 ± 2
18S	2	3.95 ± 0.3	1.95 ± 0.1	2.0 ± 0.2	0.24 ± .01	41.6±2.3
	4	3.4 ± 0.1	1.78 ± 0.1	1.62 ± 0.1	0.22 ± .01	45.5±1.9
	6	2.85 ± 0.3	1.35 ± 0.1	1.5 ± 0.2	0.23 ± .01	43.5±1.8
	8	2.71 ± 0.2	1.34 ± 0.1	1.37 ± 0.2	0.23 ± .01	43.5±1.5
	12	2.83 ± 0.3	1.35 ± 0.2	1.48 ± 0.2	0.22 ± .01	45.5±0.9
20	2	3.36 ± 0.2	1.63 ± 0.1	1.73 ± 0.1	0.24 ± .01	41.6 ± 1.8
	4	2.63 ± 0.2	1.27 ± 0.3	1.36 ± 0.3	0.21 ± .01	47.6 ± 2.8
	6	2.85 ± 0.1	1.27 ± 0.1	1.58 ± 0.2	0.23 ± .01	43.5 ± 2.9
	8	2.70 ± 0.3	1.3 ± 0.2	1.4 ± 0.1	0.22 ± .01	45.5 ± 1.8
	12	2.47 ± 0.3	1.15 ± 0.1	1.32 ± 0.1	0.21 ± .01	47.6 ± 1.4
20S	2	3.8 ± 0.2	2.1 ± 0.5	2.22 ± 0.2	0.25±.01	40±0.8
	4	2.92 ± 0.3	1.36 ± 0.3	1.56 ± 0.2	0.21±.01	47.6±1.3
	6	2.42 ± 0.2	1.09 ± 0.1	1.33 ± 0.1	0.23±.01	43.5±1.6
	8	2.4 ± 0.1	1.11 ± 0.2	1.29 ± 0.1	0.23±.01	43.5±2
	12	2.96 ± 0.3	1.4 ± 0.1	1.56 ± 0.1	0.22±.01	45.5±0.9
19	2	2.8 ± 0.2	1.33 ± 0.1	1.47 ± 0.2	0.22 ± .01	45.5 ± 1.9
	4	2.7 ± 0.3	1.28 ± 0.1	1.42 ± 0.1	0.22 ± .01	45.5 ± 1.5
	6	2.91 ± 0.3	1.38 ± 0.1	1.53 ± 0.1	0.22 ± .01	45.5 ± 1.4
	8	2.68 ± 0.3	1.19 ± 0.2	1.49 ± 0.2	0.22 ± .01	45.5 ± 1.2
	12	2.73 ± 0.3	1.3 ± 0.1	1.43 ± 0.1	0.24 ± .01	41.6 ± 1.3
19S	2	3.71 ± 0.3	1.85 ± 0.1	1.86 ± 0.1	0.24±.01	41.6 ± 2.1
	4	3.51 ± 0.5	1.62 ± 0.4	1.89 ± 0.4	0.24±.01	41.6 ± 2.5
	6	3.58 ± 0.2	1.72 ± 0.2	1.86 ± 0.2	0.24±.01	41.6 ± 1.3
	8	3.69 ± 0.2	1.84 ± 0.1	1.85 ± 0.2	0.25±.02	1.34 ± 3
	12	3.76 ± 0.3	1.85 ± 0.1	1.91 ± 0.3	0.23±.01	43.5 ± 2.6
21	2	2.81 ± 0.1	1.23 ± 0.1	1.58 ± 0.1	0.22 ± .01	45.5 ± 0.6
	4	2.65 ± 0.3	1.27 ± 0.1	1.38 ± 0.2	0.22 ± .01	45.5 ± 2.3
	6	2.92 ± 0.3	1.42 ± 0.1	1.5 ± 0.1	0.23 ± .01	43.5 ± 2.5
	8	2.84 ± 0.3	1.42 ± 0.2	1.42 ± 0.2	0.26 ± .03	38.5 ± 2
	12	2.92± 0.1	1.39 ± 0.1	1.53 ± 0.2	0.22 ± .01	45.5 ± 0.7
21S	2	3.53 ± 0.2	1.62 ± 0.1	1.91 ± 0.1	0.23 ± .01	43.5 ± 2.3
	4	2.75 ± 0.6	1.29 ± 0.3	1.46 ± 0.3	0.22 ± .01	45.5 ± 3.3
	6	3.1 ± 0.2	1.47 ± 0.1	1.63 ± 0.2	0.22 ± .01	45.5 ± 1.7
	8	3.11 ± 0.2	1.51 ± 0.1	1.6 ± 0.1	0.25± .03	40 ± 2.6
	12	3.18 ± 0.1	1.57 ± 0.1	1.61 ± 0.1	0.22 ± .01	45.5 ±0.9

See table 16 for alloy Fe-Mn-Mg levels

Table 20 Charpy impact properties of 319 alloys containing different levels of Fe, Mn, and Mg aged at 220°C.

Alloy Code	Aging Time (h)	E_T (J)	E_I (J)	E_p (J)	Time to Failure (ms)	ACS (mm/ms)
18	2	3.18 ± 0.1	1.5 ± 0.1	1.68 ± 0.1	0.22 ± .01	45.5 ± 1.2
	4	3.1 ± 0.3	1.3 ± 0.2	1.8 ± 0.1	0.23 ± .01	43.5 ± 1.9
	6	3.25 ± 0.2	1.54 ± 0.1	1.7 ± 0.1	0.24 ± .01	41.6 ± 0.4
	8	3.44 ± 0.3	1.70 ± 0.2	1.74 ± 0.2	0.25 ± .01	40 ± 1.5
	12	3.85 ± 0.5	2.0 ± 0.3	1.85 ± 0.4	0.24 ± .01	41.6 ± 2
18S	2	5.4 ± 0.3	2.35 ± 0.2	2.05 ± 0.1	0.23 ± .01	43.5 ± 1.6
	4	5.19 ± 0.4	2.49 ± 0.3	2.7 ± 0.2	0.29 ± .01	34.5 ± 3
	6	5.25 ± 0.2	2.13 ± 0.1	3.12 ± 0.2	0.25 ± .01	40 ± 1.4
	8	5.2 ± 0.2	2.7 ± 0.1	2.5 ± 0.1	0.28 ± .01	35.7 ± 0.9
	12	5.22 ± 0.4	2.73 ± 0.3	2.49 ± 0.2	0.27 ± .01	37 ± 1.7
20	2	2.85 ± 0.2	1.5 ± 0.1	1.35 ± 0.2	0.21 ± .01	45.5 ± 2
	4	2.37 ± 0.3	1.09 ± 0.1	1.28 ± 0.1	0.22 ± .01	45.5 ± 1.4
	6	2.45 ± 0.2	1.12 ± 0.1	1.03 ± 0.1	0.21 ± .01	47.6 ± 1.1
	8	2.15 ± 0.3	1 ± 0.2	1.45 ± 0.2	0.21 ± .01	47.6 ± 3
	12	2.86 ± 0.5	1.38 ± 0.1	1.48 ± 0.1	0.22 ± .01	45.5 ± 1.4
20S	2	3.32 ± 0.2	1.63 ± 0.1	1.69 ± 0.1	0.23 ± .01	43.5 ± 1.5
	4	3.54 ± 0.1	1.69 ± 0.1	1.85 ± 0.1	0.23 ± .01	43.5 ± 1
	6	3.41 ± 0.1	1.6 ± 0.1	1.81 ± 0.1	0.21 ± .01	47.6 ± 0.6
	8	3.45 ± 0.2	1.7 ± 0.1	1.75 ± 0.1	0.21 ± .01	47.6 ± 1.9
	12	3.96 ± 0.5	1.9 ± 0.1	2.06 ± 0.1	0.22 ± .01	45.5 ± 0.9
19	2	2.77 ± 0.3	1.35 ± 0.2	1.42 ± 0.1	0.22 ± .01	45.5 ± 2.5
	4	2.36 ± 0.6	1.12 ± 0.3	1.24 ± 0.3	0.22 ± .01	45.5 ± 3
	6	2.31 ± 0.5	1.12 ± 0.2	1.19 ± 0.2	0.21 ± .01	47.6 ± 2.4
	8	3.25 ± 0.3	1.56 ± 0.1	1.69 ± 0.1	0.23 ± .01	43.5 ± 0.6
	12	3.36 ± 0.1	1.66 ± 0.1	1.70 ± 0.1	0.23 ± .01	43.5 ± 1.3
19S	2	3.52 ± 0.5	1.82 ± 0.3	1.70 ± 0.3	0.26 ± .02	38.5 ± 2.5
	4	3.33 ± 0.5	1.63 ± 0.2	1.70 ± 0.3	0.24 ± .01	41.6 ± 2.8
	6	3.4 ± 0.2	1.72 ± 0.2	1.68 ± 0.2	0.24 ± .01	41.6 ± 1.9
	8	3.87 ± 0.2	1.92 ± 0.1	1.95 ± 0.1	0.25 ± .01	40 ± 0.7
	12	3.46 ± 0.4	1.70 ± 0.4	1.76 ± 0.3	0.25 ± .01	40 ± 2.6
21	2	2.86 ± 0.2	1.38 ± 0.1	1.48 ± 0.1	0.22 ± .01	45.5 ± 1.5
	4	2.29 ± 0.4	1.1 ± 0.2	1.19 ± 0.3	0.22 ± .01	45.5 ± 1.1
	6	3.09 ± 0.3	1.52 ± 0.1	1.57 ± 0.2	0.23 ± .01	43.5 ± 0.7
	8	2.81 ± 0.3	1.33 ± 0.2	1.48 ± 0.1	0.23 ± .01	43.5 ± 1.2
	12	2.82 ± 0.3	1.37 ± 0.1	1.45 ± 0.1	0.22 ± .01	45.5 ± 1.4
21S	2	3.03 ± 0.3	1.44 ± 0.2	1.59 ±0.1	0.23 ± .01	43.5 ± 1.4
	4	2.55 ± 0.2	1.25 ± 0.1	1.30 ±0.1	0.21 ± .01	47.6± 0.6
	6	2.62 ± 0.2	1.27 ± 0.1	1.35 ±0.1	0.23 ± .01	43.5 ± 2.6
	8	2.78 ± 0.2	1.31 ± 0.1	1.47 ±0.1	0.22 ± .01	45.5 ± 1.1
	12	3.00 ± 0.2	1.46 ± 0.1	1.54 ±0.1	0.23 ± .01	43.5 ± 0.9

See table 16 for alloy Fe-Mn-Mg levels

Table 21 Charpy impact properties of 396 alloys in the as-cast and solution heat-treated conditions

Alloy Code	Alloy Condition	E_T (J)	E_I (J)	E_P (J)	Time to Failure (ms)	ACS (mm/ms)
E1*	A	3.08 ± 0.3	1.54 ± 0.2	1.54 ± 0.1	0.23 ±.01	43.5 ± 2
	B	4.34 ± 0.4	2.18 ± 0.3	2.16 ± 0.2	0.25 ±.01	40 ± 1.9
E2	A	3.75 ± 0.6	1.88 ± 0.3	1.89 ± 0.3	0.25 ±.01	40 ± 2
	B	4.96 ± 0.9	2.61 ± 0.5	2.35 ± 0.4	0.27 ±.01	37 ± 1.5
E3	A	3.35 ± 0.8	1.7 ± 0.5	1.65 ± 0.4	0.24 ±.01	41.6 ± 1.7
	B	4.59±0.8	2.32 ± 0.6	2.27 ± 0.4	0.26 ±.01	38.5 ± 1.8
E4	A	2.2 ± 0.6	1.05 ± 0.3	1.15 ± 0.3	0.22 ±.01	45.5 ±1.6
	B	3.48 ± 0.8	1.68 ± 0.4	1.8 ± 0.4	0.23 ± .01	43.5 ± 1.3
E5	A	3.07 ±0.7	1.53 ±0.2	1.54 ±0.1	0.23 ± .01	43.5 ± 2
	B	4.4 ± 0.8	2.26 ± 0.5	2.14 ± 0.4	0.25 ± .02	40 ± 1.7
E6	A	3 ± 0.3	1.53 ± 0.2	1.47 ±0.2	0.23 ± .02	43.5 ± 1.7
	B	4.23 ± 0.5	2.13 ± 0.4	2.1 ± 0.3	0.25 ±.01	40 ± 1.3
***HE1**	A	2.05 ± 0.5	1.03± 0.2	1.02± 0.2	0.20 ± 0.1	50.0 ± 1.1
	B	2.24 ± 0.2	1.14± 0.1	1.1± 0.1	0.21 ± 0.2	47.6 ± 1.2
HE2	A	2.75 ± 0.5	1.45 ± 0.4	1.3 ± 0.1	0.24 ± .02	41.6 ± 1.3
	B	2.95 ± 0.4	1.55 ± 0.2	1.4 ± 0.3	0.25 ± .03	40.0 ± 1.2
HE3	A	2.48 ± 0.5	1.26 ± 0.4	1.22 ± 0.2	0.23 ±.01	43.7 ± 1.1
	B	2.75 ± 0.3	1.42 ± 0.3	1.33 ± 0.1	0.24 ±.05	41.6 ± 0.9
HE4	A	1.95 ± 0.4	1.01± 0.2	0.94± 0.3	0.19 ± .02	52.5 ± 1.2
	B	2.2 ± 0.3	1.15 ± 0.3	1.05 ± 0.4	0.21 ± .03	47.6 ± 1.1
HE5	A	2.32 ± 0.5	1.21 ± 0.5	1.11 ± 0.4	0.21 ± .03	47.6 ± 1.1
	B	2.8 ± 0.2	1.47 ± 0.2	1.33 ± 0.3	0.24 ± .02	41.6 ± 1.2
HE6	A	2.1 ± 0.3	1.07 ± 0.4	1.03 ± 0.2	0.20 ± .02	50.0 ± 0.9
	B	2.6 ± 0.4	1.34 ± 0.3	1.26 ± 0.3	0.23 ±.01	43.7 ± 0.8

*E: 396 base-alloy; 1: 0 ppm Sr; 2: 200 ppm Sr, 3: 350 ppm Sr, A: as-cast and B; Solution heat-treated; H: low cooling rate condition

Table 22 Charpy impact properties of 396 alloys containing 0.45 wt% Mn, and aged at different aging temperatures for 4, 16, and 44 hrs (samples obtained under high cooling rate conditions)

Alloy Code	Aging Conditions		E_T (J)	E_I (J)	E_P (J)	Time to Failure (ms)	ACS (mm/ms)
	Time (h)	Temp. (°C)					
E1	4	155	3.08 ± 0.23	1.39 ± 0.2	1.69 ± 0.15	0.23 ± .001	43.5 ± 0.9
		180	2.35 ± 0.22	1.07 ± 0.13	1.28 ± 0.12	0.21 ± .001	47.6 ±0.7
		200	2.41 ± 0.36	1.12 ± 0.17	1.29 ± 0.16	0.21 ±.001	47.6 ± 0.8
		220	2.62 ± 0.41	1.32 ± 0.24	1.30 ± 0.11	0.22 ± .001	45.5 ±0.9
		240	2.84 ± 0.47	1.42 ± 0.34	1.42 ± 0.13	0.22 ±.001	45.5 ± 0.8

		155	3.98 ± 0.13	2.04 ± 0.05	1.94 ± 0.1	0.25 ± .001	40 ± 1
		180	2.92 ± 0.36	1.44 ± 0.14	1.48 ± 0.1	0.23 ± .001	43.5 ± 0.7
E2	4	200	3.2 ± 0.22	1.6 ± 0.12	1.6 ± 0.1	0.24 ± .001	41.6 ± 0.6
		220	3.5 ± 0.24	1.81 ± 0.13	1.69 ± 0.11	0.24 ± .002	41.6 ± 0.8
		240	4.33 ± 0.51	2.31 ± 0.38	2.02 ± 0.14	0.27 ±.003	37 ± 0.9
		155	3.68± 0.49	1.6 ± 0.39	2.08 ± 0.2	0.25 ± .002	40 ± 1
		180	2.55 ± 0.55	1.37 ± 0.27	1.17 ± 0.15	0.21 ± .001	47.6 ±0.8
E3	4	200	2.69 ± 0.38	1.47 ± 0.37	1.22 ± 0.21	0.22 ± .003	45.5 ±0.9
		220	2.84 ± 0.59	1.53 ± 0.38	1.31 ± 0.23	0.23 ± .001	43.5 ±0.7
		240	3.05 ± 0.39	1.57 ± 0.18	1.48 ± 0.16	0.23 ± .004	43.5 ±0.5
		155	2.85 ± 0.31	1.41 ± 0.24	1.44 ± 0.11	0.22 ± .001	45.5 ± 0.9
		180	2.6 ± 0.21	1.36 ± 0.28	1.24 ±0.2	0.22 ± .002	45.5 ± 0.6
E1	16	200	2.85 ± 0.4	1.31 ± 0.32	1.54 ±0.14	0.22 ± .003	45.5 ± 0.5
		220	3.2 ± 0.2	1.64 ± 0.1	1.56 ± 0.12	0.24 ± .002	41.6 ± 0.7
		240	3.84 ± 0.41	1.89 ± 0.21	1.95 ± 0.17	0.26 ± .001	38.5 ± 0.7
		155	3.04 ± 0.4	1.47 ± 0.17	1.57 ± 0.2	0.24 ± .002	41.6 ± 0.8
		180	3.51 ± 0.4	1.78 ± 0.27	1.63 ± 0.15	0.25 ± .001	40 ± 0.4
E2	16	200	3.6 ± 0.39	1.84 ± 0.3	1.76 ± 0.16	0.25 ± .003	40 ± 0.7
		220	4.24 ± 0.39	2.16 ± 0.24	2.08 ± 0.17	0.27 ± .001	37 ± 0.6
		240	4.93 ± 0.43	2.54± 0.21	2.39 ± 0.18	0.29 ± .001	34.5 ± 0.6
		155	3.68 ± 0.22	1.74 ± 0.19	1.94 ± 0.1	0.25 ±.001	40 ± 0.9
		180	3.24 ± 0.18	1.57 ± 0.11	1.67 ± 0.14	0.25 ±.002	40 ± 0.80
E3	16	200	3.4 ± 0.16	1.71± 0.1	1.67 ± 0.13	0.25 ±.003	40 ± 0.8
		220	3.91± 0.31	2 ± 0.2	1.91 ± 0.17	0.26 ±.004	38.5 ± 0.3
		240	4.61 ± 0.45	2.44 ± 0.31	2.26 ± 0.2	0.28 ±.001	35.7 ± 0.6
		155	2.32 ± 0.45	1.06 ± 0.25	1.26 ± 0.11	0.21 ± .002	47.6 ± 0.8
		180	2.56 ± 0.2	1.19 ± 0.1	1.37 ± 0.13	0.22 ± .004	45.5 ± 0.9
E1	44	200	2.80 ± 0.45	1.35 ± 0.21	1.45 ± 0.15	0.22 ± .004	45.5 ± 0.5
		220	4.45 ± 0.41	2.34 ± 0.2	2.11 ± 0.16	0.27 ± .002	37 ± 0.7
		240	5.1 ± 0.43	2.52 ± 0.36	2.58 ± 0.12	0.29 ± .003	34.5 ± 0.8
		155	3.42 ± 0.57	1.61 ± 0.28	1.81 ± 0.2	0.24 ± .001	41.6 ± 0.9
		180	3.73 ± 0.2	1.82 ± 0.1	1.91 ± 0.19	0.25 ± .003	40 ± 0.6
E2	44	200	3.93 ± 0.54	1.93 ± 0.24	2 ± 0.15	0.26 ±.002	38.5 ± 0.7
		220	5.11 ± 0.45	2.63 ± 0.29	2.48 ± 0.17	0.29 ±.004	34.5 ± 0.9
		240	5.48 ± 0.22	2.86 ± 0.23	2.62 ± 0.12	0.30 ±.003	33.3 ± 0.8
		155	2.56 ± 0.23	1.19±0.1	1.37± 0.13	0.22 ± .003	45.5 ± 0.6
E3	44	180	3.31 ± 0.2	1.69 ± 0.1	1.62 ± 0.1	0.24 ± .002	41.6 ± 0.5
		200	3.34 ± 0.33	1.69 ± 0.2	1.65 ± 0.12	0.24 ± .004	41.6 ± 0.8
		220	4.75 ± 0.51	3.43 ± 0.24	1.32 ± 0.11	0.27 ± .001	37 ± 0.6
		240	5.3 ± 0.46	2.61 ± 0.32	2.69 ± 0.14	0.29 ± .003	34.5 ± 0.7

See table 21 for alloy Sr levels

Table 23 Charpy impact properties of 396 alloys containing 0.45 wt% Mn, and aged at 180°C and 240°C for various aging times (high cooling rate samples)

Alloy Code	Aging conditions		E_T (J)	E_I (J)	E_P (J)	Time to Failure (ms)	ACS (mm/ms)
	Time (h)	Temp (°C)					
E1	180	2	2.77 ± 0.35	1.63 ± 0.14	1.14 ±0.1	0.23 ±.001	43.5 ± 0.9
		4	2.35 ± 0.22	1.18 ±0.1	1.17 ±0.2	0.21 ±.001	47.6 ± 0.5
		8	2.54 ± 0.26	1.19 ± 0.16	1.35 ±0.1	0.22 ±.001	45.5 ± 0.6
		12	2.36 ± 0.3	1.2 ± 0.17	1.16 ±0.17	0.21 ±.002	47.6 ± 0.4
		16	2.6 ± 0.27	1.17 ± 0.21	1.43 ±0.16	0.22 ±.003	45.5 ± 0.7
		20	2.52 ± 0.4	1.2 ± 0.23	1.32 ±0.13	0.22 ±.001	45.5 ± 0.6
		24	2.54 ± 0.27	1.29±0.21	1.25 ±0.12	0.22 ±.004	45.5 ±0.5
		30	2.56 ± 0.24	1.22±0.15	1.34 ±0.1	0.22 ±.002	45.5 ± 0.4
		36	2.6 ± 0.33	1.34±0.17	1.26 ±0.12	0.23 ±.001	43.5 ± 0.7
		44	2.56 ± 0.19	1.86±0.1	0.89 ±0.13	0.23 ±.002	43.5 ± 0.8
E2	180	2	3.62 ± 0.43	1.80 ± 0.1	1.82 ± 0.12	0.25±.001	40.0 ± 1.0
		4	2.92 ± 0.36	1.51 ± 0.1	1.41 ± 0.13	0.24 ±.002	41.6 ± 0.9
		8	3.7 ±0.24	1.84 ± 0.1	1.86 ± 0.14	0.25±.001	40.0 ± 0.5
		12	3.37 ± 0.32	1.67 ± 0.2	1.70 ± 0.15	0.25±.003	40.0 ± 0.6
		16	3.51 ± 0.24	1.78 ± 0.1	1.73 ± 0.16	0.25±.004	40.0 ± 0.4
		20	3.64 ± 0.26	1.83 ± 0.2	1.81 ± 0.1	0.25±.003	40.0 ± 0.8
		24	3.84 ± 0.41	1.65 ± 0.2	2.19 ± 0.1	0.26±.001	38.5 ± 0.4
		30	3.89 ± 0.29	1.89 ± 0.1	2.0 ± 0.12	0.27±.002	37.0 ± 0.6
		36	3.74 ± 0.33	1.84 ± 0.2	1.9 ±0.13	0.25±.001	40.0 ±0.9
		44	3.73 ± 0.19	1.82 ± 0.1	1.9 1±0.1	0.26±.003	38.5 ± 0.7
E3	180	2	3.02 ±0.4	1.44 ±0.2	1.58±0.1	0.24±.001	41.6±1.1
		4	2.55 ±0.32	1.69 ±0.1	1.61±0.11	0.25±.002	40.0±0.9
		8	3.37±0.31	1.6 ±0.15	1.77±0.12	0.25±.001	40.0±0.8
		12	3.06±0.27	1.4 ±0.2	1.66±0.13	0.24±.003	41.6±0.9
		16	3.24±0.18	1.57 ±0.1	1.67±0.1	0.24±.004	41.6±0.8
		20	3.43±0.1	1.72 ±0.1	1.71±0.14	0.25±.002	40.0±0.7
		24	3.5±0.24	1.78 ±0.1	1.72±0.11	0.26±.001	38.5±0.5
		30	3.4±0.47	1.71 ±0.2	1.69±0.12	0.25±.001	40.0±0.9
		36	3.41±0.23	1.74 ±0.1	1.67±0.13	0.25±.001	40.0±0.8
		44	3.31 ±0.19	1.68 ±0.1	1.63 ±0.11	0.26±.003	38.5±0.6
E1	240	2	2.59±0.27	1.3±0.1	1.29±0.13	0.22±.001	45.5±0.8
		4	2.84±0.37	1.46±0.1	1.38±0.12	0.24±.002	41.6±0.9
		8	3.1±0.3	1.58±0.1	1.52±0.13	0.25±.003	40.0±0.3
		12	3.29±0.2	1.68±0.1	1.61±0.1	0.25±.004	40 0±0.6
		16	3.84±0.2	1.89±0.1	1.95±0.14	0.28±.003	35.7±0.8
		20	4.11±0.33	2.09±0.2	2.02±0.15	0.29±.002	34.5±0.9
		24	4.21±0.37	2.14±0.1	2.07±0.17	0.29±.003	34.5±0.6
		30	4.35±0.45	2.23±0.21	2.12±0.12	0.30±.001	33.3±0.8
		36	4.69±0.35	2.45±0.1	2.24±0.13	0.31±.002	32.2±0.4
		44	5.1±0.43	2.82±0.3	2.28±0.12	0.32±.003	31.2±0.5

		2	3.37±0.4	1.41±0.1	1.96±0.1	0.25±.002	40±0.9
		4	4.33±0.3	2.07±0.1	1.93±0.2	0.28±.005	35.7±0.8
		8	4.63±0.2	2.37±0.1	2.06±0.3	0.29±.006	34.5±0.5
		12	4.8±0.3	2.48±0.2	2.32±0.1	0.30±.001	33.3±0.4
E2	240	16	4.93±0.2	2.52±0.1	2.41±0.14	0.32±.004	31.2±0.5
		20	5.1±0.2	2.65±0.1	2.45±0.12	0.31±.003	31.3±0.6
		24	5.21±0.4	2.62 ±0.2	2.59±0.16	0.32±.002	32.2±0.7
		30	5.29±0.2	265.±0.1	2.64±0.17	0.32±.001	32.2±0.8
		36	5.39 ±0.3	2.7 ±0.2	3.92±0.11	0.33±.001	30.3±0.4
		44	5.48 ±0.1	2.76±0.1	2.72±0.1	0.34±.003	29.4±0.6
		2	2.85±0.3	1.44±0.1	1.41±0.1	0.24±.001	41.6±0.7
		4	3.05±0.3	1.53±0.1	1.52±0.11	0.25±.002	40.0±0.9
		8	3.78±0.2	1.42±0.1	2.36±0.12	0.26±.003	38.5±0.6
		12	4.23±0.4	2.14±0.2	2.09±0.14	0.28±.004	35.6±0.4
E3	240	16	4.61±0.3	2.38±0.2	2.23±0.13	0.29±.001	34.5±0.5
		20	4.7±0.4	2.49±0.2	2.21±0.17	0.30±.001	33.3±0.3
		24	4.81±0.3	2.52±0.2	2.28±0.18	0.30±.002	33.3±0.8
		30	5.1±0.4	2.56±0.2	2.54±0.16	0.30±.003	33.3±0.4
		36	5.23±0.5	2.87±0.2	2.36±0.13	0.33±.003	30.3±0.5
		44	5.3±0.3	2.8±0.1	2.5±0.12	0.33±.005	30.3±0.3

See table 21 for alloy Sr levels

Table 24 Charpy impact properties of 396 alloys containing 0.65 wt% Mn, and aged at different aging temperatures for 4, 16, and 44 hrs (samples obtained under high cooling rate)

Alloy Code	Aging conditions		E_T (J)	E_I (J)	E_P (J)	Time to Failure (ms)	ACS (mm/ms)
	Time (h)	Temp. (°C)					
		155	2.91± 0.23	1.34±0.12	1.57±0.12	0.24±.001	41.6±1.2
		180	2.51±0.22	1.29±0.12	1.22±0.13	0.22±.002	45.5±1.3
E4	4	200	2.56±0.29	1.29±0.17	1.27±0.14	0.23±.003	43.5±1.1
		220	2.78±0.36	1.2±0.14	2.58±0.15	0.24±.003	41.6±1
		240	2.81±0.25	1.56±0.1	1.29±0.12	0.25±.004	40±0.9
		155	3.54±0.33	1.96±0.11	1.58±0.12	0.26±.001	38.5±0.9
		180	2.93±0.23	1.46 ±0.17	1.47±0.11	0.24±.002	41.6±1
E5	4	200	3.45±0.23	1.61±0.18	1.84±0.14	0.25±.004	40.0±0.7
		220	3.74±0.41	1.87±0.18	1.87±0.15	0.26±.005	38.5±1.1
		240	3.75±0.41	1.92±0.2	1.83±0.1	0.27±.003	37±1.3
		155	3.2±0.15	1.72±0.1	1.48±0.12	0.24±.001	41.6±1
		180	2.68±0.27	1.34±0.14	1.54±0.14	0.23±.002	43.5±1.1
E6	4	200	3.16±0.33	1.49±0.19	1.67±0.13	0.25±.003	40.0±1.2
		220	3.24±0.35	1.47±0.17	1.77±0.15	0.25±.004	40.0±0.9
		240	3.34±0.26	1.81±0.2	1.53±0.14	0.26±.004	38.5±0.8

		155	2.62 ± 0.33	1.22 ± 0.15	1.4 ± 0.12	0.22 ± .001	45.5 ± 0.9
		180	2.66 ± 0.24	1.26 ± 0.10	1.49 ± 0.13	0.22 ± .002	45.5 ± 0.7
E4	16	200	2.92 ± 0.22	1.47 ± 0.11	1.45 ± 0.11	0.23 ±.003	43.5 ± 1.1
		220	2.98 ± 0.36	1.51 ± 0.14	1.47 ± 0.14	0.24 ± .004	41.6 ± 1.2
		240	3.05 ± 0.25	1.69 ± 0.10	1.36 ± 0.10	0.25 ± .001	40.0 ± 0.8
		155	3.23 ± 0.30	1.57±0.1	1.65±0.1	0.25±.001	40.0 ±0.9
		180	3.28 ± 030	1.62±0.15	1.66±0.12	0.25±.002	40.0 ±0.8
E5	16	200	3.67 ± 0.25	1.78±0.18	1.89±0.14	0.26±.003	38.5 ±1.1
		220	3.75 ± 0.2	1.86±0.1	1.89±0.13	0.27±.004	37.0 ± 1.0
		240	4.12 ± 0.4	2.12±0.2	2.0±0.11	0.28±.004	35.7 ± 0.7
		155	2.91±0.11	1.34±0.1	1.57±0.12	0.23±.001	43.5±0.9
E6		180	2.94±0.27	1.48±0.14	1.46±0.14	0.23±.002	43.5±1
	16	200	3.24±0.33	1.63±0.19	1.61±0.13	0.25±.003	40.0±1.2
		220	3.37±0.22	1.7±0.13	1.67±0.11	0.26±.004	38.5±1.3
		240	3.67±0.26	1.82±0.2	1.85±0.12	0.27±.005	37±0.8
		155	2.61±0.1	1.3±0.1	1.31±0.12	0.23±.001	43.5±0.9
		180	2.85±0.24	1.42±0.12	1.43±0.11	0.23±.002	43.5±0.8
E4	44	200	3.09±0.22	1.54±0.11	1.55±0.15	0.24±.003	41.6±0.7
		220	3.25±0.1	1.64±0.1	1.61±0.12	0.25±.004	40.0±1.1
		240	3.49±0.27	1.78±0.14	1.71±0.14	0.26±.002	38.5±1
		155	3.33±0.23	1.57±0.14	1.76±0.11	0.26±.001	38.5±0.9
		180	3.49±0.28	1.75±0.16	1.74±0.13	0.27±.002	37±1.2
E5	44	200	3.58±0.28	1.8±0.17	1.78±0.16	0.27±.003	37±1.2
		220	4.1±0.2	2.1±0.1	2.0±0.17	0.30±.004	33.3±0.8
		240	4.3±0.4	2.14±0.2	2.16±0.16	0.31±.003	32.2±0.7
		155	3.17±0.4	1.51±0.27	1.66±0.14	0.25±.001	40.0±0.9
E6	44	180	3.24±0.27	1.64±0.14	1.60±0.11	0.25±.002	40.0±0.8
		200	3.49±0.33	1.75±0.19	1.74±0.16	0.26±.003	38.5±1.1
		220	3.64±0.22	1.88±0.13	1.76±0.12	0.27±.001	37±1.2
		240	3.89±0.26	2.03±0.2	1.86±0.11	0.28±.002	35.7±0.7

See table 21 for alloy Sr and Mn levels

Table 25 Charpy impact properties of 396 alloys containing 0.65 wt% Mn, and aged at 180°C and 240°C for various aging times (samples obtained under high cooling rate)

Alloy Code	Aging conditions		E_T (J)	E_I (J)	E_P (J)	Time to Failure (ms)	ACS (mm/ms)
	Temp (°C)	Time (h)					
		2	2.70 ± 0.2	1.33 ± 0.11	1.37 ±0.1	0.23±.001	43.5±0.9
		4	2.51 ± 0.2	1.29 ± 0.12	1.22 ± 0.12	0.23±.001	43.5±0.7
		8	2.46 ±0.3	1.14 ± 0.14	1.32 ± 0.10	0.22±.003	45.5±0.6
		12	2.24 ±0.2	1.11 ± 0.10	1.13 ± 0.14	0.2±.003	50.0±0.8
E4	180	16	2.66 ±0.2	1.39 ± 0.13	1.29 ± 0.13	0.22±.004	45.5±0.4
		20	2.54 ±0.3	1.32 ± 0.15	1.22 ± 0.12	0.22±.005	45.5±0.6

		24	2.62 ± 0.2	1.36±0.1	1.26±0.13	0.23±.006	43.5±0.3
		30	2.71 ± 0.2	1.38±0.12	1.33±0.12	0.23±.007	43.5±0.9
		36	2.8 ± 0.20	1.42±0.16	1.38±0.14	0.24±.003	41.6±0.9
		44	2.85 ± 0.3	1.45±0.12	1.41 ±0.15	0.24±.001	41.6±0.6
		2	3.2 ± 0.3	1.57 ± 0.2	1.63 ± 0.11	0.25±.001	40.0 ±0.9
E5		4	2.93 ± 0.3	1.51 ± 0.15	1.50 ± 0.13	0.24±.002	41.6 ±0.8
		8	2.87 ± 0.2	1.41 ± 0.16	1.46 ± 0.1	0.24±.001	41.6 ±0.7
		12	2.41± 0.18	1.14 ± 0.17	1.26 ± 0.15	0.24±.003	41.6 ±0.6
		16	3.28 ± 0.3	2.36 ± 0.13	1.92 ± 0.16	0.25±.004	40.0 ±0.8
E5	180	20	2.97 ± 0.2	1.48 ± 0.16	1.49 ± 0.14	0.24±.006	41.6 ±0.8
		24	3.05 ± 0.3	1.54 ±0.17	1.51 ± 0.13	0.25±.004	40.0 ±0.9
		30	3.29 ± 0.1	1.61 ± 0.2	1.68 ± 0.10	0.25±.005	40.0 ±0.7
		36	3.46 ± 0.2	1.63 ± 0.19	1.83 ± 0.18	0.26±.001	38.5 ±0.5
		44	3.49 ± 0.2	1.74 ± 0.1	1.80 ± 0.19	0.27±.002	37.0 ±0.6
		2	2.93±0.30	1.42 ±0.20	1.51 ±0.10	0.24±.002	41.6±0.9
		4	2.68±0.20	1.34 ±0.14	1.34 ±0.12	0.23±.003	43.5±0.8
		8	2.57±0.28	1.17 ±0.20	1.40 ±0.30	0.22±.001	45.5±0.7
		12	2.33 ±0.20	1.06 ±0.10	1.27 ±0.14	0.21±.002	47.6±0.6
E6	180	16	2.94 ±0.18	1.54 ±0.13	1.40 ±0.16	0.23±.001	43.5±0.4
		20	2.69±0.25	1.33 ±0.20	1.34 ±0.15	0.23±.001	43.5±0.9
		24	2.85±0.2	1.39 ±0.13	1.45 ±0.1	0.23±.001	43.5±0.5
		30	3.02±0.23	1.49 ±0.15	1.53 ±0.2	0.25±.002	40.0±0.7
		36	3.10 ±0.19	1.54 ±0.16	1.56 ±0.14	0.25±.003	40.0±0.6
		44	3.24±0.26	1.55 ±0.14	1.69 ±0.15	0.25±.003	40.0±0.4
		2	2.33±0.19	1.17 ± 0.12	1.16 ± 0.15	0.21±.001	47.6 ± 0.9
		4	2.81 ±0.25	1.57 ± 0.13	1.24 ± 0.13	0.23±.002	43.5 ± 0.8
		8	2.74 ±0.21	1.26 ± 0.11	1.48 ± 0.16	0.23±.003	43.5 ± 0.7
		12	2.92 ±0.19	1.93 ± 0.14	0.99 ± 0.10	0.24±.001	41.6 ± 0.5
E4	240	16	3.05 ±0.24	1.49 ± 0.60	1.61 ± 0.17	0.25±.004	40.0 ± 0.9
		20	3.07 ±0.17	1.53 ± 0.17	1.54 ± 0.19	0.25±.002	40.0 ± 0.5
		24	3.16 ±0.19	1.61 ± 0.11	1.55 ± 0.20	0.26±.006	38.5 ± 0.7
		30	3.29 ±0.27	1.68 ± 0.19	1.61 ± 0.14	0.26±.005	38.5 ± 0.8
		36	3.34 ±0.30	1.71 ± 0.17	1.63 ± 0.12	0.27±.006	37.0 ± 0.8
		44	3.49 ±0.32	1.79 ± 0.18	1.70 ± 0.16	0.28±.001	35.6 ± 0.6
		2	3.07 ±0.21	1.54 ±0.13	1.53 ± 0.12	0.25±.001	40.0±0.9
		4	3.75 ±0.29	1.85 ±0.12	1.90 ± 0.13	0.26±.002	38.5±0.7
		8	3.78 ±0.26	1.97 ±0.14	1.81 ± 0.14	0.27±.003	37.0±0.5
		12	3.80 ±0.19	1.90 ±0.15	1.80 ± 0.10	0.28±.001	35.7±0.6
E5	240	16	3.84 ±0.30	1.94 ±0.10	1.86 ± 0.16	0.29±.004	34.5±0.4
		20	3.90 ±0.23	1.98 ±0.20	1.92 ± 0.15	0.30±.002	33.3±0.9
		24	3.91 ±0.34	1.94 ±0.14	1.97 ± 0.10	0.31±.006	32.2±0.4
		30	4.12 ±0.35	2.10 ±0.16	2.02 ±0.20	0.32±.003	31.2±0.5
		36	4.29 ±0.22	2.13 ±0.15	2.16 ± 0.13	0.32±.001	31.2±0.6
		44	4.50 ±0.28	2.33 ±0.14	2.17 ± 0.11	0.33±.002	30.3±0.9
		2	2.91 ± 0.2	1.46 ± 0.1	1.45 ± 0.13	0.24±.001	41.6±0.9
		4	3.34 ± 0.2	1.71 ± 0.2	1.63 ± 0.1	0.25±.002	40.0±0.7
		8	3.27 ± 0.3	1.64 ±0.14	1.63 ± 0.2	0.25±.003	40.0±0.6

E6	240	12	3.44 ±0.2	1.70±0.16	1.74 ± 0.14	0.26±.001	38.5±0.8
		16	3.51 ±0.2	1.81±0.13	1.70 ± 0.10	0.27±.001	37±0.6
		20	3.62 ± 0.3	1.82 ±0.10	1.80 ± 0.15	0.28±.004	35.7±0.4
		24	3.70 ± 0.3	1.87±0.12	1.83 ± 0.10	0.28±.001	35.7±0.5
		30	3.77 ± 0.2	1.87±0.13	1.90 ± 0.13	0.28±.006	35.7±0.6
		36	3.82 ±0.15	1.92±0.14	1.90 ± 0.15	0.29±.005	34.5±0.3
		44	3.89 ±0.2	1.95 ±0.16	1.93± 0.16	0.30±.004	33.3±0.4

*H: low cooling 396 samples; See table 21 for alloy Sr and Mn levels

Table 26 Charpy impact properties of 396 alloys containing 0.45 wt% Mn, and aged at different aging temperatures for 4, 16, and 44 hrs (samples obtained under low cooling rate)

Alloy Code	**Aging conditions**		**E_T (J)**	**E_I (J)**	**E_P (J)**	**Time to Failure (ms)**	**ACS (mm/ms)**
	Time (h)	**Temp (°C)**					
HE1	4	155	2.01 ± 0.21	0.93 ± 0.18	1.08±0.11	0.20±.001	50.0±0.8
		180	1.84 ± 0.21	0.85 ± 0.15	0.99±0.12	0.18±.002	55.5±.9
		200	1.91± 0.19	0.94 ± 0.10	0.97±0.13	0.19±.001	52.6±1.1
		220	2.01 ± 0.3	1.01 ± 0.21	1.0±0.14	0.20±.004	50.0±0.7
		240	2.08 ± 0.2	1.06 ± 0.10	1.02±0.12	0.20±.003	50.0±0.6
HE2	4	155	2.43 ± 0.16	1.18 ± 0.10	1.25±0.11	0.22±.001	45.5±1.6
		180	2.13 ± 0.2	1.12 ± 0.20	1.01±0.14	0.20±.002	50.0±0.9
		200	2.27 ± 0.33	1.17 ± 0.20	1.1±0.13	0.21±.002	47.6±0.8
		220	2.35 ± 0.20	1.19 ± 0.15	1.16±0.14	0.22±.003	45.5±0.7
		240	2.49 ± 0.17	1.23 ± 0.10	1.26±0.11	0.23±.002	43.5±0.9
HE3	4	155	2.21±0.29	1.01±0.2	1.2±0.1	0.21±.001	47.6±0.6
		180	1.97±0.12	0.99±0.1	0.98±0.14	0.20±.001	50.0±1.1
		200	2.09±0.3	1.01±0.3	1.08±0.15	0.20±.003	50.0±1.2
		220	2.21±0.19	1.11±0.12	1.1±0.13	0.21±.002	47.6±1.1
		240	2.34±0.2	1.19±0.13	1.15±0.12	0.22±.002	45.5±0.9
HE1	16	155	1.97±0.3	0.86±0.12	1.11±0.11	0.19±.001	52.6±0.8
		180	2.03±0.21	0.92±0.15	1.11±0.13	0.20±.003	50.0±0.9
		200	2.08±0.19	0.97±0.1	1.11±0.12	0.20±.002	50.0±0.7
		220	2.13±0.18	1.01±0.13	1.12±0.16	0.21±.001	47.6±0.6
		240	2.27±0.22	1.1±0.14	1.17±0.13	0.21±.003	47.6±0.5
HE2	16	155	2.28±0.19	1.09±0.11	1.19±0.14	0.21±.003	47.6±0.7
		180	2.33±0.26	1.16±0.18	1.17±0.16	0.22±.002	45.5±1
		200	2.53±0.21	1.26±0.17	1.27±0.12	0.22±.001	45.5±0.9
		220	2.61±0.14	1.29±0.1	1.32±0.11	0.23±.002	43.5±0.8
		240	2.76±0.17	1.34±0.1	1.42±0.12	0.23±.002	43.5±0.9
HE3	16	155	2.11±0.22	1.02±0.16	1.09±0.13	0.20±.001	50.0±0.7
		180	2.21±0.19	1.1±0.1	1.10±0.12	0.21±.002	47.6±0.6
		200	2.3±0.16	1.14±0.13	1.16±0.11	0.21±.004	47.6±0.8
		220	2.43±0.18	1.2±0.14	1.23±0.16	0.22±.005	45.5±0.5
		240	2.7±0.2	1.35±0.16	2.35±0.14	0.23±.002	43.5±0.9

		155	1.87±0.1	0.93±0.1	0.94±0.13	0.18±.002	55.9±1.1
		180	2.06±0.3	0.98±0.15	1.08±0.15	0.20±.004	50.0±1.2
HE1	44	200	2.11±0.16	1.03±0.1	1.08±0.16	0.20±.003	50.05±1.4
		220	2.29±1.14	1.12±0.11	1.17±0.12	0.21±.004	47.6±0.9
		240	2.65±0.22	1.35±0.1	1.30±0.14	0.21±.005	47.6±0.8
		155	2.18±0.18	1.03±0.1	1.15±0.12	0.20±.002	50.0±0.8
		180	2.39±0.21	1.17±0.13	1.22±0.13	0.21±.001	47.6±1.1
HE2	44	200	2.52±0.22	1.22±0.17	1.30±0.15	0.22±.003	45.5±0.9
		220	2.76±0.24	1.43±0.13	1.33±0.11	0.23±.004	43.5±0.7
		240	3.32±0.17	172±0.1	1.60 ±0.14	0.24±.002	41.6±0.8
		155	2.11±0.22	0.98±0.16	1.13±0.14	0.20±.002	50.0±1.2
HE3	44	180	2.23±0.2	1.06±0.19	1.17±0.12	0.20±.003	50.0±1.3
		200	2.44±0.16	1.13±0.13	1.31±0.11	0.21±.001	47.6±1.1
		220	2.6±0.18	1.29±0.14	1.31±0.13	0.22±.004	45.5±1.4
		240	3.21±0.2	1.66±0.12	1.56±0.1	0.23±.002	43.5±1.2

*H: low cooling 396 samples; See table 21 for alloy Sr and Mn levels

Table 27 Charpy impact properties of 396 alloys containing 0.45 wt% Mn, and aged at 180°C and 240°C for various aging times (samples obtained under low cooling rate)

Alloy Code	**Aging conditions**		**E_T (J)**	**E_I (J)**	**E_P (J)**	**Time to Failure (ms)**	**ACS (mm/ms)**
	Temp. (°C)	**Time (h)**					
		2	1.77 ±0.21	0.83±0.1	0.94±0.12	0.20±.001	50.0±0.9
		4	1.84 ±0.19	0.85±0.12	0.99±0.13	0.21±.002	47.6±0.8
		8	1.78 ±0.20	0.86±0.1	0.92±0.15	0.20±.003	50.0±0.5
		12	1.72 ±0.19	0.8±0.15	0.92±0.16	0.20±.001	50.0±0.3
HE1	180	16	2.03 ±0.11	1.05±0.14	0.98±0.14	0.21±.001	47.6±0.4
		20	1.87 ±0.19	0.89±0.16	0.98±0.12	0.21±.004	47.6±006
		24	1.88 ±0.17	0.93±0.13	0.95±0.13	0.21±.006	47.6±0.4
		30	1.89 ±0.11	0.97±0.17	0.92±0.17	0.21±.003	47.6±0.9
		36	2.04 ±0.10	0.99±0.12	1.05±0.19	0.22±.003	45.5±0.8
		44	2.06 ±0.12	1.02±0.13	1.05±0.18	0.22±.002	45.5±0.7
		2	1.99±0.17	1.17±0.11	0.82±0.2	0.21±.001	47.6±1.1
		4	2.13±0.1	1.01±0.12	1.12 ±0.15	0.21±.005	47.6±1.2
		8	2.11±0.11	1.05±0.1	1.06 ±0.13	0.20±.004	50.0±1.4
		12	2.15±0.14	1.08±0.17	1.07±0.1	0.19±0.3	52.6±0.9
HE2	180	16	2.33±0.13	1.16±0.19	1.17±0.14	0.20±.002	50.0±0.8
		20	2.07±0.17	0.94±0.18	1.13±0.17	0.21±.005	47.6±1.4
		24	2.09±0.16	1.0±0.14	1.09±0.18	0.21±.006	47.6±0.7
		30	2.14±0.15	1.03±0.15	1.11±0.15	0.22±.001	45.5±0.8
		36	2.16±0.14	0.98±0.13	1.18±0.12	0.22±.002	45.5±0.9
		44	2.39±0.13	1.24±0.12	1.15±0.11	0.22±.004	45.5±1.1

		2	2.12 ±0.13	0.98 ±0.14	1.14±0.12	0.21±.002	47.6±1.1
		4	1.97 ±0.12	0.98 ±0.15	0.99±0.14	0.20±.003	50.0±1.2
		8	2.13 ±0.20	1.14 ±0.10	0.99±0.13	0.21±.004	47.6±0.9
		12	2.15 ±0.13	1.05 ±0.11	1.10±0.11	0.21±.002	47.6±.08
HE3	180	16	2.21 ±0.21	1.09 ±0.20	1.12±0.18	0.20±.001	50.0±1.4
		20	2.06 ±0.19	0.99 ± 0.16	1.07±0.16	0.20±.005	50.0±1.6
		24	2.08 ±0.17	1.01 ±0.13	1.07±0.11	0.21±.006	47.6±0.5
		30	2.11 ±0.18	1.04 ±0.10	1.07±0.13	0.21±.006	47.6±0.7
		36	2.13 ±0.20	1.05 ±0.12	1.08±0.12	0.21±.004	47.6±0.9
		44	2.23 ±0.15	1.14 ±0.15	1.09±0.10	0.21±.003	47.6±0.7
		2	1.67 ±0.20	0.77±0.10	0.90±0.12	0.19±.001	52.6±1.4
		4	2.08 ±0.20	1.01±0.11	1.07±0.10	0.20±.003	50.0±1.2
		8	2.06 ±0.16	0.91±0.12	1.15±0.15	0.20±.005	50.0±1.6
		12	2.10 ±0.10	1.03±0.20	1.07±0.14	0.21±.004	47.69±1.3
HE1	240	16	2.27 ±0.20	1.02±0.16	1.17±0.17	0.21±.002	47.6±0.9
		20	2.44 ±0.20	1.25±0.14	1.19±0.18	0.21±.003	47.6±0.8
		24	2.51 ±0.17	1.29±0.17	1.22±0.10	0.22±.001	45.5±0.7
		30	2.46 ±0.12	1.19±0.13	1.27±0.13	0.22±.001	45.5±0.6
		36	2.61 ±0.15	1.21±0.18	1.40±0.12	0.23±.002	43.5±0.9
		44	2.65 ±0.13	1.34±0.11	1.31±0.17	0.23±.001	43.5±0.8
		2	2.11±0.13	1.03±0.2	1.09±0.12	0.2±.001	50.0±0.7
		4	2.49±0.17	1.32±0.11	1.17±0.13	0.2±.003	50.0±0.9
		8	2.39±0.20	1.17±0.14	1.22±0.14	0.21±.004	47.6±.8
		12	2.48±0.12	1.18±0.13	1.30±0.16	0.22±.005	45.5±0.7
HE2	240	16	2.76±0.19	1.33±0.10	1.43±0.17	0.23±.001	43.5±0.5
		20	3.15±0.15	1.37±0.17	1.78±0.11	0.25±.002	40.0±0.4
		24	3.22±0.11	1.50±0.16	1.72±0.13	0.25±.004	40.0±0.6
		30	3.30±0.16	1.54±0.15	1.76±0.12	0.26±.003	38.5±0.3
		36	3.31±0.10	1.64±0.18	1.67±0.15	0.26±.003	38.5±0.4
		44	3.32±0.16	1.73±0.12	1.59±0.18	0.27±.002	37.0±0.1
		2	2.17±0.13	1.06±0.16	1.11±0.17	0.20±.001	50.0±0.9
		4	2.34±0.20	1.16±0.13	1.09±0.16	0.20±.002	50.0±0.8
		8	2.29±0.16	1.14±0.14	1.15±0.12	0.21±.003	47.6±0.7
		12	2.56±0.18	1.19±0.12	1.37±0.10	0.22±.004	45.5±0.6
HE3	240	16	2.61±0.12	1.26±0.15	1.35±0.11	0.23±.005	43.5±0.4
		20	2.94±0.10	1.48±0.11	1.46±0.17	0.24±.006	41.6±0.7
		24	3.10±0.20	1.52±0.18	1.58±0.15	0.25±.002	40.0±0.5
		30	3.13±0.15	1.59±0.11	1.59±0.14	0.25±.001	40.0±0.8
		36	3.17±0.11	1.60±0.17	1.64±0.13	0.26±.003	38.5±0.9
		44	3.21±0.14	1.61±0.19	1.60±0.12	0.27±.003	37.0±0.4

*H: low cooling 396 samples; See table 21 for alloy Sr and Mn levels

Table 28 Charpy impact propertiesof 396 alloys containing 0.65 wt% Mn, and aged at different aging temperatures for 4, 16, and 44 hrs (samples obtained under low cooling rate)

Alloy Code	Aging conditions		E_T (J)	E_I (J)	E_P (J)	Time to Failure (ms)	ACS (mm/ms)
	Time (h)	Temp (°C)					
HE4	4	155	2.15±0.17	1.05±0.11	1.10±0.13	0.20±.001	50.0±0.9
		180	1.89±0.17	0.89±0.10	1.00±0.12	0.18±.002	55.5±1.1
		200	2.03±0.13	1.03±0.10	1.00±0.11	0.20±.003	50.0±1.3
		220	2.13±0.10	1.03±0.10	1.10 ±0.12	0.20±.004	50.0±1.1
		240	2.19±0.22	1.12±0.10	1.07±0.14	0.21±.005	47.6±0.8
HE5	4	155	2.44 ± 0.16	1.15±0.10	1.29±0.12	0.23±.004	43.5±0.7
		180	2.02 ± 0.20	0.99±0.20	1.0±0.13	0.19±.001	52.6±0.8
		200	2.17 ± 0.18	1.13±0.16	1.04±0.11	0.21±.003	47.6±1.1
		220	2.23 ± 0.20	1.18±0.11	1.05±0.14	0.21±.002	47.6±1.4
		240	2.41 ± 0.15	1.16±0.13	1.25±0.10	0.22±.005	45.5±1.2
HE6	4	155	2.32 ± 0.13	1.06±0.12	1.26±0.11	0.22±.003	45.5±0.8
		180	1.94 ± 0.12	0.98±0.1	0.96±0.12	0.19±.002	52.6±0.7
		200	2.14 ± 0.14	1.09±0.16	1.05±0.16	0.20±.005	50.0±0.6
		220	2.17 ± 0.19	1.14±0.12	1.03±0.1	0.20±.004	50.0±1.1
		240	2.30 ± 0.20	1.15±0.13	1.15±0.13	0.21±.001	47.6±1.3
HE4	16	155	1.91±0.13	0.87±0.10	1.04±0.12	0.19±.002	52.6±0.7
		180	1.97±0.18	0.93±0.13	1.04±0.1	0.20±.001	50.0±0.8
		200	2.03±0.19	0.98±0.10	1.05±0.1	0.20±.003	50.0±0.6
		220	2.08±0.15	1.03±0.12	1.05±0.13	0.21±.004	47.6±1.1
		240	2.74±0.19	1.34±0.12	1.40±0.11	0.22±.002	45.5±1.3
HE5	16	155	2.08±0.16	1.01±0.12	1.07±0.1	0.20±.004	50.0±1.1
		180	2.20±0.26	1.05±0.18	1.15±0.1	0.21±.003	47.6±1.3
		200	2.18±0.21	1.05±0.18	1.13±0.1	0.21±.004	47.6±1.2
		220	2.29±0.23	1.06±0.11	1.23±0.12	0.22±.002	45.5±10
		240	3.00±0.16	1.54±0.10	1.46±0.11	0.25±.005	40.0±0.9
HE6	16	155	2.08±0.18	0.99±0.16	1.09±0.12	0.20±.005	50.0±0.7
		180	2.11±0.15	1.05±.14	1.06±0.10	0.21±.004	47.6±0.8
		200	2.23±0.13	1.11±0.1	1.13±0.13	0.21±.001	47.6±0.6
		220	2.25±0.17	1.1±0.13	1.15±0.11	0.22±.002	45.5±0.4
		240	2.94±0.13	1.46±0.13	1.54±0.13	0.23±.005	435.5±0.8
HE4	44	155	2.00±0.19	0.93±.1	1.07±0.12	0.20±.003	50.0±0.7
		180	2.03±0.21	0.95±0.15	1.08±0.1	0.20±.001	50.0±0.6
		200	2.07±0.17	1.01±0.11	1.06±0.11	0.20±.004	50.0±0.9
		220	2.10±0.12	1.04±0.1	1.06±0.1	0.21±.002	47.6±1.1
		240	3.07±0.21	1.57±0.14	1.50±0.15	0.22±.003	45.5±0.4
HE5	44	155	2.13±0.18	1.06±0.1	1.07±0.13	0.21±.001	47.6±0.6
		180	2.21±0.21	1.13±0.11	1.08±0.11	0.21±.002	47.6±0.8
		200	2.61±0.20	1.29±0.13	1.32±0.1	0.23±.001	43.5±0.4
		220	2.8±0.19	1.4±0.15	1.4±0.1	0.23±.002	43.5±0.6

		240	3.34±0.17	1.67±0.10	1.60±0.12	0.25±.004	40.0±0.9
HE6	44	155	2.05±0.16	0.98±0.12	1.07±0.11	0.20±.003	50.0±0.8
		180	2.13±0.29	1.03±0.19	1.10±0.12	0.21±.001	47.6±0.7
		200	2.27±0.16	1.11±0.13	1.16±0.13	0.22±.005	45.5±0.5
		220	2.57±0.16	1.24±0.11	1.33±0.10	0.23±.002	43.5±0.4
		240	3.27±0.20	1.61±0.12	1.66±0.12	0.24±.004	41.6±0.6

*H: low cooling 396 samples; See table 21 for alloy Sr and Mn levels

Table 29 Charp impact properties of 396 alloys containing 0.65 wt% Mn, aged at 180°C and 240°C for various aging times (low cooling rate samples)

Alloy Code	Aging conditions		E_T (J)	E_I (J)	E_P (J)	Time to Failure (ms)	ACS (mm/ms)
	Temp (°C)	Time (h)					
*HE4	180	2	1.84±0.15	0.88±0.10	0.96±0.13	0.19±.001	52.6±0.9
		4	1.89±0.17	0.94±0.12	0.95±0.14	0.19±.001	52.6±0.8
		8	1.83±0.20	0.84±0.13	0.99±0.15	0.18±.002	55.5±0.7
		12	1.95±0.20	0.89±0.14	1.06±0.11	0.20±.003	50.0±1.1
		16	1.97±0.11	0.97±0.12	1.0±0.12	0.20±.004	50.0±1.3
		20	1.93±0.18	0.93±0.14	1.0±0.15	0.20±.005	50.0±0.7
		24	2.01±0.14	0.98±0.15	1.03±0.16	0.21±.006	47.6±0.8
		30	2.03±0.12	1.01±0.11	1.02±0.12	0.21±.004	47.6±0.6
		36	2.07±0.15	1.04±0.12	1.03±0.13	0.21±.003	47.6±1.4
		44	2.03±0.12	1.03±0.1	1.00±0.11	0.21±.004	47.6±1.3
HE5	180	2	1.90±0.22	0.96±0.13	0.94±0.12	0.19±.001	52.6±0.9
		4	2.02±0.21	1.01±0.12	1.01±0.13	0.20±.003	50.0±0.8
		8	2.06±0.15	1.03±0.15	1.03±0.15	0.20±.004	50.0±0.7
		12	2.11±0.13	1.06±0.14	1.05±0.14	0.21±.005	47.6±0.6
		16	2.20±0.14	1.10±0.11	1.10±0.16	0.21±.001	47.6±0.9
		20	2.23±0.12	1.12±0.17	1.11±0.11	0.22±.002	45.5±0.8
		24	2.21±0.11	1.11±0.18	1.10±0.13	0.22±.006	45.5±0.7
		30	2.10±0.10	1.05±0.12	1.05±0.14	0.21±.001	47.6±0.9
		36	2.06±0.16	1.03±0.11	1.03±0.11	020±.002	50.0±0.5
		44	2.21±0.17	1.09±0.10	1.12±0.12	0.21±.003	47.6±0.9
HE6	180	2	1.90±0.18	0.94±0.12	0.96±0.13	0.19±.001	52.6±1.1
		4	1.94±0.14	0.98±0.13	0.96±0.11	0.19±.002	52.6±1.4
		8	2.02±0.12	1.01±0.14	1.01±0.10	0.20±.003	50.0±0.9
		12	2.08±0.19	1.03±0.10	1.05±0.15	0.20±.004	50.0±1.3
		16	2.11±0.13	1.11±0.13	1.00±0.14	0.21±.001	47.6±1.4
		20	2.16±0.16	1.03±0.12	1.13±0.11	0.20±.002	50.0±1.2
		24	2.07±0.10	0.97±0.11	1.10±0.10	0.20±.003	50.0±0.9
		30	1.97±0.15	0.89±0.16	1.08±0.15	0.19±.004	52.6±0.8
		36	2.01±0.12	0.94±0.15	1.07±0.17	0.20±.003	50.0±0.7
		44	2.13±0.10	1.02±0.10	1.11±0.11	0.21±.002	47.6±1.1

		2	2.21±0.11	1.08±0.12	1.13±0.1	0.21±.001	47.6±0.9
		4	2.19±0.12	1.04±0.14	1.15±0.12	0.21±.002	47.6±0.8
		8	2.45±0.23	1.18±0.13	1.27±0.11	0.22±.003	45.5±0.7
		12	2.65±0.15	1.21±0.11	1.44±0.13	0.22±.001	45.5±0.9
HE4	240	16	2.74±0.16	1.28±0.10	1.46±0.14	0.23±.004	43.5±0.5
		20	2.93±0.17	1.42±0.16	1.51±0.10	0.24±.005	41.6±0.6
		24	2.97±0.14	1.49±0.15	1.48±0.10	0.24±.006	41.6±1.1
		30	3.01±0.18	1.54±0.10	1.47±0.10	0.25±.001	40.0±1.2
		36	3.04±0.16	1.59±0.11	1.45±0.10	0.25±.002	40.0±0.7
		44	3.07±0.12	1.60±0.12	1.47±0.20	0.25±.003	40.0±0.5
		2	2.40±0.14	1.16±0.13	1.14±0.12	0.22±.001	45.5±0.9
		4	2.41±0.12	1.31±0.14	1.10±0.13	0.23±.002	43.5±0.8
		8	2.76±0.16	1.37±0.16	1.39±0.14	0.23±.003	43.5±0.7
		12	2.91±0.11	1.42±0.11	1.49±0.11	0.23±.001	43.5±0.4
HE5	240	16	3.00±0.15	1.44±0.10	1.56±0.16	0.24±.004	41.6±0.6
		20	3.12±0.10	1.50±0.17	1.62±0.15	0.25±.006	40.0±0.9
		24	3.21±0.12	1.56±0.14	1.65±0.17	0.25±.005	40.0±1.1
		30	3.28±0.18	1.61±0.13	1.67±0.13	0.25±.003	40.0±1.4
		36	3.24±0.11	1.66±0.12	1.58±0.10	0.25±.002	40.5±0.3
		44	3.34±0.17	1.67±0.12	1.66±0.12	0.26±.001	38.5±0.7
		2	2.38±0.15	1.12±0.14	1.26±0.12	0.22±.001	45.5±0.9
		4	2.30±0.14	1.14±0012	1.16±0.14	0.22±.002	45.5±0.8
		8	2.49±0.11	1.27±0.11	1.22±0.15	0.23±.001	43.5±0.4
		12	2.67±0.13	1.33±0.10	1.34±0.17	0.24±.005	41.6±0.7
HE6	240	16	2.94±0.18	1.40±0.15	1.54±0.10	0.24±.004	41.6±0.2
		20	3.04±0.12	1.45±0.14	1.59±0.13	0.24±.003	41.6±0.3
		24	3.11±0.17	1.53±0.16	1.58±0.12	0.25±.006	40.0±0.6
		30	3.14±0.19	1.57±0.10	1.57±0.11	0.25±.005	40.0±0.7
		36	3.19±0.10	1.61±0.13	1.58±0.14	0.26±.007	38.5±1.2
		44	3.27±0.13	1.63±0.11	1.64±0.16	0.26±.001	38.5±1.3

*H: low cooling 396 samples; See table 21 for alloy Sr and Mn levels

Appendix 3

Chemical Composition, Vol. Fraction of Intermetallics and eutectic Si particle Characteristics Data for 396 Alloy Samples Selected for Fractography

Table 30 Chemical composition, codes, and conditions of the 396 alloy samples selected for fractographic analysis

Alloy Code	Alloy	Condition
E1	Non-modified 396 – 0.45 % Mn – High cooling rate	As-Cast
E2	Sr-modified 396 – 0.45 % Mn – High cooling rate	
E4	Non-modified 396 – 0.65 % Mn – High cooling rate	
E5	Sr-modified 396 – 0.65 % Mn – High cooling rate	
HE1	Non-modified 396 – 0.45 % Mn – Low cooling rate	As-Cast
HE2	Sr-modified 396 – 0.45 % Mn – Low cooling rate	
HE4	Non-modified 396 – 0.65 % Mn – Low cooling rate	
HE5	Sr-modified 396 – 0.65 % Mn – Low cooling rate	
E1T	Non-modified 396 – 0.45 % Mn – High cooling rate	SHT*
E2T	Sr-modified 396 – 0.45 % Mn – High cooling rate	
E4T	Non-modified 396 – 0.65 % Mn – High cooling rate	
E5T	Sr-modified 396 – 0.65 % Mn – High cooling rate	
HE1T	Non-modified 396 – 0.45% Mn – Low cooling rate	SHT
HE2T	Sr-modified 396 – 0.45 % Mn – Low cooling rate	
HE4T	Non-modified 396 – 0.65 % Mn – Low cooling rate	
HE5T	Sr-modified 396 – 0.65 % Mn – Low cooling rate	

*SHT: solution heat-treated

Table 31 Total volume fraction of the intermetallic phases present in the 396 alloy samples listed in Table 30 [119]

Alloy Code	Alloy Condition	Average Volume Fraction of Al_2Cu Phase		Average Volume Fraction of α-Fe Phase	
		Av.	SD	Av.	SD
E1	As-Cast	1.13	± 0.3	3.92	± 0.58
E2		1.37	± 0.6	3.61	± 0.56
E3		1.5	0.69	3.75	± 0.92
E4		1.44	± 0.4	4.42	± 0.41
E5		1.36	± 0.7	4.37	± 0.65
E6		1.4	± 0.96	4.41	± 0.91
E1	SHT	0.43	± 0.2	4.94	± 0.48
E2		0.43	± 0.3	4.08	± 0.52
E3		0.71	± 0.54	3.58	± 0.33
E4		0.5	± 0.5	5.03	± 0.58
E5		0.27	±0.1	4.7	± 0.97
E6		0.58	±0.23	4.73	±0.71
***HE1**	As-Cast	0.66 =	± 0.1	2.95	± 0.32
HE2		0.96	± 0.6	3.02	± 0.96
HE3		0.89	±0.22	2.42	±0.38
HE4		0.81	± 0.1	3.05	± 0.52
HE5		1.26	± 0.4	2.3	± 0.36
HE6		1.48	± 0.69	2.73	± 0.54
HE1	SHT	0.49	± 0.1.	3.03	± 0.29
HE2		0.76	± 0.2	3.53	± 0.21
HE3		0.98	± 0.41	3.25	± 0.34
HE4		0.49	± 0.1	3.08	± 0.39
HE5		0.9	± 0.5	2.74	± 0.82
HE6		0.88	± 0.6	2.3	± 0.31

*E sample: high cooling rate (SDAS ~ 45 μm); HE samples: Low cooling rate (SDAS ~ 120 μm); SHT: solution heat-treated; see table 30 for alloy Sr and Mn levels

Table 32 Characteristics of eutectic Si particles of the 396 alloy samples listed in Table 30 [119]

Alloy Code	Alloy Condition	Particle Area (μm^2)		Particle Length (μm)		Particle Aspect Ratio		Particle Roundness		Density Number/ mm^2
		Av.	SD	Av.	SD	Av.	SD	Av.	SD	
E1	As-Cast	36.83	61.7	12.72	16.1	2.62	1.49	53.5	32.4	2300
E2		5.3	10.1	4.1	5.1	2.25	1.17	62.5	27.9	20616
E4		38.9	59.6	13.72	16.6	2.61	1.45	50.5	31.8	2298
E5		7.18	12.0	5.18	5.7	2.5	1.29	56.6	28.7	14574
E1	SHT	57.4	76.5	16.7	17.8	2.58	1.39	52.6	30.1	1386
E2		5.5	8.5	3.4	3.4	1.86	0.97	76.7	21.4	26362
E4		59.1	73.5	18.09	18.9	2.61	1.4	49.5	30.6	1342
E5		3.57	5.76	2.65	2.57	1.71	0.66	80.2	18.3	36840
HE1	As-Cast	47.7	86.8	16.5	22.7	2.94	1.76	50.06	32.4	1351
HE2		46.02	67.6	15.3	16.5	2.83	1.65		29.1	2186
HE4		58.8	96.3	17.2	21.8	2.83	1.73	50.3	31.6	1376
HE5		27.5	55.3	9.63	13.4	2.37	1.3	51.7 58.3	29.5	4220
HE1	SHT	54.9	91.7	16.7	21.6	2.83	1.7	56.2	32.1	1557
HE2		12.6	26.9	6.4	7.2	2.39	1.29	64.4	26.4	10465
HE4		48.3	80.1	14.5	18.5	2.69	1.78	57.3	32.4	1826
HE5		66.4	109.2	19.2	26.0	2.45	1.48	58.4	33.3	1049

*E sample: high cooling rate (SDAS ~ 45 μm); HE samples: Low cooling rate (SDAS ~ 120 μm); SHT: solution heat-treated

REFERENCES

1. T. Kobayashi, *Strength and Toughness of Materials*, Agne Gijutsu Center, Springer – Verlag Tokyo, 2004.
2. F. Paray, B. Kulunk and J. E. Gruzleski, "Impact properties of Al-Si foundry alloys," *International Journal of Cast Metals Research*, 2000, Vol. 13, pp. 17-37.
3. A. M. Samuel, F. H. Samuel and H. W. Doty, "Observations on the Formation of β-Al_5FeSi Phase in 319 Type Al-Si Alloys," *Journal of Materials Science,* Vol. 31, 1996, pp. 5529-5539.
4. Z. Li, A. M. Samuel and F. H. Samuel, "Effect of alloying elements on the segregation and dissolution of $CuAl_2$ phase in Al-Si-Cu 319 alloys," *Journal of Material Science*, Vol. 38, 2003, pp. 1203-1218.
5. J. E. Gruzleski and B. M. Closset, *The Treatment of Liquid Aluminum–Silicon Alloys*, American Foundrymen's Society, Des Plaines, IL, 1990, pp. 74-94.
6. J. Gilbert Kaufman, *Fracture Resistance of Aluminum Alloys: Notch Toughness, Tear Resistance and Fracture Toughness*, 1st Edition, ASM International, Materials Park, OH, USA, 2001.
7. John. E. Hatch, *Aluminum: Properties and Physical Metallurgy*, 2nd Edition, American Society for Metals, Metals Park, OH, 1984, pp. 134-197.
8. Z. Li, A. M. Samuel, F. H. Samuel, C. Ravindran, H. W. Doty and S. Valtierra, "Parameters controlling the performance of AA319-type alloys - Part II. Impact properties and fractography," *Materials Science and Engineering A*, Vol. 367, 2004, pp. 111-122.
9. Z. Li, A.M. Samuel, F.H. Samuel, C. Ravindran, S. Valtierra and H.W. Doty, "Parameters controlling the performance of AA319-type alloys - Part I. Tensile properties," *Materials Science and Engineering A*, Vol. 367, 2004, pp. 96-110.
10. F. H. Samuel, A. M. Samuel and H. W. Doty, "Factors controlling the type and morphology of copper-containing phases in 319 aluminum alloy," *AFS Transactions*, Vol. 104, 1996, pp. 893-901.
11. A. Couture, "Iron in Aluminum Casting Alloys - A Literature Survey," *AFS International Cast Metals Journal*, Vol. 89, 1981, pp. 9-17.
12. O. Vorren, J. E. Evensen and T. B. Pedersen, "Microstructure and Mechanical Properties of AlSi (Mg) Casting Alloys," *AFS Transactions*, Vol. 92, 1984, pp. 459-466.
13. Peyman Ashtari, Hiroyasu Tezuka and Tatsuo Sato, "Influence of Sr and Mn Additions on Intermetallic Compound Morphologies in Al-Si-Cu-Fe Cast Alloy," *Materials Transactions*, Vol. 44(12), 2003, pp. 2611-2616.

14. S. S. Sreeja Kumari, R. M. Pillai and B. C. Pai, "Effects of individual and combined additions of Be, Mn, Ca and Sr on the solidification behaviour, structure and mechanical properties of Al-7Si-0.3Mg-0.8Fe alloy," *Materials Science & Engineering A*, Vol. 460-461, 2007, pp. 561-573.

15. L. F. Mondolfo, *Aluminum Alloy: Structure and Properties*, Butterworths, London-Boston, 1976, p. 971.

16. L. Bäckerud, G. Chai and J. Tamminen, *Solidification Characteristics of Aluminum Alloys, Vol. 2: Foundry Alloys*, AFS/Skanaluminium, Des Plaines, IL, 1990, pp. 71-229.

17. Q. G. Wang, P. E. Jones and M. Osborne, "Effect of Iron on the Microstructure and Mechanical Properties of an Al-7%Si-0.4%Mg Casting Alloy," Advanced Materials Engineering, GM Powertrain, report No. 2003-01-0823, pp. 449-457.

18. J. Barresi, M. J. Kerr, H. Wang and M. J. Couper, "Effect of Magnesium, Iron and Cooling Rate on Mechanical Properties of Al-7Si-Mg Foundry Alloys," *AFS Transactions*, Vol. 108, 2000, pp. 563-570.

19. S. Shivkumar, L. Wang and C. Keller, "Impact Properties of Al-Si-Cu Alloys," *Zeitschrift für Metallkunde,* Vol. 85(6), 1994, pp. 394-399.

20. K. G. Basavakumar, P. G. Mukunda and M. Chakraborty, "Influence of grain refinement and modification on microstructure and mechanical properties of Al-7Si and Al-7Si-2.5Cu cast alloys," *Materials Characterization*, Vol. 59, 2008, pp. 283-289.

21. K. G. Basavakumar, P. G. Mukunda and M. Chakraborty, "Impact Toughness in Al-12Si and Al-12Si-3Cu Cast Alloys - Part 1: Effect of Process Variables and Microstructure," *International Journal of Impact Engineering*, Vol. 35, 2008, pp. 199-205.

22. K. G. Basavakumar, P. G. Mukunda and M. Chakraborty, "Effect of melt treatment on microstructure and impact properties of Al-7Si and Al-7Si-2.5Cu cast alloys," *Bulletin of Materials Science*, Vol. 30(5), Oct. 2007, pp. 439-445.

23. J. Gilbert Kaufman, *Introduction to Aluminum Alloys and Tempers*, 1st Edition, ASM International, Materials Park, OH, USA, 2000, pp. 87-118.

24. J. Gilbert Kaufman, and E. L. Rooy, *Aluminum Alloy Castings*, 1st Edition, American Foundrymen's Society, Inc., Schaumburg, IL, 2004, pp. 17-20.

25. J. Y. Hwang, H. W. Doty and M. J. Kaufman, "The effects of Mn additions on the microstructure and mechanical properties of Al-Si-Cu casting alloys," *Materials Science and Engineering A*, Vol. 488, 2008, pp. 496-504.

26. J. L. Jorstad, W. M. Rasmussen and D. L. Zalensas, *Aluminum Casting Technology*, 2nd Edition, American Foundrymen's Society, Des Plaines, Il, 1993, pp. 19-104.

27. George E. Totten and D. Scott Mackenzie, *Handbook of Aluminum, Physical Metallurgy and Processes*, Marcel Dekker, Inc., New York, Vol. 1, 2003, pp. 604-606.

28. E. Tillová and M. Panušková, "Effect of Solution Treatment on Intermetallic Phases Morphology in AlSi9Cu3 Cast Alloy," *Metalurgija*, Vol. 47 (3), 2008, pp. 207-210.

29. D. Apelian, S. Shivkumar and G. Sigworth, "Fundamental Aspects of Heat Treatment of Cast Al-Si-Mg Alloys," *AFS Transactions*, Vol. 97, 1989, pp. 727-742.

30. C. W. Meyers, "Solution heat treatment effects in A357 alloys," *AFS Transactions*, Vol. 93, 1985, pp. 741-750.

31. N. Crowell and S. Shivkumar, "Solution Treatment Effects in Cast Al-Si-Cu Alloys," *AFS Transactions*, Vol. 103, 1995, pp. 721-726.

32. F. Paray and J. E. Gruzleski, "Microstructure-mechanical property relationship in a 356 alloy. Partl: Microstructure," *Cast Metals*, Vol. 7(1), 1994, pp. 29-40.

33. J. W. Martin and R. D. Doherty, *Stability of Microstructure in Metallic Systems*, 2nd Edition, Cambridge University Press, Cambridge, U.K., 1997, pp. 239-251.

34. S. Shivkumar, "The interactive effects of Sr modification and heat treatment on the mechanical properties of cast aluminum alloys," *17th ASM Heat Treating Society Proceedings including the 1st International Induction Heat Treating Symposium*, 15-18 Sep., Indianapolis, Indiana, 1997, pp. 265-269.

35. L. A. Narayanan, F. H. Samuel and J. E. Gruzleski, "Dissolution of iron intermetallics in Al-Si alloys through nonequilibrium heat-treatment," *Metallurgical and Materials Transactions A*, Vol. 26(A), 1995, pp. 2161-2174.

36. C. Villeneuve and F. H. Samuel, "Fragmentation and dissolution of β-Al5FeSi phase during solution heat treatment of Al-13wt%Si-Fe alloys," *International Journal of Cast Metals Research,* Vol. 12, 1999, pp. 145-160.

37. P. N. Crepeau, "Effect of iron in Al-Si Casting Alloys: A Critical Review," *AFS Transactions*, Vol. 103, 1995, pp. 361-366.

38. L. H. Zheng, "Effects of solution, aging, natural aging and pre-aging treatment on the tensile properties and microstructure of an Al-7%Si-0.4 % Mg alloy," PhD Thesis, The University of Queensland, Australia, 1998, P. 25.

39. J. A. Taylor, D. H. StJohn, J. Barresi and M. J. Couper, "Influence of Mg Content on the Microstructure and Solid Solution Chemistry of Al-7Si-Mg Casting Alloys During Solution Treatment," *Materials Science Forum*, Vol. 331-337, 2000, pp. 277-282.

40. A. Taylor, D. H. StJohn, L. H. Zheng, J. Barresi and M. J. Couper, "Solution Treatment Effects in Al-Si-Mg Casting Alloys: Part 1. Intermetallic phases," *Aluminum Transactions*, Vol. 4-5, 2001, pp. 95-110.

41. *Metals Handbook, Vol. 15: Casting*, Ninth Edition, American Society for Metals, Metals Park, OH, 1988, pp. 290-295.

42. L. Pedersen and L. Arnberg, "The Effect of Solution Heat Treatment and Quenching Rates on Mechanical Properties and Microstructure in AlSiMg

Foundry Alloys," *Metallurgical and Materials Transactions A*, Vol. 32(A), 2001, pp. 525-532.

43. I. J. Polmear, *Light Alloys*, Edward Arnold, London, UK, 1981, pp. 147-157.

44. G. E. Dieter, *Mechanical Metallurgy*, 3rd Edition, McGraw Hill, UK, 1986, pp. 241-272.

45. Marc André Meyers and Krishan Kumar Chawla, *Mechanical Behavior of Materials*, 2nd Edition, Cambridge University Press, New York, 2009.

46. R. E. Smallman and A. H. W. Ngan, *Physical Metallurgy and Advanced Materials*, 7th Edition, Butterworth Heinemann, Boston, 2007, pp. 385-404.

47. O. H. Wyatt and D. Dew-Hughes, *Metals, Ceramics and Polymers*, Cambridge University Press, Bentley House, London, 1974, pp. 444-452.

48. R. X. Li, R. D. Li, Y. H. Zhao, L. Z. He, C. X. Li, H. R. Guan and Z. Q. Hu, "Age hardening behavior of cast Al-Si base alloy," *Material Letters*, Vol. 58, 2004, pp. 2096-2101.

49. H. K. Kang, M. Kida and H. Miyahara, "Age hardening characteristics of Al-Si-Cu-base cast alloys," *AFS Transactions,* Vol. 107, 1999, pp. 507-515.

50. S. Shivkumar, C. Keller, M. Trazzera and D. Apelian, "Precipitation hardening in A356 alloys," in *Proceedings. International Symposium on Production, Refining, Fabrication and Recycling of Light Metals*, Hamilton, Ontario, Aug. 26-30, 1990, M. Bouchard and P. Tremblay (Eds), Pergamon Press, New York, 1990, pp. 264-278.

51. S. Shivkumar, C. Keller and D. Apelian, "Aging Behavior in Cast Al-Si-Mg alloys," *AFS Transactions*, Vol. 98, 1990, pp. 905-911.

52. G. V. R. Ragavan, K. Raghukandan, U. T. S. Pillai, K. Sukumaran and B. C. Pai, "General aspects of heat treatment processes on Al-Si-Mg alloys," *Indian Foundry Journal*, Vol. 50(4), 2004, pp. 28-34.

53. *Metals Handbook, Vol. 8: Mechanical Testing and Evaluation*, Tenth Edition, American Society of Metals, Metals Park, OH, 2000, pp. 596-611.

54. N. Komatsu, M. Nakamura and Y. Yamamoto, "Metallurgical Structure and Impact Strength of Al-Si Alloys," *Technical Report of Toyota R&D Center,* TR-11, 1975, pp. 1-46 (in Japanese).

55. M. Tsukuda, S. Koike and M. Harada, "The Heat Treatment of Al-7%Si-0.3Mg Alloy," *Journal of Japan Institute of Light Metals* (in Japanese), Vol. 28(1), 1978, pp. 8-14

56. S. Shivkumar, L. Wang and C. Keller, "Impact Properties of A356-T6 Alloys," *Journal of Materials Engineering and Performance,* Vol. 3, Feb. 1994, pp. 83-90.

57. M. C. Srivastava, O. Lohne, L. Arnberg, H. I. Laukli and H. Gjestland, "Energy absorption of HPDC aluminum and magnesium alloys," in *Proceedings*: *High Tech Die Casting*, 2006, Vicenza, Italy, P. 10.

58. L. Lu and A. K. Dahle, "Iron-Rich Intermetallic Phases and Their Role in Casting Defect Formation in Hypoeutectic Al-Si Alloys," *Metallurgical and Materials Transactions A*, Vol. 36(A), 2005, pp. 819-835.

59. Cameron M. Dinnis, John A. Taylor and Arne K. Dahle, "As-cast morphology of iron-intermetallics in Al-Si foundry alloys," *Scripta Materialia*, Vol. 53, 2005, pp. 955-958.

60. M. Tsukuda, M. Harada, T. Suzuki and S. Koike, "The effect of Si, Mg, Fe on the mechanical properties of Al-Si-Mg alloys for casting," *Journal of Japan Institute of Light Metals*, Vol. 28(3), 1978, pp. 109-115.

61. A. Ikenaga, M. Tsujikawa, K. Okabayashi and M. Kawamoto, "Relation between Fracture Properties and Microstructure of Hyper-eutectic Al-Si Alloy Castings," *Transactions of the Japan Foundrymen's Society*, 1987, pp. 18-22.

62. D. K. Dwivedi, Sumit Sood and Virender Thakur, "Influence of Microstructure on Mechanical Properties of Cast Al-Si Base alloy; Effect of Grain Refinement and Artificial Aging Hardening on Hardness and Toughness," *Indian Foundry Journal*, Vol. 47(10), October 2001, pp. 34-37.

63. M. A. Moustafa, F. H. Samuel, H. W. Doty and S. Valtierra, "Effect of Mg and Cu additions on the microstructural characteristics and tensile properties of Sr-modified Al-Si eutectic alloys," *International Journal of Cast Metals Res*earch, Vol. 14, 2002, pp. 235-253.

64. M. A. Moustafa, F. H. Samuel and H. W. Doty, "Effect of solution heat treatment and additives on the microstructure of Al-Si A413.1 automotive alloys," *Journal of Material Science*, Vol. 38, 2003, pp. 4507-4522.

65. M. A. Moustafa, C. Lepage, F. H. Samue and H. W. Doty, "Metallographic observations on phase precipitation in strontium-modified Al-11.7%Si alloys: Role of alloying elements," *International Journal of Cast Metals Research*, Vol. 15, 2003, pp. 609-626.

66. S. Murali, K. S. Raman and K. S. S. Murthy, "Effect of magnesium and iron (impurity) and solidification rates on the fracture toughness of Al-7Si-0.3Mg casting alloy," *Material Science and Engineering*, A, Vol. 151, 1992, pp. 1-10.

67. T. Nakayama, K. Ninomiya and N. Ohnishi, "Effect of magnesium content on mechanical properties of Al-2% Si casting alloy solution treated at high temperature," *Journal of Japan Institute of Light Metals*, Vol. 48(7), 1998, pp. 340-345.

68. F. J. Tavitas-Medrano, J. E. Gruzleski, F. H. Samuel, S. Valtierra and H. W. Doty, "Effect of Mg and Sr-modification on the mechanical properties of 319-type aluminum cast alloy," *Materials Science and Engineering A*, Vol. 480, 2008, pp. 256-264.

69. J. A. Taylor, "Metal-related castability effects in aluminum foundry alloys," *Cast Metals*, Vol. 8 (4), 1995, pp. 225-252.

70. B. Markoli, S. Spaić and F. Zupanic, "The Intermetallic phases containing transition elements in common Al-Si cast alloys," *Aluminum*, Vol. 80(1/2), 2004, pp. 84-88.

71. S. S. Sreeja Kumari, R. M. Pillai and B. C. Pai, "Effect of Iron in Al-7Si-0.3Mg Alloy," *Indian Foundry Journal*, Vol. 48(1), 2002, pp. 27-31.

72. S. Murali, K. S. Raman and K. S. S. Murthy, "Effect of Trace Additions (Be, Cr, Mn and Co) on the Mechanical Properties and Fracture Toughness of Fe-Containing Al-7Si-0.3Mg Alloy," *International Journal of Cast Metals Research,* Vol. 6(4), 1994, pp. 189-198.

73. Y. Awano and Y. Shimizu, "Non-Equilibrium Crystallization of AlFeSi Compound in Melt-Superheated Al-Si Alloy Casting," *AFS Transactions*, Vol. 98, 1990, pp. 889-905.

74. L. A. Narayanan, F. H. Samuel and J. E. Gruzleski, "Crystallization Behavior of Iron-Containing Intermetallic Compounds in 319 Aluminum Alloy," *Metallurgical and Materials Transactions A*, Vol. 25(A), 1994, pp. 1761-1773.

75. Y. Kaneko, H. Murakami, K. Kurada and S. Nakasaki, *Die Casting Engineer*, May-June 1979, P. 26.

76. T. Kobayashi, "Fracture Characteristics of Aluminum Casting Alloys," in *Proceedings of 6th International Conference on Aluminum Alloys (ICAA-6), Aluminum Alloys: Their Physical and Mechanical Properties*, July 5-10, 1998, Japan, pp. 127-138.

77. S. S. Sreeja Kumari, R. M. Pillai and B. C. Pai, "A study on the structural, age hardening and mechanical characteristics of Mn and Ca added Al-7Si-0.3Mg-0.6Fe alloy," *Journal of Alloys and Compounds*, Vol. 453, 2008, pp. 167-173.

78. E. Kato and T. Kobayashi, "Effect of solidified structure on the fracture toughness of unidirectionally solidified Al-Si system alloys," *Journal of Japan Institute of Light Metals*, Vol. 30(3), 1980, pp. 140-146.

79. Mattia Merlin, Giulio Timelli, Franco Bonollo and Gian Luca Garagnani, "Impact behaviour of A356 alloy for low-pressure die casting automotive wheels," *Journal of Materials Processing Technology*, Vol. 209, 2009, pp. 1060-1073.

80. B. Closset and J. E. Gruzleski, "Structure and Properties of Hypoeutectic Al-Si-Mg Alloys Modified with Pure Strontium," *Metallurgical and Materials Transactions A*, Vol. 13(A), 1982, pp. 945-951.

81. T. Kobayashi, M. Miinomi, M. Yamaoka, T. Harata and M. F. Hafiz, "Effect of Sr addition on fracture characteristics of high purity Al-Si-Mg type casting alloy," *Journal of Japan Institute of Light Metals*, Vol. 43(9), 1993, pp. 472-477.

82. B. M. Closset, "Modification of Quality Low Pressure Al-Si Castings," *AFS Transactions*, Vol. 96, 1988, pp. 249-260.

83. M. F. Hafiz and T. Kobayashi, "Mechanical Properties of modified and non-modified eutectic Al-Si alloys," *Journal of Japan Institute of Light Metals*, Vol. 44(1), Jan. 1994, pp. 28-34.

84. M. F. Hafiz and T. Kobayashi, "Effect of Microstrctural Variation on Tensile Properties and Impact Toughness of Hypoeutectic Al-Si Alloy," *Transactions of the Japan Foundrymen's Society*, Vol. 12, Oct. 1993, pp. 115-123.

85. M. F. Hafiz and T. Kobayashi, "A Study of the Microstructure-Fracture Behavior Relations in Al-Si Casting Alloys," *Scripta Metallurgica et Materialia*, Vol. 30, 1994, pp. 475-480.

86. C. L. MacAdam and D. C. Jenkinson, "The stability of silicon fibres in aluminium-silicon alloys and their influence on mechanical properties," in *Proceedings 27th Annual Congress of the Australian Institute of Metals*, 20-24 May 1974, Christchurch, New Zland, Vol. 27, 1974, pp. 58-63.

87. D. L. Zhang, L. H. Zheng and D. H. StJohn, "Effect of a short solution treatment time on microstructure and mechanical properties of modified Al-7 wt.%Si-0.3 wt.%Mg alloy," *Journal of Light Metals*, Vol. 2, 2002, pp. 27-36.

88. J. Gurland and J. Plateau, "The Mechanism of Ductile Rupture of Metals containing Inclusions," *Transactions of Metallurgical Society of AIME,* Vol. 56, 1963, pp. 442-454.

89. A. Gangulee and J. Gurland, "On the Fracture of Silicon Particles in Aluminum-Silicon Alloys," *Transactions of Metallurgical Society of AIME,* Vol. 239, 1967, P. 269.

90. S. F. Frederick and W. A. Bailey, "The Relation of Ductility to Dendrite Cell Size in as-Cast Al-Si-Mg Alloy," *Transactions of Metallurgical Society of AIME,* Vol. 242, Oct. 1968, pp. 2063-2067.

91. R. C. Voigt and D. R. Bye, "Microstructural Aspects of Fracture in A356," *AFS Transactions,* Vol. 99, 1991, pp. 33-50.

92. Q. G. Wang and C. H. Cáceres, "The Fracture Mode in Al-Si-Mg Casting Alloys," *Materials Science and Engineering A,* Vol. A241, 1998, pp. 72-82.

93. Charlie R. Brooks and Ashok Choudhury, *Metallurgical Failure Analysis*, McGraw-Hill, Inc., New York, 1993.

94. N. Fatahalla, M. Hafiz, and M. Abdulkhaliek, "Effect of Microstructure on the Mechanical Properties and Fracture of Commercial Hypoeutectic Al-Si alloy modified with Na, Sb and Sr," *Journal of Materials Science,* Vol. 34, 1999, pp. 3555-3564.

95. A. Saigal and J. T. Berry, "Study of the Effects of Volume Fraction, Size and Shape of Silicon Particles on Mechanical Properties in Al-Si Alloys Using Finite Element Method," *AFS Transactions,* Vol. 93, 1985, pp. 699-704.

96 M. D. Dighe and A. M. Gokhale, "Relationship Between Microstructural Extremum and Fracture Path in a Cast Al-Si-Mg Alloy," *Scripta Materialia,* Vol. 37(9), 1977, pp. 1435-1440.

97. C. H. Cáceres and J. R. Griffiths, "Damage by the Cracking of Silicon Particles in an Al-7Si-0.4Mg Casting Alloy," *Acta Materialia,* Vol. 44(1), 1996, pp. 25-33.

98. C. H. Cáceres and J. R. Griffiths, "Fracture Micromechanisms in an Al-Si-Mg Casting Alloy," *Strength of Materials, ICSMA 10*, The Japan Institute of Metals, Sendai, Japan, Aug. 1994, pp. 22-26.

99. K. Okabayashi, M. Kawamoto, A. Ikenaga, M. Tsujikawa and K. Nomura, "Relationship between Fracture Properties and Microstructure of Hyper-Eutectic Al-Si Alloy Castings," *Imono (Journal of the Japan Foundrymen's Society),* Vol. 57(2), 1985, pp. 108-112.

100. A. M. Samuel and F. H. Samuel, "A Metallographic Study of Porosity and Fracture Behavior in Relation to Tensile Properties in 319.2 End Chill Castings," *Metallurgical and Materials Transactions A,* Vol. 26A, 1995, pp. 2539-2372.

101 M. K. Surappa, E. W. Blank, and J. C. Jaquet, "Microstructural Approach to Deformation and Fracture of Cast Al-7Si-0.3Mg," *3rd International Conference on Solidification Processing,* Sheffield, UK, 1987, pp. 424-427.

102. C. H. Cáceres, C. J. Davidson and J. R. Griffiths, "The Deformation and Fracture Behavior of an Al-Si-Mg Casting Alloy," *Materials Science and Engineering* A, Vol. 197, 1995, pp. 171-179.

103. A. M. Samuel, F. H. Samuel, C. Villeneuve, H. W. Doty and S. Valtierra, "Effect of Trace Elements on β-Al_5FeSi Characteristics, Porosity and Tensile Properties of Al-Si-Cu (319) Cast Alloys," *International Journal of Cast Metals Research,* Vol. 14, 2001, pp. 97-120.

104. S. Murali, A. Trivedi, K. S. Shamanna and K. S. S. Murthy, "Effect of Iron and Combined Iron and Beryllium Addition on the Fracture Toughness and Microstructures of Squeeze-Cast Al-7Si-0.3Mg Alloy," *Journal of Materials Engineering and Performance,* Vol. 5(4), 1996, pp. 462-468.

105. E. Kato, "Relationship between Fracture Process of Al-Si Alloy Castings and Shape of Iron Compounds," *Journal of Japan Institute of Light Metals* (in Japanese), Vol. 45(1), 1995, pp. 9-14.

106. *Metals Handbook, Vol. 8: Mechanical Testing and Evaluation,* Tenth Edition, American Society for Metals, Materials Park, OH, 2000, pp. 416-418.

107. William D. Callister, Jr., *Materials Science and Engineering - An Introduction,* 7th Edition, John Wiley & Sons, Inc., York, PA, 2007, pp. 155-160.

108. John A. Taylor, "The Effect of Iron in Al-Si Casting Alloys," Cooperative Report, Research Center for Cast Metals Manufacturing (CAST), University of Queensland, Brisbane, Australia, pp. 1-10

109. O. El Sebaie, F. H. Samuel, A. M. Samuel and H. W. Doty, "The Effects of Mischmetal, Cooling Rate and Heat Treatment on the Eutectic Si Particle

Characteristics of A319.1, A356.2 and A413.1Al-Si Casting Alloys," *Materials Science and Engineering A*, Vol. 480, Issues 1-2, 15 May 2008, pp. 342-355.

110. A. Taylor, D. H. StJohn, L.H. Zheng, J. Barresi and M. J. Couper, "Solution Treatment Effects in Al-Si-Mg Casting Alloys: Part II. Solid Solution Chemistry," *Aluminum Transactions*, Vol. 4-5, 2001, pp. 111-124.

111. Q. G. Wang and C. J. Davidson, "Solidification and precipitation behavior of Al-Si-Mg Casting Alloys," *Journal of Materials Science*, Vol. 36, 2001, pp. 739-750.

112. O. El Sebaie, A. M. Samuel, F. H. Samuel and H.W. Doty, "The effects of mischmetal, cooling rate and heat treatment on the hardness of A319.1, A356.2 and A413.1 Al-Si casting alloys," *Materials Science and Engineering A*, Vol. 486, 2008, pp. 241-252.

113. M. M. Tash, "Effect of Metallurgical Parameters on the Machining Behavior of 356 and 319 Alloys (Drilling and Tapping Study)," PhD Thesis, Université du Québec à Chicoutimi, Chicoutimi, Canada, July, 2005.

114. Z. Ma, A. M. Samuel, F. H. Samuel, H. W. Doty and S. Valtierra, "Effect of Fe Content and Cooling Rate on the Impact Toughness of Cast 319 and 356 Aluminum Alloys", *AFS Transactions*, paper 03-101, 2002, pp. 1-11.

115. G. Sigworth, D. Apelian, and S. Shivkumar, "The Influence of Molten Metal Processing on Mechanical Properties of Cast Al-Si-Mg Alloys," *AFS Transactions,* Vol. 97, 1989, pp. 811-824.

116. Victor Paramo, Rafael Colas, Eulogio Velasco and Salvador Valtierra, "Spheroidization of the Al-Si Eutectic in a Cast Aluminum Alloy," *Journal of Materials Engineering and Performance*, Vol. 9(6), Dec. 2000, pp. 616-622.

117. F. H. Samuel, P. Ouellet, A. M. Samuel and H. W. Doty, "Effect of Mg and Sr Additions on the Formation of Intermetallics in Al-6 Wt Pct Si-3.5 Wt Pct Cu-(0.45) to (0.8) Wt Pct Fe 319-Type Alloys," *Metallurgical and Materials Transactions A*, Vol. 29A(12), 1998, pp. 2871-2884.

118. G. Ran, J.E. Zhou and Q.G. Wang, "Precipitates and tensile fracture mechanism in a sand cast A356 aluminum alloy," *Journal of Materials Processing Technology*, Vol. 207, 2008, pp. 46–52.

119. Z. Ma, E. Samuel, A. M. A. Mohamed, A. M. Samuel, F. H. Samuel and H. W. Doty, "Parameters controlling the microstructure of Al-11Si-2.5Cu-Mg alloys," *Materials and Design*, Vol. 31, 2010, pp. 902-912.

120. S. G. Shabestari and F. Shahri, "Influence of modification, solidification conditions and heat treatment on the microstructure and mechanical treatment of A356 aluminum alloy," *Journal of Materials Science*, Vol. 39, 2004, pp. 2023-2032.

121. Z. Ma, E. Samuel, A. M. A. Mohamed, A. M. Samuel, F. H. Samuel and H. W. Doty, "Influence of Aging Treatments and Alloying Additives on the Hardness of Al-11Si-2.5Cu-Mg Alloys," *Materials and Design,* in Press, 2010.

122. M. V. Kral, "A crystallographic identification of intermetallic phases in Al-Si alloys," *Materials Letters*, Vol. 59, 2005, pp. 2271-2276.

123. F. H. Samuel, A.M. Samuel, H.W. Doty and S. Valtierra, "Decomposition of Fe-Intermetallics in Sr-Modified Cast 6XXX Type Aluminum Alloys for Automotive Skin," *Metallurgical and Materials Transactions A*, Vol. 32A, 2001, pp. 2061-2075.

124. G. Pucella, A. M. Samuel, F. H. Samuel, H. W. Doty and S. Valtierra, "Sludge formation in Sr-modified Al-11.5%Si die-casting alloys," *AFS Transactions*, Vol. 107, 1999, pp. 398-405.

125. A. M. A. Mohamed, F. H. Samuel, A. M. Samuel and H. W. Doty, "Influence of additives on the impact toughness of Al-10.8% Si near-eutectic cast alloys," *Materials and Design*, Vol. 30, 2009, pp. 4218-4229.

126. M. F. Hafiz, T. Kobayashi, and N. Fat-Halla, "Role of microstructure in relation to the toughness of hypoeutectic Al-Si casting alloy," *Cast Metals*, Vol. 7, 1994, pp. 103-111.